DISSERTATION / DOCTORAL THESIS

Titel der Dissertation /Title of the Doctoral Thesis

„From geometric morphometrics to clinical classification: using bending energy to assess the functional significance of nasoseptal deformity in a nonsurgical Austrian sample"

verfasst von / submitted by

Peter Currie MSc

angestrebter akademischer Grad / in partial fulfilment of the requirements for the degree of

Doctor of Philosophy (PhD)

Wien, / Vienna 2018

Studienkennzahl lt. Studienblatt / degree programme code as it appears on the student record sheet:	A 794685437
Dissertationsgebiet lt. Studienblatt / field of study as it appears on the student record sheet:	Biologie
Betreut von / Supervisor:	Prof. Dr. Fred Bookstein

Acknowledgements

This thesis represents not only seven years of work at the University of Vienna, and shuttling between Canada and Vienna, but also a long fascination with the airway and midface morphology. During a concurrent career in dentistry I had been long frustrated by the inconclusively demonstrated relationship between airway obstruction and dental malocclusion. This thesis presents a novel approach that may be useful in exploring this relationship.

I would like to thank my supervisor, Prof. Dr. Fred L. Bookstein. Without his guidance, wisdom and support this project would never have been completed. It has been an honour being associated with this great scholar. A gifted statistician, editor, and mentor, he conceptualized the partial warps – bending energy innovation of this project. Thank you also for your insights on the vagaries of American politics, Vienna, and art.

I would like to thank Prof. Dr. Rudolf Slavicek, one of the world's great dental educators, for the opportunity to study in Vienna, for his support, and for all that he has taught me in the past. Thank you to Dr. Cinzia Fornai for instructing me in Amira and segmentation, and Mr. Martin Dockner for IT support.

A special thank you to Dr. Michael Coquerelle for instruction in all aspects of the GMM toolkit, digitization and the use of Viewbox, for instruction in R and for many lines of code. Without your support this all would have been impossible.

Most of all I thank my wife Susan for her continuing love and support. Not only in our life together, but in what must have seem to be a quixotic pursuit of this Ph.D.

Table of Contents

Chapter I

Introduction
Anatomy of the Nasal Septum and Current Diagnostic Systems

The pharynx is part of both the digestive and respiratory systems, extending from the base of the skull to the larynx (respiratory) and the esophagus (digestive). It is comprised of three sections: the nasopharynx, the oropharynx, and the laryngopharynx. This study is focused on the nasopharynx (and in particular the nasal septum) which extends from the base of the skull to the hard palate, and includes the internal nares, nasal conchae, nasal septum, and adenoids.

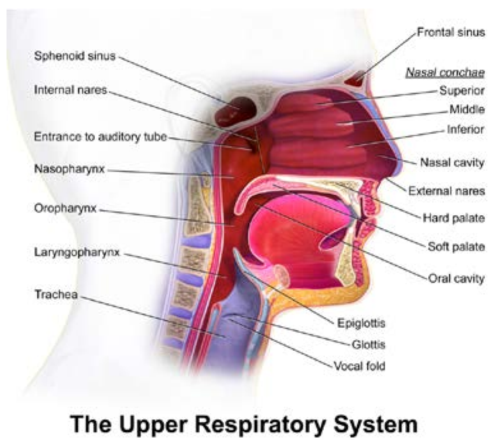

Figure 1: The upper respiratory system (diagram from Wikipedia)

The nasal septum is a slightly nonplanar midline structure comprised of cartilage, the perpendicular plate of the ethmoid, maxillary crest, and the vomer (Figs. 1 and 2). It supports the nose and turbinates and maintains separation of the right and left nasal cavities. Deviation of the nasal septum to the left or right, and deformity of the septum into S, C, or other shapes can result in reduced airflow through the nasal pharynx.

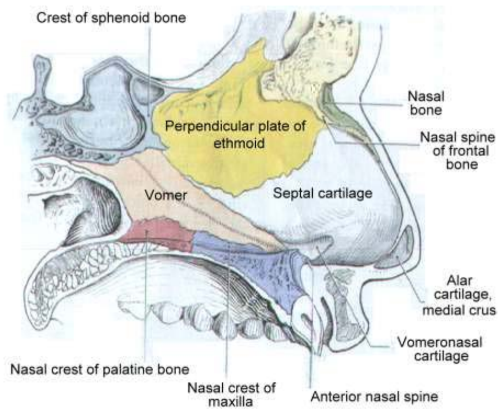

Figure 2: Diagram showing the anatomical units of the nasal septum

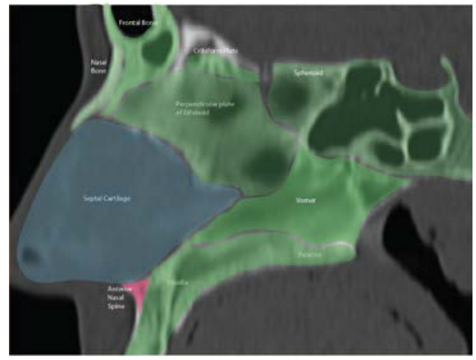
Figure 3: CT with anatomical units of the nasal septum

There may be considerable confusion regarding the anatomy of the nasal septal complex. This will be discussed in detail in conjunction with nasal septal deformity classification.

What is Nasal Septal Deviation?

Gray (1965) defined deviated nasal septum as either anterior nasal cartilage deformity or combined septal deformity; these may occur independently or together. The anterior nasal cartilage deformity is localized to the anterior quadrilateral cartilage, while the combined septal deformity may involve the vomer, the perpendicular plate of the ethmoid bone, and the quadrilateral cartilage. Gray notes that there may be a “kinking or spur deformity” of the vomer/ethmoid junction, a “C or S shaped bending or deviation,” or a combination of all these elements. The shape of this bending is significant and will be identified and discussed in later chapters.

Deviated septum has also been described as “displacement from flat of the nasal septum”, with no implication that treatment is required. This definition has been modified in one patient information website from that of normal anatomical variation, to an implication of pathology that should be corrected. A "deviated septum" occurs when the septum is severely shifted away from the midline” (American Academy of Otolaryngology Head and Neck Surgery 2017). This over simplifies a complex problem that doesn’t have clear parameters as to what is normal versus what is pathological.

In contrast to an implication of pathology, Ryo Takahashi describes the deviated nasal septum and its etiology in the context of his “concept of evolutionary paradox” where “nasal septal deformity should not be interpreted as an isolated human phenomenon but as one that occurred during the evolution from non-primate mammals to primates” (Takahashi 1987, p.152).

The rationale for an assessment of nasoseptal form is a functional one: the reduced airflow to the nasopharynx associated with rhinosinusitis, septal deviation and other respiratory problems (Becker 2003, Maqbool 2013). The problem is that current approaches to “treating” airflow problems by surgical intervention do not appear, in practice, to arrive at the anticipated functional improvements (Sundh, 2015).

Over 600,000 sinonasal surgical procedures were performed in the USA in the year 2006. This included 260,000 septoplasties and 134,000 plastic surgery cases (Cullen 2009). In England during 2012 and 2013, there were 3.8 septoplasties per 10,000 inhabitants, while in the Netherlands in 2010 there were 6.0 septoplasties per 10,000 (Van Egmond 2015). The efficacy of these procedures may be questioned in light of the UK CRS Epidemiology Study (CRES) that reported a 19.1% surgical revision rate at 5 years for these procedures (Philpott 2015).

There is an extensive literature on airway obstruction and nasal septal surgery; however, there is very little objective evidence to support most surgical procedures. This is compounded by a frequent failure to ascertain the quality of the literature that meets research criteria. In this review of the literature, I consider whether the paper meets the criteria of evidence based medicine (Burns 2011, Howick 2011) as set out by the Oxford Centre for Evidence-Based Medicine (OCEBM) criteria (Table 1). The OCEBM is a division of the Centre for Evidence Based Medicine of Oxford University (CEBM), a not-for-profit organisation dedicated to the practice, teaching and dissemination of high quality evidence based medicine to improve healthcare in everyday clinical practice. Further guidance on evidence medicine is provided by the Grading of Recommendations Assessment, Development and Evaluation working group (GRADE, 2017).

Oxford Centre for Evidence-Based Medicine 2011 Levels of Evidence

Question	Step 1 (Level 1*)	Step 2 (Level 2*)	Step 3 (Level 3*)	Step 4 (Level 4*)	Step 5 (Level 5)
How common is the problem?	Local and current random sample surveys (or censuses)	Systematic review of surveys that allow matching to local circumstances**	Local non-random sample**	Case-series**	n/a
Is this diagnostic or monitoring test accurate? (Diagnosis)	Systematic review of cross sectional studies with consistently applied reference standard and blinding	Individual cross sectional studies with consistently applied reference standard and blinding	Non-consecutive studies, or studies without consistently applied reference standards**	Case-control studies, or "poor or non-independent reference standard**	Mechanism-based reasoning
What will happen if we do not add a therapy? (Prognosis)	Systematic review of inception cohort studies	Inception cohort studies	Cohort study or control arm of randomized trial*	Case-series or case-control studies, or poor quality prognostic cohort study**	n/a
Does this intervention help? (Treatment Benefits)	Systematic review of randomized trials or *n*-of-1 trials	Randomized trial or observational study with dramatic effect	Non-randomized controlled cohort/follow-up study**	Case-series, case-control studies, or historically controlled studies**	Mechanism-based reasoning
What are the COMMON harms? (Treatment Harms)	Systematic review of randomized trials, systematic review of nested case-control studies, *n*-of-1 trial with the patient you are raising the question about, or observational study with dramatic effect	Individual randomized trial or (exceptionally) observational study with dramatic effect	Non-randomized controlled cohort/follow-up study (post-marketing surveillance) provided there are sufficient numbers to rule out a common harm. (For long-term harms the duration of follow-up must be sufficient.)**	Case-series, case-control, or historically controlled studies**	Mechanism-based reasoning
What are the RARE harms? (Treatment Harms)	Systematic review of randomized trials or *n*-of-1 trial	Randomized trial or (exceptionally) observational study with dramatic effect			
Is this (early detection) test worthwhile? (Screening)	Systematic review of randomized trials	Randomized trial	Non -randomized controlled cohort/follow-up study**	Case-series, case-control, or historically controlled studies**	Mechanism-based reasoning

*** Level may be graded down on the basis of study quality, imprecision, indirectness (study PICO does not match questions PICO), because of inconsistency between studies, or because the absolute effect size is very small; Level may be graded up if there is a large or very large effect size.**

**** As always, a systematic review is generally better than an individual study.**

Table 1 (Above): OCEBM Classification [(Burns 2011, Howick J 2011)]**.** In the table each row describes a series of steps to be followed in order to find the strongest evidence. Usually the strongest evidence is found towards the left and the weakest towards the right. The levels are not intended to provide a definitive judgment about the quality of evidence. Each column anticipates the types of questions that a clinician is likely to ask, in the order that they are likely to be encountered. The OCEBM classification does not replace systematic reviews, which are better than individual studies at assessing the strength of evidence (GRADE) and assumes that a systematic review has been used. The OCEBM classification is appropriate when individual studies are only available and/or are preferable. A CEBM glossary may be found at http://www.cebm.net/glossary/.

The GRADE working group has developed a transparent approach to grading quality (or certainty) of evidence and strength of recommendations. Many international organizations have provided input into the development of this approach and GRADE claims that it is considered the standard in guideline development.

A physical examination of the nasal cavity is self-limiting as there are no existing criteria as to the degree of nasal septal deformity or turbinate hypertrophy that must be present in order to justify surgery, and there is also no standard methodology to measure airway function. Singh (2006) noted the need for objective evidence to support surgery as the subjective clinical findings do not necessarily correlate with the patient's symptoms. They undertook a meta-analysis to examine the evidence that surgery can improve nasal airflow. Data bases (Medline, Embase, Cochrane, and Royal Society of Medicine) were searched for the period 1966 – 2005. Objective reporting criteria that measured the outcomes of septal surgery using rhinomamometry, peak nasal inspiratory flow, or acoustic rhinometry were reviewed. 942 articles were identified; however, only 13 were prospective papers that used objective techniques, and only 3 met the study criteria: older studies (1988, 1990, and 1997), which would have scored at level 4 on the OCEBM scale, and had inconsistent findings.

Jessen (1989) demonstrated a greater reduction of airway resistance at 9 years as compared to 9 months post-operative (suggesting spontaneous bone-cartilage changes); however, patient evaluation of no nasal obstruction at 9 months (51%) declined to 26% at 9 years. The authors concluded that despite extensive literature on septal surgery, demonstrating a short term reduction of obstruction following surgery, both objective and subjective changes may occur later than 9 months after functional septoplasty. The methodology that most of the studies employed to measure nasal airway resistance was often flawed, and there is little objective evidence about the value of these procedures. Because of the large size of the original pool (942 papers selected), while only 3 papers were eligible for analysis, Singh (2006) did not believe that their results could sustain a definitive and objective conclusion in favor of surgery.

Rhee (2008) identified the need for a systematic review of the literature supporting surgical techniques to treat nasal obstruction due to nasal valve collapse. Following a PubMed search of the English-language from 1982 through 2007, 44 of 861 citations met their inclusion criteria, which addressed the question: “In adult subjects with nasal airway obstruction related to a structural nasal deformity, does a functional rhinoplasty and/or nasal valve repair effectively improve the nasal airway obstruction?” 42 studies met level 4 evidence (case studies) but only 2 met level 2b (systematic review) criteria (Howick 2011). The authors conclude that the substantial level 4 evidence supports the use of rhinoplasty to treat nasal obstruction due to nasal valve collapse, while acknowledging that under the Oxford Centre for Evidence Based Medicine (OCEBM), the studies reviewed only merit an aggregate grade C. The authors point out that randomized controlled trials may not be feasible, and conclude that the OCEBM guidelines “fall short in helping to differentiate the studies within the level 4 quality”. However the 2011 OCEBM background paper (Howick 2011) addresses these concerns in requiring level 1 studies to answer “Which treatment, from among all the available alternatives, has the most favorable benefit/harm balance?” To date (January, 2018) no papers have addressed this question.

While Rhee (2008) demonstrates weak OCEBM grade C evidence supporting rhinoplasty, they conclude that some of the level 4 studies “demonstrate compelling evidence that the intervention is effective”. This indeed misconstrues the meaning of “compelling”, which when used correctly definitely proves a hypothesis, as in Hackshaw (1997) confirming the relationship between lung cancer and environmental tobacco smoke. In a later paper Rhee acknowledges the limitations in usefulness and reproducibility of objective diagnostics such as rhinomanometry and acoustic rhinometry, along with the subjectivity of physical examination (Rhee 2009), pointing out the potential of computational fluid dynamics, and also highlighting the potential of facial anthropometrics. Rhee further maintains that due to the high failure rate of surgery for nasal septal obstruction (NAO) and the lack of standard objective measures, Nasal Obstruction Symptom Evaluation (NOSE) and visual analog scale (VAS) subjective measures can be equally meaningful measures of surgical outcomes (Rhee 2014). In my opinion this inference doesn’t appear to be logical. If surgical failure rates are high and objective measurements are lacking, how can this satisfy the criteria of which procedure has the most favorable benefit/harm balance (Howick 2011)?

In an effort to assess the subjective sense of nasal obstruction and the objective scores of acoustic rhinometry and rhinomanometry, Andre (2009) performed a structured literature search from 1980 to 2009. Studies were rated as per the OCEBM criteria. Sixteen studies meet the 2009 OCEBM criteria (4 as II-a, and 12 as II-b). [Under the 2011 OECBM criteria the sublevels were abandoned and the studies would score as level 3 as they were not randomized, did not have controls, or were not selected consecutively.] This well constructed study failed to find a correlation between subjective symptoms of nasal airway obstruction and objective measurements. The authors concluded that the elevation of improved objective measurements over the patient’s subjective symptoms is unfounded. They further concluded that further research or refinements on methods to measure nasal patency is unlikely to solve the problem and that the patients' subjective sense of patency still gives the most valuable information on obstruction. This leaves unresolved the question of when to perform surgery and how to measure outcomes.

Concerned that health authorities in the United Kingdom (UK) might restrict or abolish nasal septal surgery, the association representing ear, nose, and throat (ENT) specialists in the UK published a position paper supporting a surgical approach(UK 2010).

In response to these doubts over the benefits of nasal septal surgery, Moore and Eccles undertook another systematic review of the literature to identify any functional benefits of septal surgery (Moore 2011). Their aim was to determine if there was any improvement in the patency of the nasal airway as measured by the objective techniques of rhinomanometry, acoustic rhinometry, and peak nasal inspiratory flow. The literature was searched for the period between 1950 and 2010 using Pubmed, Medline, Embase, and the Cochrane Controls Trials Register. Three different assessments of nasal patency were encountered:

> Rhinomanometry: Measures airflow and the pressure gradient that moves the airflow.
>
> Acoustic Rhinometry: Measures the cross-sectional area at the narrowest point of the nasal airway (MCA).
>
> Nasal Peak Inspiratory Flow: Measures the maximum nasal airflow at maximum effort.

Pre- and postoperative results for septoplasty were measured in seven studies. The aggregate of the studies reported a statistically significant increase in airflow for an improvement in patency in 67% of subjects. However only one study (Jessen 1984) had a control group (OCEBM level 2) while the rest were a mix of consecutive and non-consecutive case studies (level 4). Acoustic rhinometry results were expressed as MCA scores in units of cm^2. Of the six studies reviewed, only three demonstrated a statistically significant increase in MCA for a pooled increase of 36%. Peak inspiratory flow was measured in only one small study which failed to report if the increase in flow was significant. In total, 14 studies demonstrated an objective improvement in nasal patency as measured by rhinomanometry and acoustic rhinometry. While an improvement in nasal patency was measured, a correlation with subjective symptoms was not established. In reviewing the individual papers that comprised this study, Pirila and Tikanto noted that only 40% of patients had a subjective assessment of being totally free from nasal obstruction post-operatively (Pirila 2001). Pirila found "there is sufficient evidence in the literature to conclude that septal surgery improves objective measures of nasal patency and that improved nasal airflow *may* have beneficial effects for the patient." This conclusion fails to meet the OCEBM criteria that a study must determine the most favourable benefit/harm balance.

In a further attempt to reconcile weak objective evidence to support surgical procedures for nasal valve compromise (NVC) with frequently reported conflicting subjective patient reported measures, Cannon and Rhee postulate that a distinction should be made between weak evidence and lack of evidence for efficacy. The weak evidence does show a consistent benefit for nasal valve repair (Cannon and Rhee 2012). This conclusion that procedures “may” have a benefit and could be unrelated to the problem at hand while being used as a rationale for their continued use, is remarkable.

Is surgery being done too frequently in an effort to manage airway obstruction secondary to septal deviation?

As long ago as 1926, Horne opined on the subject of nasal septal surgery, writing: “The end-results, however gratifying to the surgeon, are not always equally satisfactory to the patient.” In 2012, a long term (10 years) retrospective study of 222 patients who had undergone septoplasty used the NOSE scale questionnaire to measure subjective outcomes. The topics probed included:

- Symptoms of nasal obstruction prior to surgery
- Satisfaction with the measures employed
- Grade of change in their nasal breathing
- Satisfaction with the overall result.

Toyserkani and Frisch (2012) reported improved nasal breathing in 68% of the patients, but an overall surgical satisfaction rate of only 55.9%. Thirty patients had more than one septoplasty with no improvement in the level of overall satisfaction in this subgroup (the paper doesn’t clarify whether failure was due to the decision to choose surgery or due to choice of the no surgery option.) 12% of patients had improved breathing but still reported dissatisfaction. Former smokers who stopped smoking following surgery also had a higher satisfaction score (70%) than those who continued to smoke (43.5%). The authors caution surgeons that patients should be warned that correction of septal deviation may not resolve their problem, and that smokers should first attempt a smoking cessation program.

In an attempt to measure long-term symptom relief and the degree of obstruction remaining following septoplasty, Sundh and Sunnergren (2015) compared long-term (3 to 5 years) symptom relief of nasal obstruction following septoplasty with short term (6 months) effects. All patients were identified who had a septoplasty in one hospital, performed in 2008, 2009, and 2010. Data for the 6 month period was retrieved from the Swedish National Quality Registry for Septoplasty, while in 2013 the same questionnaire was repeated with an additional question of “whether they still had nasal obstruction”. The basic questionnaire asked 4 questions to 111 patients:

Symptoms	Short-term	Long-term
My symptoms are gone	52.9%	18.2%
My symptoms are almost gone	27.9%	27.3%
My symptoms remain	14.7%	46.5%
My symptoms have worsened	4.4%	6.1%
Symptoms	**Report Nasal Obstruction in 2013**	**Report No Nasal Obstruction in 2013**
My symptoms are gone	3.3%	13.3%
My symptoms are almost gone	24.4%	3.3%
My symptoms remain	50%	0%
My symptoms have worsened	5%	0%

Table 2: Subjective evaluation of the effectiveness of septoplasty. Table entries are expressed as a fraction of yes answers. From Sundh and Sunnergren (2015).

Thirty four to seventy months following septoplasty, 53% of patients reported that their symptoms had remained or worsened, 83% reported nasal obstruction at long term follow up, and those reporting that “their symptoms had gone” declined from 53% at 6 months to 18% at 34-70 months. For any surgical procedure these results would be discouraging.

For patients who elected not to have surgery similar results were found. Thulesius (2009) selected 44 patients who had been selected for surgery but who had declined due to fear (27/44), elected treatment with nasal steroids (12/44), or weight loss or uvulopalatopharyngoplasty (5/44). An earlier initial examination and rhinomanometry had selected these patients for septoplasty. A follow up examination following the same format plus rhinomanometry determined that 38% had improved while 67% had unimproved or worsening symptoms. These results are similar to post-surgical studies: Sundl and Sunnergren (2015) 53% symptoms remained or worsened, Jesson (1989) found that only 26% were subjectively free from obstruction after 9 years. Where Thulesius found that 38% had improved without surgery, Bohlin and Dahlqvist (1994) found that 39% had improved with surgery. These papers would suggest that there is no measurable outcome difference between surgical and non-surgical therapy.

With the uncertainty regarding whether nasoseptal deformity is normal human variation or a frequent condition that requires surgical correction, the following sections will review the incidence, the anatomical variation of the nasal septum, and the classification of nasoseptal deformities.

Incidence of Nasal Septal Deviation

Horne (1926) observed that "some irregularity of the cartilaginous portion of the nasal septum is the rule rather than the exception". Widely differing incidences of nasal septal deviation have subsequently been reported:

Author	Type	Year	Sample Size (M/F)	Deviation Rate
(Gray LP 1965)	Infants	1965	2094	57%
(Gray LP 1965)	Adults	1965	2152	79%
(Takahashi R 1987)	Mixed	1987	5317	98.7%/ 90.5%
(Earwaker 1993)	Adults	1993	800 (360/440)	44%
(Perez-Pinas I 2000)	Adults	2000	110 (57/53)	58%
(Uygur K 2002)	Infants	2002	200	15.6%
(Harugop AS 2012)	Infants	2009	250 (132/118)	20%
(Mohebbi A 2012)	Adults	2012	463	47%

Table 3: Incidence of nasal septal deviation (a summary of the published literature)

The wide variation in the reporting of septal deviation way be a consequence of whether "septal deviation" is defined as any lateral deviation from the midline or whether deviation occurs only in conjunction with nasal airway obstruction. This leads to a wide divergence in the reported rates of septal deviation. Takahashi, in a large and comprehensive study, identifies failures to note deviation prior to birth (25% deviated, and to measure any deviation that occurs in adolescence and early adulthood (Takahashi 1987). Takahashi's rate for fetal deformity alone exceeds the total rate reported by other authors.

Anatomical Variation of the Nasal Septum

Beyond the linear measurements or angulation of the nasal septum, the biologist interested in the function of a three dimensional structure needs to consider its anatomical variation. Earwaker (1993) identified deformity of the chondro-vomeral junction (CVJ), septal ridges and spurs (lateral protuberance), and middle turbinate pneumatisation (concha bullosa). His identification of the chondro-vomeral junction deformity is consistent with both the findings of

Takahashi (1987, page 37) and those of this study. The presence of middle turbinate pneumatisation may be relevant if associated with septal deformity; however, it may only be a space filling lesion.

Gray (1965) classified two types of surface curvature for septal deviation, a cartilaginous type involving the anterior cartilage with dislocation at the chondro-vomeral junction, and a cartilaginous-osseous type involving the whole septum . This is consistent with Takahashi's view, however, Takahashi further sub-divided bending of the septum into eight types of septal surface curvature (Takahashi 1987 p.19-20)

In my opinion, consistent with the great variation of the reported incidence of nasal septal deviation and my detailed examination of numerous nasal septal CTs, there will be few, if any non-deviated nasal septa in any sample. It would appear the term "deviated septum" is applied when an individual examiner determines that the septal surface curvature exceeds a particular threshold of bending or when there in an obstruction of nasal airflow. The question then arises: are there certain "deviations" positioned in a particular anatomical location of the septum that alter the morphology of the septum enough that airflow is interrupted? What distinguishes the large majority of humans with nasal deformity who are asymptomatic from those that are symptomatic?

Miles (2007) measured the septal deviation of 57 cadavers, grading both the amount of deviation and whether it was in the cartilaginous or osseous part of the septum.

Lateral Septal Deviation	**Grade**	**Cartilaginous**	**Osseous**
0-2mm	I	25	13
2-4mm	II	12	13
4-6mm	III	9	17
6-8mm	IV	6	8
>8mm	V	4	6

Table 4: Septal deviation and Distribution from Miles (2007).

It was Miles who called to my attention an infrequently referenced study:

> "Ryo Takahashi (1987) provided the most comprehensive body of work ever produced in the study of the nasal septum. The work of Takahashi primarily focused on the development, function, and etiology of septal deformity".

This complex work merits a separate chapter here (Chapter 5) as it provides not only clarity into the evolution, development, function, and etiology of the nasal septum, but offers insights into the interpretation of nasal septal "deviation".

Diagnosis and Classification of Nasal Septal Deviation

Historical Diagnostics

The modern era of describing diagnosis and correction of "deflected noses" began in the 1880s. Trendelenburg in 1886 reported on the correction of deflected noses, and Asch in 1890 described a "new operation for deviated cartilaginous septum (Meyer 2012). By 1892 the topic was being discussed at medical meetings.

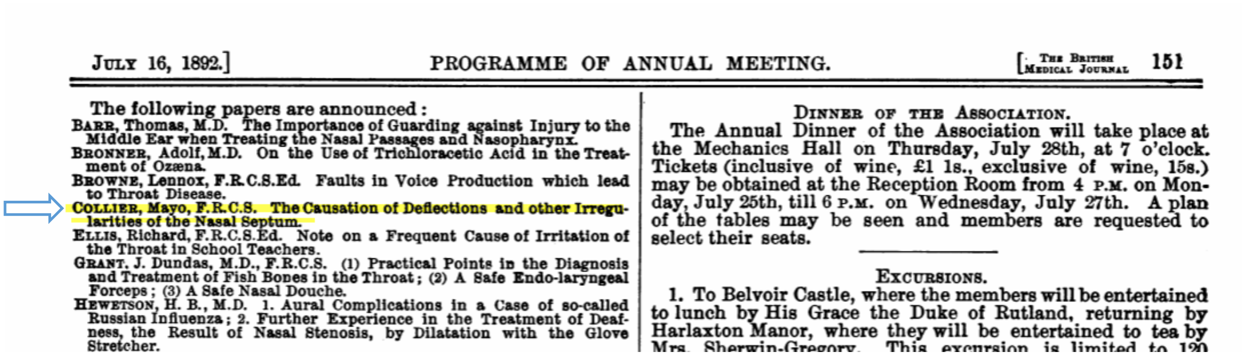

JULY 16, 1892.] PROGRAMME OF ANNUAL MEETING. [THE BRITISH MEDICAL JOURNAL 151

The following papers are announced:
BARR, Thomas, M.D. The Importance of Guarding against Injury to the Middle Ear when Treating the Nasal Passages and Nasopharynx.
BRONNER, Adolf, M.D. On the Use of Trichloracetic Acid in the Treatment of Ozæna.
BROWNE, Lennox, F.R.C.S.Ed. Faults in Voice Production which lead to Throat Disease.
COLLIER, Mayo, F.R.C.S. The Causation of Deflections and other Irregularities of the Nasal Septum.
ELLIS, Richard, F.R.C.S.Ed. Note on a Frequent Cause of Irritation of the Throat in School Teachers.
GRANT, J. Dundas, M.D., F.R.C.S. (1) Practical Points in the Diagnosis and Treatment of Fish Bones in the Throat; (2) A Safe Endo-laryngeal Forceps; (3) A Safe Nasal Douche.
HEWETSON, H. B., M.D. 1. Aural Complications in a Case of so-called Russian Influenza; 2. Further Experience in the Treatment of Deafness, the Result of Nasal Stenosis, by Dilatation with the Glove Stretcher.

DINNER OF THE ASSOCIATION.
The Annual Dinner of the Association will take place at the Mechanics Hall on Thursday, July 28th, at 7 o'clock. Tickets (inclusive of wine, £1 1s., exclusive of wine, 15s.) may be obtained at the Reception Room from 4 P.M. on Monday, July 25th, till 6 P.M. on Wednesday, July 27th. A plan of the tables may be seen and members are requested to select their seats.

EXCURSIONS.
1. To Belvoir Castle, where the members will be entertained to lunch by His Grace the Duke of Rutland, returning by Harlaxton Manor, where they will be entertained to tea by Mrs. Sherwin-Gregory. This excursion is limited to 120

Figure 4: 1892 announcement of a meeting where "deflections and other irregularities of the nasal septum) were to be discussed. From British Medical Association (1892).

Douglass (1899) wisely noted that not all "deflection from the perpendicular" requires treatment unless the deflection produces symptoms. Early on, Roe (1908) emphasized the need for careful preliminary study not only of the condition of the nose but also of the possibility of successful surgery. He published this early classification:

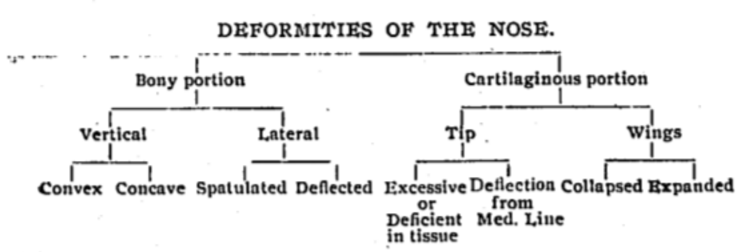

Figure 5: Early classification of deformities of the nose. From Roe (1908).

While the Roe (1908) classification is dated regarding the aetiology of nasal septal deformities, attributing NSD to trauma, abnormal growth, or a luetic (syphilitic) history, the classification is consistent with Takahashi (1987), dividing the septum into a bony and cartilaginous portions. The vertical bony portion (perpendicular plate) frequently has a "C" shaped curvature with convex and concave surfaces. The tip of the cartilaginous portion may become deflected with ridge formation at the chondro-vomeral junction (Earwaker 1993). This is consistent with the current consensus about the septal form likeliest to generate airflow obstruction in the valve region (Wen 2008).

Subsequently there have been numerous classifications of nasal septal deviation to assist in the diagnosis and treatment of septal deformities. The paradox is that the phenomena may or may not be related to airway obstruction and may or may not be amenable to successful surgical correction.

Ironically, little appears to have changed regarding the complexity of nasal septal shape from when Gibb (1907) observed "….the utter lack of unanimity of opinion" when describing defects of the nasal septum. Gibb questioned the aetiology of septal deformity: "Rather does it show that the form the septum may assume because of interference with the proper and normal development or as a result of traumatism is so varied as to baffle accurate description". However this prescient observation has not deterred over 100 years of efforts to classify septal morphology as "defects".

Modern era classifications

Author(s)	Year	Classification
Williams	1908	1: C-shaped deviations bowed towards one side or the other in an anterior-posterior or vertical plane. 2: S-shaped deviations bowing in one direction anteriorly or below and in the opposite direction posteriorly or above. 3: Spurs, crests, or spines. Early classification virtually identical to many modern derivatives (Lee and Baker 2013, Cerkes 2011, Rohrich 2002, Guyuron 1999, Lawson 1978).
Shahney and Sinha	1964	Deviations are scored as mild, moderate, and marked. Cartilage and bony deflection, dislocation of septal cartilage and skeletal asymmetry.
Lawson)	1978	Two basic types: C-shaped, S-shaped twist, deviated nose, twisted nose, and skeletal asymmetry.
Mladina	1987	Type 1: Anterior unilateral vertical septal deviation that doesn't touch the valve wall. Type 2: Anterior unilateral vertical septal deviation that touches the valve wall. Type 3: Unilateral vertical deviation (more posterior) that touches the wall. Type 4: S-shaped vertical deviation touching the wall on the left and right. Type 5: Septal spur with no deviation on the contra-lateral side of the septum. Type 6: Anterior maxillary deviation with contra-lateral groove and posterior deviation. Type 7: Combination of types 1-6.
Guyuron et al	1999	1: Septal tilt deformity. 2: C-shaped anteroposterior deviation. 3: C-shaped cephalocaudal. 4: S-shaped anteroposterior. 5: S-shaped cephalocaudal. 6: Localized deviations or large spurs. A modification of William's classification.

Rohrich et al	2002	3 types with subtypes: Type I: Caudal septal deviation: Subtype a: straight septal tilt, b: C-shaped, c: S-shaped. Type II: Concave dorsal deformity: Subtype a: C-shaped, b: reverse C-shaped. Type III: Concave/convex dorsal deformity (S-shaped). A modification of William's classification.
Buyukertan et al	2003	Nasal septum divided into 10 segments obtained by the use of coronal and horizontal planes are as follows: anteriosuperior (AS), anteriomedia (AM), anterioinferior (AI), mediosuperior (MS), mediomedia (MM), medioinferior (MI), posteriosuperior (PS), posteriomedia (PM) and posteroinferior (PI), caudal end of the septum nasi (CE). Deviation is measured from a line joining the upper and lower extremes of the septum (coronal view).
Rao et al	2005	Type I: Midline septum or mild deviations in the vertical or horizontal plane. Type II: Anterior vertical deviation. Type III: Posterior vertical deviation. Type IV: S-shaped. Posterior to one side and anterior to the other side. Type V: Spur on one side (with or without deviation). Type VI: Type V with a deep groove on the concave side. Type VII: Combination of Types 1-VI. This is a modification of the Mladina classification.
Baumann and Baumann	2007	Type I: Septal crest (ipsilateral vomeral spur). Type II: Cartilaginous deviated nose (ipsilateral subluxation and/or contralateral vertical septal deviation. Type III: High septal crest deviation (contralateral septal crest) Type IV: Caudally inclined septum (contralateral subluxation, ipsilateral vertical septal deviation, ipsilateral septal crest, ipsilateral vomeral spur). Type V: Septal crest (contralateral vomeral spur). Type 6: Caudally inclined septum (contralateral subluxation, ipsilateral vertical septal deviation, contralateral septal crest, contralateral vomeral spur). Concomitant pathologies in parenthesis.
Jin et al	2007	Type I: localized deviation included spur, crest or caudal deflection. Type II: Non-localized curved/angulated deviation. Type III: Curved/angulated with a localized deviation. Type IV: Curved/angulated with an external deformity.
Cerkes	2011	1: Caudal septal deviation (septal tilt). 2: Anteroposterior C-shaped. 3: Cephalocaudal C-shaped. 4: Anteroposterior S-shaped. 5: Cephalocaudal S-shaped. Classification is similar to that of Williams 1907.
Reitzen et al	2011	Classification as a measure of the tortuosity of the septum. Tortuosity was defined as the ratio of the "actual" length of the septum (T) to the "ideal" length (I) of the septum, which was defined as the length of a straight line drawn from the superior to the inferior aspect of the septum. Tortuosity = T/I. Increased with age.
Lee and Baker	2013	Classification used as a guide for septal surgery: 1: Straight septum but deviated from midline. 2. C-shaped deformity in either vertical or horizontal plane. 3. S-shaped deformity in either vertical or horizontal plane. Classification is similar to that of Williams 1907.
Vidigal et al	2013	Classification relating obstructive sleep apnea syndrome (OSAS) to increased rate of nasal septal deviation (NSD). Degree I: Deviation didn't reach lower turbinate, Degree II: Deviation reached the lower nasal turbinate, Degree III: Deviation reached the lateral wall and compressed the lower nasal turbinate.
Salihoglu et al	2014	Classification based on the % obstruction of the nasal cavity. Grade 1: 0-33%. Grade 2: 34-66%. Grade 3: 67-100%. NSD present in 46.6% of subjects (comparable to studies using Mladina classification.

Lin et al	2014	A computed tomography study using MATLAB and OsiriX. Compared deviated septum contours with a straight septum.

Table 5: Table of Classification systems. From Teixeira (2016) with amendments.

Many of the modern era classifications are variations of Williams' 1908 description of nasal septal deformities. Williams believed that most nasal septal deformity was linked to the susceptibility of the cartilaginous nasal septum to trauma and the effects of trauma on this region. He described C-shaped and S-shaped deviations of the septum in an anteroposterior direction and vertical planes and identified their frequent association with dislocation of the cartilage from the vomer often accompanied by ridges and thickenings proximal to the dislocation. Spurs, crests, and spines were described, alone and in association with fractures along with vertical fractures of the cartilage and their consequences. While Williams' classification and its derivatives described the anatomical variation of the nasal septum, they do not facilitate a visualization of the deformity that is associated with a particular "type" of deviation. Mladina's 1987 classification changed this.

Before reviewing the Mladina classification, I will first review the anatomy of the nasal septum, particularly the premaxilla, vomer, ethmoid, and cartilaginous structures and their interrelationship. The anatomy of this region is complex and highly variable, with inconsistent and confusing nomenclature (Hur 2016, Huizing 2003, Tripathi 2017). This has resulted in classifications of nasal septal deformity (NSD) that often simplify or misunderstand the complex structures at play.

Mosher (1907) provided the first comprehensive modern review of the region. Although he incorrectly attributed the aetiology of nasal septal deviation as largely to trauma, he accurately described the role of the hypertrophic vomer in the development of ridges and spines. "The cartilage of the septum is thrown out of its bed in the vomer for a very considerable distance and the septum is deviated as a consequence" (Mosher 1907 p. 841). His great contribution was the description of the vomer, premaxillary, incisal spine relationship at birth and adulthood. The limitations imposed by interconnectedness and variability of this region underscore the need for quantitative methods to map the regional morphology.

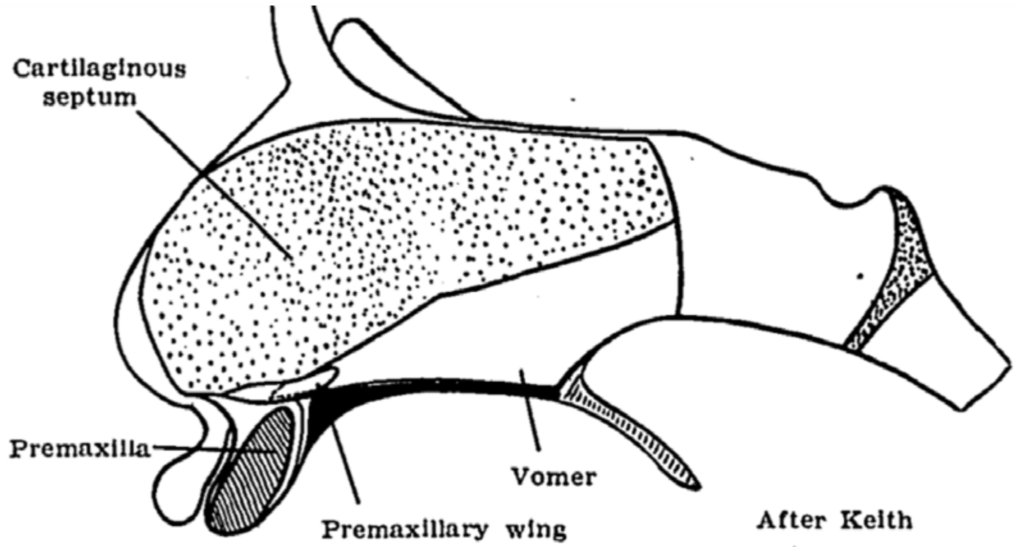

Figure 5: The nasal septum at birth from Mosher 1907 p.845

Mosher described the nasal septum at birth, with both the premaxillary wings and the vomer having two leaves connected at their base and forming a groove on their superior surface. Takahashi (1987) provides an extensive guide to the growth and development of the vomeral groove to adulthood.

Remarkably, Mosher's description of the adult septum both captures the complexity of the vomer, premaxilla, and septal cartilage region that is consistent with recent research (Hur 2016).

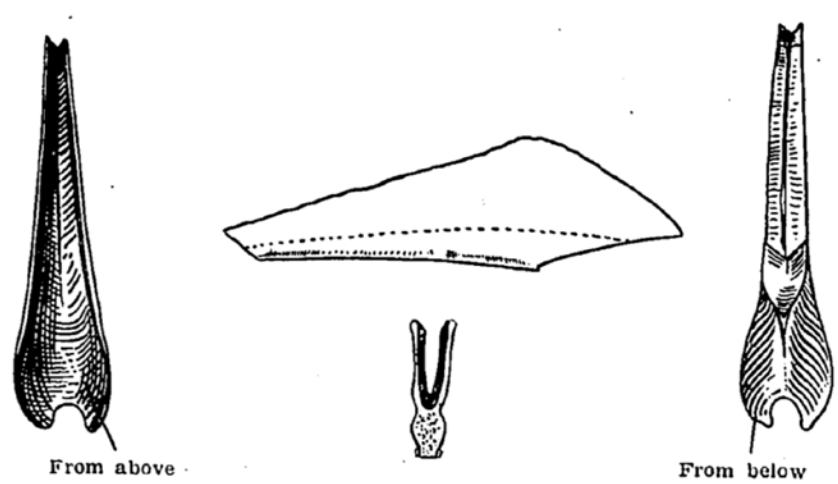

Figure 6: The vomer at birth with the two leaves (wings) and the groove (gutter) they form. From Mosher 1907 p.845

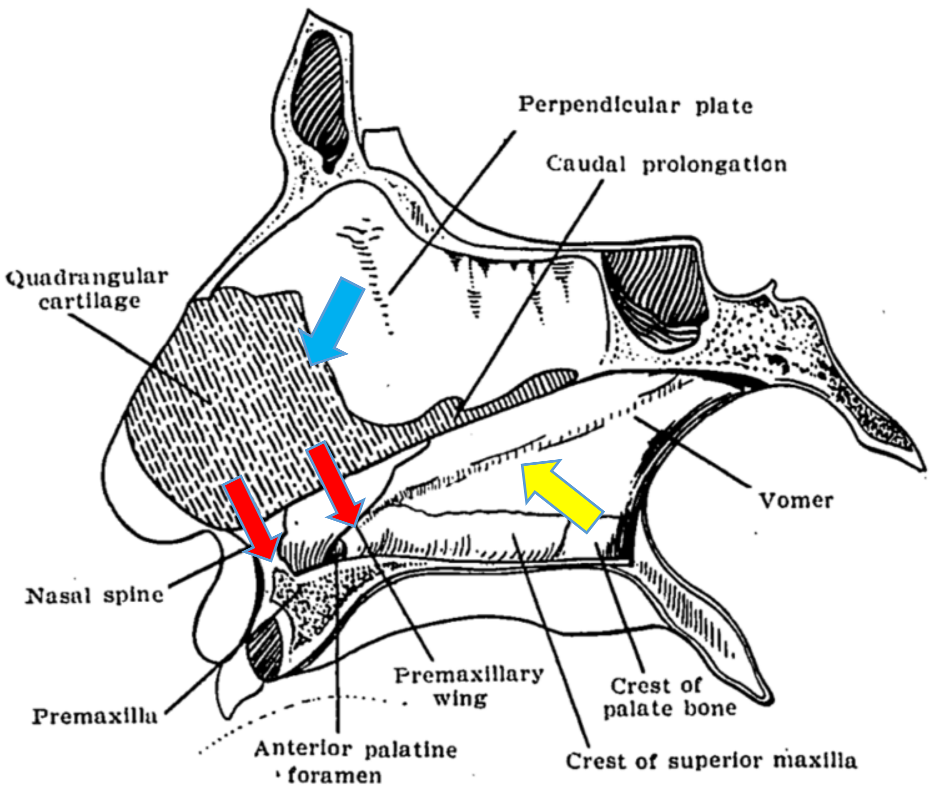

Figure 7: The adult nasal septum from Mosher 1907 p. 847. Note the three regions of regions of deformity. Blue arrow: Ossification line between the septal cartilage and the perpendicular plate of the ethmoid (Buckling and curvature). Yellow arrow: Chondro-vomeral junction (ridges and spines). Red arrow: Vomer, premaxillary wing, nasal spine and septal cartilage (complex deformities: (Mladina 1987 T6, Earwaker 1993).

Mosher describes the cartilaginous projection of the septal cartilage posteriorly as the “caudal prolongation”, an extension of the cartilaginous portion of the vomeral junction with the septal cartilage and perpendicular plate which increases the possibility of deformation.

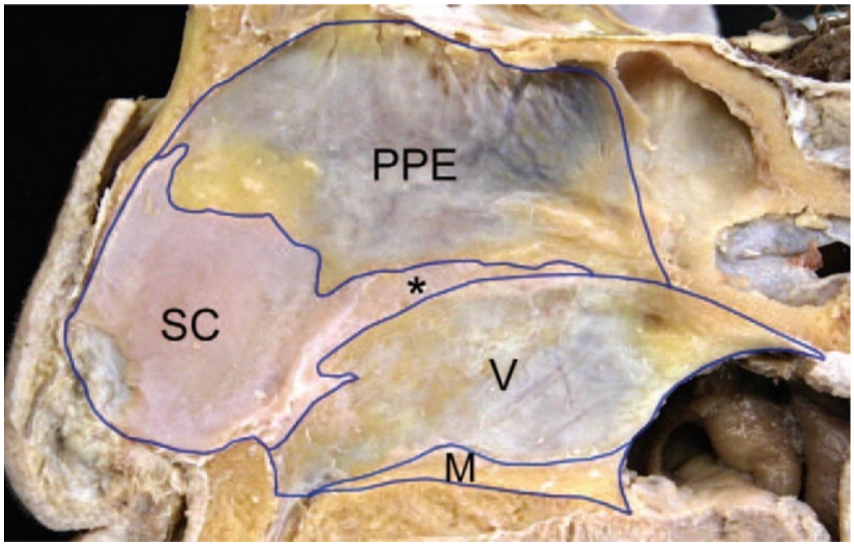

Figure 8: Nasal septum from Hur 2016. Septal cartilage (SC), Posterior extension of the SC (*). Perpendicular plate of the ethmoid (PPE), Vomer (V), Maxilla (M)

Hur’s 2016 dissection and image of the nasal septum captures the posterior cartilaginous extension and variability is across specimen’s with the vomer-septum boundary almost entirely cartilage/bone with only a small bone/bone junction between the vomer and the perpendicular plate.

Mosher describes the complex anatomy of the anterior nasal septal region: “Here the mosaic of the septum is the smallest, here the tip of the vomer lies in the groove of the premaxillary wings…” (Mosher 1907 p.847) and “Projecting horizontally forward from the anterior edge of the upper face of the premaxilla is a pointed process called the nasal spine….but projecting obliquely upwards and outwards is another process, the premaxillary wing….When the two premaxillary wings are placed together the wings mortice into one another so that they form a sizable gutter. Into this, in the complete septum, fits the tip of the vomer also a gutter. The premaxillary wings act as cleats on either side of the vomer to hold it in place.” (Mosher 1907 p. 849)

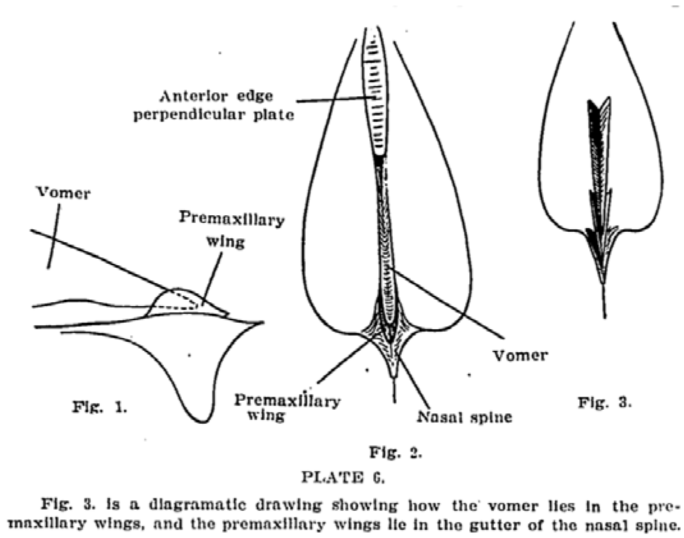

Figure 9: Vomer, premaxillary wing, and nasal spine. Note the inhomogeneity. From Mosher 1907

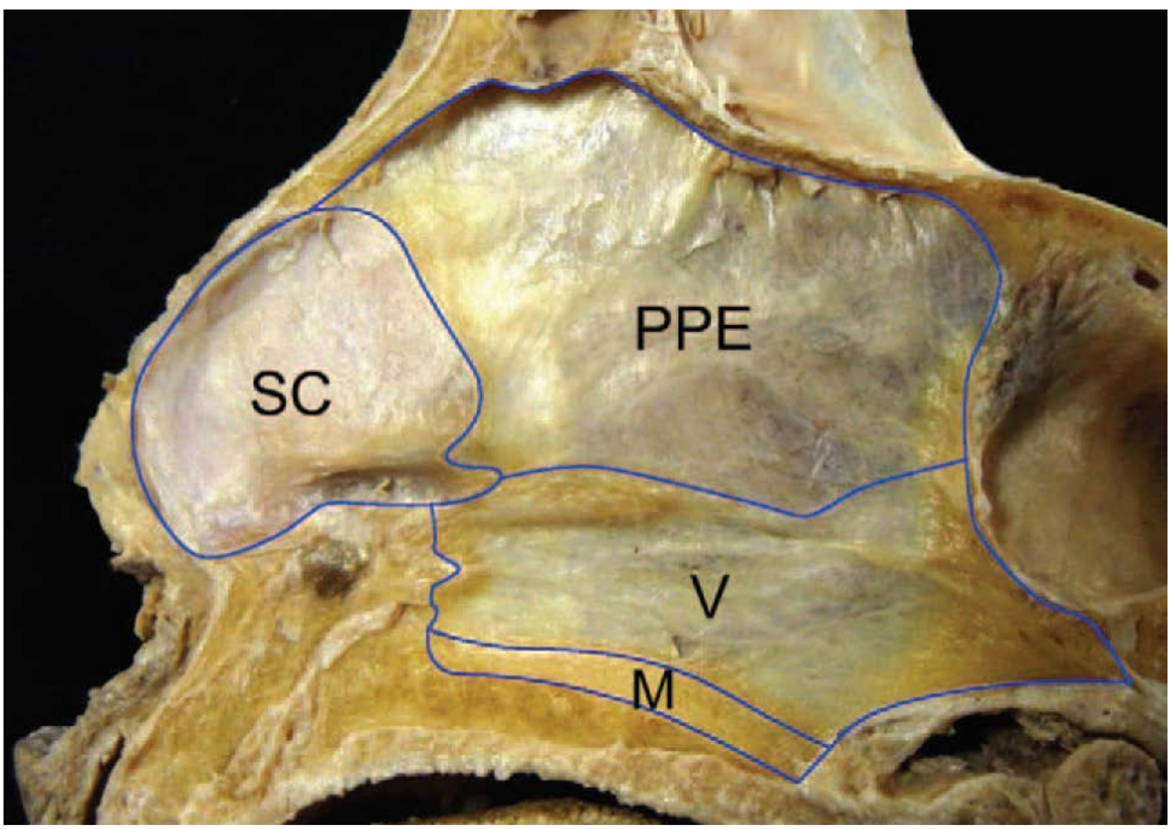

Figure 10a: M: nasal crest of the maxilla PPE: perpendicular plate of the ethmoid SC: septal cartilage V: vomer
From Hur (2016)

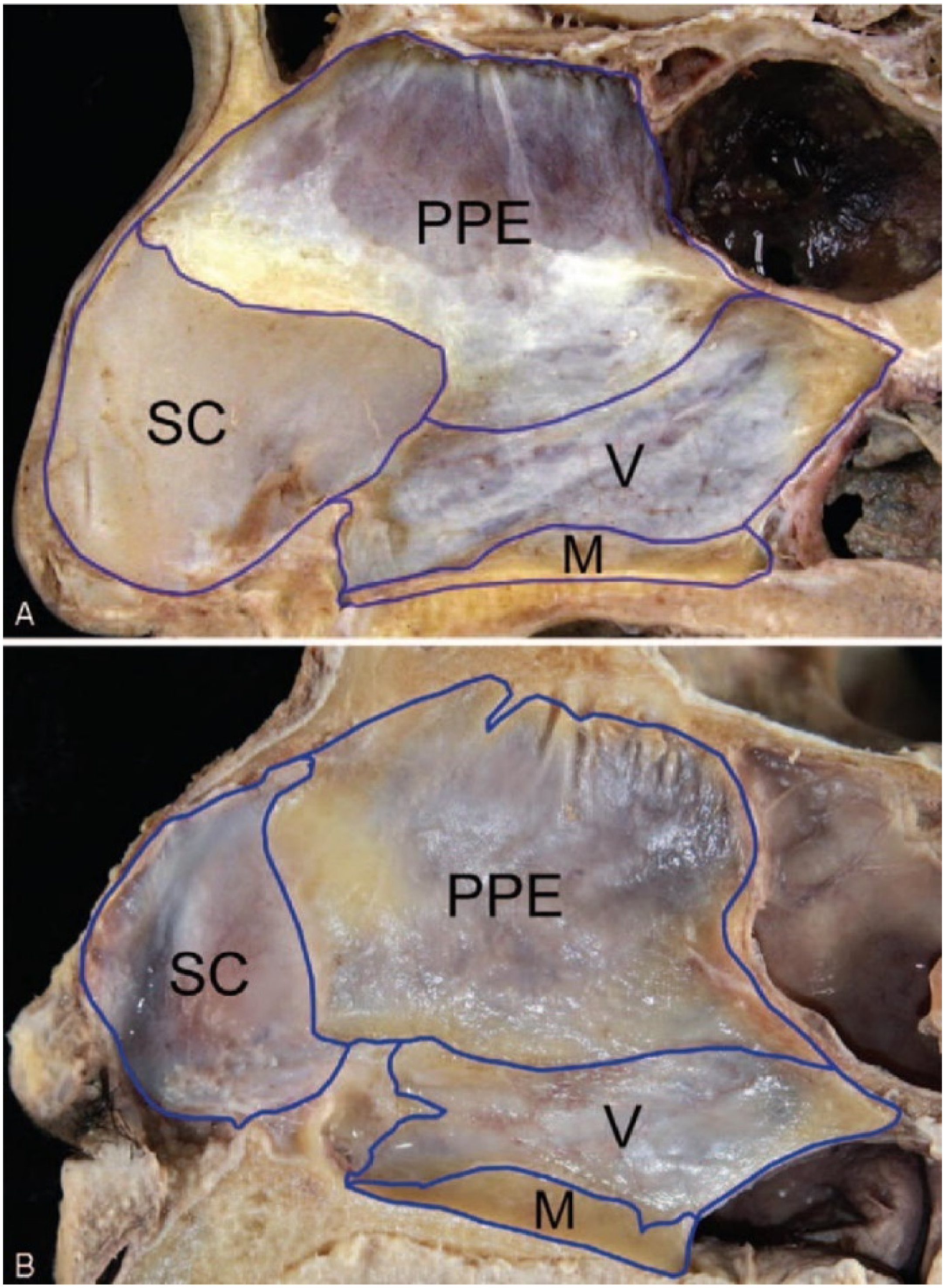

Figure 10b: Views of the nasal septum from Hur 2016. (A) Both the maxillary wing and vomer contact the septal cartilage. (B) The vomer doesn't contact the septal cartilage. From Hur (2016)

Figure 11: (Below) Views of the nasal septum demonstrating great variability between the septal cartilage, vomer, and maxillary wings. (C) No contact between vomer and septal cartilage, maxillary wings in contact with large perpendicular plate. From Hur 2016.

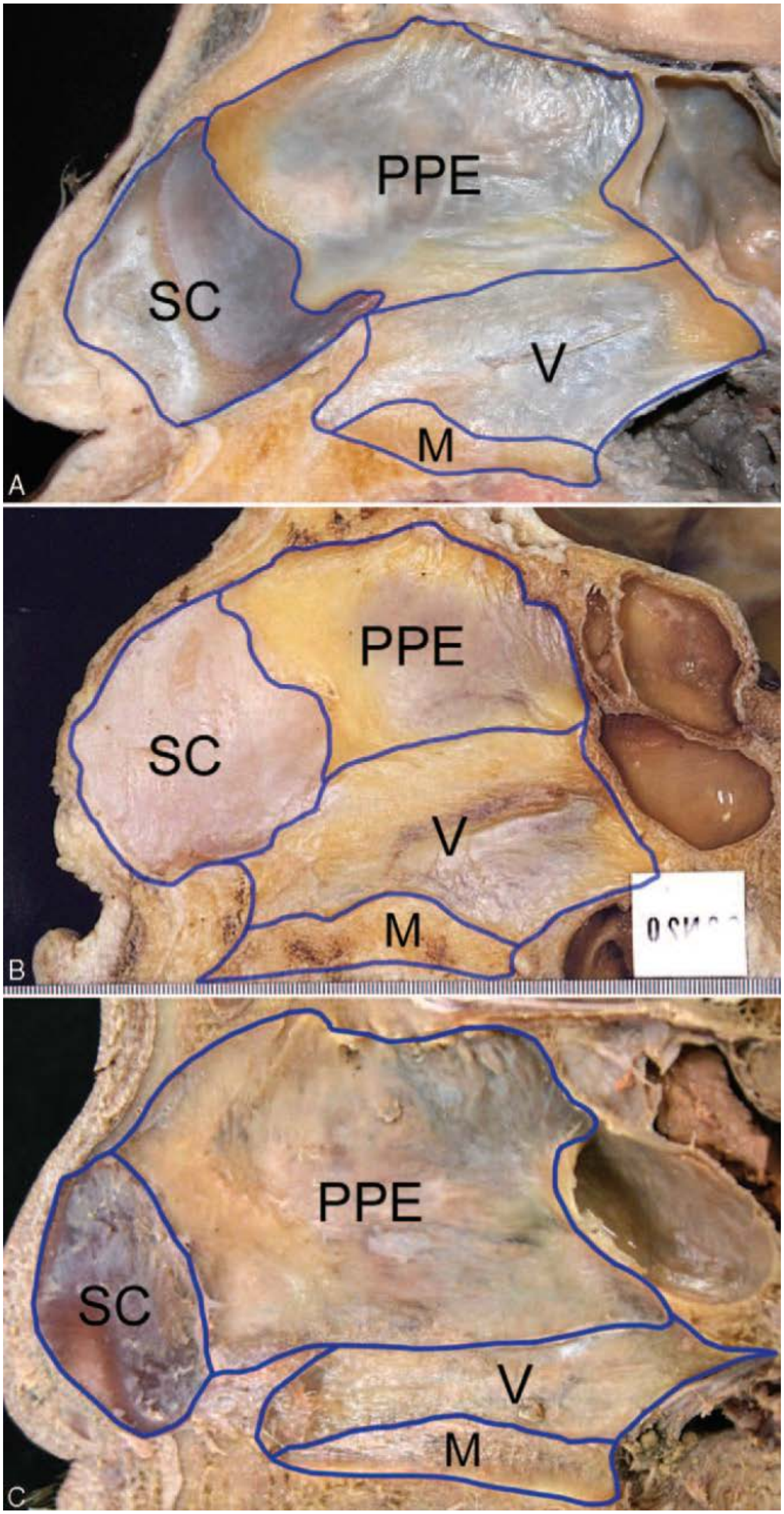
PPE
SC
V
M
A
PPE
SC
V
M
B
PPE
SC
V
M
C

While the above drawings and photos document the complexity and variation of this region, other papers simplify the structure of the region. Cottle describes the nasal septum as "in general having its surfaces parallel" Cottle 1958 p. 301, and names trauma as a major cause of NSD. Cottle states that anterior deformity is linked to the maxillary crest and maxilla, with no mention of the vomer in his associated surgical guide for the region. While this paper is problematic, Mladina 2015 references it, noting "The first attempts to systematize septal distortions were given as early as 1958 by Cottle" (Mladina 2015 p. 137). This is simply incorrect as it ignores the historiography referenced earlier in this chapter, as well as more recent research by Hafkamp (1999) and Barteczko (2004). Mladina's (2015) citation of Cottle while ignoring Takahashi is of concern in light of Takahashi's concern of Cottle's understanding of the nasal septum:

> "I feel that Cottle failed to observe the distinctive characteristic of the septal cartilage (growth controlled by intrinsic genetic factors) and the control of the relationship between the septal cartilage and the vomer by local epigenetic and local environmental factors." (Takahashi 1987 p. 99)

Cottle, Moss, and by extension Mladina's concept of nasal septal growth has subsequently been proven to be erroneous. This is discussed further in Chapter 5.

Mladina 2015 doesn't discuss the role the vomer, and when referencing a type 6 deformity refers to "… a typical horizontal groove located between the septum and, big laterally protruding *intermaxillary* bone wing…" (Mladina 2015 p. 144). Hafkamp describes the cartilaginous-bone region as follows: "The caudal margin of the cartilaginous septum rests, from ventral to dorsal, on the anterior nasal spine, the premaxilla, and the vomer. The connections between the cartilaginous plate and these bony structures are crucial to the stability of the cartilaginous part of the nasal pyramid" (Hafkamp 1999 p. 21). Barteczko correctly summarizes the vomer-premaxilla relationship: "We focused on the relation of the developing premaxilla to the forming nasal septum moving from the ventral to dorsal and the *intercalation* with the vomer. Thus the premaxilla acts as a stabilizing element within the facial skeleton comparable with the keystone of a Roman arch" (Barteczko 2004 p. 417). This is relevant as it is impossible to accurately determine the vomer-premaxilla borders on a CT, with the incisal canal region being identified with both the vomer (Botti 2017) and premaxilla.

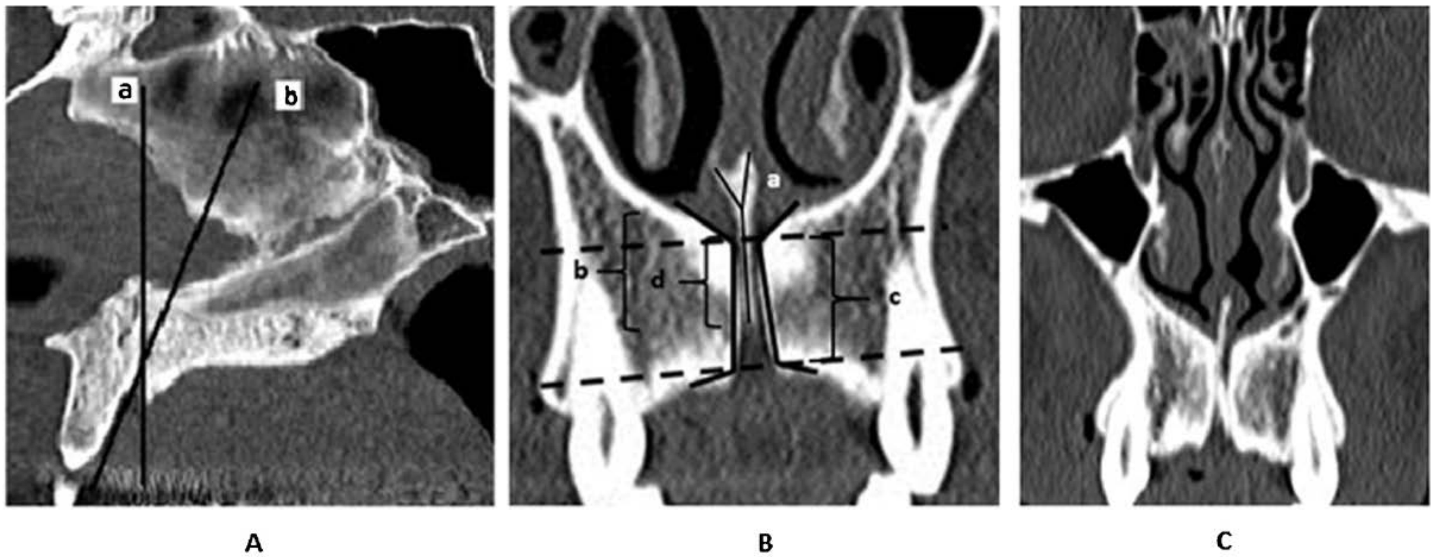

Figure 12: Imaging in the area of the incisal canal with the vomer visualized as both I and Y shaped. (A) Sagittal section through the incisal canal (a) axis of the standard coronal section. (b) axis of modified coronal section passing through the incisal canal. (B) Coronal section through the incisal canal. (a) Y shaped vomer groove (b) vertical segment of the vomer (c) height of the incisal canal (d) height of vomer in the incisal canal (C) I shaped vomer (no groove or wings). From Botti (2017).

While the images identified by Botti (2017) are of the vomer, can the premaxilla-vomer border be ascertained? Dissection images as per Hur (2016) make it clear that on different CT scans, the premaxilla, vomer, or both may be imaged. Thus when discussing anterior deformation of the nasal septum it is critical to recognize the importance of the whole premaxilla, vomer, septal cartilage structure in the region's evolutionary and development. The term "premaxillary complex) which is comprised of the premaxilla and the vomer is probably the most appropriate terminology (Murthy 2016).

Mladina 1987 introduced his classification of nasal septal deformities in 1987 and has presented subsequent revisions (Mladina 2008) and with clinical revisions (Mladina 2015). He differentiates between nasal septal deviations and deformities, describing deviations as a "slight declination from the medio-sagittal plane" whereas deformity is described as "the change of shape or form". The 1987 classification had six basic types with a seventh combination type. Types 1-4 are termed vertical deformities with a longer axis in the vertical plane which Mladina describes as creating "unilateral crooks" secondary to forces acting on the septum in an anteroposterior direction. Horizontal deformities have a longer axis in the horizontal plane and deform (crook) as if forces have been applied against the septum from a superior to inferior direction. {Note: the verb "crook" is now archaic in English]. Subsequently a number of authors have presented modifications of the Mladina classification: Guyuron 1999, Buyukertan 2003, and Baumanns 2007. Types five and six are described as horizontal deformities with the long axis of the septum in the horizontal plane. Type seven is a combination of the other six types.

Type I

There is a mild unilateral ridge in the valve area which results in a slight interference in function with mild clinical significance and no change in the patient's subjective perception of normal nasal breathing.

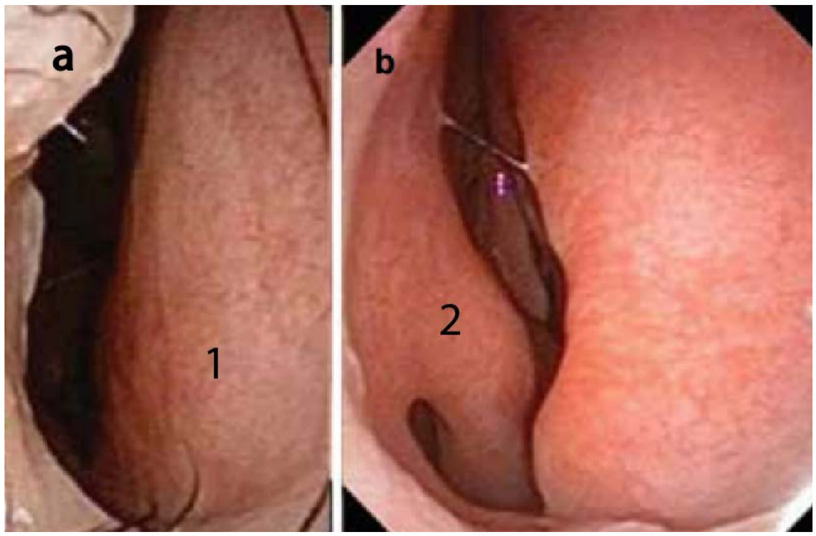

Figure 13: (a) Inferior turbinate: 1 (b) Middle turbinate: 2 with partially obstructed airway. From Madina (2015)

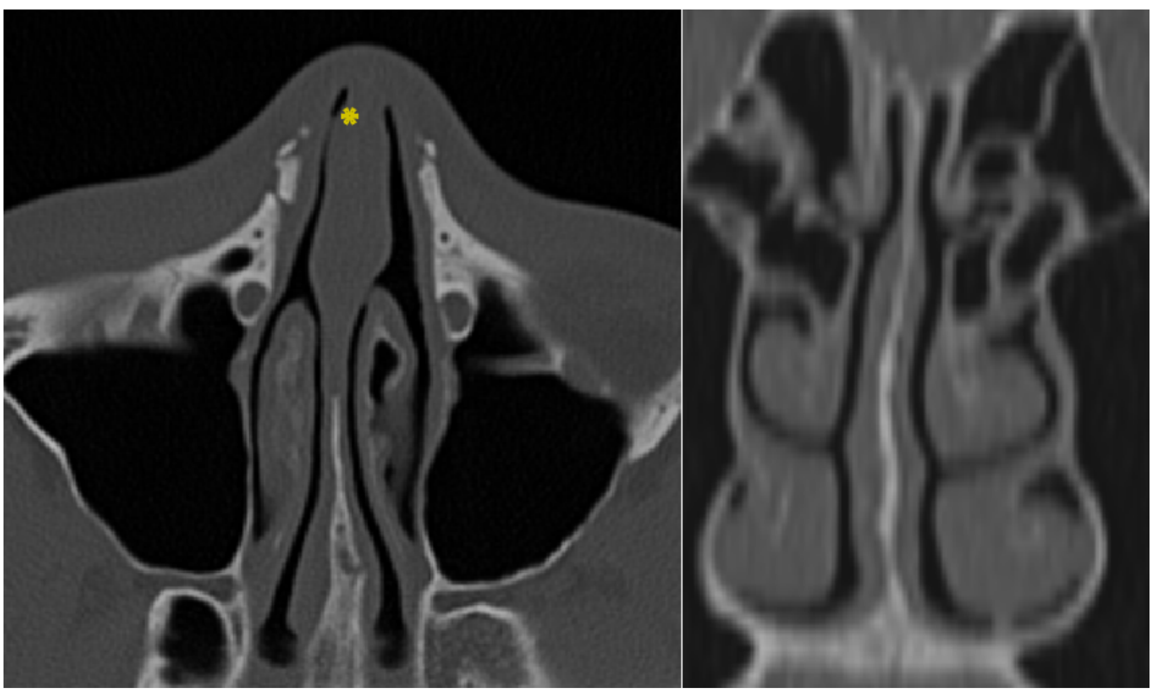

Figure 14: Specimen 63. Constriction of the airway in the valve region *

Type 2

There is a unilateral vertical ridge that is close to or in contact with the anterior nasal valve which interferes with or blocks airflow on the affected side resulting in impaired breathing.

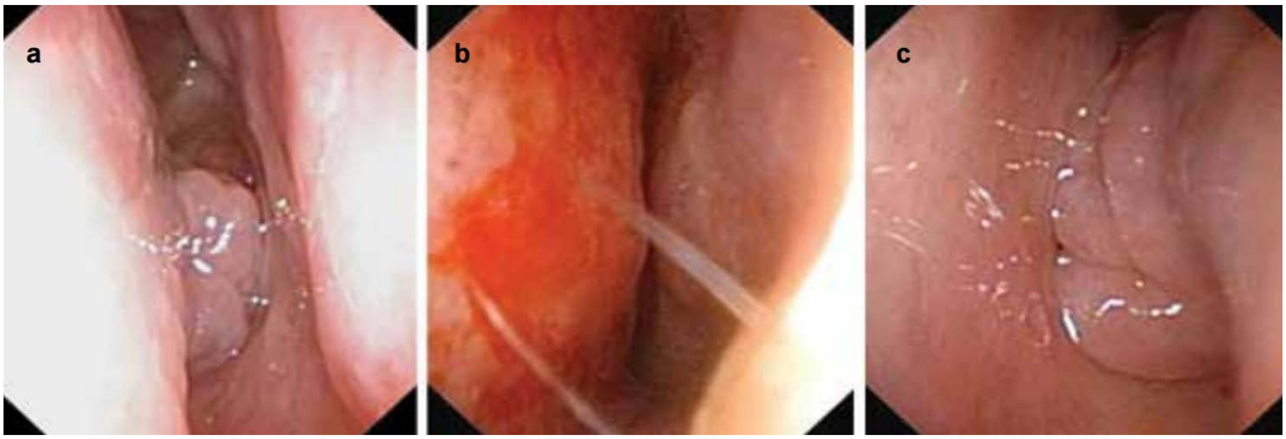

Figure 15 a: Left side type 2 with choana blocked by hypertrophic mucosa. b: Left side type 2 with mucosa of the left inferior turbinate tail visible. c: a and b images taken with decongestion, note hypertrophic mucosa in c without decongestion. From Madina 2015.

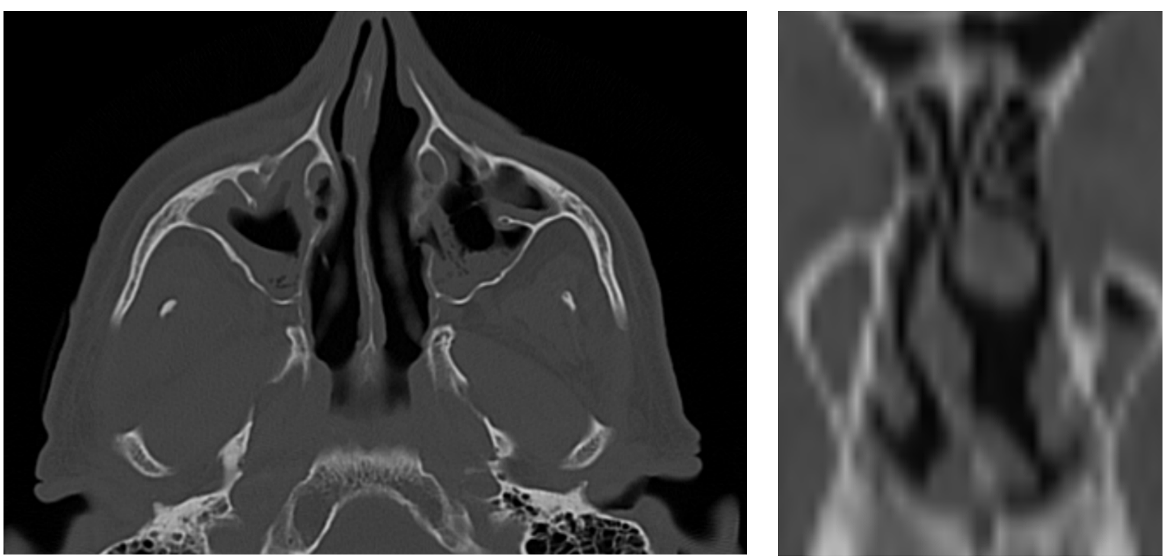

Figure16: Specimen 91. Constriction of the airway in the valve region due to close contact of septal ridge with wall

Type 3

This is a more posterior unilateral vertical deformity located at the anterior edge of the middle turbinate. Mladina claims type 3 occurs frequently, is associated with chronic rhinosinusitis, "C" or "reverse-C" shape of the external nose, and is mainly associated with a type 3 deformity.

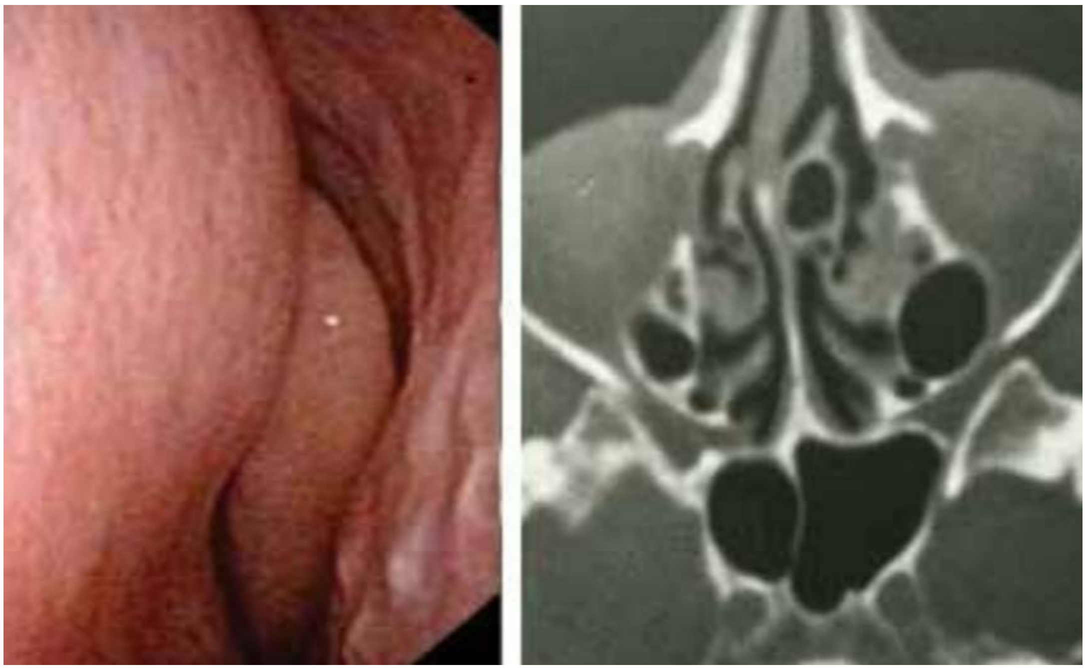

Figure 16 Left side type 3 with the deformity covering the view of the middle turbinate. Note contact of the septum with the middle turbinate. From Mladina (2015).

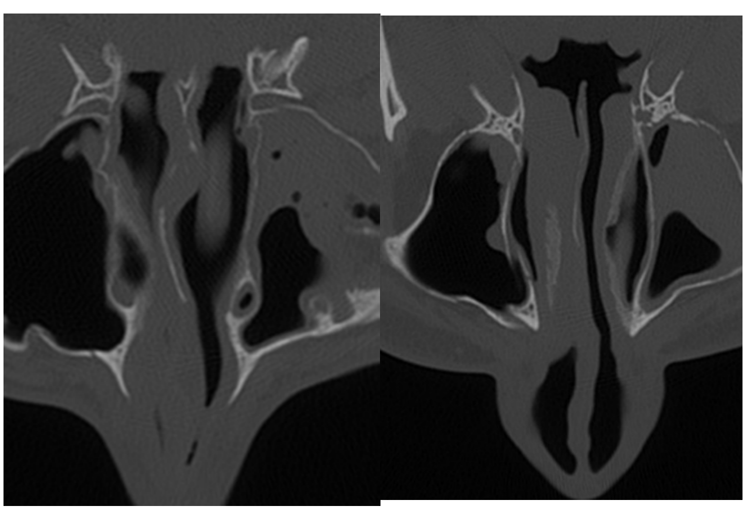

Figure 17: Specimen 013 (18)

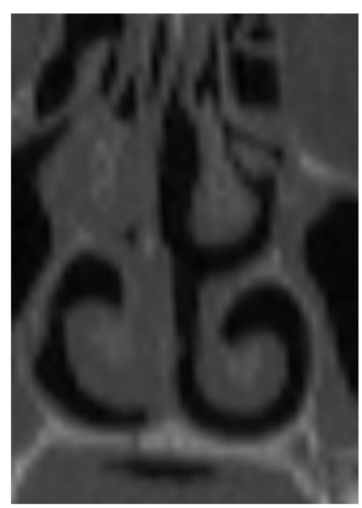

Figure 18: Specimen 013 (18)

Type 4

This is a combination of an anterior type 2 deformity on one side and a more posterior type 3 deformity on the contra-lateral side which results in an “S” shaped nasal septum. Type 4 has the clinical implications of both types 2 and 3.

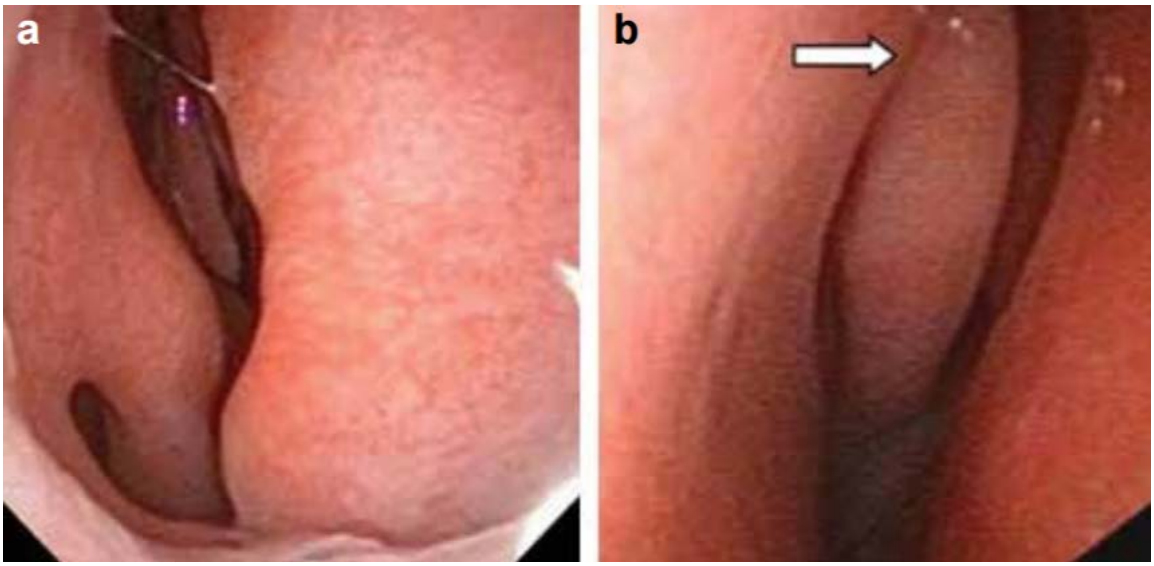

Figure 19 a: Type 4 with anterior right side type 2 component close to the head of the inferior turbinate. b: Type 4 with more posterior Type 3 component next to the head of the middle turbinate (white arrow)

Figure 20: Specimen 036 (13)

Figure 21: Specimen 059 (33)

Type 5

This is a unilateral horizontal deformity, known by physicians as a septal spur. Starting anteriorly as a crest it projects laterally, and posteriorly its tip usually contacts the proximal wall. The opposite side of the septum is usually flat. This usually results in impaired nasal breathing and is not seen in children until puberty. It is not due to trauma.

Mladina claims that Type 5 deformities are associated with a contact point headache often called Sluder's, as the tip of the spur may be in close contact with the sphenopalatine nerve. The spur may affect the drainage of the ostiomeatal complex to the nasopharynx resulting in fluid directed towards the Eustachian tube orifice. This is difficult to confirm as "Sluder's neuralgia and the phenomenology it describes have essentially been subsumed by the more refined nosology of the IHCD (Headache Classification Committee of the International Headache Society, **2013**), and the term should not further be used" (Eller 2016 p. 4).

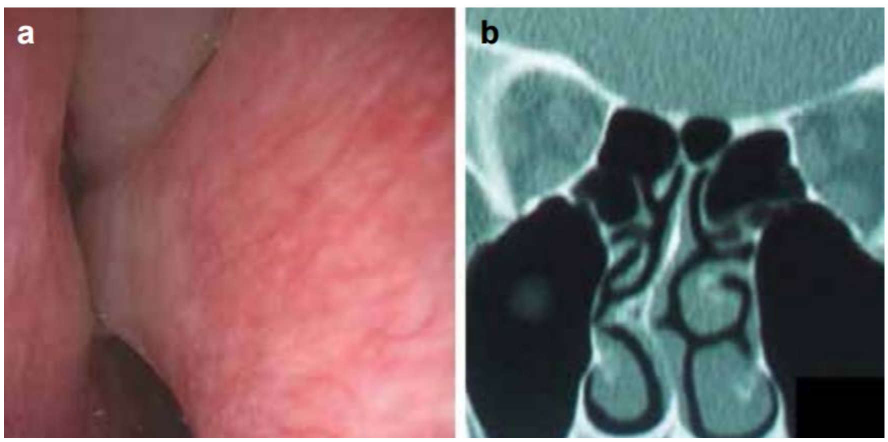

Figure 22 Right side type 5. a: Spur with close contact with the lateral nasal wall. b: Coronal CT with spur deep in the nose (only orbital apex is visible)

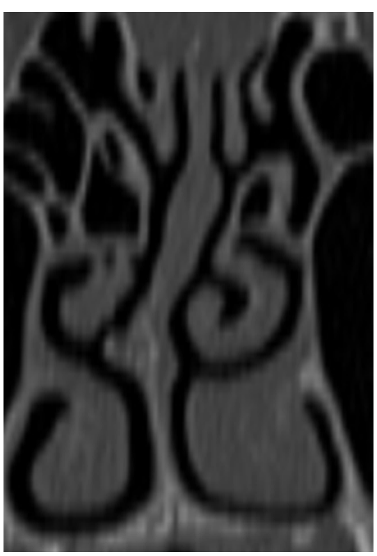

Figure23: Specimen 018 (50)

Figure24: Specimen 088 (07)

Figure 25: Specimen 000 (05)

Type 6

This is an anterior horizontal deformity with two components. There is an anterior basal septal crest on one side with a large wing on the opposite side. Between the septum and the wing there is a horizontal groove (which may be shallow or deep) that is characteristic of type 6. The groove defines the side of the deformity with the anterior basal crest on the opposite side. According to Mladina, it becomes evident at puberty and further develops during adolescence.

This defect is present in 96% of all children with a cleft lip/palate and 76% of their parents, and is also present in most patients with recurrent epistaxis (nosebleeds). Mladina believes that like the type 5, this deformity is not associated with exogenous trauma.

Takahashi (chapter 5) is much more systematic about developmental defects like this.

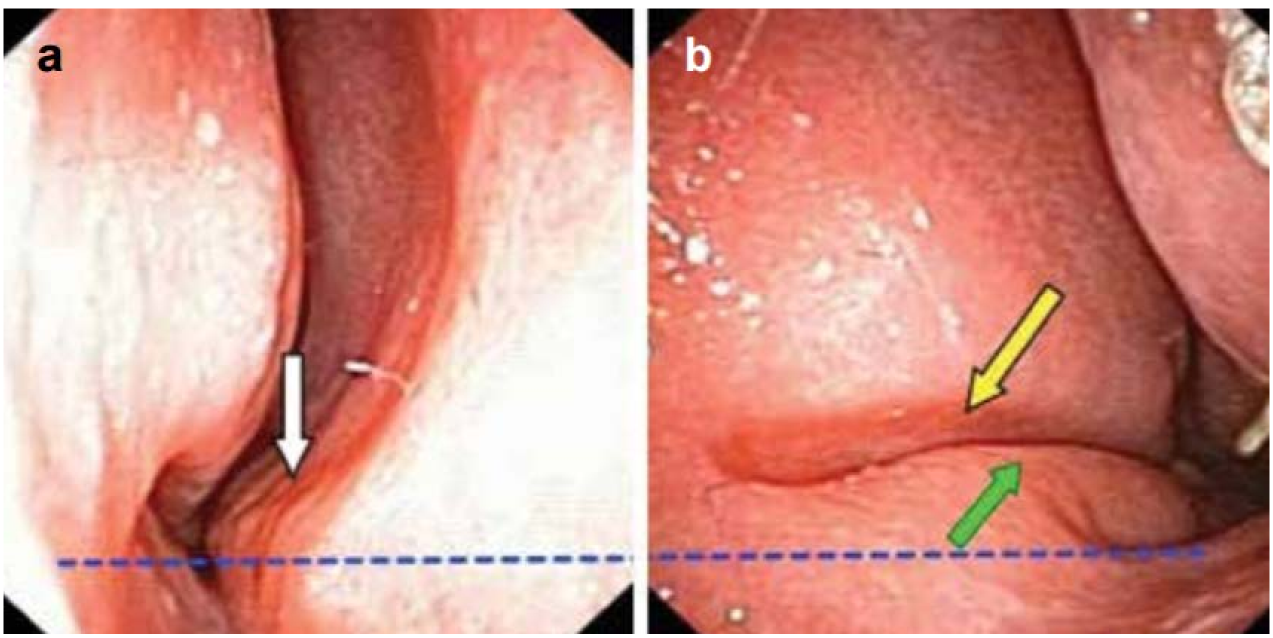

Figure 26: a: Type 6 with anterior basal crest (white arrow). Blue line is nasal floor). b: Septal groove (yellow arrow) above the inter-maxillary bone wing (green arrow). From Mladina (2015).

Mladina type 6 describes the deformity that had previously been described by Gray 1965 as "kinking or spur deformity" of the vomer ethmoid junction, and a "C or S shaped bending or deviation". Earwaker 1993 later described this as a deformity of the chondro-vomeral junction (CVJ). We will see in chapter 6 that the Mladina type 6 is the only one that is reliably discriminated by a morphometric approach. In effect it is the "most serious" of the deformities, the one most in need of a surgical correction if any of them are.

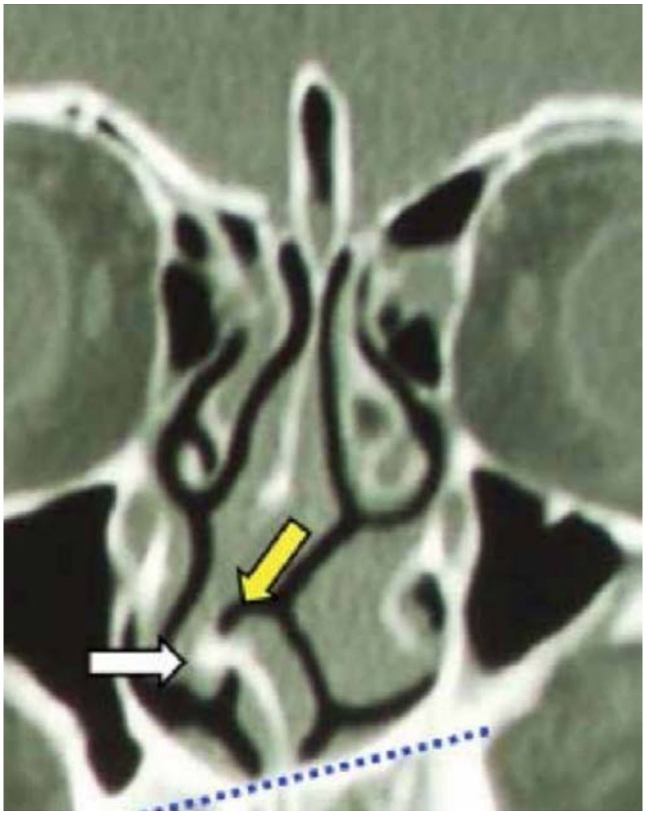

Figure 27: Mladina type 6 deviation. From Mladina (2015)

Figure 28: Specimen 007 (34)

Yellow arrow: typical groove of T6

White arrow: basal crest

Dotted line: asymmetry of nasal floor

Type 7

This combination deformity involves a horizontal deformity (type 5 or type 6) along with one of the vertical deformities (types 1-4).

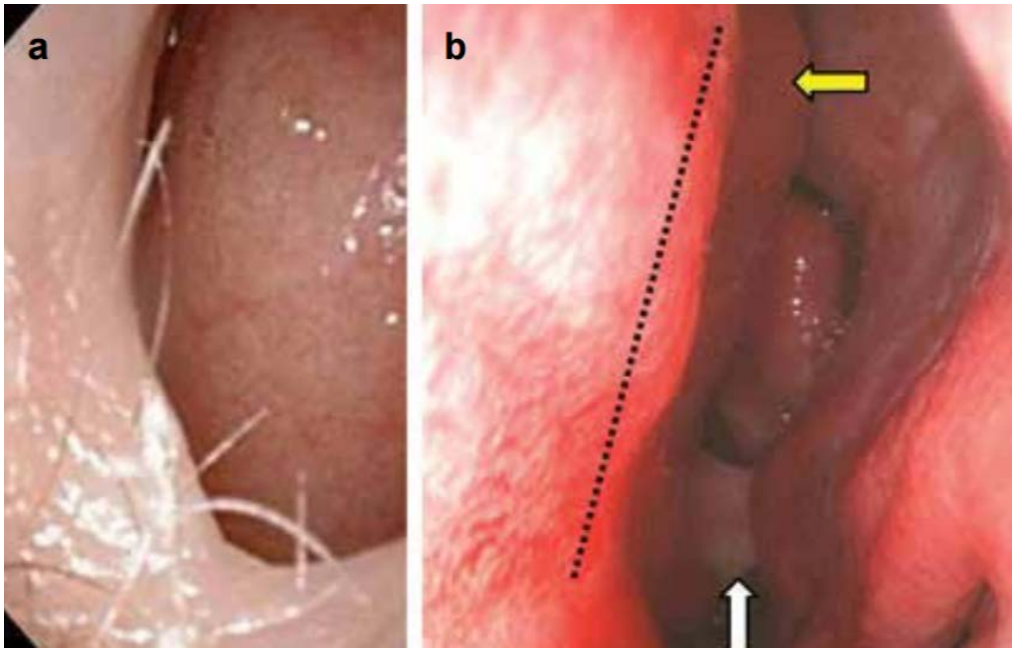

Figure 29: Type 7 where a: the right nasal cavity is almost completely blocked by the deformity. b: The left nasal cavity with the type 3 deformity superiorly (yellow arrow) and a type 5 spur inferiorly and deeper. The dotted line demarcates the internal caudal border of the type 3 which extends to the right, obstructing the entrance to the right nasal cavity (as seen in a). From Mladina 2015

Figure 30: Specimen 015 (50)

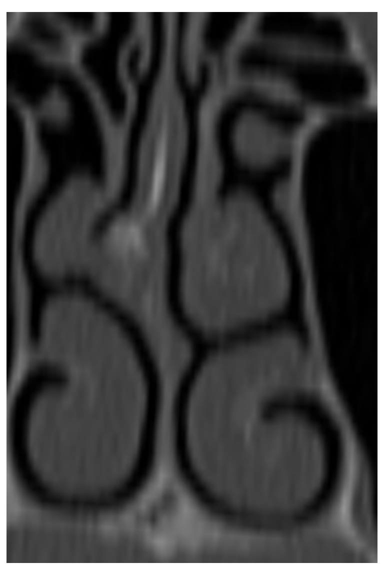

Figure 31: Specimen 016 (51)

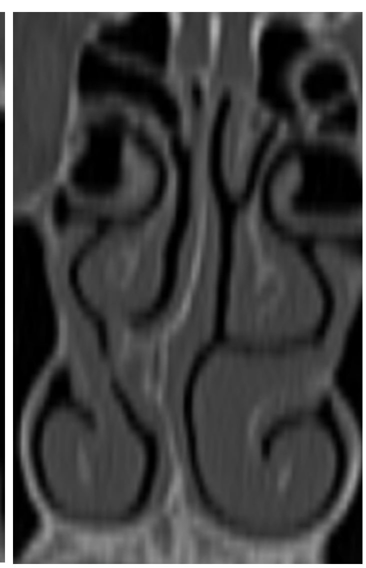

Figure 32: Specimen 025 (48)

Modifications of the Mladina Classification

Guyuron (1999) classified 93 patients (71F, 22M) into six types:

1. Septal tilt (40% of patients). The septum is straight but tilted to one side anteriorly and the opposite side posteriorly.
2. C-shape antero-posterior deviation (32%). The septum has a C-shaped curvature in the antero-posterior direction. The maxillary crest and nasal spine may also be deviated.
3. C-shape cephalocaudal (4%). Similar to the type 2 except the curvature is in the cephalocaudal direction.
4. S-shape antero-posterior (9%). Guyuron described this as two curvatures next to each other but in opposite directions that form a S.
5. S-shape cephalocaudal (1%). Similar to type 4 except the direction is cephalocaudal.
6. Localized deviations or spurs (14%). Invariably accompanied by an enlarged inferior turbinate on the affected side.

This descriptions of curvature in term of compass directions appears odd, quantification and with more precise directional coordinates would have been helpful.

Guyuron Classification	**Mladina Classification**	**Baumann and Baumann Classification**
	T1 Unilateral vertical partial (anterior)	
	T2 Unilateral vertical completer (Anterior)	
T2 Antero-posterior C	T3 Unilateral vertical (Posterior)	Type 6
T4 Antero-posterior S	T4 Bilateral vertical “Z”	
T6 Spur	T5 Spur	Type 1 and 2
T5 Cephalocaudal S	T6 Basal crest/septal groove	Type 3
	T7 Combination	Type 4 and 5

Table 6: Classification commonalities, Guyuron, Mladina, and Baumann

It is interesting that the various classifications are selective as to which septal variations there describe. Other than Guyuron type 3 cephalocaudal, the Mladina and Guyuron classifications are very similar, but use different descriptions. As with the Mladina classification there is no quantification of the deformity, nor is there any indication of the relationship with a disruption in airflow. In general this sort of morphometric approach is absurd (Bookstein 2019).

Buyukertan (2002) divided the coronal CT image of each side of the nose into 9 segments. The length and height were each divided into thirds, with lines connecting the upper and lower extremes of the septum in that sector.

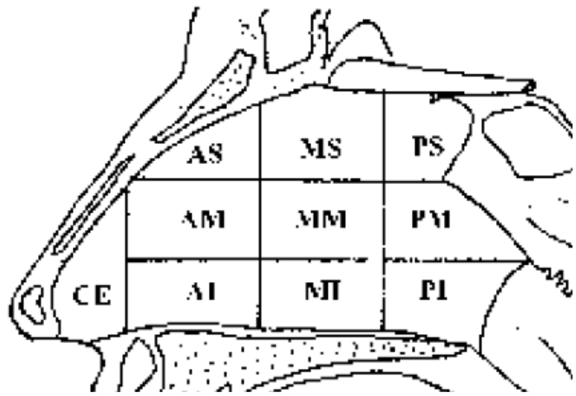

Figure 33: Antero segments AS, AM, and AI, Medio segments MS, MM, and MI, Postero segment PS, PM, and PI. CE segment not used. From Buyukertan (2002). Note: These are not English terms)

While this classification gives a rough location of the septum to a particular segment, it failed to reveal any information regarding shape or form.

Baumann and Baumann (2007) developed a classification whose aim was to improve surgical outcomes, based on the outcomes of 1088 surgical patients. Following surgery intraoperative drawings were made, and data was recorded regarding subluxation of the septum, inclined septum, nasal crest, vomeral spur, direction of septal deviation, turbinate hypertrophy, and presence of concha bullosa. Patients were classified as one of six types:

1. Septal crest with possible ipsilateral vomeral spur.
2. Cartilaginous deviated nose with possible ipsilateral subluxation, or contralateral vertical septal deviation.
3. High septal deviation with contralateral septal crest.
4. Caudally inclined septum with possible contralateral subluxation, ipsilateral vertical septal deviation, ipsilateral septal crest, or ipsilateral vomeral spur.
5. Septal crest with possible contralateral vomeral spur.
6. Caudally inclined septum with possible contralateral subluxation, ipsilateral vertical septal deviation, contralateral septal crest, or contralateral vomeral spur.

The use of the term “subluxation” is perplexing (a partial dislocation (“a subluxation associated with a fracture", a slight misalignment of the vertebrae, regarded in chiropractic theory as the cause of many health problems). It is of no help using a term greatly deprecated in the USA, due to its association with chiropractic and unrelated to the nasal septum.

Baumann and Baumann state “that types 1, 2, and 5 should be corrected under the guidance of an experienced surgeon, while types 3, 4, and 6 should be reserved for experienced surgeons.” This begs the question as to why each type of septal deviation requires correction.

This classification lacks a descriptor of “S” or “reverse “S” septa, namely the Mladina type 4 or the Guyuron T4. It also is unrelated to quantification or precise location of the defect, or the relationship with airflow disruption.

Noting that “there is no widely accepted classification system for septal deformities that is able to quantitatively measure and characterize the nature of the deviation”, Lin 2014 set as a goal “… to develop a method to quantitatively describe the curvature, extent of deviation, and often complex shape of a nasal septum…” (Lin 2014 p.183). Using coronal CT images, the septal contour drawn, and a MATLAB algorithm used to simulate a “straight septum” once the start and end points were selected (arbitrary selection). Deviation was quantified by measuring the distance between actual and a subjectively determined “ideal” septal contour, the deviation area was calculated between the two contours, and the RMS values of the septal contour vs the straight septum fit was calculated to represent the amplitude of the deviation. Both the actual and ideal septal contours are isolated from any biological reference, e.g. the mid-sagittal plane. Without reference to such a structure, it is unknown whether the ideal contour itself deviates from the mid-sagittal plane. The area of the deviation is unlikely to provide any information regarding the effect of the deformity on air flow as it doesn’t provide any information on the degree of obstruction. The RMS was used to measure the mean deviation from a baseline that itself was arbitrary.

Mladina’s classification and other classifications have grave deficiencies in that they do not actually measure anything. The definitions of the various types of deformity described by Mladina as “the change of shape or form” are pure words, devoid of objective meaning. Other than the classification by Lin 2014, the classifications in table 5 have all failed to provide measurements of shape change in relation to the “normal” nasal septum. Additionally, no evidence is provided as to what the shape of a “normal nasal septum” actually is. It is that lack of quantification of the ideal septum that renders classifications meaningless and makes surgical outcomes so difficult to appraise. In spite of regular introduction of new subjective classifications, review articles of nasal septal classification systems (Teixeira 2016), and reviews of the measurement tools used for the diagnosis of nasal septal deviation (Aziz 2014), the current clinical literature fails to offer any objective diagnostic guidance pertaining to nasal septal deformity.

Chapter 2

Selected methods of geometric morphometrics

Introduction

Reyment described as classics Bookstein's 1978 and 1986 papers that heralded "the dawning of the new era for the study of shape and growth". These publications and the 1989 paper and 1991 book "lie centrally located at the origin of the modern development of geometric morphometrics" (Reyment 2010). In a 1993 review, Rohlf and Marcus considered this period to be a "revolution" in morphometrics . Adams and Rohlf graphically stylized that work of the 1980's into what would become known as the "toolkit" of geometric morphometrics (Adams 2013). The figure below outlines the steps used in the "toolkit":

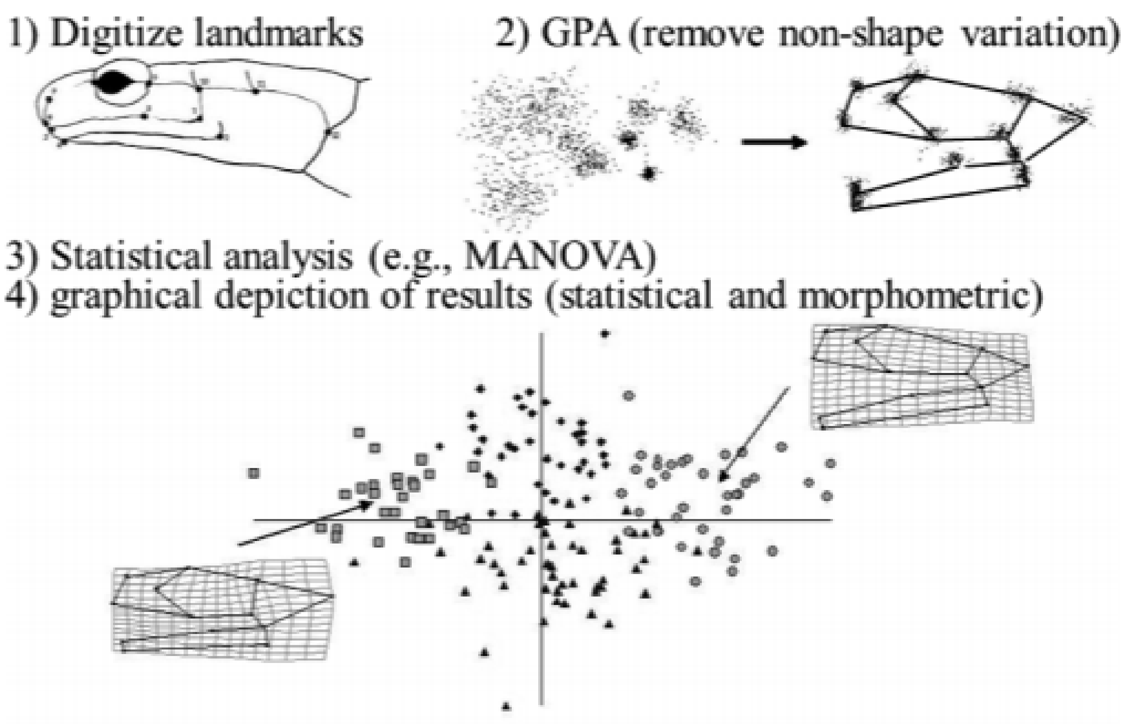

Figure 34: Graphical Depiction of the "Toolkit" of geometric morphometrics. From Adams (2013).

Step 1 Landmark coordinates in 2 or 3 dimensions define the relative positions of anatomical locations. These represent discrete anatomical points that correspond among all the forms of the data set

Step 2 A generalized Procrustes analysis (GPA) is performed. The specimens are translated to a common origin, scaled to a common centroid size, centroids are superimposed, and rotated in order to minimize the total sum of squared deviations of the coordinates from their average configuration. Bookstein 1991 argued that this frees morphometric statistical analysis from a reference coordinate system, implying that "differences of groups of landmark shapes are….independent of the system of shape coordinates by which the landmark locations are represented."

Step 3 Multivariate statistical methods can be used to describe shape differences, multivariate regression or partial least squares and to identify patterns of covariation between shape and other variables. However as early as 1991, Bookstein urged caution when making shape comparisons, noting that "we need to re-express all the statistical findings "inside the organism, an organism that only by accident finds itself sharing space with the mathematical manifold over which the landmarks, in reality bound together biologically, have been algebraically scattered" (Bookstein 1991 p.256-257). He cautioned that the utility of the Procrustes superposition may be limited, and that it may be "systematically misleading". This limitation derives from the fact that we can force the Procrustes superposition to use any homologous pair of locations that we choose, thus eliminating the ability to measure shape change. Biological processes involve the change of shape, yet "…every Procrustes fit to a pair of stages differing in age is missing a term for shape change, and thus is automatically mis-specified" (Bookstein 1991 p.261). Similarly in the presence of growth gradients, each fit to a pair of stages differing in age is missing the ability to measure shape change.

The limitations of the Procrustes analysis are further expounded in Bookstein 2016. He notes that "…the geometrical structure of a set of Procrustes shape coordinates—some pairs of variables, but not others, pertain to the same landmark point; some pairs but not others represent coordinates aligned in the same direction—is not coded anywhere in the conventional matrix of their values" (Bookstein 2016 p. 286). He describes the Procrustes problem: "The spacing of semilandmarks is arbitrary, and likewise their weighting in any overall geometric formulation" (Bookstein 2016 p. 287).

Step 4 Graphical measures can be used to visualize shape change. Principal components analysis (PCA) can represent the dispersion of shapes in tangent space. In an effort to better capture the information about the mean form, thin plate spline transformation grids can visualize shape differences, transforming (warping) one object into another. The GPA – PCA methods are limited in biology by the requirement of homology which can be corrected by substituting the TPS – bending energy model, for the Procrustes model. It is the low-pass version of this alternative method that we use in Chapter 5.

For an overview of GMM see Bookstein (2014) (Measurement and Reasoning) or Dryden and Mardia (2016) (Statistical Shape Analysis).

Semilandmarks which were introduced by Bookstein in 1991 and enabled the extension of landmark-based statistics to smooth curves and surfaces. Bookstein (1996) further developed the algebra to curves and surfaces in three dimensions. Points are allowed to slide along a curve or surface. For the purpose of this project the optimization of shape difference is achieved either through the minimization of the bending energy of the thin plate spline.

Recently Bookstein (2015) has questioned the uncritical expansion of the use of the Procrustes shape coordinates and principal components "toolkit" to explain functional morphology. Rather than using statistical properties to bridge geometric morphometrics to function, the necessity of using geometry to facilitate the bridge is proposed.

The remainder of this chapter will expand on this introduction, exploring the "toolkit" and its deficiencies, while discussing a more robust application.

1. Geometric morphometrics (GMM) for landmarks, what Procrustes analysis does, and associated problems.
2. GMM for surfaces, semi-landmarks and sliding, and undesired effects.
3. A new method for midline surface GMM.

GMM, Landmarks, and Procrustes Analysis

In light of current concerns pertaining to biological correspondence, it is relevant to review Bookstein's early emphasis on the differences between multivariate analysis outside morphometrics and morphometric data. Homology defined as a matter of correspondence between parts, lacks information regarding length or structures that curve inconsistently between their endpoints. Measurement is of the relation between forms, and we are ultimately measuring not shape but homology, and homology must be considered a mapping function, "a correspondence relating points to points rather than parts to parts". These points that represent the data base being studied are called landmarks. Bookstein 1991 posits that "landmarks delimit our explanations of effects upon form, and are the points at which one's explanations of biological processes are grounded". The assumption of homology when using the toolkit is particularly problematic when examining a structure like the nasal septum which deforms unpredictably and has functional implications.

The three types of landmarks identified by Bookstein (1991) , have been superseded by the six types of landmark points reviewed by Bookstein and Weber (2011).

Type 1: Discrete juxtapositions of tissues, including points where three structures intersect such as the junctions of bony sutures (Nasion), intersections of curves, branching points of tree structures, etc.

Type 2: Extremes of curvature or other local morphogenetic processes. These include tips of extrusions (tips of teeth, claws, and bony processes) and valleys of invaginations.

Type 3: Landmark points defined locally by multiple curves and by symmetry.

- 3a. Intersection of a ridge curve and the mid-curve on the same surface (foramen magnum).
- 3b. Intersection of an observed curve and the mid-curve (posterior border of the hard palate).
- 3c. Intersection of a ridge curve and an observed curve on the same surface (suture crossing a ridge curve).

Type 4: Semilandmarks on curves. Controlled by an energy term such as the bending energy of the thin plate spline.

Type 5: Semilandmarks on surfaces. Constrained to slide with respect to a combination of point landmarks and curve semilandmarks.

Type 6: Constructed semilandmarks: Various loci not covered previously. Projections of one structure onto another, "starts and finishes" of curves, places where curves come closest to each other, etc.

Landmarks are recorded as Cartesian coordinates. These Cartesian coordinates may be either two or three dimensional and may originate from many sources; coordinate digitizer, computed tomography (CT), or magnetic resonance imaging (MRI). To perform a statistical analysis of shape on these coordinates, they must first be separated from the confounding information of size, position, and orientation.

The three steps of the Procrustes superimposition, scaling to centroid size set to 1, translation to the same centroid, and superimposition of the centered and scaled configurations, result in the centered, scaled, and rotated *Procrustes shape coordinates*. The summed squared differences between two sets of Procrustes shape coordinates is the *Procrustes distance*. The Procrustes average is the shape whose sum of squares difference to other shapes is minimal, and the individual differences from this average shape are the *Procrustes residuals.*

Procrustes Adjusted Differential Methodology

Bookstein (2014) has proposed the following alternative to a typical geometric morphometric analysis when a functional measurement on the same data is available. Using a 6 landmark, 2D configuration, the typical GM calculates the relative warps (RW), of which only two of eight principal components are meaningful. Unfortunately the correlations between the cosine of the angle of interest and the eight relative warps imply that the most predictive RW is one of the meaningless ones. The alternative is to construct a functional index; the differential of the functional space measure as an explicit direction in Procrustes dual space. The example he uses is the normalized dot product of the two sides of a triangle divided by the product of their lengths. The differential of the functional index is then expressed in terms of the differentials of the Procrustes shape coordinate pairs. The differentials are computed as linear combinations. To diagram this method, the Procrustes mean locations and the sample means are substituted. This partials out translation and linear approximations of size and rotation as independent orthogonal geometric maneuvers.

This method finds the local changes that deform the thin plate spline while leaving unchanged the form of the remaining landmarks and their relationship (centering and net orientation) to the centroid of the triangle of the three landmarks involved in the functional measurement. Although there is a restriction to using conventional descriptors only, that aren't describing any specific biological question, the above approach via explicit index construction "is correct on *a priori* geometrical grounds" (Bookstein 2014).

If we had indices of function for nasal septal deformity, Bookstein (2018) presents a method using the linear combinations of the underlying variables of either measurement block of the partial least squares computations. When that block consists of shape coordinates, from the PLS covariance extracted, the same splining tool can be used to represent it as a grid. This method wasn't used in this study, instead using bending energy as per (Rohlf and Conti 2000).

Rigidly Registered Non-Procrustes Morphometrics

Initially the quantification of these classes was by applying the GMM toolkit to my segmentation of the septal surfaces. GMM, a specialty of the department of Bioanthropology of the University of Vienna, expresses a data set of biological forms as a collection of Cartesian coordinates (x, y, and z) of labelled points (landmarks) along with chains of points (semilandmarks) along curves and meshes of points upon surfaces (surface semilandmarks). The points I digitized included five landmarks (most anterior/inferior point on the NS, foramen caecum, ethmoid-sphenoid, sphenoid-vomer, vomer-palatine), two curves (anterior nasal septum, posterior nasal septum), and a mesh for each of the two surfaces with 132 separate points. In addition there were 5 other landmarks (Basion, pharyngeal attachment to the sphenoid, sella turcica (floor), sella turcica (posterior), and opisthion) chosen on the posterior cranial base in order to define an “anatomical mid-plane” with respect to which the septum’s deviations would be assessed.

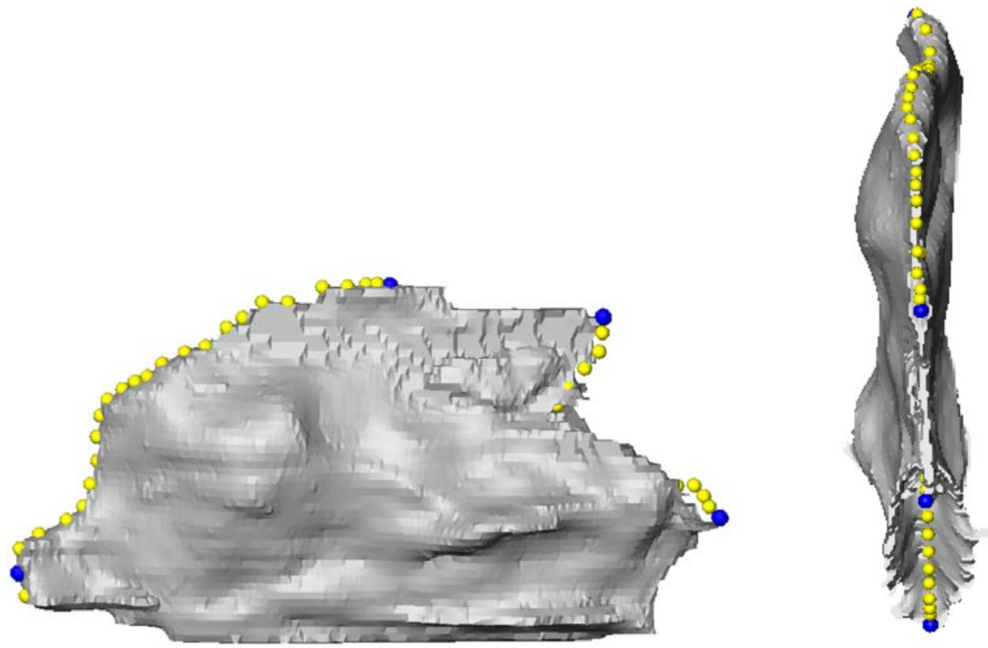

Figure 35a: Landmarks (Blue) Semilandmarks on Anterior and posterior nasal septal curves (Yellow). From specimen 046 (40).

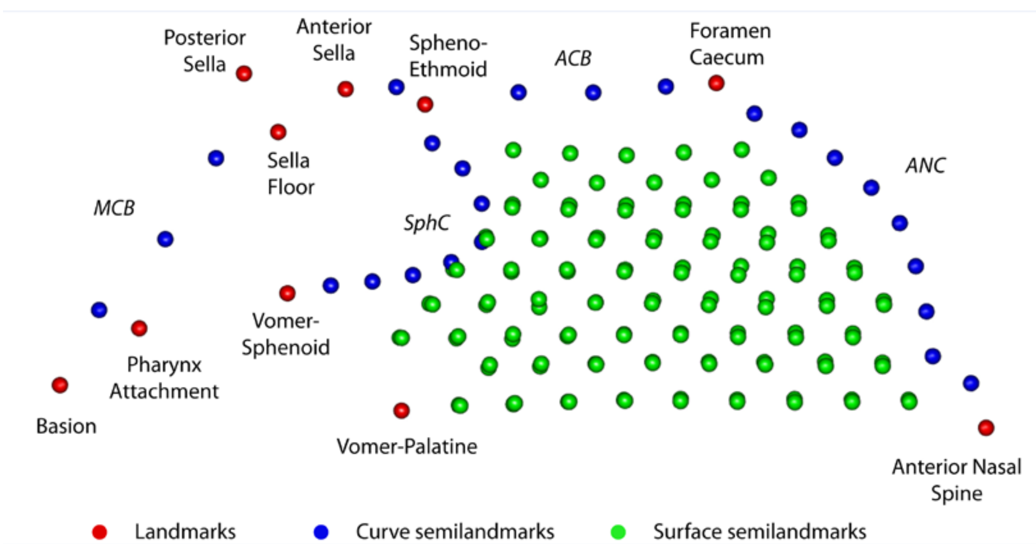

Figure 36b: Nasal septum template with cranial base and nasal septum landmarks, anterior and posterior nasal septum curve’s semilandmarks, and surface semilandmarks.

Application of a new method of midline surface GMM

For some types of investigations the translational and rotational freedom of the Procrustes procedure is inappropriate. For such problems including mine in this thesis, a quite different method of rigid registration from methods commonly used (Hill 2001) has been chosen in preference to the more frequently encountered Generalized Procrustes Analysis (GPA) (Gower 1975). GPA entails the loss of information about the position and orientation of the NS relative to the midsagittal plane due to centering and rotation (Bookstein 2015), whereas the lateral deviation of a nasal septum ought to be analysed with respect to this specific plane. The specimens' midsagittal plane was estimated. Then a rigid registration of all specimens' midsagittal planes was performed. After rigid registration of the midsagittal planes, each specimen's NS (Fig. 46: NS Block to align) was aligned according to its registered plane and rotated using the corresponding rotation matrices generated by the rigid registration. This procedure, which we call a block rigid registration or equivalent method as applied in Senck (2012), was carried out via a routine written by MC in R software. After rotation, the medial–lateral coordinates of the NS, measuring the deviation from the mid-sagittal plane, were extracted and submitted to statistical analysis. In a septum that bends, the left and right anti-mirror will shift in the same direction.

Visualization of nasal septum

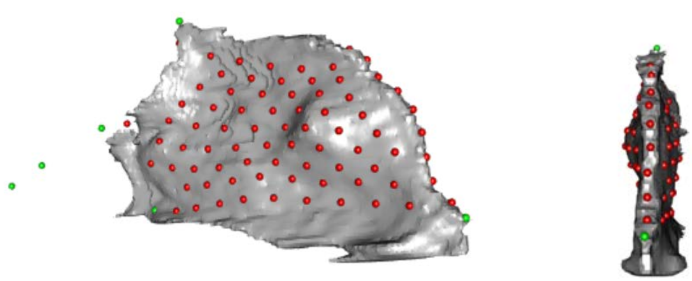

Figure 36: Specimen 062: Landmarks and semi-landmarks

Raw matrix of cranio data into and array

Visualization of cranio data

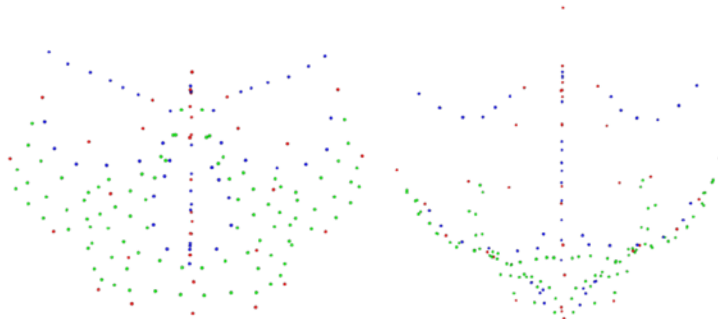

Figure37: Specimen 062: landmarks and semi-landmarks

Reorganizing the data: The mid-sagittal plane and nasal septum arrays were created.

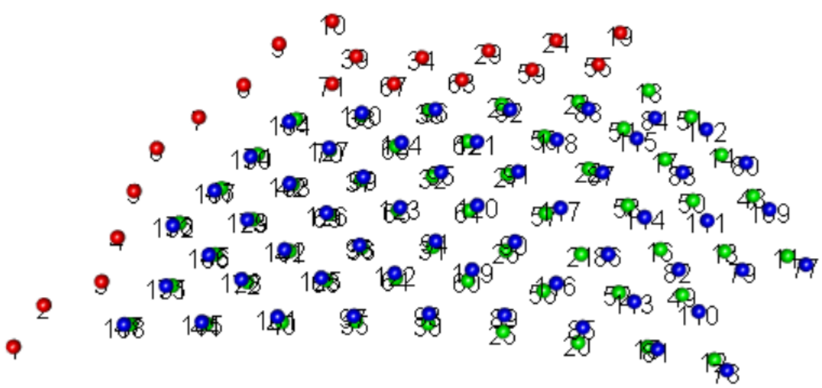

Figure 38: Nasal septum data

Figure 39: Cranial Base Reference Block

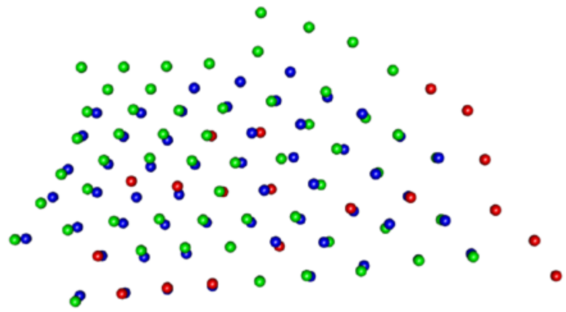

Figure 40: Nasal Septum Block to align

Rotation of the specimen’s nasal septum via the specimen’s mid-sagittal plane rotation matrix.

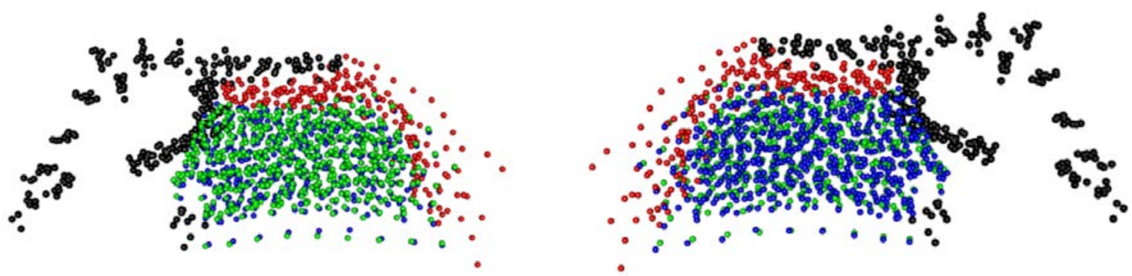

Figure 41: 2nd Rotation

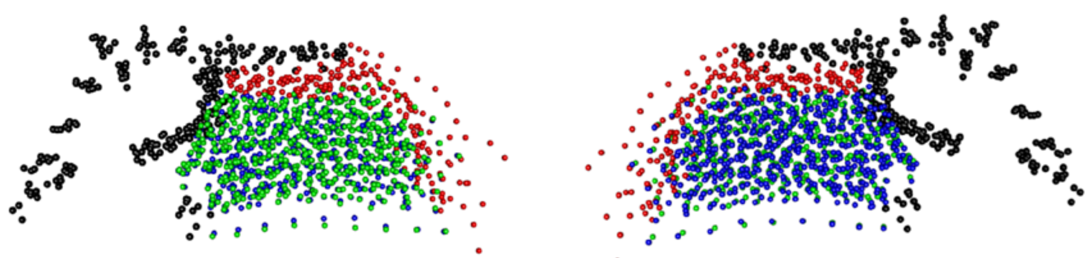

Figure 42: After 4 iterations

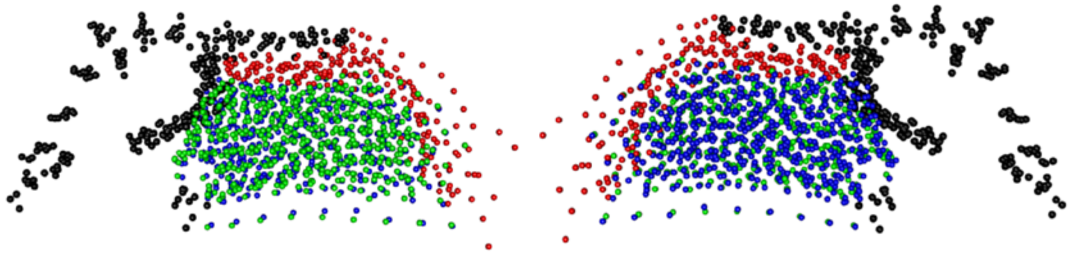

Figure 43: After n rotations, final configuration.

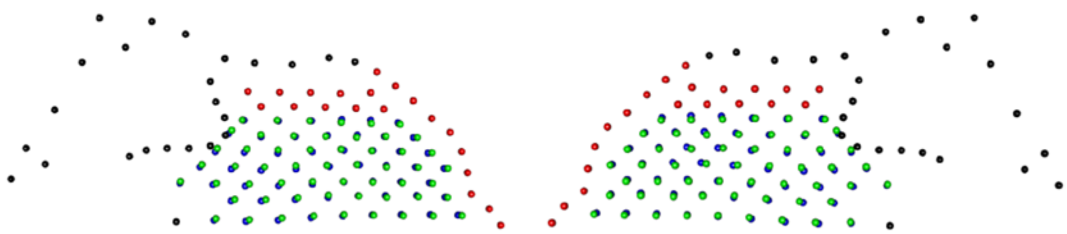

Figure 44: Example (Specimen 4)

Summary:

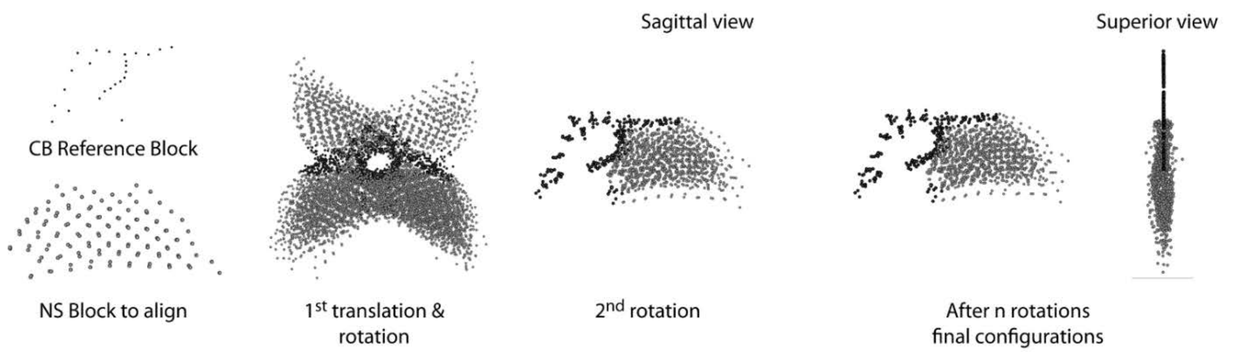

Figure 45: Block rigid registration. CB: Cranial Base: NS: Nasal Septum. Rigid registration of all specimens' CB planes (CB Reference Block). After rigid registration, each specimen's NS (NS Block to align) was aligned according to its registered CB plane and rotated using the rotation matrices generated by the rigid registration. Deviation of the septum from the mid-sagittal measured by their axial coordinates.

Registration based on the mid-sagittal structures. Nasal septum rotated according to the mid-sagittal rotation matrix. Rotation against specimen 1. A SVD of the transpose of the data (specimen 1 against each specimen needs the first step to orient the specimens, then calculate the average mean.

For 1st rotation i_2 to *n*

$$\mathrm{D}_i(X_i'^T X_i')$$

$$\mathrm{U}_i\mathrm{V}_i^T$$

$$X_i'\mathrm{U}_i\mathrm{V}_i^T$$

$$Y_i'\mathrm{U}_i\mathrm{V}_i^T$$

2nd Rotation (594-622). Rotation of all specimens after 1st rotation. Re-calculate the average mean for iteration i_1 to *n.*

All z coordinates were treated as having at the mean positions of the semilandmarks in the medial plane.

Chapter 3

The Data Set

The general plan was to obtain a sample of patients who satisfied the exclusion principles, assign a Mladina classification type, quantify the septa, and then determine if the resultant statistics could reconstruct the Mladina classes.

Data Collection

It was anticipated that data collection would face a number of obstacles. The inquiry required computed tomography (CT) of individuals with an intact nasal pharynx including the nasal septum, and at least a partially dentulous dentition. Radiation exposure standards precluded a prospective study of a healthy cohort that met these requirements. Therefore a retrospective study of subjects who required a CT of the head and neck for reasons other than trauma or malignancy, and who met the above requirements would have to be done.

The Medical University of Graz, Department of General ENT provided a sample of CTs appropriate for my investigation. From in excess of 2000 CTs, ninety two CT scanned adult patient images for me to look at as potential specimens were provided by (Medical University of Graz, Austria – Department of General Otorhinolaryngology, Head and Neck Surgery, Dr. Peter Tomazic (PVT) and his assistant). Drs. Currie (PC) and Coquerelle (MC) selected these to be the present study sample in consideration of exclusion factors. The sample I selected comprised 52 CT scanned adult patients (18 females, 34 males), from age 17 to 77. The most common reasons for exclusion was missing facial structure (nose, mandible or superior aspect of the septum was missing from the CT) or poor resolution (vertical slices having a 3.0mm or greater interval between slices). There were several subjects who were edentulous or had previous nasal surgery. During the analysis phase it was discovered that one subject had nasal surgery and was dropped from the sample, while two other subjects (052 and 062) who comprised the non-deviated specimens were dropped as a subset of two is too small. This resulted is a final sample of 49.

The entire sample has presented at the ENT department of the Medical University at Graz, the sample group had presented for complaints unrelated to the nasal cavity, none of those selected had been diagnosed and/or treatment planned for procedures related to the nasopharynx or nasal septum, nor had any related structure been altered by trauma, surgery, or neoplasm. The collection of 49 is not representative of any biological or demographic population. Biostatisticians would refer to such a collection as a “sample of convenience,” since all the sample is deviated it is unlikely to be of any value for the description of normal variation; that was not our goal.

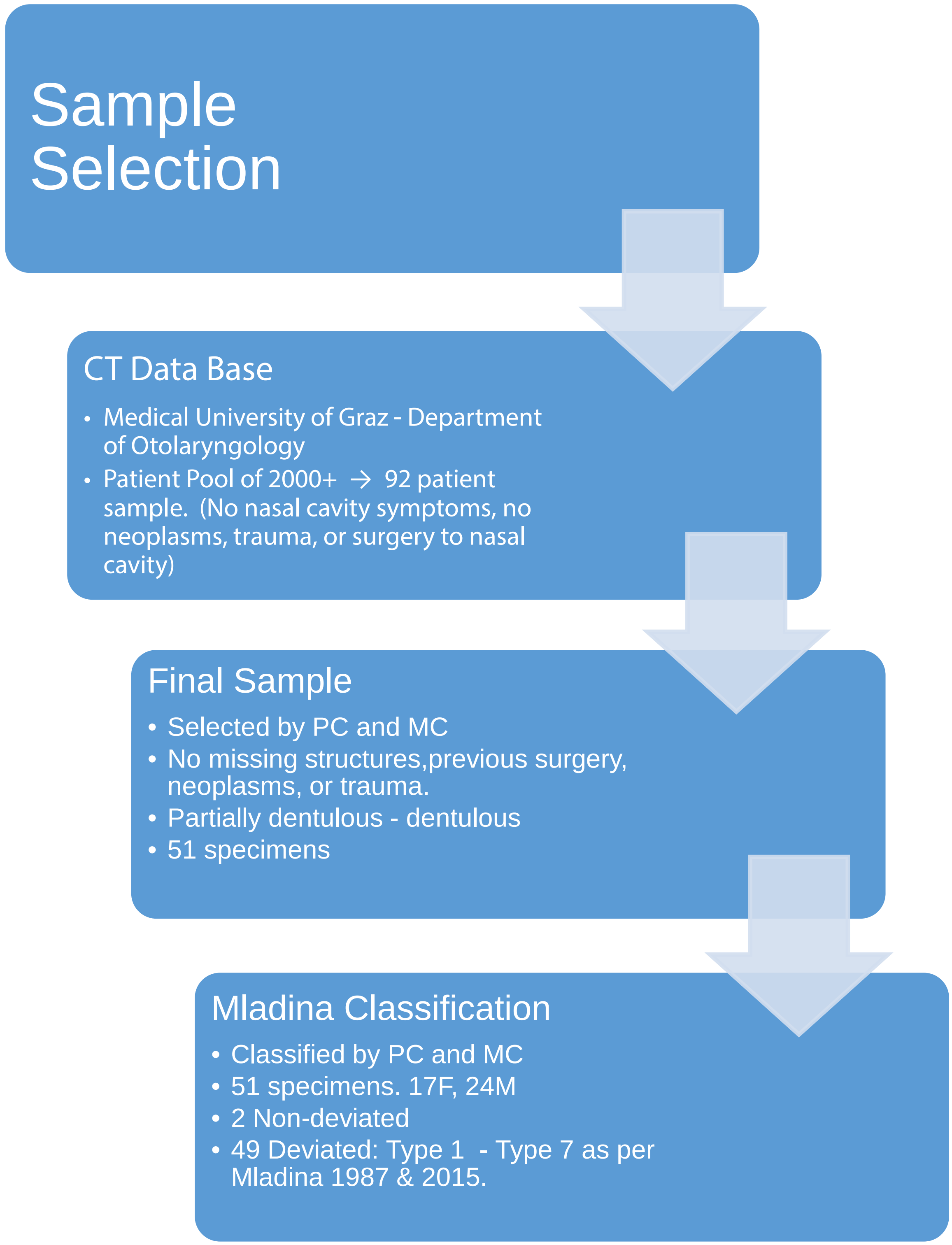

Figure 46: Diagnostic flowchart

The approach of what to examine in this study and the method of data analysis went through two phases in this study.

In the first phase a traditional GMM analysis was used to examine a sample that was set up to: 1. Assess if the standard toolkit of geometric morphometrics (GMM) – the statistics of biological form when applied to segmentations of the (two-sided) septal surface would confirm the validity of an existing classification (Mladina). 2. Distinguish what anatomical variations (concha bullosa, adenoids) might be associated with the different Mladina classification types. This led to the ambiguous findings as discussed in chapter 4.

The first phase grouping is exemplified in figure 47.

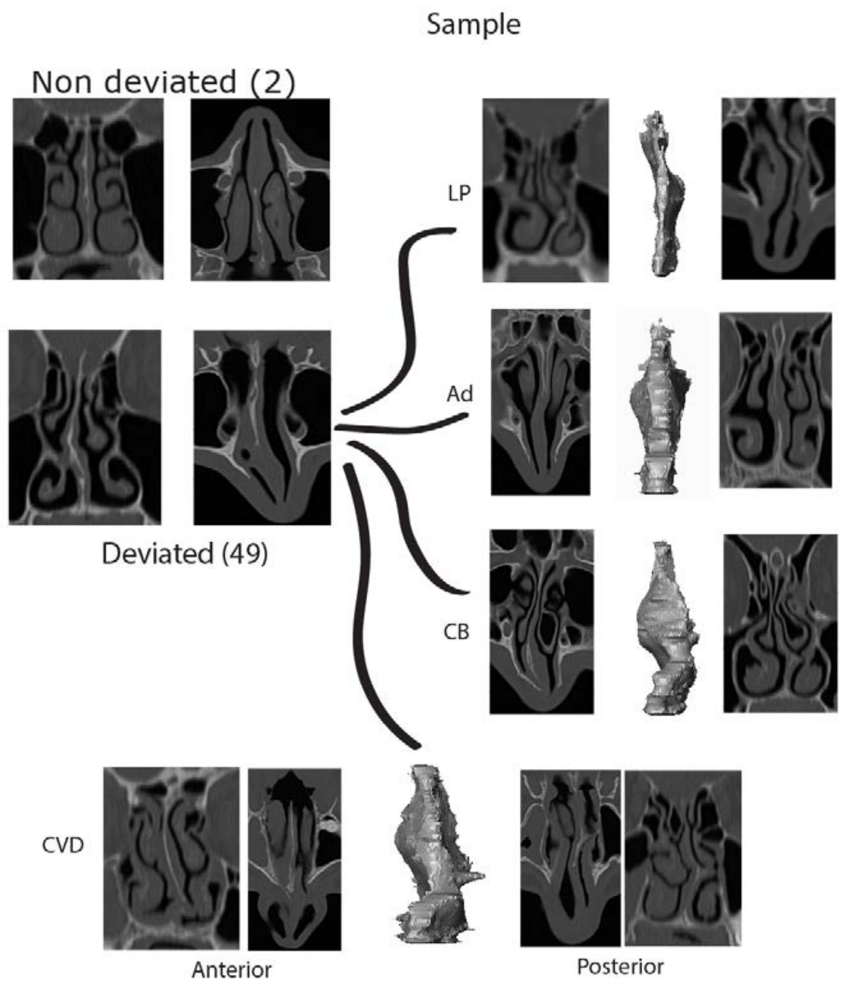

Figure 47: Examples of the anatomical variations examined in the first phase of the study: Non-deviated (2) (Deviated), and Deviated (49). Deviated groups may have anatomical variants such as lateral protuberance (LP) ridge, spur, or spine, concha bullosa (CB), or Chondro-vomero disturbance (CVD) as per Earwaker (1993).

The discovery of the work of Ryo Takahashi resulted in a second phase where the sample was examined in the context of the effect of evolution, growth, and development on the deformation of the nasal septum. The deformation of the septum was analysed using a severe modification of GMM centered on the thin plate spline and it's bending energy. This methodology was used to determine which specimens were most severely deformed and relate this to the Mladina classification. These findings are discussed in chapter 6.

With the help of MC the sample was further classified as per Mladina 1987 where the subjects were classified from T1 to T7.

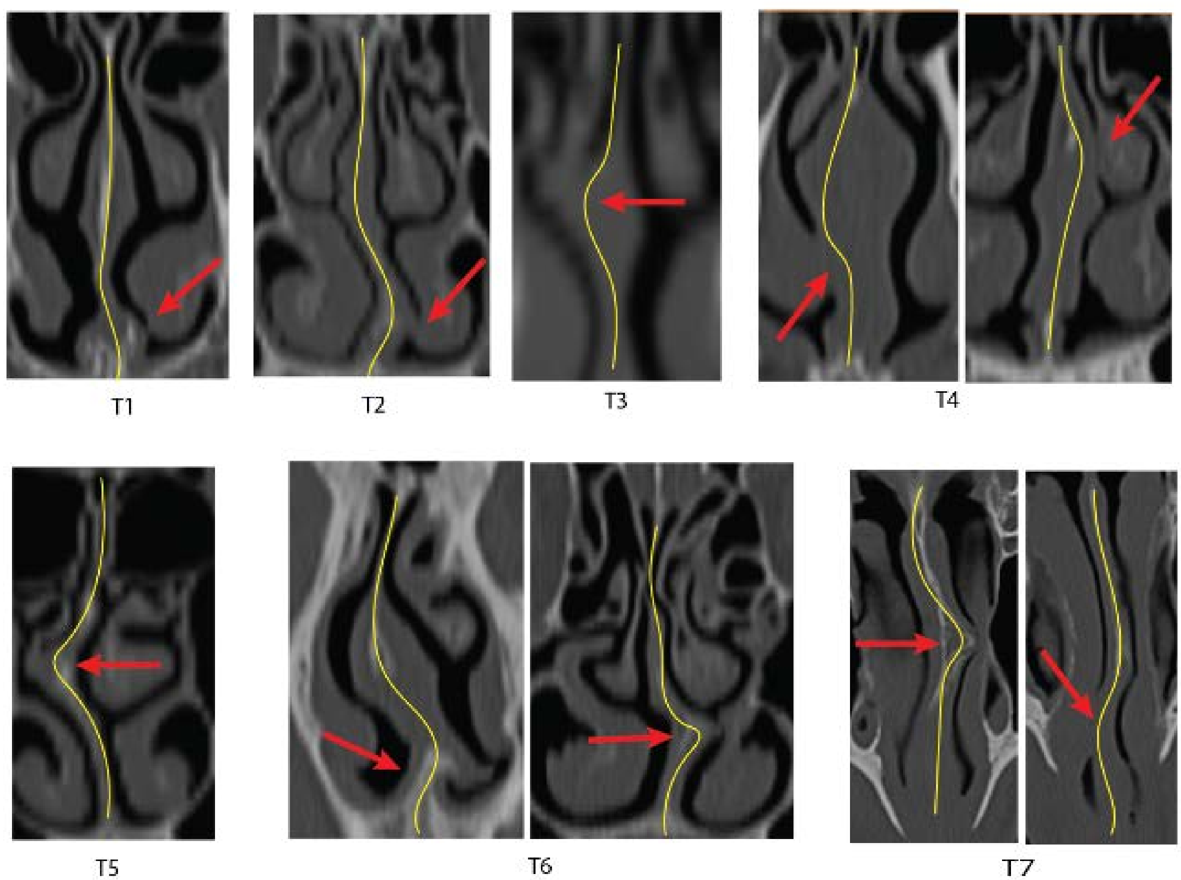

Figure 48: Study specimen examples of the Mladina classification: T1 Unilateral vertical ridge in the valve area, T2 Similar to T1 but a more severe obstruction and a disturbance of the nasal valve, T3 Unilateral vertical ridge at the level of the head of the middle turbinate, T4 Combination of T3 plus either a T1 or T2, T5 Horizontal septal crest in contact with the lateral nasal wall, T6 Prominent maxillary crest contralateral to the deviation with a septal crest on the deviated side, T7 Combination of previously described septal deformity types. The arrows indicate where the septal deformity is contacting the nasal cavity wall resulting in airflow disruption,

Details of Data Collection

The data have been collected in a number of Excel spreadsheets, summarized below in table 19. Following screening of the anonymized CT data files for the previously described exclusion factors, 49 subjects remained. Image segmentation, landmark digitization, and data analysis proceeded initially with considerable difficulty. Automatic segmentation was incapable of visualizing cartilaginous tissue, requiring careful and extremely time consuming manual segmentation with careful attention paid to Hounsfield values. Data analysis was complicated with ambiguous results, and the failure of the traditional GMM toolkit. This also resulted in a considerable wastage of time, ultimately requiring the development of a new methodology.

Data Summary (Table 7)

ID #	Number assigned in order that data was inputted into spreadsheet.
ID airway	ID number assigned to anonymized specimen.
Sex	M or F
Age	At time of CT
Cb	Presence of concha bullosa
Ads	Presence of adenoids
LatProb	Lateral protrusion (Spur, ridge or spine)
Spur	Bony spur
Ridge	Bony ridge
MaxCrest	Deformation of maxillary crest or chondro-vomeral junction
Mladina	Mladina classification (Types 1 – 7)
MladinaRgS	Mladina classification and presence of ridge or spur
ND	Non deviated

ID #	ID airway	Sex	Age	Cb	Ads	LatProb	Spur	Ridge	MaxCrest	Mladina	MadlinaRgS
1	Air047	M	22	No	No	Lp	No	Rg	No	T3	T3Rg
2	Air039	F	51	No	No	Lp	No	Rg	No	T3	T3Rg
3	Air078	M	18	No	No	Lp	S	No	No	T5	T5S
4	Air074	F	21	No	No	No	No	No	No	T3	T3
5	Air000	F	46	No	No	No	No	No	No	T1	T1
6	Air091	M	48	Cb	No	No	No	No	No	T2	T2
7	Air088	F	16	No	No	Lp	S	No	No	T5	T5S
8	Air090	M	30	Cb	No	Lp	S	No	No	T5	T5S
9	Air089	M	77	No	No	No	No	No	No	T1	T1
10	Air087	M	27	No	No	Lp	No	Rg	No	T3	T3Rg
11	Air086	M	32	Cb	No	Lp	No	Rg	No	T3	T3Rg
12	Air079	M	44	No	No	No	No	No	No	T1	T1
13	Air036	M	16	Cb	AD	Lp	No	Rg	No	T4	T4Rg
14	Air030	M	27	No	No	Lp	S	No	No	T5	T5S
15	Air029	M	16	No	AD	No	No	No	No	T3	T3
16	Air028	M	22	Cb	No	No	No	No	No	T2	T2
17	Air027	F	34	No	No	No	No	No	No	T3	T3
18	Air013	M	20	No	No	No	No	No	No	T3	T3
19	Air012	M	63	No	No	No	No	No	No	T3	T3
20	Air015	F	41	No	No	Lp	No	Rg	No	T7	T7Rg
21	Air077	M	23	No	No	No	No	No	No	T2	T2
22	Air076	M	73	No	No	No	No	No	No	T2	T2
23	Air071	M	33	No	No	Lp	No	Rg	DmxA	T6	T6Rg
24	Air070	M	53	Cb	No	No	No	No	No	T1	T1
25	Air069	F	27	Cb	No	No	No	No	No	T4	T4
26	Air068	F	70	Cb	No	Lp	S	No	No	T5	T5S
27	Air066	F	60	Cb	No	Lp	S	No	No	T3	T3S
28	Air064	M	53	Cb	No	Lp	No	Rg	DmxA	T6	T6Rg
29	Air063	M	24	Cb	No	No	No	No	No	T1	T1
30	Air062	F	45	No	No	No	No	No	No	ND	ND
31	Air061	M	54	No	No	No	No	No	DmxA	T6	T6
32	Air053	M	24	No	No	Lp	No	Rg	No	T3	T3Rg
33	Air059	M	48	No	No	No	No	No	No	T4	T4
34	Air007	M	44	No	No	Lp	No	Rg	DmxA	T6	T6Rg
35	Air057	F	16	Cb	No	No	No	No	No	T4	T4
36	Air056	F	47	No	No	No	No	Rg	No	T3	T3Rg
37	Air055	M	22	Cb	No	No	No	No	No	T4	T4
38	Air052	M	37	No	No	No	No	No	No	ND	ND
39	Air051	F	51	Cb	No	Lp	No	Rg	No	T2	T2
40	Air046	M	56	Cb	No	Lp	S	No	DmxA	T6	T6S
41	Air043	M	21	No	No	Lp	No	Rg	No	T7	T7Rg
42	Air042	M	18	No	AD	No	No	No	No	T2	T2
43	Air035	M	30	No	No	No	No	No	No	T1	T1
44	Air009	M	48	Cb	No	No	No	No	No	T3	T3
45	Air002	M	41	No	No	Lp	No	Rg	No	T2	T2Rg
46	Air031	M	21	No	AD	Lp	S	No	No	T3	T3S
47	Air026	F	29	No	No	No	No	No	No	T1	T1
48	Air025	M	29	No	AD	Lp	No	Rg	No	T7	T7Rg
49	Air021	M	17	No	AD	Lp	No	Rg	No	T3	T3Rg
50	Air018	M	57	No	No	Lp	S	No	No	T5	T5S
51	Air016	F	37	Cb	No	Lp	S	Rg	No	T7	T7S

Table 7: Data Summary. Mladina (Deviation type:, Cb (Concha bullosa), Ads (Adenoids), LatProt (Lateral protrusion [spur or ridge], MaxCrest (Maxillary crest deviation), (MladinaRgS (Mladina classification and presence of a ridge or spur),

The Mladina classification protocols were strictly adhered to. Table 7 summarizes this. The sample classified as per Mladina is described in Table 8.

Mladina - Group	**Number per Type**
T1	7
T2	7
T3	15
T4	5
T5	6
T6	5
T7	4
Total	49

Table 8: Mladina classification. Sample of 49 subjects with breakdown according to type.

Chapter 4

Findings I

(*Note to the reader*) this represents an attempt to apply classic GMM tools to the data. It is an obvious failure. After separate principal component analyses (PCA) of the NS centered axial coordinates, left and right we examined the distribution of the NSD according to the Mladina T group classification. Keep in mind that the PC analysis is on the signed mediolateral coordinates of the 76 lateralized semilandmarks. We used a mesh of surface semilandmarks on a template specimen and the TPS interpolation function computed from the landmarks and curve semilandmarks to warp the mesh from the template unto each specimen.

Using a statistical test borrowed from Anderson (Coquerelle 2011, Bookstein 2014), it was found that for either side of the surface the characteristic values (variance of the PC scores) from PC3 onwards, were nearly equal and hence their ordination is more likely than not to be expressing only noise. Therefore, only the first two PCs of either side separately were considered for interpretation and visualization.

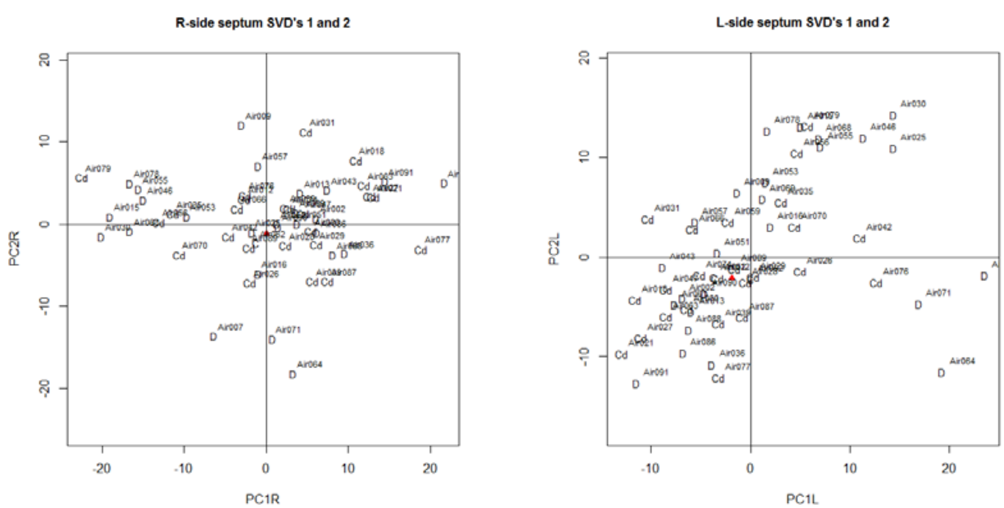

Figure 49: Left and right PC1 and PC2 of septal SVDs.

The triangulated surface of one asymptomatic, non-deviated individual was warped towards the sample mean form using the TPS interpolation function (Bookstein 1991) in order to create the sample mean surface.. Thereafter, surface deviation characterizing NSD represented by the eigenvectors of a particular PC was visualized as a TPS deformation from the sample mean surface, plus or minus the principal components. A surface deviation analysis was performed based on the minimal Procrustes distances between the surface vertices and was displayed as a colour map of the sample mean nasal surface.

NS Surface Analysis

The first two PCs account for 28.9% and 28.2% of the total form variation of the left and right NS surfaces, respectively. Figure 49 shows the distribution of the NSD along PC1 and PC2 grouped according to T-group. The T groups T1, T2, T3, T4, T5, and T7 overlap to a great extent, whereas T6 specimens which corresponds to CVD specimens clearly diverge.

While three of the five T6 specimens are widely separated from the remainder of the specimens along PC2, two T6 specimens are not (figure 50). On visual inspection all the T6 specimens are severely deformed, yet two show no separation from the other groups in figures 50 and 52). Clearly the analysis is yielding ambiguous results if all the most severely deformed specimens cannot be identified. Furthermore there is no pattern to the distribution of the other Mladina types with some T2s more widely scattered that supposedly more severely deformed T4s and T5s.

Furthermore there is similar failure to identify the next most severely deformed specimens (T7). Not only are they not identified as a group, they are not identified proximal to the most severely deformed T6 group. There is a clear failure of the GPA-PCA technique of GMM toolkit to be of any utility is the identification of morphological deformation in a biological structure such as the nasal septum.

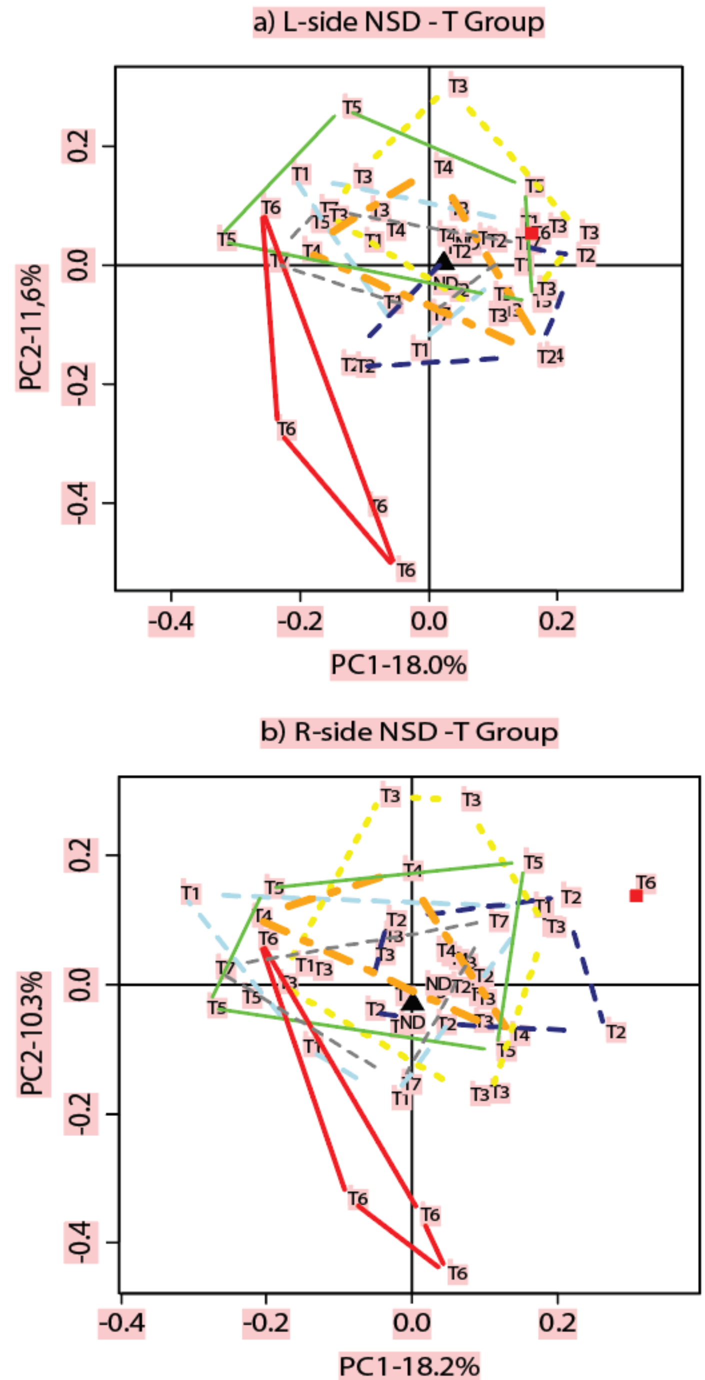

Figure 50: T-Group distributions: Right and left convex hull distributions of the principal components analysis (PC1 vs PC2) for the T groups. T6 group is the only group that shows little overlap with the other overlapping groups

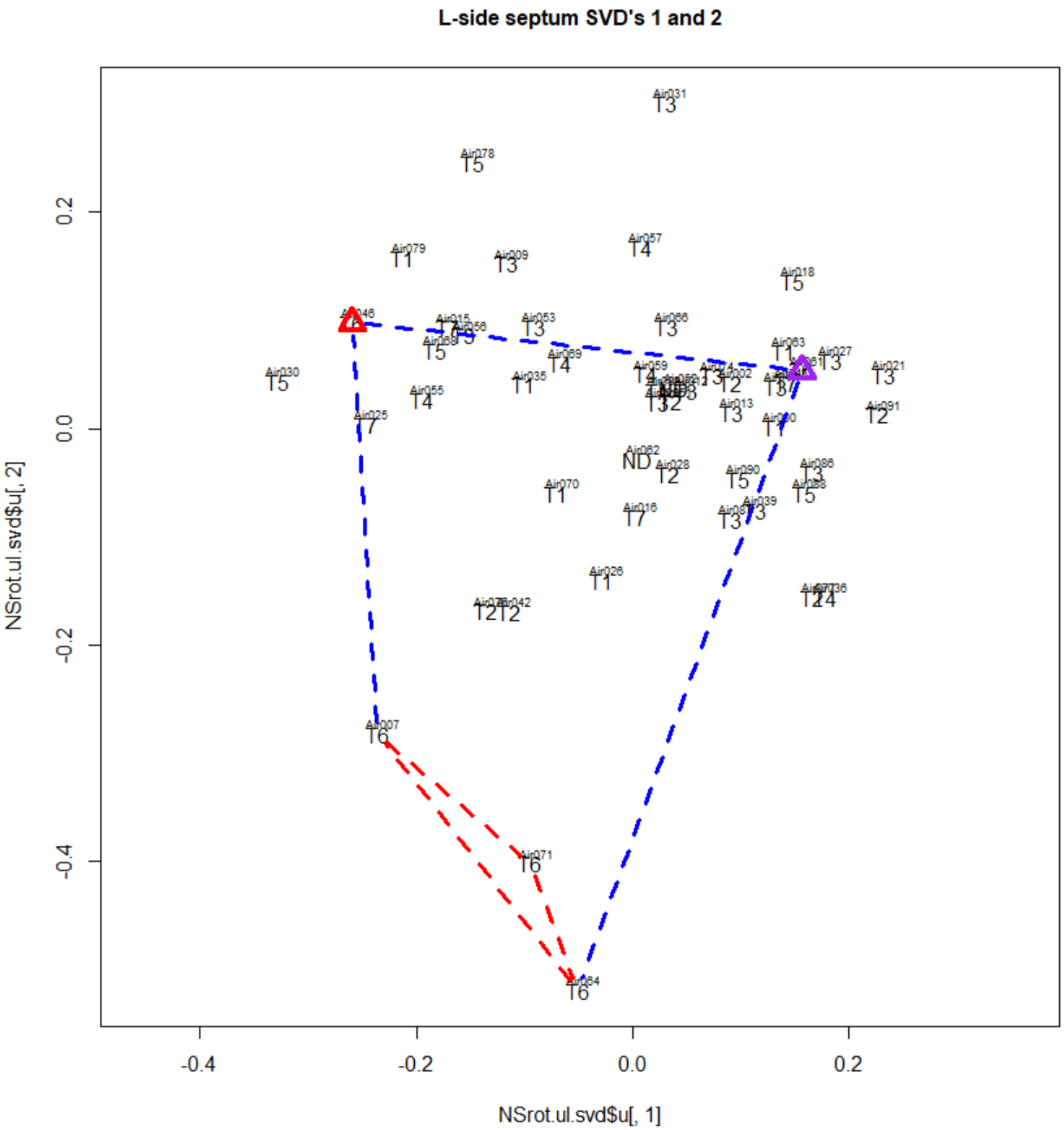

Figure 51: Convex hulls for Mladina classification: (UL).) Convex hull type 6. Red: 3 T6 that group together) Convex hulls type 6. (Blue: All 5 widely dispersed T6)

As shown in figured 52a and 52b, PC 1 relates to the central and posterior regions of the NS which are predominantly osseous. The higher the PC1 scores, the greater the horizontal deviation between the junction of the septal cartilage and the ethmoid plate (leading to a pronounced C-shaped NS). Posteriorly where the vomer, septal cartilage, and the ethmoid plate collide (increased negative and positive PC1 scores for the left and right surfaces respectively), the surface deviation corresponds to the formation of a large lateral protuberance. This highlights the difficulties with using PCs as this combines two functionally unrelated features.

PC2 in contrast, is a deviation of the anterior region of the NS, which is predominantly cartilaginous. This region is characterized by less deformation of the ethmoid plate and more deformation of the most anterior cartilaginous region of the NS in the opposite direction. Again, there is no biological sense to combining these.

In the context of later chapters following our discovery of Takahashi's texts, the deformation of the anterior cartilaginous region will be discussed in relation to Takahashi's concept of nasal septal deformity.

The higher the PC2 score, the greater the deviation from the anterior midline of the ethmoid plate and the septal cartilage at its junction with the anterior nasal spine, resulting in a pronounced S-shaped deformation, characteristic of the CVD specimens.

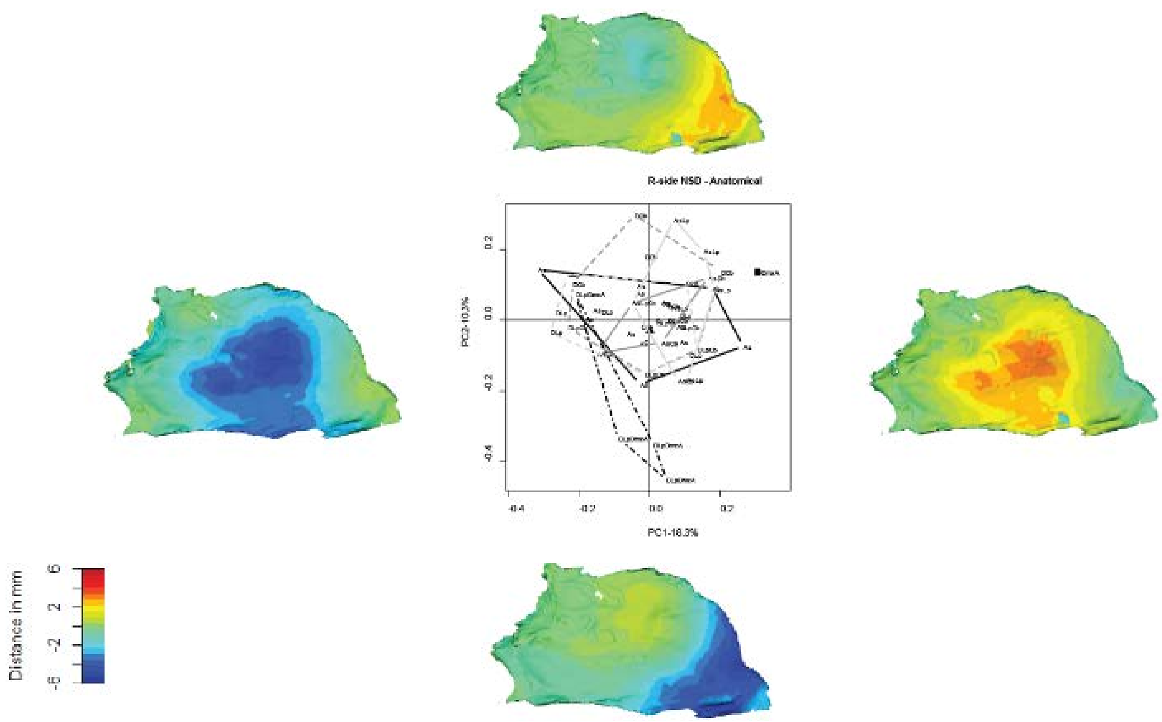

Figure 52a: NSD along PC1 and PC2 (RS)

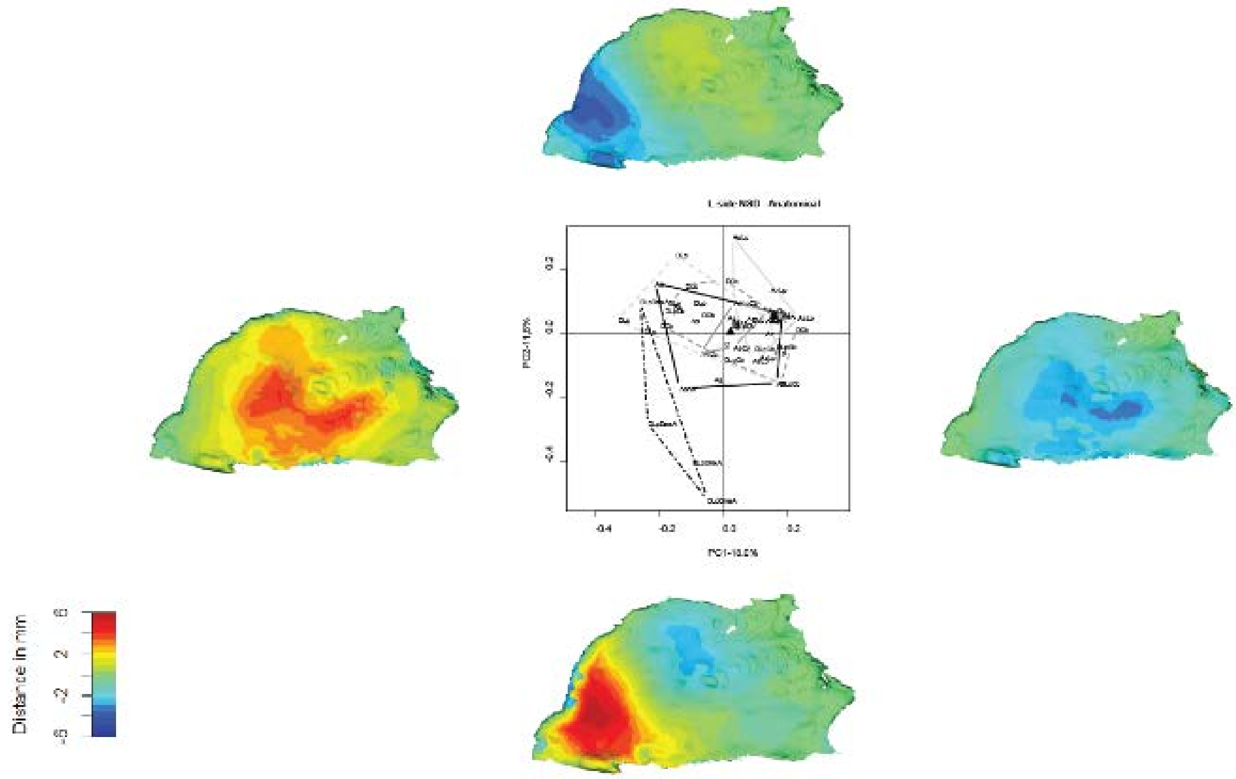

Figure 52b: NSD along PC1 and PC2 (LS)

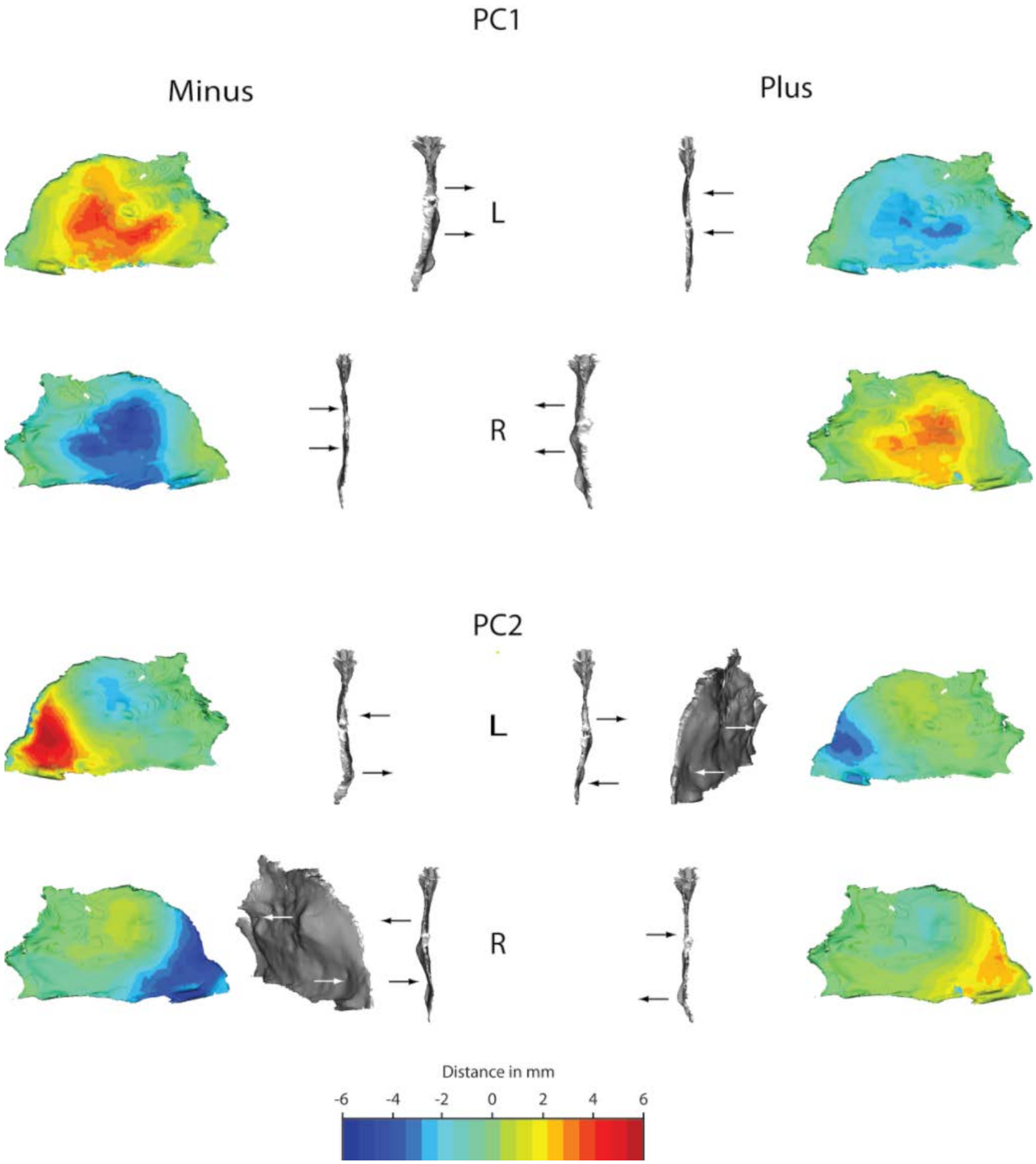

Figure 53: Nasal septal deviations along PC1 and PC2 (LS and RS): On PC1 the septal deviations produce a "C "shaped septum. On PC2 the deviations produce a "S" shaped septum.

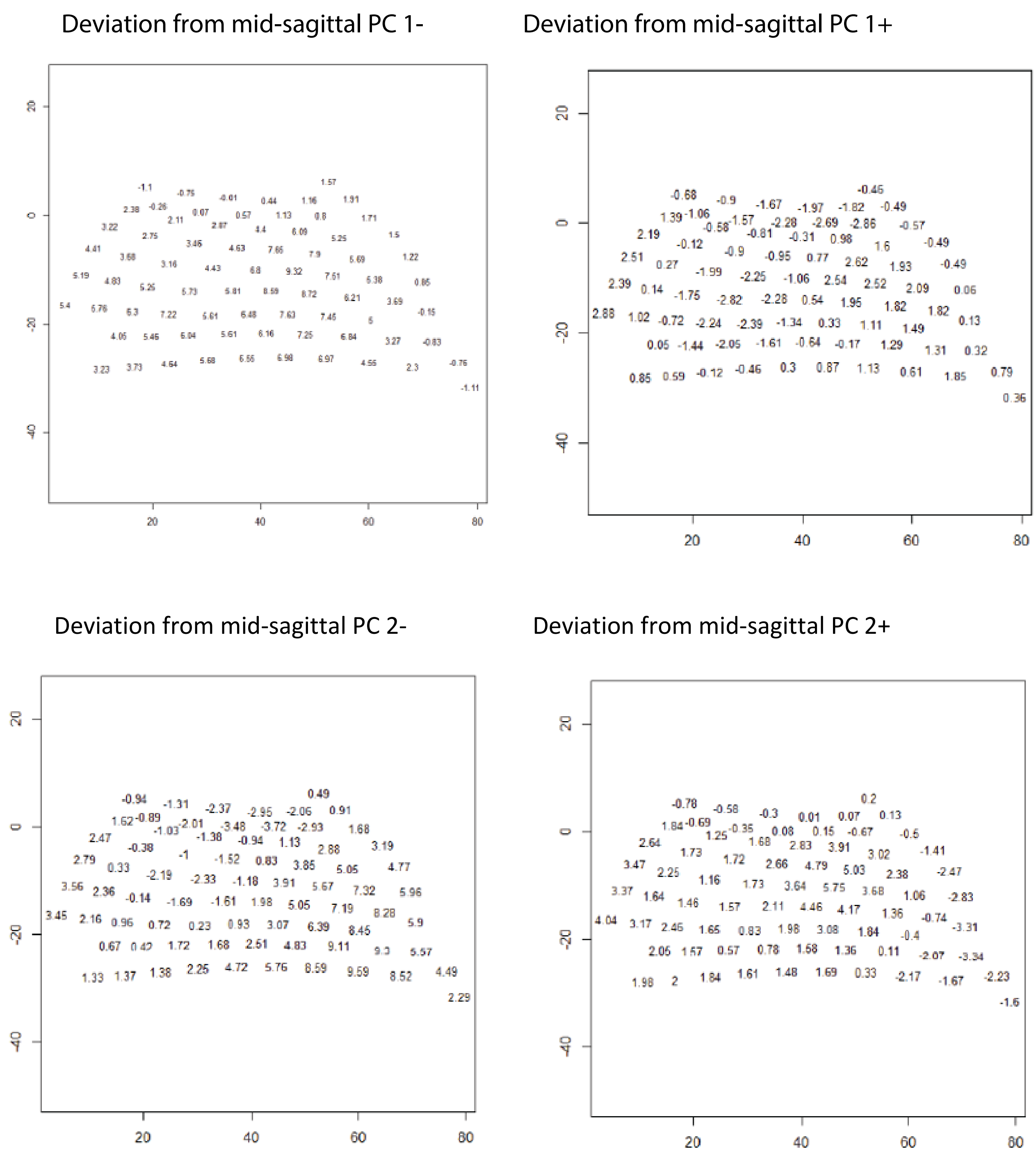

Figure 54: Deviation from mid-sagittal plane on PC 1 and PC2

These results show that the T-group classification has only a very limited association with septal shape except for one anatomical variant corresponding to the deformation of the chondro-vomeral junction (Gray 1965, Earwaker 1993). This deformity mostly concerns the cartilaginous septum, and as previously mentioned is predominantly left sided and with a large lateral protuberance. However even this was inconsistent. On the right nasal septum, 3 specimens 007 (35), 064 (28), and 071 (23) were strongly deviated along PC1, while the remaining two T6 specimens were deviated along PC2 but in opposite directions. It would be wise to find an approach that left the type 6smore tightly clustered. See chapter 6 for just such an approach.

Type 6 is associated with the greatest deformity in the vomer region with a large lateral protrusion (or projection) and increasing concavity of the anterior–inferior edge of the perpendicular plate as the severity of the nasal septal deformity increases. Overall, type 6 is the most severe deformity, with complex curvature of the septal cartilage and significant ridge formation anteriorly resulting in reduced airflow in the valve region, and ridge or spine formation centrally.

For the T groups T1 to T5 and T7, Miles (2007) noted a variability of the nasal septum, which is supported by our study. About 88% shows a maximum NS deviation of approximately 5mm from the mid-sagittal plane. Miles in his sample of cadavers, 82% showed a maximum deviation lower than 6 mm as measured from the septal midline.

The range of deformity described by Miles can be found across all types. When the nasal septum is viewed axially, the septal curvature can be viewed as representative of each types in in figure 55. Whether noting curvature of deformity on clinical visual inspection or on a computed tomogram, these classification reveal nothing regarding quantification of the deformity or resultant interruption in air flow.

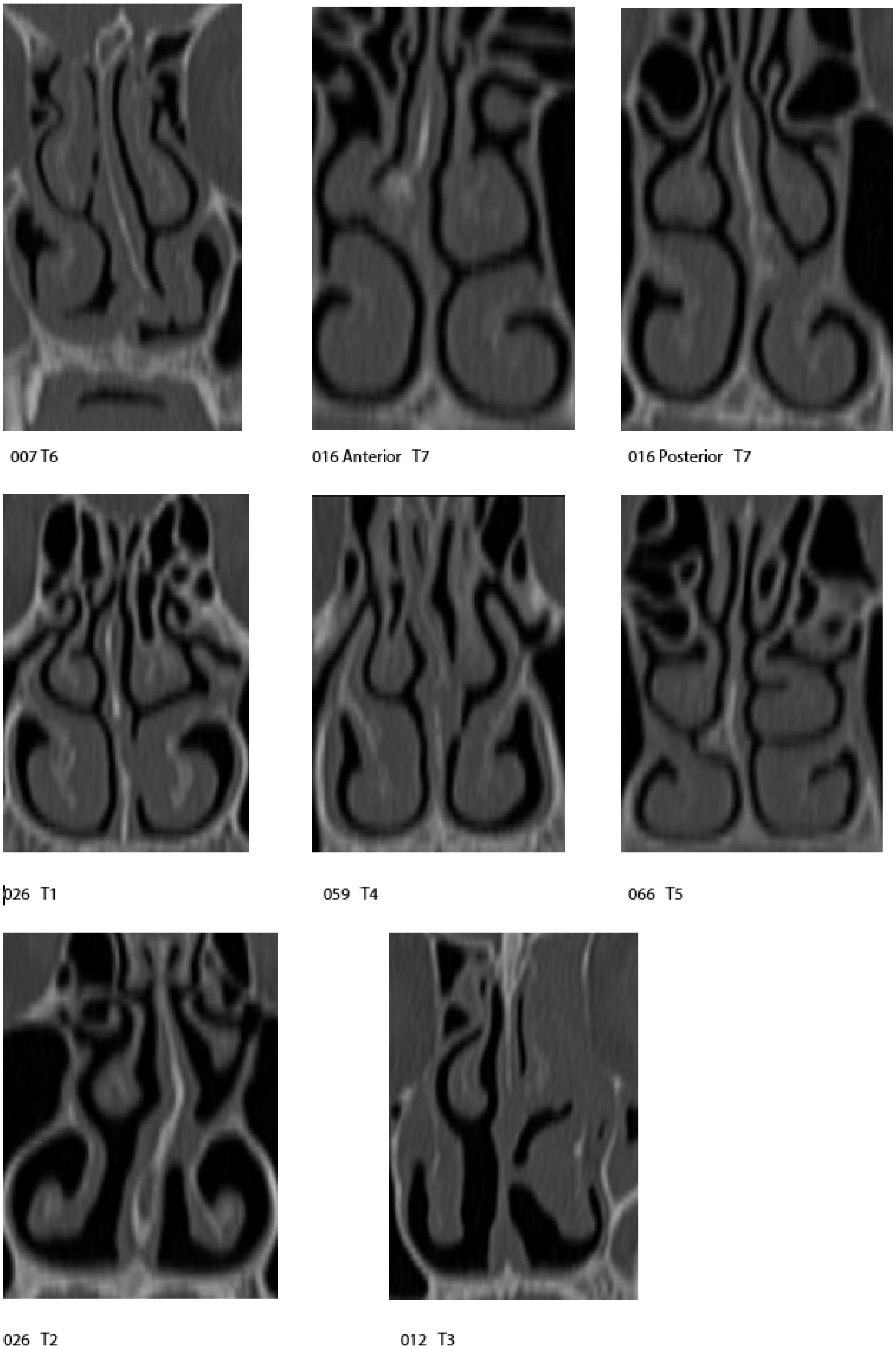

Figure 55: Axial view septal curvatures for Mladina types 1to 7.

Furthermore, the fallacy in attempting to describe a nasal septal deformity by attaching a convenient label to it is that it may fail to differentiate between very dissimilar deformities. As an example, the three specimens most severely displaced on the PC2-axis are 007, 071, and 064. They have a deformation of the vomer-cartilaginous junction and the vomeral groove as typified by Mladina T6 or DmxA. Though they are T6 deformities, the septa appear quite different radiographically and on visual inspection.

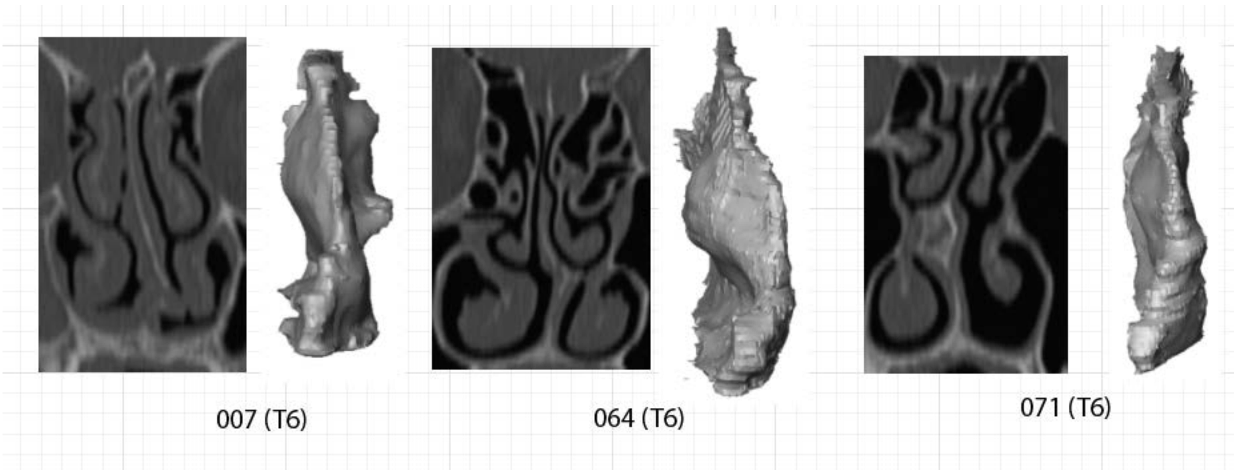

Figure 56: Axial CTs and surfaces for the three T6s on PC2

On PC2 the most displaced are 009 and 031. The central perpendicular plate (ethmoid) - cartilage ossification line disturbance results in a "C" curvature. However both 009 and 031 are Mladina T3s, which are described by Mladina 2015 as unilateral vertical deformities, and don't appear severely deformed. Is it the classification methodology that is failing to identify the most severely deformed septa or the traditional GMM method of Procrustes analysis using principal components misidentifying the most deformed? Actually both, as will become clear in chapter 6.

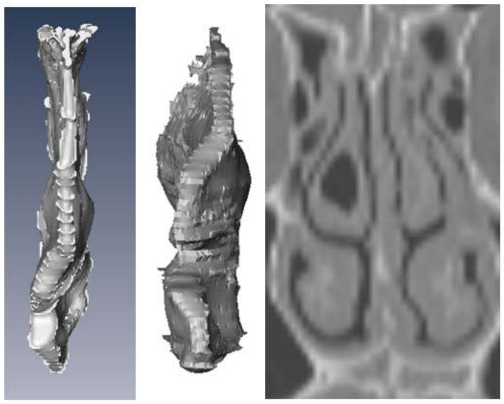

009 T3 Coronal & Axial surfaces & CT

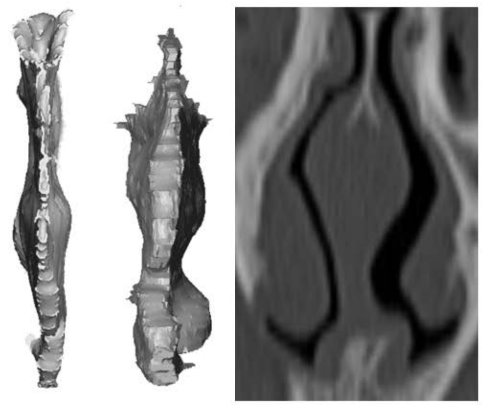

031 T3 Coronal & Axial surfaces & CT

Figure 57: Coronal and axial surface views and axial CT views of Type 3 deformities.

On PC1- specimens 030, 070, and 077 are most displaced:

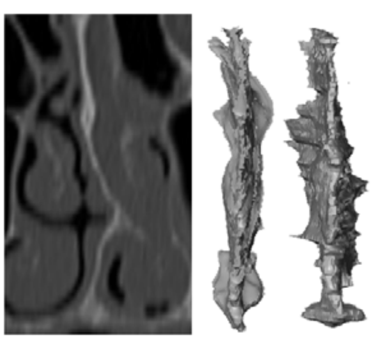

030 T5

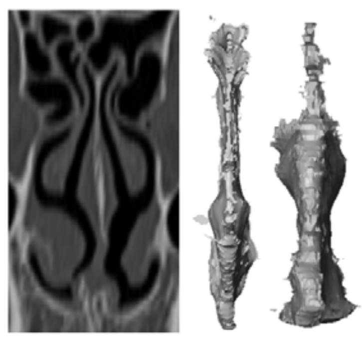

070 T1

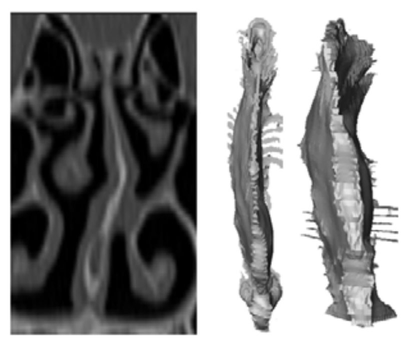

077 T2

Figure 58: Coronal and axial surface views and axial CT views of T1, T2, and T5 deformities.

On PC1+ specimens 076, 086, and 088 are most displaced:

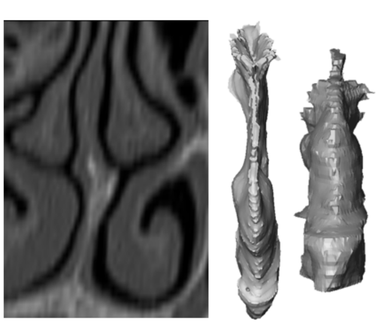

Fig. 67: 076 T2

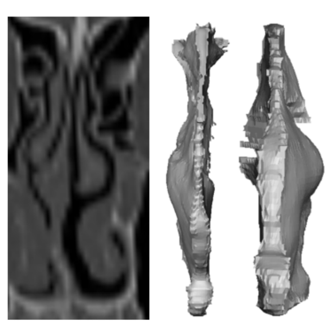

Fig. 68: 086 T3

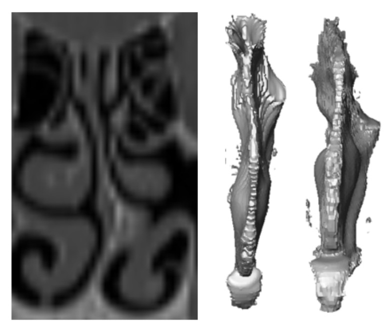

Fig. 69: 088 T5

Figure 59: Coronal and axial surface views and axial CT views of T2, T3, and T5 deformities.

Similarly for the cases of extremely high or low PC1 scores, the most displaced cases are comprised of a variety of types (T1, T2, T3, and T5) with varying degree of airway obstruction on visual inspection of the CT. None of these specimens are among the most severely deformed as determined by the methods of chapter 6. Takahashi 1987 noted that morphological change was consistent with the severity of the nasal septal deformity, as the severity increased so did the concavity of the perpendicular plate of the ethmoid. While principal components do not measure severity, this analysis apparently failed to offer any meaningful insights into the clinical variation of the nasal septum.

Just as it appeared that traditional GMM approach produced an ambiguous, non-quantitative result, our fortuitous discovery of the extensive work of Ryo Takahashi in an equally fortunate combination with Bookstein's underused concept of partial warps has culminated in a revision of nasal septal analysis. First a review of Takahashi's extensive research of nasal septal deformities is in order, as it is in that context that the revised analysis finds coherence.

Chapter 5

The Concept of Evolutionary Paradox

A comprehensive review of the evolution and formation of the nasal septum, and the etiology of septal deformity.

Revisiting a masterpiece.

While producing the earliest revision of this thesis, I came across a description of a paper in Miles (2007). As previously noted, Miles wrote, "*Ryo Takahashi provided the most comprehensive body of work ever produced in the study of the nasal septum. The work of Takahashi is primarily focused on the development, function, and etiology of septal deformity*". Obtaining this paper proved elusive as it wasn't available locally but a copy was found by my supervisor (FB) in a German used bookstore. Later a copy of an equally impressive manuscript, "A collection of ear, nose and throat studies" (Takahashi 1971) also turned up in a German used bookstore. (Note added in proof: As of 1 January, 2018, no copy of either of these books is available anywhere in the universe of internet bookstores [www.bookfinder.com]).

Ryo Takahashi, a Japanese rhinologist born in 1911, was active from 1938 to 2005 in medical research and education and in rhinology organizations. He was professor and director of the Department of Otorhinolaryngology at Jikei University School of Medicine, Tokyo, Japan. His publications were almost entirely in Japanese other than his English language treatises of 1971 and 1986, and a summary published in 1988. Language and difficulty of access probably account for the low citation count (36 in Google Scholar for the 1986 paper, and 17 for the 1988 paper as of January, 2018). In spite of this, the paper (1987) and the book (1971) are masterpieces of observation, analysis, and thoughtful natural history of an almost universal design flaw in H. *sapiens,* explaining the 95% incidence of nasal septal deviation in an evolutionary context.

None of the 16 classification schemes reviewed for this project cited Takahashi. As Takahashi (1987) notes: "Most have tried to classify the great variety of morphological types of deformity by clinical observation. As the process of formation of septal deformity has come to be elucidated and histological findings have been made, these classifications appear simplistic. This was a natural consequence of classification system originally based on intranasal findings alone, and which failed to take etiology into account."

In his "Evolution of the Human Head," Lieberman (2011) fails to cite Takahashi, offers a brief explanation of nasal septal and nasal cavity growth, and makes no mention of nasal septal deformity. Of the papers I reviewed, only four cite Takahashi. Other than the note by Miles, Verwoerd (2005), refers to Takahashi when noting that nasal development ends later in males and that the ethmoido-vomeral junction may show developmental variations. Holton (2011) cites Takahashi when indicating that both the nasal septum and the vomer may be affected by nasal septal deviation, and Hartman (2016) cites Takahashi in the references but makes no mention of his work in the body of the text. The superficiality of these citations would suggest that Takahashi appears to have been writing for scholars of craniofacial evolution, not clinicians.

This chapter reviews Takahashi's thoughts on the formation of the nasal septum and the etiology of the nasal septum. Alone in presenting a comprehensive review of the nasal septum and integrating that knowledge into a hypothesis of nasal septal deformity, Takahashi's paper necessitates a careful review. From the order in which he presents the material, and from his analysis of the implications of those findings, it is remarkable how it helps the interpretation of our findings. It is the consistency of his research and theoretical musings with our findings, not those of earlier classifiers, that merits this full chapter review.

Takahashi (1987) used the following human sample:

Takahashi's Human Sample

Age	10s	20s	30s	40s	50s	60s	70s	80s	Totals
Male	10	31	27	50	35	19	7	2	181
Female	6	21	13	12	14	4	6	0	76
Total	16	52	40	62	49	23	13	2	257

Table 9; Human sample composition from Takahashi 1987 p. 19

Takahashi's Work

Starting in 1938, usually in Japanese, Takahashi wrote extensively on the nasal septum and related structures. Here are 18 of his findings:

1. There is an association between the length of the processus vomeris and the severity of projections of the nasal septum (ridges and spines). The shorter the processus vomeris, the more severe the projections (this is later related to the cranial base angle).
2. The surface area ratios of the septal cartilage, perpendicular plate and vomer have varied over evolution from non-primate mammals to man.

Non-Primate Mammals	Primates	H. sapiens	Evolutionary Effect
→	Septal Cartilage	→	↓ Decreased area
→	Perpendicular Plate	→	↑ Increased area
→	Vomer	→	↔ Unchanged

Table 10: Surface area ratio: Septal Cartilage: Perpendicular Plate: Vomer. From Takahashi 1987, p8.

3. Biomechanics of Nasal Septal deformity.

The effects of the application of physical stress to the nasal cavity will vary with location. This is explored in depth later in this chapter in the discussion on biomechanics.

Location	Effect of Stress
Nasal septum	Curving of the upper anterior portion of the nasal septum
Within the nasal septum	Formation of ridges and spines due to buckling between the septal cartilage and the vomer.
Area between the perpendicular plate and the septal cartilage.	Curvature of the region proximal to the ossification line.

Table 11: The effect of stress on regions of the nasal septum. From Takahashi 1987 p. 9

4. The region of ossification between the cartilaginous and osseous regions of the perpendicular plate is termed the ossification line. In the presence of a deformity, the line of ossification forms an acute angle with the convex side of the septum. This is a mechanical functional adaptation to reinforce the convexity. The ossification line is most conspicuous at the anterior aspect of the processus vomeris. If the deformation extends into the groove, the base of the groove will have a marked modification. As the deformation increases in severity, the lateral surface of the septum extends to the lateral surface of the groove on the side of the deformity. The anterior vomer is most likely to be affected by growth and development of the septal cartilage (Takahashi 1987 p. 9)

5. Nasal Growth and septal deformity (Takahashi 1987 p. 11)

0 – 10 years	High incidence of projections.
10+	Increasing curvature of the upper portion of the nasal septum
Puberty	Severe curving and spines
17-18	Deviated nose begins to be seen.
Infancy and childhood:	Greatest growth along the anterior – posterior axis.
Puberty and adult:	Growth increases on the superior – inferior axis. There is no relationship between the length of the palate and NSD.

6. The fetal nasal septum (Takahashi 1987 p. 11)

In a sample of 78 human fetuses, 25% do not have a straight nasal septum. One at 10 months exhibited severe NSD, one at 7 months showed moderate NSD, two and five months and one at 8 months showed slight NSD, while one at 5 months, two at 7-8 months, and 1 at 10 months exhibited very slight NSD.

7. Birth and the nasal septum (Takahashi 1987 p. 13)

There is no relationship between the morphology of the nasal septum and the duration of parturition, fetal lie, normal versus C-section, or maturity of the fetus and the morphology of the nasal septum.

8. Incidence of nasal septal deformity in the Takahashi sample (Takahashi 1987 p. 13)

Sample of 5317 individuals

Age 0 – 12	Low incidence of NSD. 50% straight septa.
End of Puberty	10% straight septa.
Age 21	<u>1.3% of males with straight septa.</u>
	<u>9.5% of females with straight septa.</u>
	98.7% of males and 90.5% of females deviated
	Equal L – R deviation at age 20

9. Nasal septum relationship to middle and superior conchae (Takahashi 1987 p. 14)

Excessive growth and development of the middle and superior conchal walls (on the side that becomes the concave side of the nasal septal curvature.

⇩

Pressure on the nasal Septum

⇩

Curving of the nasal septum (Usually caused by pressure on the middle conchae)

⇩

Usually affects the thin upper posterior half of the nasal septum.

⇩

As the nasal septum curves, the concha act as a space-filling lesion.

10. Evolution of the Nasal Septum and Nasal Septal Deformity

Takahashi believes that nasal septal deformity results from the imbalance caused by the enlargement of the neurocranium and retraction of the maxillo-facial region that evolved during the descent of Homo. The most conspicuous changes in the shape of the cranium occurred during the transition from Homo neaderthalensis to Homo sapiens.

Australopithecus

⇩

Homo erectus ⇨ Neurocranium is enlarged and lengthened.

⇩

Homo neanderthalensis (Dolichocephalic)

⇙

Homo sapiens: Brachycephalic

Retracted maxillo-facial region ⇨ Deformity of the NS

Increased flexion of the cranial base (135°

Takahashi's early work laid the groundwork for his comprehensive "evolutionary paradox" theory. Point 1 speaks to Takahashi's early focus on the role of the vomer in nasal septal deformity, from the length of the processus vomerus and later deformation of the chondro-vomeral junction. Point 2 deals with the changing relationship between the septal cartilage, perpendicular plate, and the vomer during primate evolution. In point 3 the elucidation of the effects of physical stress on the nasal septum is later integrated with the evolutionary and developmental forces on the septum. With point 4, Takahashi outlines the connection between ossification of the perpendicular plate in terms of functional adaptation and future deformity. The early incidence of NSD in fetal life, and the increasing frequency during growth underscore the relationship between NSD and growth and development in point 5. Points 6 and 7 relate NSD to growth, thus discounting the trauma association. The frequency of NSD in point 8 corresponds to our study's finding. Point 9 considers the effects of hypertrophic conchae while point 10 presents an evolutionary explanation of NSD that is consistent with hominid evolution and current data on NSD.

Takahshi's classification of nasal septal deformity is more comprehensive than any of the previously described classifications, not only being more descriptive of nasal septal morphology but including the septum's relationship to proximal structures. It is not a classification in the context of Mladina or any of the other traditional classifications. It is rather a guide as to how to examine the nasal septum in consideration of the frequency of the factors, characteristics, inter-relationships related to NSD, and his above summarized theory "evolutionary paradox".

Classification I: Severity and Laterality of NSD according to Takahashi (1987)

Grade	**Description**	**Frequency (%)**
I	Straight or very slight curving	9.3
II	Very slight – slight moderate curving. Mainly projection of the vomer	16.8
III	Slight – severe curving. Mainly projection superior and inferior to the vomerine groove.	18.0
IV	Very slight – severe curving. Mainly curving of the perpendicular plate.	17.6
V	Slight to severe curving. Mainly curving of the perpendicular plate and vomer in continuum.	15.2
VI	Slight to severe curving. Mainly curving of the perpendicular plate and projection of the vomer. (DmxA or Mladina T6)	12.5
VII	Very slight – severe curving. Curving of the perpendicular plate and ipsilateral projection of the vomer.	3.5
VIII	Slight –severe curving. Mainly tilting of the perpendicular plate in one direction	7.0

Table 12 : Classification of the severity and laterality of nasal septal deformity (NSD) from Takahashi 1987 p. 24

This classification was made on dry skulls where the cartilaginous portion of the septum wasn't present. Therefore the classification represents the relationship between the perpendicular plate and the vomer. The diagnostic position corresponds to an estimated cross-section one third the distance from the anterior end of the nasal septum to the posterior. The upper 3/4 represents the perpendicular plate and the remaining represents the vomer.

The Takahashi type 6 coincides with Mladina T6 and our DmxA. More importantly, the 12.5% rate of occurrence reported by Takahashi coincides with the rate of severe deformity that we report using different GMM analytics employing the quantification of bending energy. This is discussed in detail later in the next chapter.

11. Characteristics of Classification I NSD

Relationship	Description
Severity of Deformity and Morphology of Deformity	Vomeral region projections resulted in severest deformity
Curvature and Projections	Majority had curvature to left and no projections.
Severity and ridges, ridges spines and spines.	42.6% curvature and no projections (Least severe NSD) 38.4% curvature and ridges 12.0% curvature and ridged spines 7.0% curvature and spines (most severe NSD)
Morphology of deformity and relative position of Inferior conchae (Distance of conchae from NS)	No correlation between Conchae - Perpendicular Plate and NSD Correlation between Conchae – Vomer and NSD
Perpendicular Plate and Middle Conchal walls. The warping of the concha walls = asymmetry.	Those that were strongly asymmetrical had some middle conchae that extended over the midline into the curvature concavity, but others did not. Important from etiological, morphogenetic and clinical viewpoints.
Morphology of NSD and the classification by degree of asymmetry of the superior I/2 of the nasal cavity.	83.9% showed asymmetry and 36.4% showed strong asymmetry. There is a correlation between the degree of asymmetry of the superior ½ and the morphology of NSD. *Both the conchae and nasal septum develop from cranial base cartilage.*

Table 13: Characteristics of nasal septal deviation from Takahashi 1987 p. 21-22.

Classification II: Relationship between Nasal Septum and Middle and Superior Conchal walls.

Type	**Nasal Septum Curvature**	**Sub-type description**
A	The NS is straight	4 Subtypes: Conchal walls are mostly parallel to the NS. Subtype Ac is the only one showing asymmetry. The NS isn't involved in the NSD.
B	Septal curvature	2 Subtypes: The middle conchal wall on the concave side is parallel to the curvature of the nasal septum.
C	Usually septal curvature	4 Subtypes: Usually the space between the septum and the middle conchal wall on the concave side has widened. The middle conchal wall is not involved in the septal curvature.
D	Septal curvature	4 Subtypes: Some or most of the middle conchal wall on the curvature side has moved toward the septum.

Table 14: Relationship between the nasal septum and the conchal walls from Takahashi 1987 p. 23-24

12. Relationship between Classification II and the degree of NSD:

There is a close correlation between Classification II and the degree of NSD:

Type A	Less severe NSD	More space between the NS and the middle and upper conchal walls (Ethmoid)
⇩	⇩	⇩
Type D	More severe NSD	Less space between the NS and the conchae

Table 15: Relationship between the nasal septum and the conchal walls from Takahashi 1987 p. 25-27

13. Relationship between Classification I and II:

Classification II Type	Correlation	Relationship to Classification I
A, B, C, D	Yes	There was a general correlation between the classifications by the positional relationship of the NS and the upper and middle conchae and the 8 types of NSD
A, C	No	The middle and superior conchal walls on the concave side of the NS are not involved in NSD
B, D	Yes	These types are involved with NSD
B**, D (Type II)**		2.4% of specimens were Type II where the vomer alone is involved with NSD
B, D (Types III – VIII)		35.0% of specimens are Types III – VIII where the curving Perpendicular Plate is involved with NSD. The middle and superior conchal walls on the concave side of the NSD are related.

Table 16: Relationship between Takahashi Classifications I and II from Takahashi 1987 p. 25

14. Classification III: Relationship between the shape of the lower anterior edge of perpendicular plate and the degree of NSD.

Takahashi classified the boundary between the Perpendicular Plate and the septal cartilage (line of ossification) into 4 types:

	Shape of the Anterior-Inferior edge of the Perpendicular Plate			
NSD	**Straight**	**Concave-Convex**	**Convex**	**Concave**
Straight	5	0	1	3
Very Slight	13	6	5	3
Very Slight-Slight	14	9	6	5
Slight	20	17	15	6
Slight-Moderate	17	12	9	2
Moderate	16	13	17	10
Severe	8	9	10	9
Totals	93	66	63	38

Table 17: Nasal septal deviation and curvature of the perpendicular plate of the ethmoid from Takahashi 1987 p. 27.

Recall the definition of the ossification line (p. 65). This boundary represents how the ossification mechanism proceeded. In general, with more pronounced ossification, the perpendicular plate tends to be concave and NSD tends to be more severe.

15. Plane of fusion between the anterior edge of the Perpendicular Plate and Septal cartilage and the relationship to the degree of NSD.

Takahashi determined that a concave plane of fusion points in the direction of the curvature of the deformity in 38.1% of cases. With severe NSD the plane of fusion was more likely to be concave, with flat or convex planes more often seen with a minor degree of NSD. In order of severity of deformity (Severe to mild) the plane goes from concave to flat to convex to irregular.

The rate of ossification is dependent on the position of the plane of fusion.

Upper	Smooth surface of plane (ossification is first completed in the upper region.
↓	↓
Lower	Rough surface (incomplete ossification – surface concavities indicate ossification is still in progress)

16. Relationship between the degree of deformity of the Perpendicular plate and the Vomer.

Takahashi determined that while it is possible for the Vomer to be straight or only slightly deformed even when the Perpendicular Plate is considerably deformed, the opposite wasn't true. When the Vomer is considerably deformed, the Perpendicular Plate is equally deformed. There is no relationship between the thickness of the Perpendicular Plate and the thickness of the superior edge of the Vomer.

17. Classification IV: Abnormalities of the anterior edge of the Perpendicular Plate

Type	Description
A	A small, low, conical protuberance found on one side of the upper part of the anterior edge of the Perpendicular Plate.
B	A low, rounded protuberance found over the upper two thirds of the Perpendicular Plate immediate posterior to its posterior edge.
C	A small hemispherical protuberance with well-defined borders seen at the anterior edge of the Perpendicular Plate.

Table 18: Classification of perpendicular plate anterior edge abnormalities from Takahashi 1987 p. 28.

18. Classification V: Classification by degree of morphological abnormality of the vomer.

The Vomer exhibits curvature along both the anterior-posterior and superior-inferior axes. Takahashi has classified this by age and morphology. The classification includes illustrations and is reproduced below as a figure.

S_1 to S_4 corresponds from several months in the fetal period to age 10. The Vomerine groove is open at its upper edge. The upper aspect of the groove is **Y** shaped in early fetal life, then deepening and becoming **U** shaped. Ossification begins on one side of the inside surface of the superior edge. (Ossification begins as soon as superior edge comes into contact with the area of the ossification line). By the S_4 stage, both sides of the groove are in contact and ossification occurs on both sides

F_1 to F_2 begins when the surfaces of the vomerine groove begin to fuse, closing the groove and forming the vomerine canal.

T_1 to T_3 occurs from 20-60 years of age. The vomer increases in height and undergoes compaction.

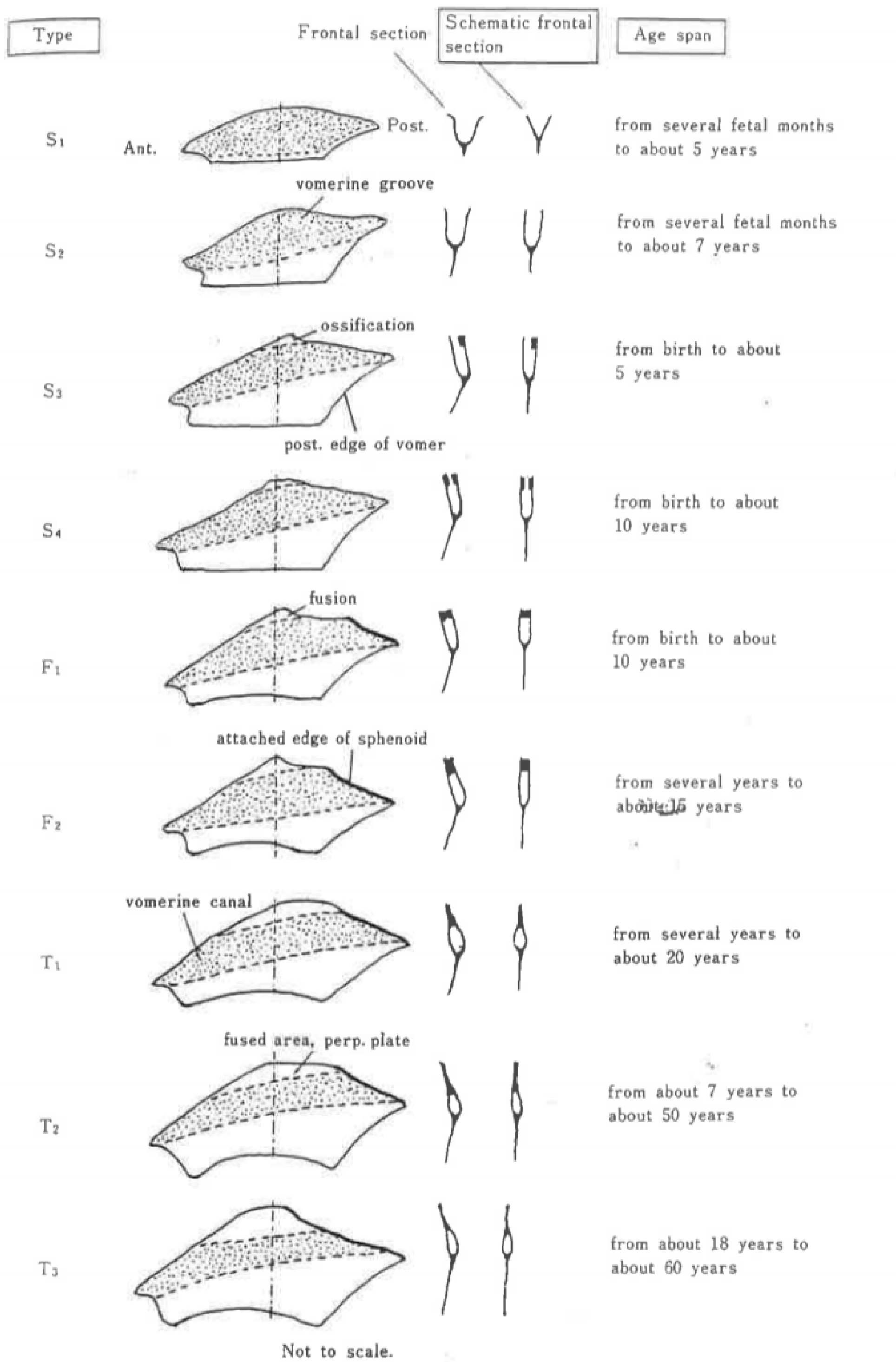

Fig. 16. Classification by configuration of vomer and vomerine groove.

Figure 60: Classification of the configuration of the vomer and the vomerine groove from Takahashi 1987 p. 37.

Takahashi's focus on the vomerine groove and the vomer is the key to understanding the "Evolutionary Paradox". Retraction of the mid-face in humans and the resultant restrictions on vomer length, he emphasizes and stresses on the chondro-vomeral junction leads to ridge and spine formation and curvature of the septum. Takahashi asked why ossification occurs at this site.

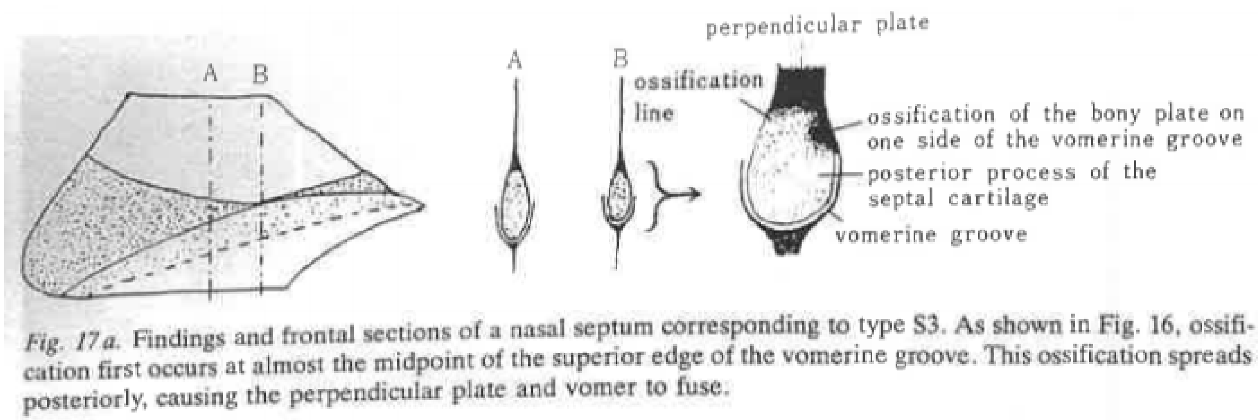

Figure 61: S_3 classification of the nasal septum and its relationship to the vomerine groove and the ossification line from Takahashi 1987 p. 38.

He determined that as soon as the ossification line between the cartilaginous nasal septum and the developing perpendicular plate (mesethmoid) contacts either the right or left plate of the vomer, ossification begins at that contact point. The ossification then comes in contact with both vomer plates, resulting in type S_4 (figure 60).

The left and right plates of the vomer fuse resulting in type F_1. By age 15 the vomer is a type F_2, with the vomer bone becoming thinner. Types T_1 (age 20) to T_3 (age 60) develops with the vomer increasing in height (figure 60)

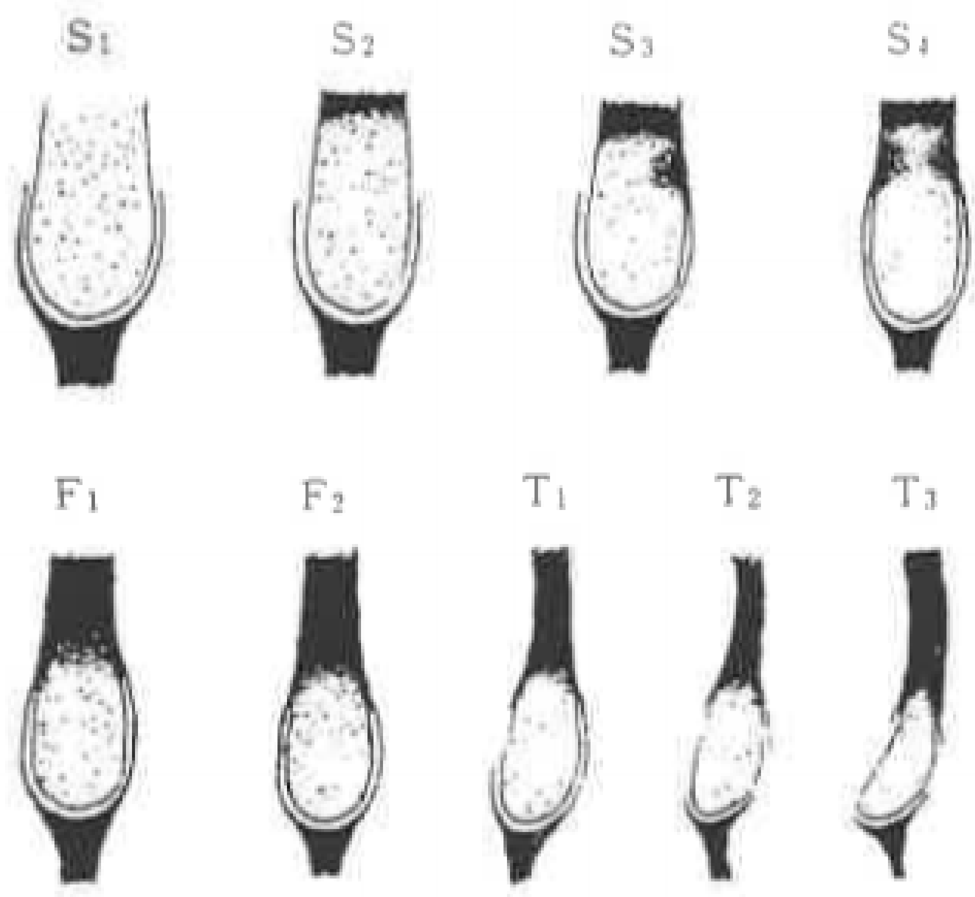

Figure 62: Schematic representation of Classification V (Morphological classifications of the Vomer based on its development as per Takahashi 1987 p. 38.

The Nasal Septum in Primates other than Man

As outlined previously, Takahashi has comprehensively detailed the characteristics, relationships, and classifications of nasal septal deformity in man. In a series of studies he has compiled similar analyses of other primates. This helps determine which aspects of NSD are a consequence of a failure to adapt to evolutionary change, and which are due to life experiences such as birth and trauma. A summary of the primate studies is presented in the table below:

Relationship	**Apes** (Chimpanzees, Gorillas)	**Monkeys** (Macaques, Colobus, Squirrel,Rhesus)	**Prosimians** (Lemurs, Indris)
Incidence of NSD according to severity	NSD = 50.8%	Macaque 33.6%, Rhesus 22.7% Squirrel Monkey 5.4%	0%
Incidence of NSD according to sex	Chimps:39.3%M,45.3%F Gorilla: 69.2%M,53.5%F	Macaque: 40.8%M, 28.6%F. Rhesus: 22.3%M, 23.1%F Squrirrel 5.7M, 5.1F	0%
Location of NSD (As reflected by Vomer)	Less chance between vomer & septal cartilage	Macaque 17.5% Rhesus 10.0% Red Colobus 6.6% King Colobus 20.0% Squirrel 100%	0%
Location of NSD (As reflected by PP)	More likely between PP & septal cartilage	Macaque 82.5% Rhesus 80.0% Red Colobus 93.3% King Colobus 80% Squirrel 0%	0%
Curvature	Curvature (50.2% with slight). No projections without curvature. Extend from Septal Cartilage to PP, usually in upper half of NS.		Extremely slight curvature found in only 1 male lemur.
Projections	Projections were slight even if curvature was marked. Projections form between Septal cartilage & vomer.		0%
Vomer	Thin in Chimp. Very thick in Gorilla.		
Perpendicular Plate	Thin in both chimp. And gorilla. Shape of Anterior edge: Chimp: Convex (46%) Straight (27%). Gorilla: Straight (34%), Concave (32%)		
Conchal Walls	NSD associated with Conchal wall abnormalities: Chimps (20.9%), Gorilla (14.2%)	NSD associated with Conchal wall abnormalities: Macque (4.1%) Colobus (1.2%) Squirrel (0%)	0%

Table 22: Nasal septal deformity for different species. From Takahashi 1987 p. 41 – 53.

The fundamental differences among the groups concern the incidence of nasal septal deformity. This is summarized by Takahashi in the following charts:

62 *R. Takahashi*

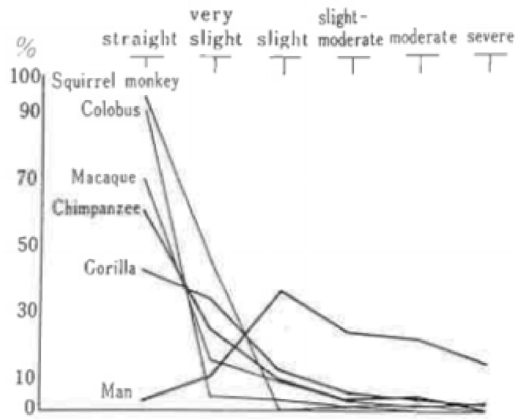

Fig. 22. Degrees of septal deformity in Man and primates.

Figure 63: Degree of deformity in man and primates, from Takahashi 1987 p. 62

Takahashi concluded that NSD first occurred in monkeys, markedly increased with the apes, and became very varied with man. Overall incidence is given in figure 18

Table 34. Incidences of septal deformitiy in prosimians, monkeys, apes, and Man (%).

	degrees of deformity	straight	very slight	slight	slight-moderate	moderate	severe
Man		3.1	22.9	22.6	16.3	21.0	14.0
ape	chimpanzee	58.6	25.1	10.2	2.3	3.2	0.5
	gorilla	39.7	31.9	16.8	4.8	4.8	1.8
	orangutan	64.3	21.4	14.3			
catarrhine	macaque	71.8	15.5	7.3	1.7	1.9	1.7
	colobus	86.6	3.5	3.0	1.2	0.8	
platyrrhine, squirrel monkey		94.6	4.4		0.9		
prosimian	lemur	96.2	3.8				
	indri	100.0					

Figure 64: Nasal septal deformity by species. From Takahashi 1986 p. 62.

Takahashi concludes that NSD first arose in monkeys, increased in incidence in apes, and became the norm in *Homo*. Coupled with the occurrence of projections in humans, Takahashi proposed the following mechanism:

A projection first manifests as a ridge in the lower anterior region of the nasal septum (border between the septal cartilage and the vomer).

⇩

The ridge extends posteriorly, and at the posterior end forms a ridged spine (projecting posteriorly at the site of processus vomeris).

⇩

Growth of the septal cartilage reduces, the ridge regresses, and only a spine (spur) remains.

This mechanism is unique to humans. In all the non-human specimens studied, Takahashi found only two apes with projections: one chimpanzee with moderate left spinous projection and curvature, and one gorilla with slight left spinous projection and curvature. Similarly the asymmetry of the nasal cavity involving the perpendicular plate, is to a slight degree present in lower primates and becomes marked in man. Simultaneously the asymmetries of the middle and superior conchal walls exert pressure on the vomer in man. Takahashi concluded that while in non-human primates, NSD is a consequence of the growth and development of the septal cartilage and its ossification, in humans it is the response of the superior edge of the vomer to the influence of the ossification line and the septal cartilage that accounts for the increased asymmetry in humans. Thus the septal deformity in humans is unique involving both the influence of the septal cartilage on the perpendicular plate through its ossification, and the influence of the septal cartilage on the vomer through its growth and development.

Let me summarize Takahashi to this point under different headings.

1. Growth and development

   Takahashi concludes that there are two types of nasal septal deformities:

   a. Septal cartilaginous deviation of the septum (active): This most frequently occurs in the anterior portion of the septum. This type is a result of an unbalance in the development of the septal cartilage and the surrounding bony framework.

   b. Conchal deviation of the septum (passive): This is seen in the upper posterior half of the septum, in the perpendicular plate of the ethmoid. Milder than the first type but with the septal walls in contact with the conchal walls or with adhesion of the opposing walls.

   Takahashi demonstrated that septal abnormalities began to appear with catarrhines (monkeys), increased through the apes, and then abruptly and greatly increased with hominization. These abnormalities appear early in human fetal life (25%) and continue to increase well into adulthood. Takahashi concluded that the increase in abnormalities is driven by the chondroseptum, which doesn't grow uniformly and exhibits curvature on both the anterior-posterior (A-P) and superior-inferior (S-I) axes. This results in curvature of the vomer and affects the premaxilla, maxilla, and sphenoid.

   Takahashi infers clinically from age related changes on the side of the deformity, that the incidence of the deformity is linked to the development process. Deformity is predominantly left sided during the fetal stage, becoming balanced left and right from the neonatal period until puberty, and then becoming more right sided. He concludes that during the transition from the fetal to postnatal period, the upper posterior chondroseptum ossifies to eventually form the perpendicular plate. This process occurs along the ossification line (anterior edge to the inferior edge of the perpendicular plate) which continues to ossify long after overall growth has stopped and further intensifying septal deformity.

   Unlike in other primates, in humans the relative areas of the septal cartilage decreases over time, the perpendicular plate increases, and the vomer remains unchanged. This is a result of the positional change between the neurocranium and maxillofacial cranium and between the maxillofacial cranium and the cranium base which in turn causes a change from cartilaginous to osseous tissue. With development this changes the growth direction of the nasal septum from anterior–posterior to superior-inferior. This directional change affects the vomero-ethmoidal junction in that as soon as the osseous tissue of the superior edge of the vomero-groove contacts the ossification line, it initiates fusion of the perpendicular plate and vomer.

Ossification between the perpendicular plate and the mesethmoid (ethmoidal synchondrosis) can occur until age 40. Takahashi believes that this is an ossification center (Scott 1953, Scott 1958) from the fetal period until immediately after birth) and an ossification site (Moss 1960, Moss 1968, Moss 1972) thereafter. Takahashi (1987) supports this based on chondrocyte research by Suzuki, demonstrating that the proliferation of cartilaginous tissue is promoted by the chondrocytes themselves through their production of the growth promoting cartilage-derived-factor (CDF). Suzuki found that chondrocytes that have differentiated from mesodermal cells synthesize a matrix of high-molecular substances during fetal and juvenile periods, and concluded that cartilage plays an important role in the morphogenesis of the maxillo-facial cranium. (Note to reader: Takahashi (1987) cites Suzuki and Sakuta. He refers extensively to these papers, however I have not reviewed the primary sources as they are only available in Japanese).

Vetter (1984) concluded that human septal cartilage has intrinsic growth potential. Takahashi (1987) concludes that "The above experimental results obtained by Long, Vetter, Pirsig, Suzuki, and Sakuta all clearly support the Scott theory rather than the Moss theory. He states: "I feel that it is particularly necessary to recognize as a fundamental principle that the growth potentiality and growth activity of nasal septal cartilage is generally area dependent and age dependent" (Takahashi, 1987, p. 93-95).

This is an interesting concept, as neither, Scott's or Moss's theory is able to fully explain the development of the nasal cavity. The greater part of the septal cartilage undergoes endochondral ossification, becoming the perpendicular plate, while the inferior edge (ossification line) continues to develop through intramembranous ossification, thus creating an imbalance resulting in bending. Exacerbated by the change of growth direction from A-P to S-I, this loss of balance results in a non-physiologic dysfunction in the form of morphological abnormalities. Takahashi believes that concomitant recession of the jaw and enlargement of cranial capacity further made adaptation to this imbalance impossible so that the nasal septum naturally began to exhibit abnormalities over the course of otherwise "normal" growth.

2. Biomechanics and Bio kinetics

The location of septal abnormality was highest at the junction between the perpendicular plate and the vomer, lower at the inferior edge of the perpendicular plate, and lowest at the superior edge of the vomer. The incidence of abnormality was highest in humans, lower in apes, and lowest in catarrhines. The thickness of the perpendicular plate is similar between humans, gorillas, and chimpanzees, while the vomer thickness varies. The consequence of a force on the perpendicular plate differs from a similar force on the vomer.

Utilizing a framing analogy, Takahashi postulates that a framing structure must be more rigid and stable than structures within the frame. The structures within the nasal cavity are framed by the strong and rigid maxillo-facial cranium. When stress generated by growth is strong, the structures within the nasal cavity (septum, vomer, and conchae) will deform. Stresses not dissipated by those structures will shift elsewhere resulting in protrusion of the external nose.

Weinstock (2018) has recently advanced a similar explanation for nasal deformity.

3. Function

The incidence of abnormality of the perpendicular plate in apes is one-third that of humans, while the incidence of vomer abnormality in apes is twice that of humans. Takahashi inquired as to why "what functions physiologically in non-primate mammals became unable to do so in Man." Examining Moss's theory of the functional matrix, Takahashi emphasized that Moss failed to explain how the functional matrices control growth or how that control proceeds at the cellular and molecular levels. Furthermore, why is the regulatory function of the functional matrix unable to cope with the stresses of growth to prevent morphological abnormalities? It is unknown if Moss ever cited Takahashi.

This question of whether the nasal septum is an active growth control center (Scott) or passive (Moss) responding to soft tissue control has defied resolution for 50 years. More recent research has supported Scott's theory that the cartilaginous septum is a primary cartilage representing the anterior extension of the cranial base, and like other primary cartilages the septum acts as a growth center.

Al Dayeh (2013) monitored real-time anteroposterior growth of the nasal septal cartilage and the nasalfrontal suture in pigs in high resolution with real-time monitoring. Their results supported Scott's theory that the septal cartilage drives sutural growth. Goergen (2017) while studying early development variation concluded that the cartilaginous nasal septum remains an active growth center until age 6 to 8.

Marulanda (2017),has shed further light on this issue. Using a mouse model for Keutal syndrome, Marulanda studied severe midface hypoplasia in Mgp-/- mice. The Mgp promotor is highly active at the cranial sutures, cranial base synchondrosis, and nasal septum. While the cranial suture remained active with a mild increase in mineralization with no reduction in the length of the cranial base, the nasal septum was abnormally mineralized. The authors believe that their data supports the original theory proposed by Scott that the nasal septum acts as a critical growth element during facial development. Takahashi was prescient in synthesizing his theory of facial growth and development by melding those of Scott and Moss.

Takahashi believes that the difficulty lies with the conflict between the chondrogenesis of the cranial base and nasal septum and the skeletogenesis of the vomer and facial bones. The chondrobasicranium develops slowly, in 3D, and under the control of genetic factors, while the desmocranium grows rapidly, in 2D, and under the involvement of environmental factors. He concludes that unless the growth of the nasal septum and ethmoid (chondrobasicranium) is stronger than the facial skeleton and vomer (desmocranium), the control of craniofacial formation will be difficult.

Takahashi's salient point is that the chondrovomeral junction (chondrocranium and desmocranium junction) "bears the strain of evolution", and that "the septal component represents the response of the chondrovomeral junction to evolution".

4. Evolution

Takahashi terms a "Paradox of Evolution", the intranasal morphological abnormalities that began with hominization. Since morphological abnormalities can be seen in presently living apes, current human abnormalities must be an intensification of previously existing morphological abnormalities. There is growth of the chondrocranium initiated by the chrondrobasicranium and chondroseptum, then later growth and ossification of the cartilaginous nasal septum and development of the nasal cavity under mucosal control.

Takahashi notes that the most distinctive finding in the human nasal septum is the imbalance in the occurrence of septal spines. Not seen in non-primate mammals or lower primates, and less than 1% of apes, spines occur in 7.0% of humans. Proximal to the nasal septum, an imbalance is manifested in warping of the middle and superior conchae (which have the same embryologic origin as the nasal septum) and asymmetry of the inferior concha.

Of interest, Takahashi notes that “In Man, these have resulted in the warping of the nasal cavity which I feel should be emphasized as having topographical and clinical significance”.

Takahashi’s early work (1954, republished in 1971), emphasised the unique presence of almost universal septal deformity in *Homo sapiens*, infrequent occurrence in other primates, and absence in other mammals. The principal difference between man and other mammals is centred on the vomeral groove. While in non-primates the vomeral grove is filled with fatty tissue in which the nasal cartilage is embedded, in primates this fat-filled groove no longer exists. Takahashi noted that in man the groove frequently shows structural changes that, he hypothesized, are a consequence of pressure exerted by cartilaginous growth.

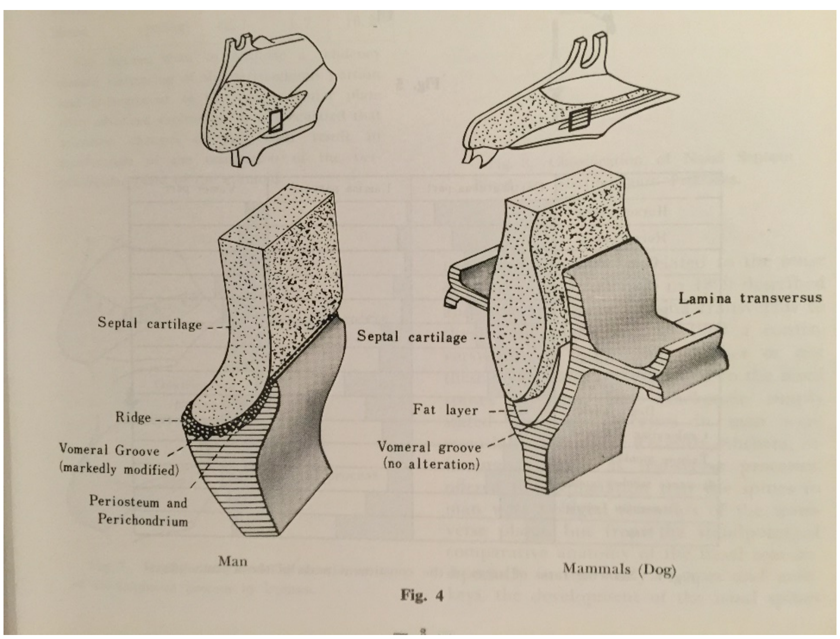

Figure 65: Left (*Homo),* right (dog). From Takahashi R, Malformations of the nasal septum, fig.4, p. 3, 1971.

From a photo-elasticity experiment,Takahashi reports findings of pronounced stress exerted from the base of the skull to the junction of the vomer and the perpendicular plate of the ethmoid. He remarked “on the peculiar structure of the vomeral process of the septum in man and on the intimate relationship of its development and ossification to the static construction of the cranial and facial bones, due to which the nasal spines are formed.” Thus the changes due to the growth of the nasal septum on the vomeral groove which supports the septum from below and which together with the forces acting inside the septum cause deformity of the septum.

It is Takahashi’s belief that there are two mechanisms involved in the malformation of the nasal septum: 1. Deformation is due to relative forces exerted by the growth of the septum itself. 2. The surrounding bony frame and its inhibitory actions deform the septum. Takahashi’s concept that a nasal septum “clamped” within a rigid osseous structure (framing structure) and confined at its base by the vomer will deform under the pressures of growth and development in a predictable fashion is illustrated by the deformation in the photo-elasticity image in figure 66.

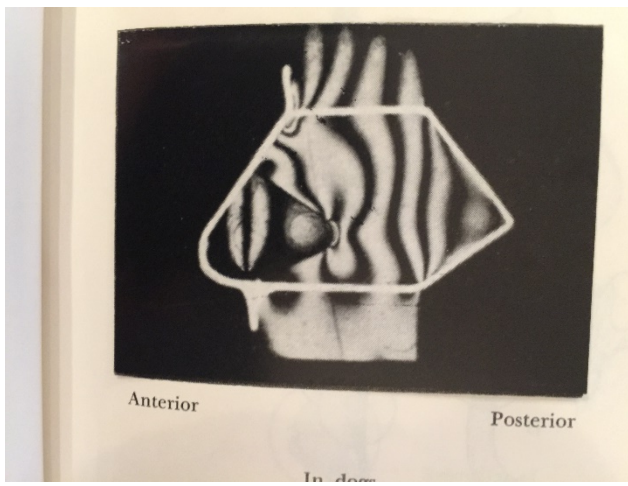

Figure 66a: From Takahashi R, Malformations of the nasal septum, fig.24, p. 21, 1971.

As the septum bends under stress forming a deep concavity in the perpendicular plate of the severely displaced samples, there was variation in the depth of the concavities. In a mechanical study on the deviation of the nasal septum, Takahashi conceptualizes the nasal septum as a column like structure set in a frame which borders most of its superior, inferior, anterior, and posterior sides. When a column is subjected to increasing pressure, at some point it will bend and then buckle.

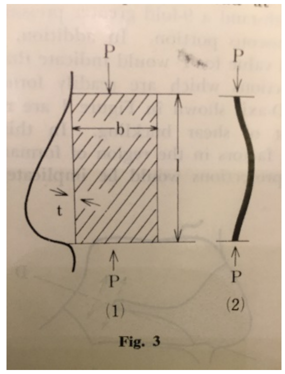

Figure 66b: The nasal septum as a column-like structure. P = value of force when buckling occurs. B = width of column. L = height of column. T = thickness of column. From Takahashi 1971 p. 89.

Assuming that the nasal septum is a weight bearing structure composed of cartilage, the top and bottom can be regarded as rotating ends. The curvature of the septum with respect to the sagittal plane that results in the concavity can be regarded as a type of buckling and can be calculated from Euler's formula:

$$P = \frac{\pi^2 EJ}{l^2} = \frac{\pi^2 Ebt^3}{12l^2} = 0.94\ kg \qquad \text{(Equation 5.1)}$$

Where l = height of column (40 mm), E = Young's modulus (7.7 kg/mm²), b = width of column (30 mm), t = thickness of column (2 mm) and P = value of the force when buckling occurs.

The upper posterior of the septum is composed of bone and must be considered as a structure with both ends fixed with a 4X increase in the value of *P* in equation 5.1. *J* is proportional to t^3 and as the bony septum is very thin (approx. 0.1mm). The resulting resistance to buckling load is very small (approx. 100g) leaving the cartilaginous part of the septum nine times more able to withstand buckling than the osseous aspect. This would suggest that part of the septum couldn't function as a loadbearing column and that bony projections are not the result of shear buckling (Takahashi 1971, p. 88-94).

Takahashi proposed that when $\boldsymbol{\beta}$ (the angle of NPD, figure 68) is small, the vomeral process is shortened and the lateral projections may be associated with the growing force of the process and its ossification.

However, the bony projections must be due to local factors along the D axis (figure 68) as the thin bony plate above and below the D axis exerts tension that resists curvature along the axis.

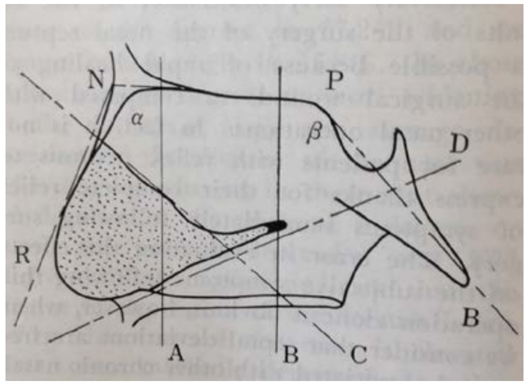

Figure 68: From Takahashi, 1971, fig 4, p88.

Anteriorly, the quadrangular cartilage may be treated as a column with free ends. This column will bend when a force (P) exceeding the critical load P_c is applied. When P exceeds P_c by 1 percent, the deflection is 9%, so that even a small additional force will cause significant curvature of the cartilage and surrounding structures. Thus when force is applied to the lower posterior region of the cartilage a severe projection will occur, and when the force is applied to the upper anterior region of the cartilage a curvature of the septal cartilage and nose will be the result.

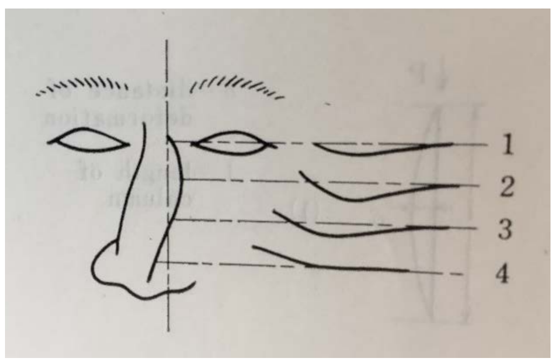

Figure 69: From Takahashi, 1971, fig 8, p92.

The load exerted by the frame will be largest in region 1-2 with the great curvature (figure 69), decreasing toward region 3-4, elevating the nasal ridge. The loads places on regions 1-4 are greatest at 2 (twice the buckling load P) and least at 4 (one quarter the buckling load P). At the same time the external nose tilts due to a tendency of the mid-sagittal plane of the external nose to rotate. This tipping of the nose occurs much more readily in cartilage than in bone.

Takahashi concludes that there are two types of nasal septal deformities:

a. Septal cartilaginous deviation of the septum (Active): This most frequently occurs in the anterior portion of the septum. This type is a result of an unbalance in the development of the septal cartilage and the surrounding bony framework.

b. Conchal deviation of the septum (Passive): This is seen in the upper posterior half of the septum, in the perpendicular plate of the ethmoid. Milder than the first type but with the septal walls in contact with the conchal walls or with adhesion of the opposing walls.

A single summary figure

The “Evolutionary Paradox” identified by Takahashi, the adjustment between the septal cartilage, perpendicular plate, and vomer resulted in an imbalance characterized by three types of morphological abnormalities:

- Curvature of the septal cartilage.
- A ridge at the junction between the septal cartilage and the vomerine groove (C’).
- A spine at the tip of the cartilaginous processus vomerus (D’).

Below (figure 70) is my favourite single summary of the evolutionary changes that have induced Takahashi’s “Evolutionary Paradox”. It maps not only the evolutionary changes, but the stresses of growth and development and the regions likely to “warp” when subjected to these forces.

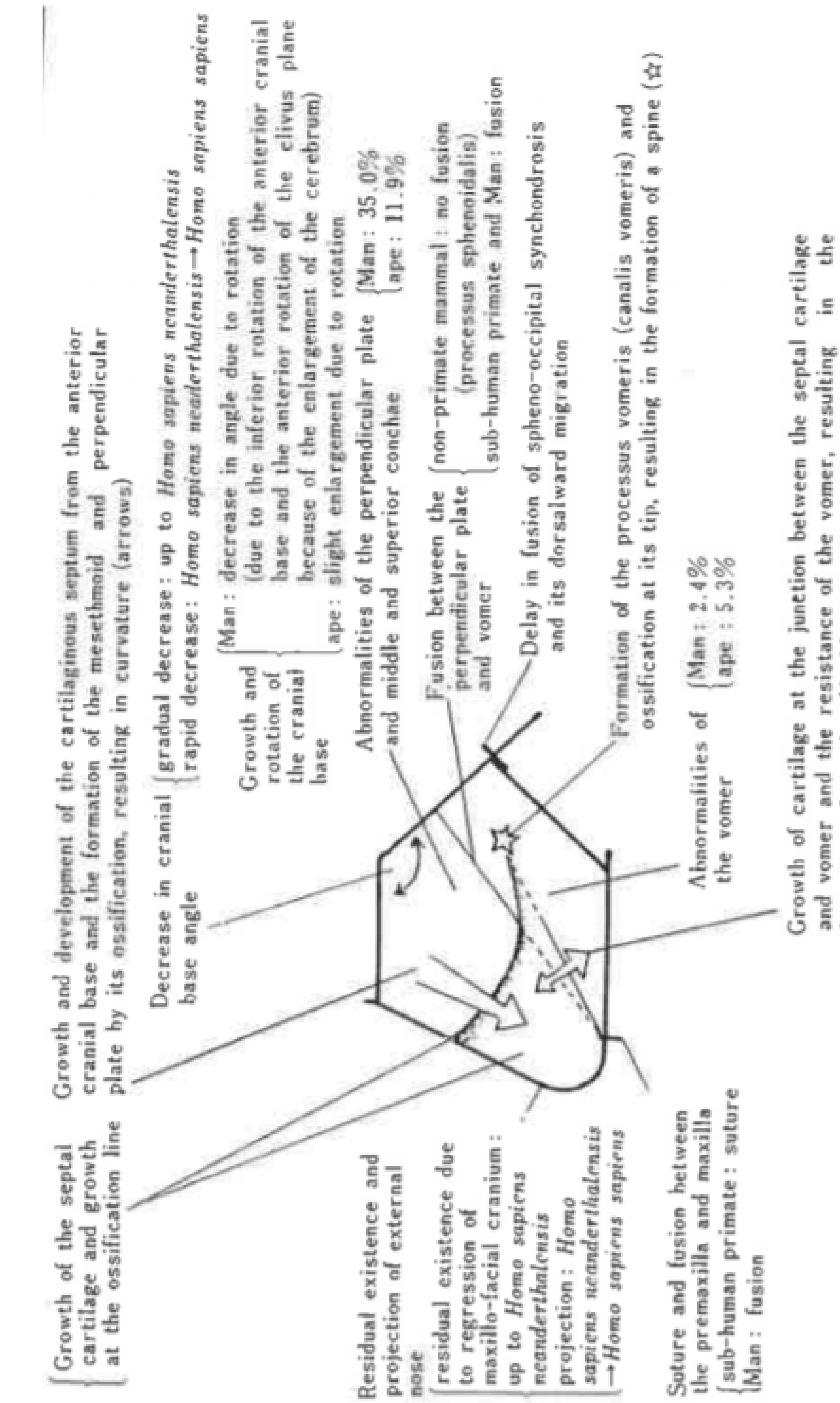

Figure 70: From Takahashi, 1987, fig 78, p 153.

What can we learn from Takahashi?

Takahashi's classifications and diagrams let us take a more analytical approach to the analysis of the nasal septum.

Takahashi Inspired Analysis

1. Sex: While septal deformity is nearly universal in males (98.7%), one in ten females (90.5%) will have a straight septum.
2. Septal Curvature:

   Type: C or S shape (C shape is less severe involving curvature of the perpendicular plate. S shape will usually involve both curvature of the perpendicular plate and vomer-cartilaginous projection)

   Location:

   Axial: Anterior or posterior? An anterior position is more likely to obstruct the valve resulting in a more severe obstruction.

   Contact with the concha or wall?

   Airway obstruction? This is subjective when viewing from a CT.

   Coronal: Superior or inferior?

   Contact with concha?
3. Lateral protrusion (my term) or projection (Takahashi)

   Ridge: Location, contact with wall and obstruction

   Spine (spur): Location, contact with wall?
4. Nasal Septum and relationship with middle and superior conchae

   Determine the Takahashi classification: Type A, B, C, D.

In particular Type D merits attention. Thirty-five percent are associated with severe NSD and it causes curvature of the septum.

Has the space between the concha and nasal septum been reduced?

Chapter 6

Findings *II*

In 1991 Bookstein cautioned as to the limitations of the traditional GMM toolkit in the analysis of non-homologous biological structures with the admonition:

> "It is no accident that they work wonderfully for grains of sand, which do not evolve by descent with modification, or grow" (Bookstein 1991).

In retrospect, the disappointing results described in chapter 4 for descriptive classification systems of nasal septal deformity and traditional GMM analysis were predictable. While the initial period of this project has been a disappointment, heeding Goethe one must move on: "By seeking and blundering we learn" (Eckermann 1848). This has resulted in the exploitation of an under-utilized but powerful aspect of GMM that fortunately supports Takahashi's findings in his conceptualization of nasal septal deformity.

In chapter 4 our data analysis based on principal components hinted, but only ambiguously at certain characteristics of septal deformity. In this chapter, the same data haves been analyzed using an alternate methodology. This necessitates a review of 1. Thin plate splines, 2. Principal warps, 3. Partial warps, and 4. Decomposition and the components of deformations.

From the data a transverse bending energy analysis was performed derived from the technique of thin plate splines (TPS) which computes the bending energy that is required to bend an infinitely thin, infinitely flat, metal plate to match the surface being studied (Bookstein 1989). Using the same data and landmark set as previously described, partial warp scores were used to determine information about the scaling of form features. Usually the coordinate basis that is rotated to produce the partial warps is the Procrustes shape coordinates. Instead the coordinates of the *actual surfaces* (the mediolateral), in place of the standard relative warp scheme (principal components in 3D) was used. We considered these variations without centering, in only one dimension (the mediolateral), as expressed in terms of an a-priori system of orthogonal patterns, the partial warps that describe the way a thin-plate spline arrives at its minimization of bending energy by a spectrum of patterns at different spatial scales. Thus after rotation of the head to the mid-sagittal plane, the partial warps concern the widths of the septal surfaces for this plane per se.

In an analogous study, Stoyanova (2015) has attempted to move age-at-death estimation from an observation/classification technique to an objective quantitative method. The paper acknowledged the limitations of variance based methods and instead chose to utilize the technique of thin plate splines (TPS).

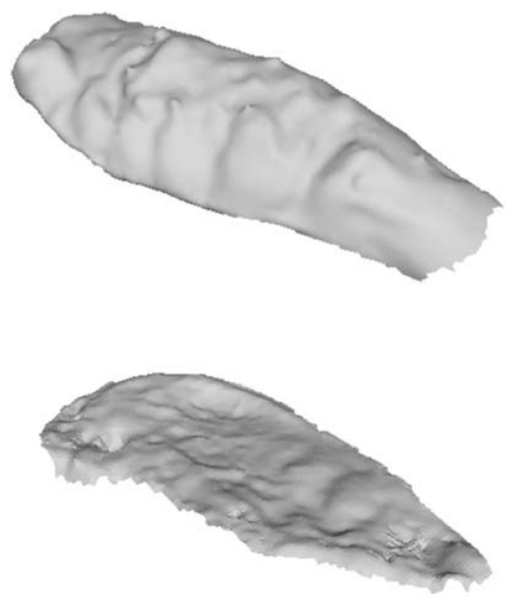

Figure 71: Top image: high billowed surface of 19 year old. Bottom image: flattened surface of 59 year old. From Stoyanova (2015).

In figure 71, the image on the top is derived from a high billowing surface while the one on the bottom is from the flattened surface of an older specimen. While a variance based method is unable to differentiate between the two specimens, the bending energy method separates the higher bending energy of the billowing surface (younger specimen) from the lower bending energy of the flattened surface (older specimen).

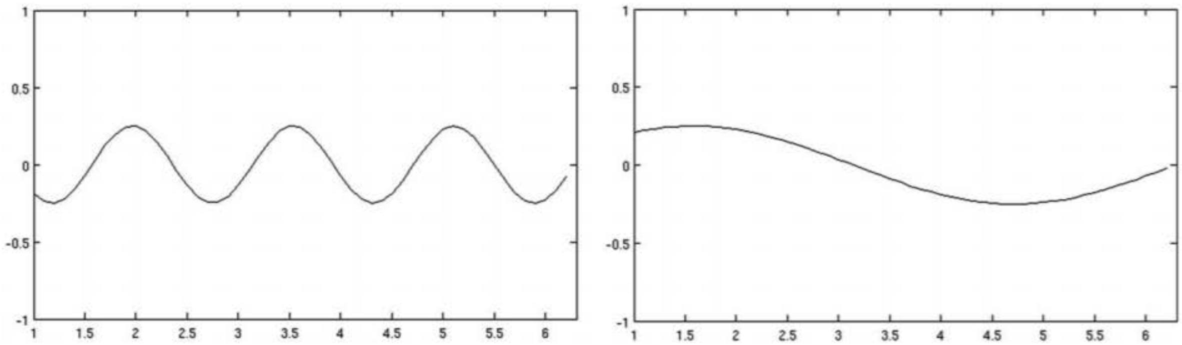

Fig. 6. Examples of surfaces that have the same variance but a higher minimum bending energy (left) and lower minimum bending energy (right).

Figure 72: From Stoyanova et al, 2015, figure 6.

In figure 72, both graphs have the same variance but different bending energies illustrating the limitations of a PCA when dealing with an organismal biological structure.

Thin plate splines

The thin plate spline permits visualization of the geometry of geometric morphometric multivariate patterns. D'Arcy Thompson developed a deformation grid method of shape modelling with an approach that used line drawings of a specimen, superimposing a grid on the first image and then performing a number of transformations that mapped point location coordinates of the first grid onto the second, thus creating a summary image of a geometric transformation. Thompson used these grids to demonstrate both linear (uniform) and non-linear (non-uniform) transformations. His method could map a transformation from one form to another but couldn't summarize geometric information for a large data sample.

Huxley, Teissier, Jolicoeur, Mosimann, Sneath and others further advanced Thompson's modelling (MacLeod 2010), but it wasn't until the 1970s when thin plate splines (called surface splines) were discovered by Harder and Desmarais. Defining the surface spline as a mathematical tool for interpolating a function of two variables. It is based upon the small deflection equation of an infinite plane" (Harder 1972). Duchon (1976) published his work on "le principe de la flexion des plaques minces" (the principle of thin plate bending). These works were done in the context of aircraft and engineering studies. The most quoted theoretical foundation remains Wahba (1990).

Bookstein's development of shape coordinates (Bookstein 1986) permitted moving from a distance based model to geometric morphometrics using the landmark coordinate values. In a review of deformation grids, Mitteroecker and Gunz credit Bookstein with introducing the method of thin plate spline (TPS) interpolation to compute deformation grids in the style of Thompson and Dürer (Mitteroecker 2009). With principal warps, thin-plate splines and the decomposition of deformations, Bookstein developed the concept of the thin plate spline, applying it to geometric morphometrics and creating the basis of the revised analysis employed in this project (Bookstein 2014). Bookstein provides a succinct review of the thin plate spline in 2D and 3D, which is summarized in turn as follows.

The thin plate spline algorithm computes a mapping function between scattered point configurations at which the height of the surface is known. If the change in position between two landmarks is measured by the deformation between the two images by using the principal axes of the transformation, the pictorial depiction of the decomposition results in a diagram of what the warp represented by the TPS does to the positions on a grid when it deforms. The thin plate spline is an interpolant that smoothly interpolates the space between points, and that minimizes the bending energy of the deformation. The bending energy of the deformation is a global figure of energy, a scalar quantity that is a quadratic form in the vector of the heights with the landmark spacing in the starting form determining the spacing. This is equal to the integral of the squared second derivatives of the deformation. The thin plate spline model can be used for both 2D and 3D data. It is a mathematical metaphor for an infinitely thin metal plate in 4D with a square grid applied to its surface, or the same in 6D with a 30 grid unit "hypersurface."

The formulas for the 2D case are as follows:

"Let U be the function $U(r) = r^2 \log \mathrm{r}$, and let $P_i = (x_i), (y_i)$, $i = 1,\ldots,k,$ be k points in the plane. Writing: $U_{ij} = U(P_i) - (P_j)$, build up matrices

$$K = \begin{pmatrix} 0 & U_{12} & \cdots & U_{1k} \\ U_{21} & 0 & \cdots & U_{2k} \\ \vdots & \vdots & \ddots & \vdots \\ U_{k1} & U_{k2} & \cdots & 0 \end{pmatrix},\ Q = \begin{pmatrix} 1 & x_1 & y_1 \\ 1 & x_2 & y_2 \\ \vdots & \vdots & \vdots \\ 1 & x_k & y_k \end{pmatrix}, L = \begin{pmatrix} K & Q \\ Q^t & O \end{pmatrix}, (k+3)\ X\ (k+3) \qquad (6.1)$$

Where O is a 3 X 3 matrix of zeros.

Write $H = (\mathrm{h}_1 \ldots \mathrm{h}_k\ \ 0\ \ 0\ \ 0)^t$ and set $W = \left(w_1 \ldots w_k\ a_0\ a_x a_y\right)^t = L^{-1}H$

Then the thin-plate spline $f(P)$ having heights (values) h_i at points $P_i = (x_i, y_i),\ i = 1, \ldots, k,$ is the function

$$f(P) = \sum_{i=1}^{k} w_i\, U(P - P_i) + a_0 + a_x x + a_y y. \qquad (6.2)$$

(The affine part of the spline: $a_0 + a_x x + a_y y$ is now an ordinary shear, metaphorically a shadow of the original plate, tilted and rescaled but not bent)

This function $f(P)$ has three crucial properties (attributed to Duchon and Meinguet):

1. $f(P_i) = h_i$, all i. The function f interpolates the heights h_i at the landmarks P_1.
2. The function f has a minimum bending energy of all functions that interpolate the heights h_i in that way: the minimum of

$$\iint_{R^2} \left(\left(\frac{\partial^2 f}{\partial x^2}\right)^2 + 2\left(\frac{\partial^2 f}{\partial x\, \partial y}\right)^2 + \left(\frac{\partial^2 f}{\partial y^2}\right)^2 \right) \qquad (6.3)$$

   Where the integral is taken over the entire picture plane. This is also called the integral quadratic variation. The integrand is the sum of squares of all the second derivatives of the warping function.

3. The value of the bending energy is

$$\frac{1}{8\pi} W^t K W = \frac{1}{8\pi} W^t \cdot H = \frac{1}{8\pi} H_k^t L_k^{-1} H_k , \qquad (6.4)$$

   Where L_k^{-1}, the bending energy matrix, is the $k\ x\ k$ upper left submatrix of L^{-1}, and H_k is the initial k vector of H, the vector of k heights."

For 2D data two splined surfaces are computed, for the x – coordinates (f_x) in which the vector of height is loaded, and for the y coordinates (f_y). For k landmarks there are k – 3 principal warps are eigenvectors of L_k^{-1} where the first principal warp has the smallest eigenvalue corresponding to the largest scale of bending. The resulting map $\left(f_x(P), f_y(P)\right)$ represents the deformation of one picture plane onto the other, mapping the landmarks onto their homologues with the minimum bending energy.

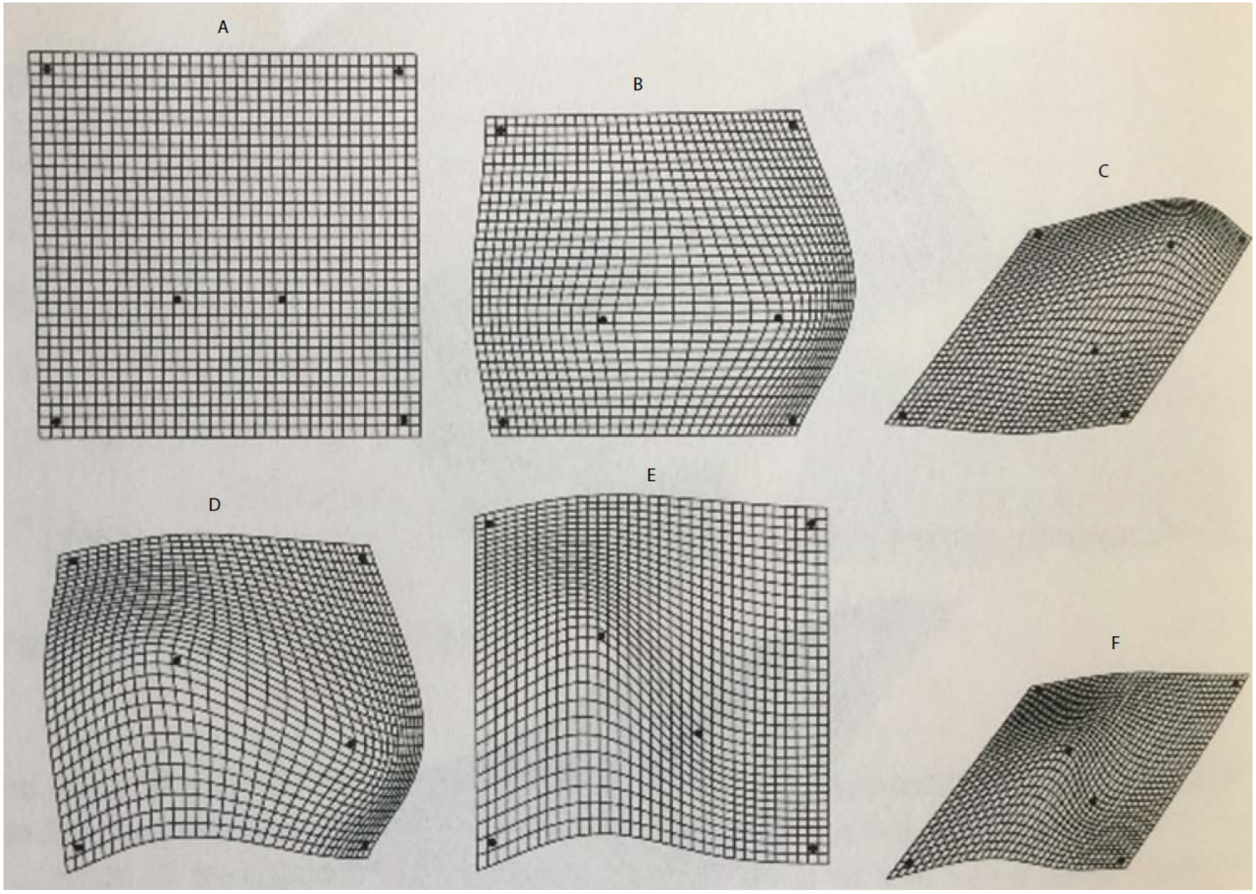

Figure 73: The TPS as a surface in four dimensions. Bookstein, 2014: p.422.

a. Starting configuration with 2 points eccentrically placed inside the square.
b. Grid where lines of y coordinates are not bent.
c. Perspective view: Rightmost inner landmark is raised in the x direction.
d. Final configuration with x and y coordinates form center are combined.
e. Grid where lines of x coordinates are not bent.
f. Perspective view: Leftmost inner landmark is raised in the y direction.

Principal and Partial Warps

L_k^{-1} has k eigenvectors that, as a set, are very useful to us.There are three eigenvectors of eigenvalue zero that correspond to the 3D family of planes over any landmark configuration, and $k-3$ non-zero eigenvectors called the principal warps. The principal warps localize within group variation of landmark data, depend only on the landmarks of one form, the "starting" or “mean form”, and are computed values of bending energy at successively lower levels of bending energy corresponding to features of deformation at successively larger values of physical scale:

Tangent eigenvalue = small feature

Smallest positive eigenvalue = relatively large feature

Because $W = L^{-1}H$ at equations 6.1 and 6.2, the spline are linear in the coordinates H of the right hand form, and the x and y coordinates are actually displacements of the shape coordinates. It is the eigendecomposition of the bending energy matrix of the mean landmark configuration of the thin plate spline results in eigenvectors of the bending energy matrix:

$$L_k^{-1} = UDU^t$$

With U orthogonal and $D = diag(e_1, \ldots, e_{k-3}, 0, 0, 0)$

The principal warps are the first $k - 3$ columns $u_1, \ldots, u_{k-3}$ of U

The partial warps derive from the eigenvectors of L_k^{-1} by weighting them by the H-vector of x-coordinates and then the y’s. Dryden and Mardia (2016) do all of this in one consistent notation. Partial warp scores are rotation of any system of Cartesian coordinates to a new orientation offering information about the scaling of form features. Omitting the affine term, they represent the superimposition of all the localizable parts of the actual warping observed. This displays the effect of a principal warp on both Cartesian coordinates as the sum of displacements in the plane of the data that represent the decomposition of a single deformation. As Bookstein (1989) indicated, the principal warps only involve the mean configuration of landmarks. In what will become significant in the analysis of the nasal septal data; the partial warps display the effect of one principal warp on both Cartesian coordinates at once, while permitting interpretation not as a surface but as a displacement in the plane of the data (Bookstein 1996; Bookstein 1989; Bookstein 1991; Bookstein 2014).

As it will be demonstrated in this chapter, the use of partial warps offer the possibility of maintaining biological meaning. The partial warps of a landmark configuration, which are still eigenvectors of their thin plate spline, contain all the information pertaining to landmark configuration that lies atop the Procrustes shape coordinates matrix and which would be rearranged arbitrarily in a principal components analysis.

In the traditional GMM toolkit the coordinate basis that is rotated to produce the partial warps is usually the set of Procrustes shape coordinates. For 2D data the warps specify an abstract “surface in four dimensions or for 3D data an analogous hypersurface in six dimensions. *For this* *project just one of the coordinates (the mediolateral) is converted into components of real surfaces that are ordered according to the scale of their relief features*. Displacements left or right of their average positions, not the position on the midsagittal plane.

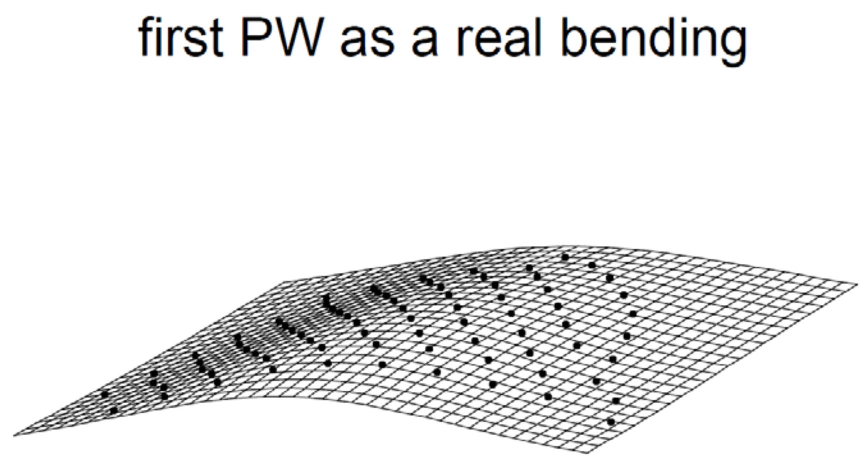

Figure 74: First PW of Nasal Septum

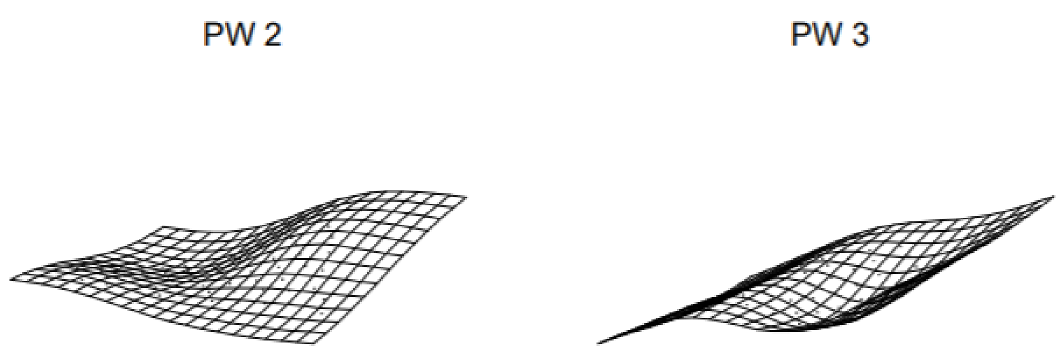

Figure 75: PW 2 and 3. PW 2 is a bending describes an S curve of the septum in an A-P direction. PW 3 describes similar bending only caudally.

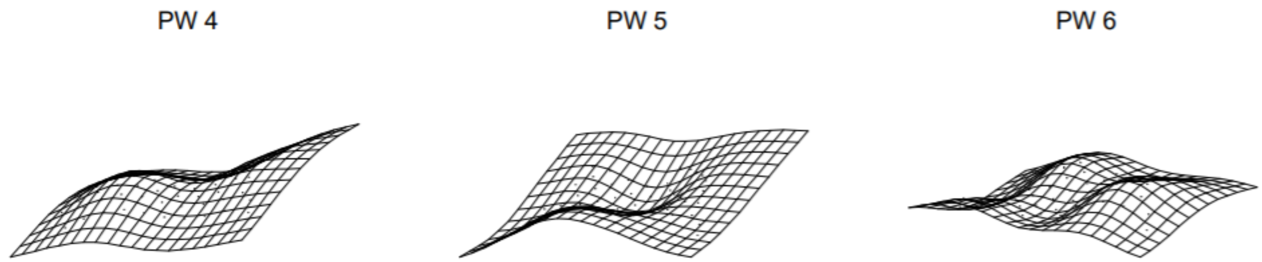

Figure 76: PWs 4, 5, and 6 describe well delineated spurs or ridges on the unilateral septal surfaces.

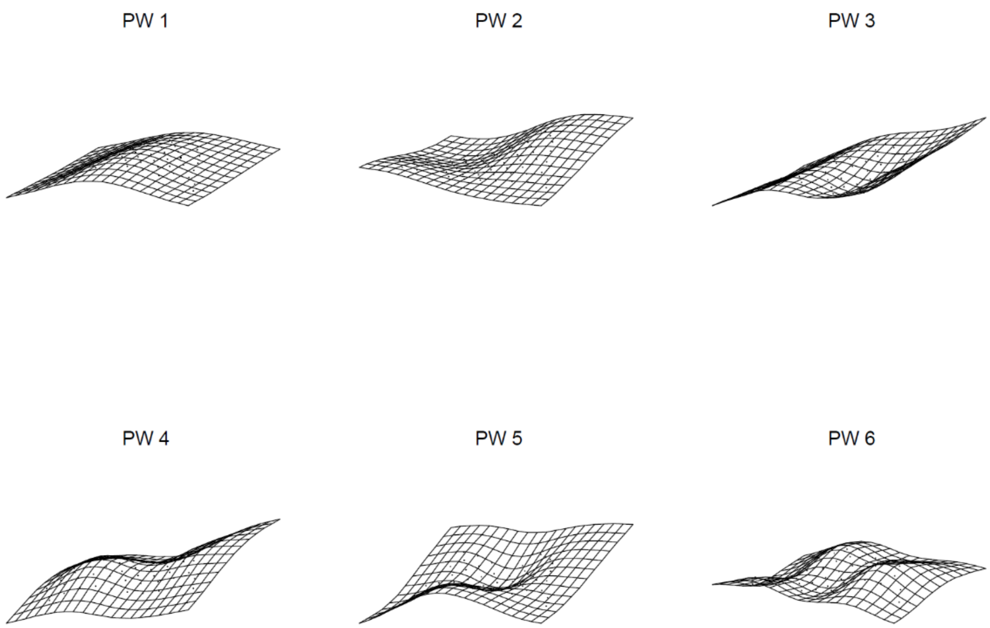

Figure 77: PW 1 to 6

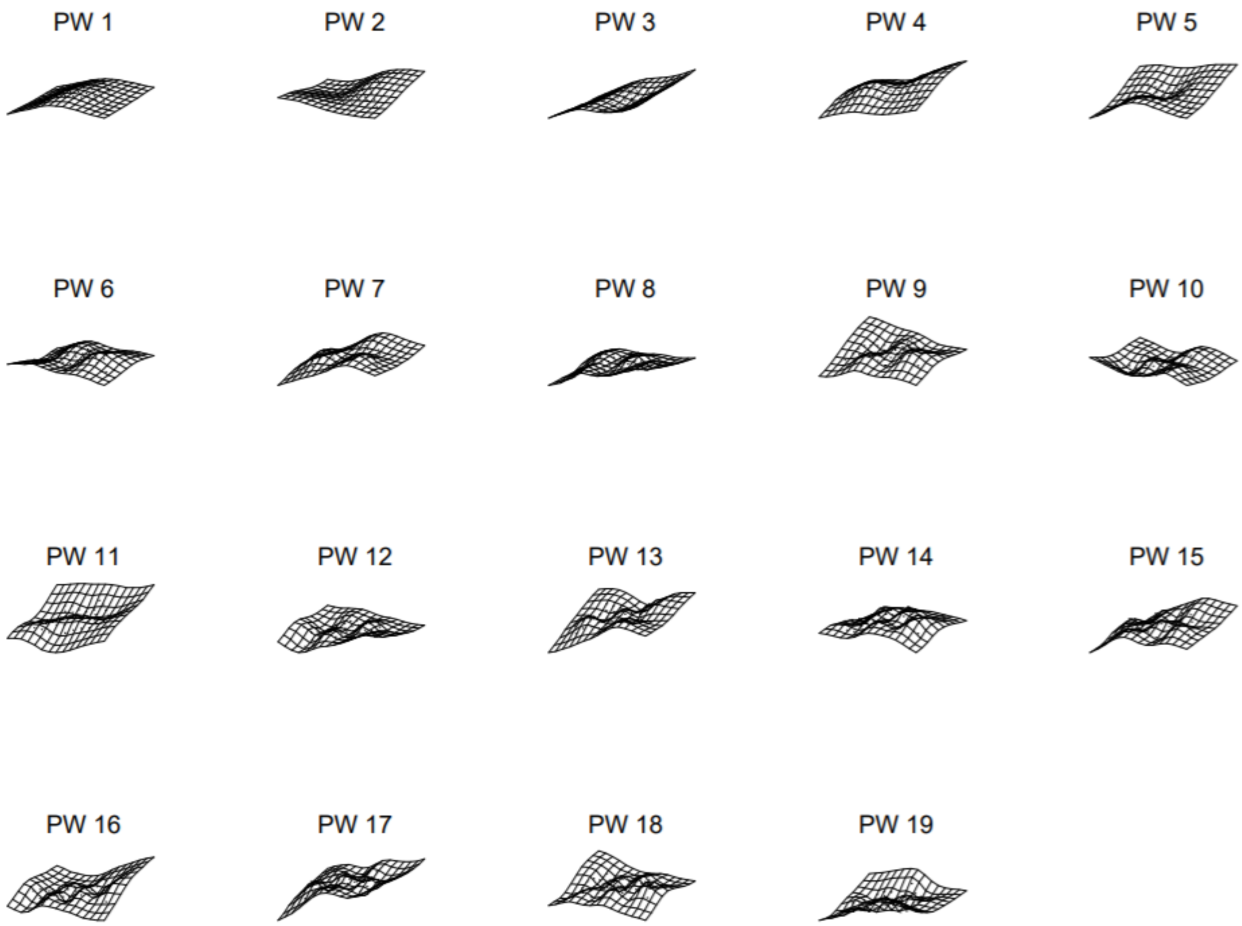

Figure 78: PWs 1 – 19. All 19 of the partial warps covered by the bandpass filter we eventually selected.

The first nontrivial partial warp (actually the fourth as the first three correspond to three degrees of freedom) is the largest-scale bending of the surface. Constraints on the deformation around the outline of the semilandmarks are not taken ito account. The bending integrates the deviations of the grid squares from their neighbours over the whole picture plane, but according to the L_k^{-1} formula, it permits analysis by linear transformations of the mediolateral cartesian coordinates. The second partial warp is a S shaped bending in an antero-cranial orientation, while the third partial warp bends obliquely to the second in an antero-caudal orientation. Partial warps 4 – 6 represent different versions of ridges.

Partial warps 1 – 19 describe part of the space of possible patterns of height in terms of bulges at many different scales and locations. By the final warp (PW 73) all possible patterns of heights as they covary around a common flat pattern over the full set of semi-landmark locations will be exhausted (warps 20 through 73 are not shown).

Bending Energy – Partial Warp Variance

The bending energy-partial warp scores drive a recent alternative (Bookstein 2015) to principal component based GMM analysis that resolves a number of problems associated with PCA (Bookstein 2017), while being sufficiently sensitive to identify the most deformed nasal septal specimens as discussed in chapter 4, at the same time replacing the either/or paradigm of "integration or modularity" with one of "integration – self similarity – disintegration", which permits integration accompanied by modularity while separating global from local effects. This truly represents a paradigm shift from the integration or modularity model.

In the context of Brownian motion where the statistical properties of the process are dependent on one parameter, the diffusion coefficient (or, for a discrete random walk, the step variance), Bookstein has adapted this concept of scaling to shape comparisons with the use of thin plate splines, and principal and partial warps. Through the thin plate spline (TPS), the individual shape of a landmark configuration can be represented as a deformation of the sample mean shape. The bending energy of the TPS is a quadratic form of the coordinates of the landmark points where the principal warps represent any single shape change with the partial warps as the horizontal and vertical coordinates.

Integration Dimension

Bookstein (2015) has described a method of unifying the un-integrated model of a subspace within the space of shape covariance structures, where the Procrustes model lies at one extreme and the strongest growth-gradient models at the other.

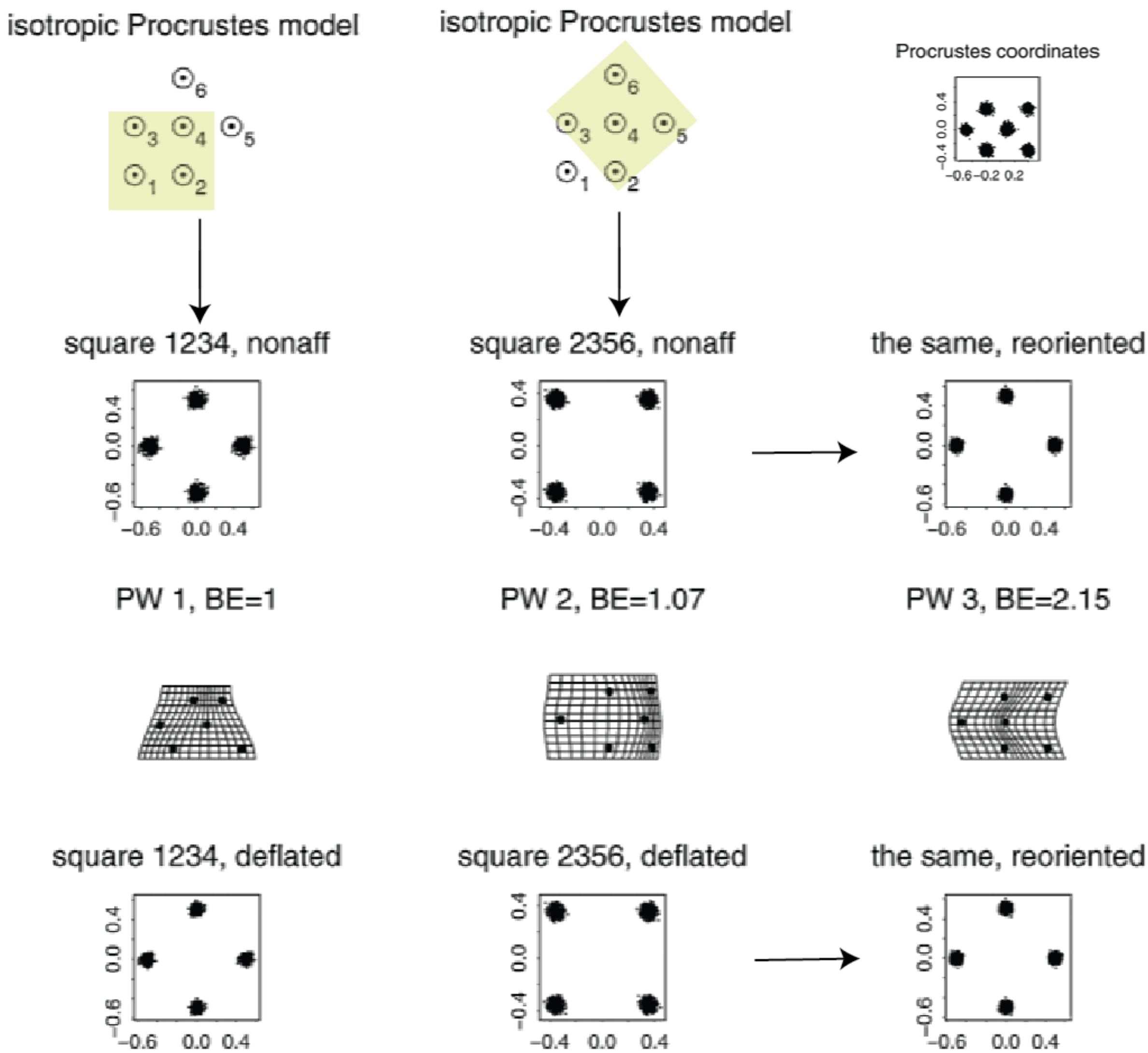

Figure 77: Derived from, Bookstein 2015, figure 1.

Start with an offset isotropic Gaussian model consisting of six landmarks: the circles around the points represent 2 standard deviations of the underlying circular normal (Gaussian) variation assigned to each landmark independently. To the upper right is the conventional Procrustes shape coordinate plot. In the top row, there are 2 squares formed by landmarks 1,2,3,4 (Small square) and landmarks 2,3,5,6 (Large square). These sub-configurations have the same shape but are different sizes.

In row 2, the variance of any single Cartesian coordinate at any landmark if the small square is 0.001247 Procrustes units. The variance of the larger square after orientation of the square upon the original form is 0.000662 Procrustes units.

Row 3 contains the grids of the principal warps of the configuration of 6 landmarks. Above each is its bending energy (net integral of summed squared second derivatives or the eigenvalues of the bending energy matrix for this mean landmark configuration). The eigenvalues are proportional to 1: 1.07:2.15. The principal warps are functions of the mean configuration, perpendicular in shape space, and are a statistically arbitrary orthogonal rotation of the original Procrustes variation (spherical in all eight of its dimensions). There is no spatially differentiated pattern, as the four orthogonal 2D subspaces of the 8D space have shape variances of 0.00337, 0.00359, 0.00350, and 0.00344, which do not meaningfully differ. With the data lacking special structure, it is "disintegrated" with no biological connection.

As noted previously, Bookstein indicated in his 1989 "Orange book", principal warp analysis only involves the starting configuration of landmarks. If the change in position between two landmarks is visualized on a thin plate spline, the resultant partial warps represent the localizable part of the warping (except the affine term) observed.

Dryden and Mardia (2016) define a pair of thin-plate splines (PTPS). The equations for this are presented in Appendix II.

In what will become significant in the analysis of the nasal septal data, the partial warps display the effect of one principal warp on both Cartesian coordinates at once.

By deflation of the observed Procrustes variation, and by reducing the variance of each partial warp by a factor proportional to its bending energy, a shape distribution is produced for which the equality of variances of potentially very informative features is replicated regardless of scale. The distribution of non-affine shapes of square sub-configurations of landmarks is the same at every geometric scale (self-similar). "The variance of the non-affine components of the shape of these perturbations of squares is *independent of scale*". Therefore the principal components with respect to the bending energy can be used across the full range of scales available for living or dead organisms (Bookstein 2015). We are doing something similar with this study's nasal septum. I am using the thin plate spline in its original sense, a lofted surface. That is why it isn't GMM.

Bookstein describes this method as being similar to the normalization of random walks and diffusions such as Brownian motion, linking it to the bending energy mathematical generalization of the Brownian motion.

The difference between the isotropic Procrustes model and a self-similarity model can be illustrated by a set of landmarks in a 5 X 5 grid, upper left, figure 78. Upper right image is a Procrustes scatter of the landmarks. Lower left image after deflation by bending energy. The lower right image of the proportionality of variance after deflation to bending energy is found in the form of the log-log plot with slope -1 for the self-similarity model, and the upper line of figures with slope 0 for the Procrustes model.

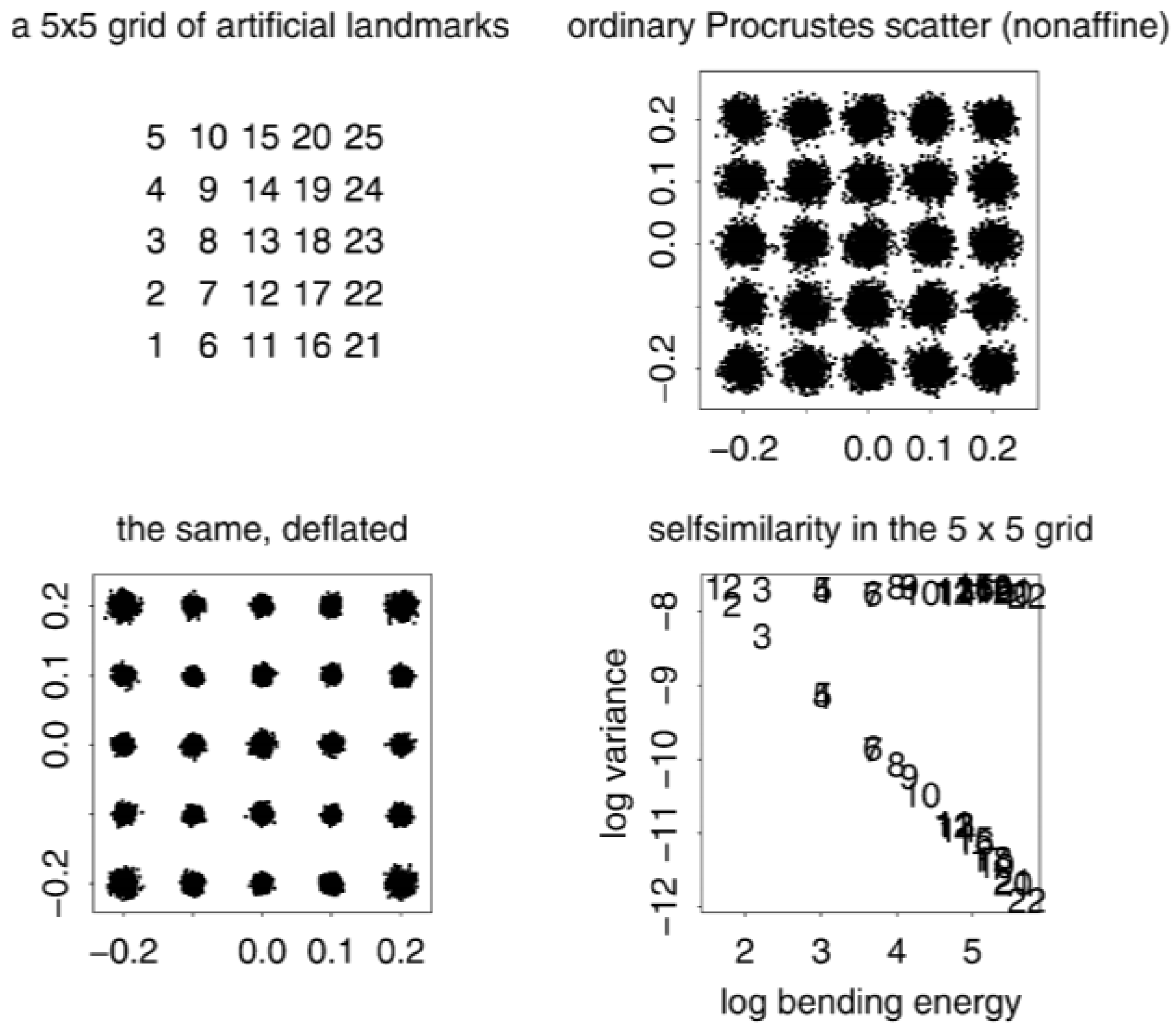

Figure 78: From Bookstein (2015).

The Procrustes model with slope ~ 0, is therefore disintegrated. This cannot serve as a null model for development as death would have occurred before growing into such a configuration. It is also not a good null model for the nasal septum, as we saw already in chapter 3. The self-similarity model breaks the non-biological symmetries of Procrustes shape space in favour of a model incorporating the mean landmark configuration in conjunction with the deflation step (Bookstein 2015).

The affine and non-affine transformations are segregated. Here the affine transformations (which are derived from the uniform component that is free from bending and leaves parallel lines parallel) are not used. By reducing the variance of each partial warp score by a factor proportional to its bending energy a *deflation* of the Procrustes variation can be produced.

The partial warps remain (representing the non-affine transformation), as an ordination of all the shape changes of the deformation in a single dimension of the increasing bending energy per unit Procrustes length. The log partial warp variance is plotted against the log bending energy: $BE - PWVplot$. The slope (α) differentiates between integration, self-similarity, and disintegration. Integration implies large scale variation (global patterns) while disintegration is small scale variation (local patterns). Windhager (2017) makes a salient point in summarizing the outcomes:

> "Small-scale features may be correlated but they cannot be "integrated" in our morphometric sense unless the deformations of the spaces around them are correlated as well meaning the integration must be at a large scale" (Windhager 2017).

Slopes steeper than -1 correspond to integration, processes such as growth which affect all regions (global patterns). Slopes shallower than -1 correspond to disintegration (local patterns). A slope of exactly 1 corresponds to self-similarity with an absence of special features, equivalent to Brownian motion. The method here assumes a slope of exactly -1; for real data, which slope itself is an observation.

In a BE-PWV plot, the vertical axis is the logarithm of the variance of the partial warp scores (projections of a sample on each on each of the patterns analogous to those in the previous two figures. The horizontal axis is the logarithm of the corresponding bending energy, eigenvalue of the pattern with respect to the bending energy matrix L_k^{-1}. The short vertical segment in figure 77 indicates the boundary of the low pass filter used. The BE-PWV scatters for the left and right septa seem mildly inequivalent.

The slope of the nasal septal BE-PWV plot is an indication of biological integration/ disintegration. In Bookstein 2015, the slopes of the paper's examples varied from -0.56 (mildly disintegrated to -2.2 (clearly integrated). When the nasal septal data is analysed in BE-PWV plot from our data, there is a near linear plot with slopes of -0.76 (left septal surface) and -0.88 (right septal surface) which connotes mild disintegration, a slight excess of uncorrelated local features. This result is entirely consistent with the deformities of the nasal septum as described by Takahashi (1987) as I will discuss later in this chapter.

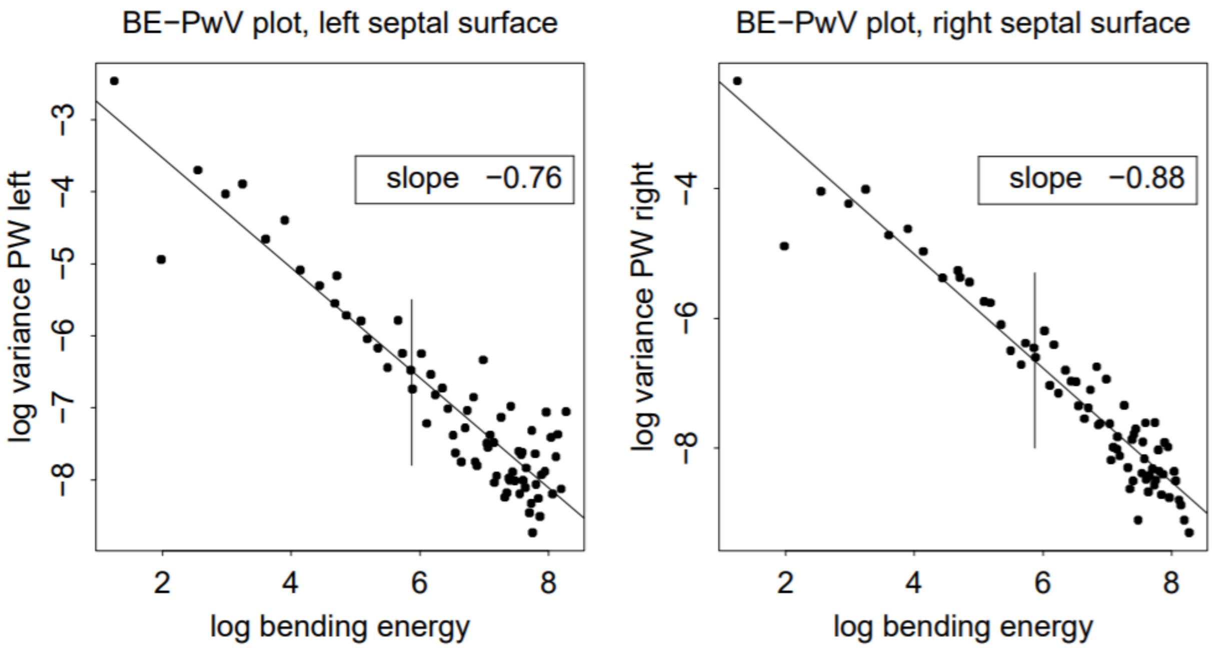

Figure 79: Bending energy – partial warp variance (BE – PWV) plot. From Bookstein (2015)

The partial warps provide an ordination of all possible shape changes along the single dimension of progressively greater bending per unit length of the deformation. The steepness of the slope is a measure of the fall of the ordination. For another application of this see Bookstein (2017). Following the principles of that paper, instead of the observed roughness variance partial warp by partial warp, we use the variance as corrected for a linear fit (figure 77) of the theoretically more appropriate slope, which in the context of respiratory function is just about -1.0. So we consider possible filters of individual partial warp vectors using the squared adjusted lengths from PW1 (figure 79) through PW*k*, where the optimal k is 19 (figure 80). The analysis is now in explicit units of bending energy, not Procrustes distance.

Lowpass Filter

All possible filter banks were considered (on the possibility that a single low pass filtering would separate the septa for which surface form is functionally relevant from the others) from PW 1 through the fifteenth and thirtieth partial warp of which the net amplitude of bending over all the partial warps, divided between the first 19 PWs versus the remainder. In a personal communication, Bookstein suggested that "acoustically, a lowpass filter bank might be the aspect of septal form that would lead to rumbling as air passes over". This approach is closely analogous to what is done the related fields of biometeorology and micrometeorology with the property of turbulence associated with fluid flow.

In our study, a lowpass filter to separate roughness has been used, because we believe that the greater the deformity (prominent spurs, ridges, and concavities) the greater the turbulence due to greater “roughness.” As it turns out, these severely deformed “rough” surface specimens have been efficiently selected by this new methodology.

As noted, cutting the partial warp spectrum between PW19 and PW20 corresponds to the short vertical lines in figure 81. The plotted bending energy is not the variance of the PWs but is each warp’s contribution to the total bending energy (total integral of summed squared second derivatives of the “height” field interpolated over the z-coordinates of the data). After each is “connected” by multiplication by its own bending energy, thus converted from a Procrustes distance to an abstract energy. The vertical axis is the Mladina T (type) number and the plotted number is the Sample number (1 – 51 specimens and with the two ND’s omitted). Figure __ shows the “best” of these filters, the one that most clearly separates Mladina’s group T6, the most clinically relevant group from the others. Note how much more effective the low-pass filter is than the high-pass.

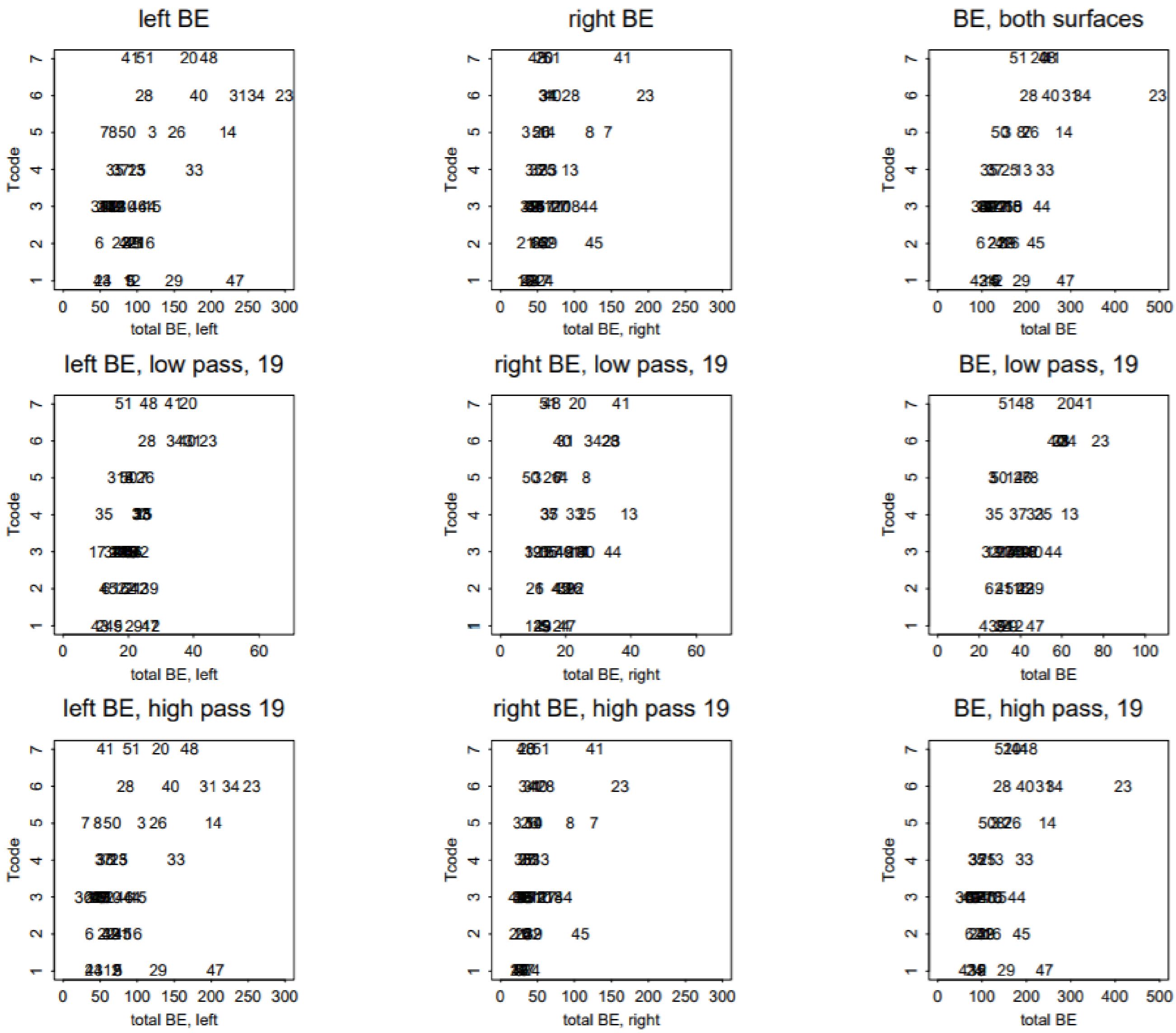

Figure80: Total bending energy – T code. From Bookstein . Left (left nasal septal surface), Right (Right nasal septal surface), T code (Mladina nasal septal deviation type), Number 1-51 (Specimens 1 – 51, two ND are omitted)

For the top row, in the upper right panel specimen 23 was noted as an outlier in the SVD1/SVD2 plots but is more divergent in the bending energy plot. Similarly in the upper left panel specimens 31 and 34 are extreme for their bending energy for the left septum but not the right.

When each side is subdivided into high and low bandpass net energy, the strongest statistical signal is given by the total (left and right) lowpass bending energy (see figure 80).

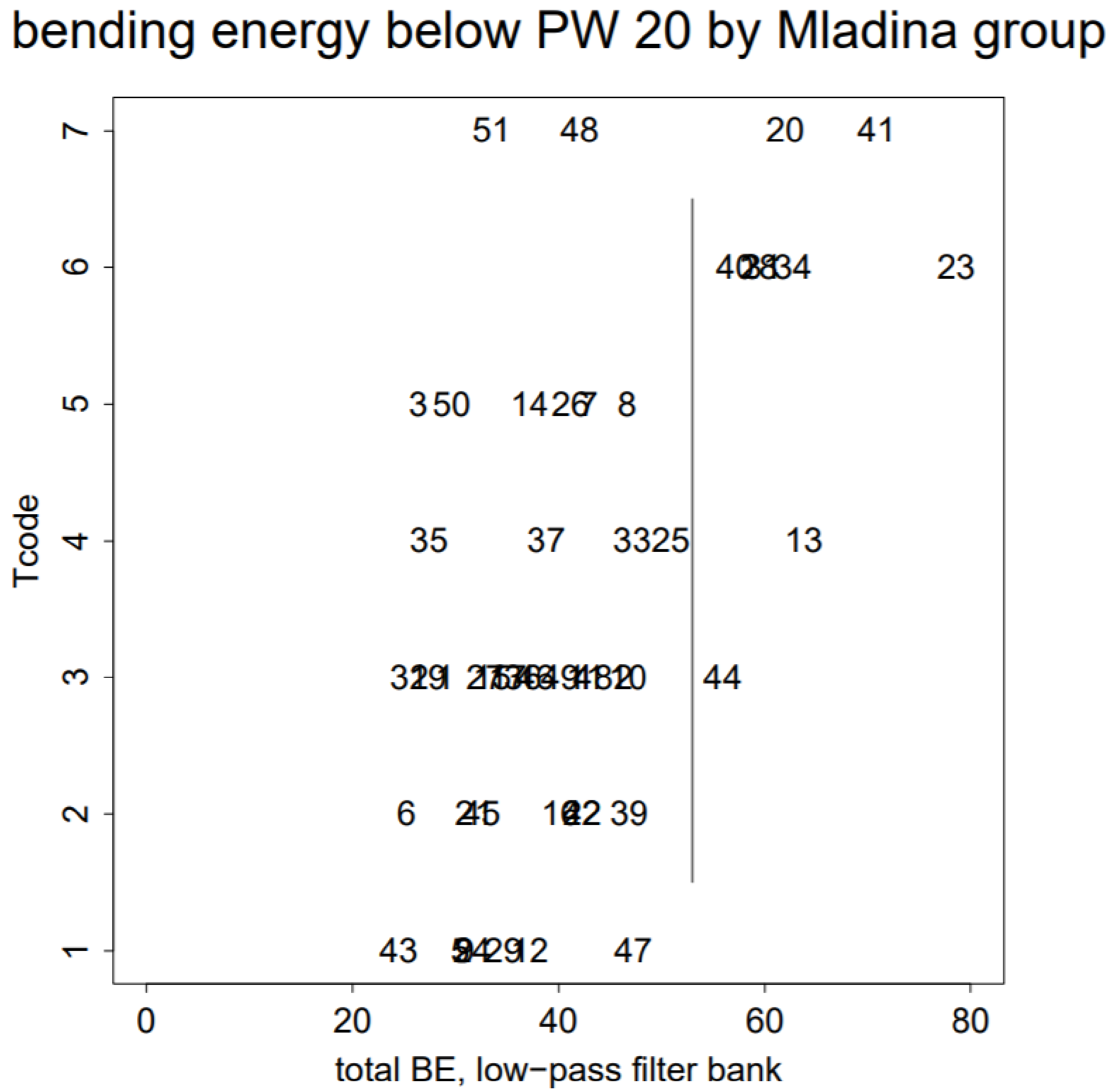

Figure 81: Our principal finding: Enlargement of the panel in the third column, second row. Numbers are the specimens' numbers from the data set of 51 including the two ND's (original specimen numbers were relabelled 1-51, conversion list is in appendix 2). The two ND's are not in the plot.

The single scalar quantity which is the bending energy of the first 19 partial warps divides the sample into two groups. The strongest low-pass bending energy group includes all five Madina T6 specimens as well as four others: (# 20 T7, 41 T7, 13 T4, and 44 T3). To repeat, the bending energy plotted here is not the variance of the partial warps but instead the actual contribution of each warp to the total bending. These calculations are determined by the energetics of the thin-plate spline, not the sum of squared distances as per the usual Procrustes analysis. Total low-pass bending energy proves to be a very good classifier of Mladina T6 group as well as the other severely deformed specimens.

Contour mapping of the nasal septum

Using the loess and contour algorithms from the R statistical package permits the nine extreme specimens to be explored in more detail by creating contour maps. The loess algorithm interpolates the height field over a scatter to a superimposed squared grid.

The contour algorithm interpolates from a field of heights upon a squared grid to a contour map.

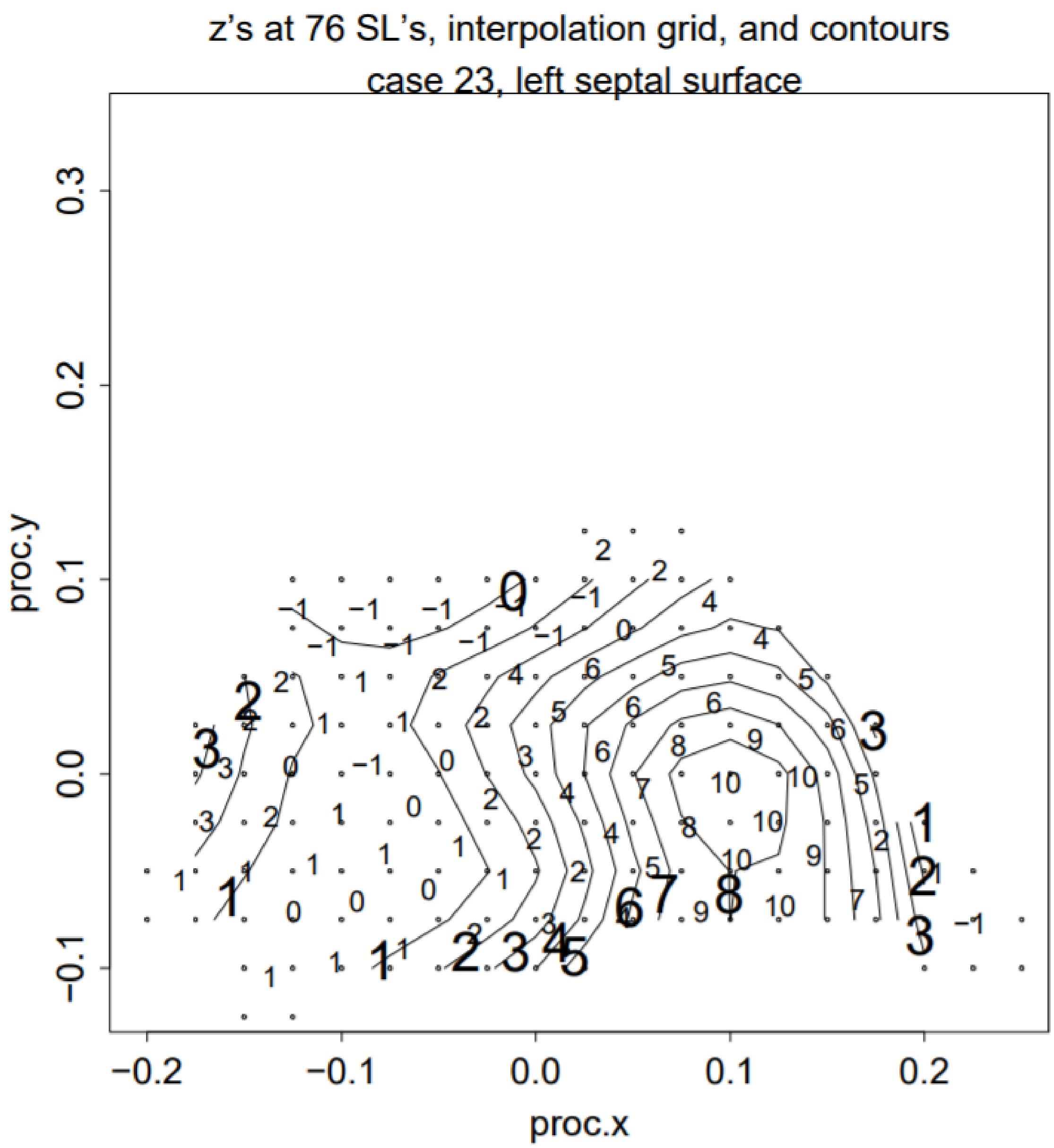

Figure 82: Case 23 (T6) interpolation grid and contours, left septal surface.

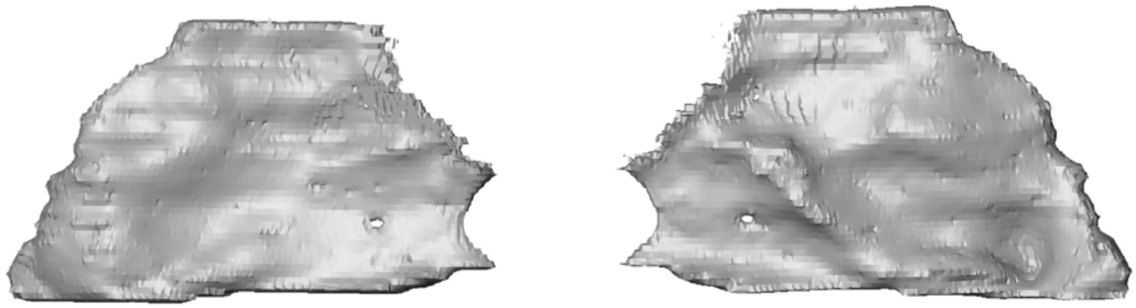

a. b.

Figure 83: Case 23 (T6): a. left septal surface. b. right septal surface.

Figure 83 displays the most extreme case from figure 84 (Case 23 T6). The digits in small font represent the actual z-coordinates of the left septal surface. The tiny open circles correspond to the nodes of the coordinate grid centered on the Procrustes system. The loess algorithm interpolates from the height data onto each of the grid nodes and the contour algorithm creates the contour map.

The nine pairs corresponding to the right and left septa of the specimens classified as the most highly bent by the lowpass filter are displayed in figure 84. These are displayed in descending order of net bending where total bending energy is close to a function of the summed squared reciprocals of the distances between neighbouring contours (the restrictions to the 19 dimensions of this surface height field that represent bending at the 19 largest spatial scales).

Most of the contour maps show a strong resemblance to one another, but not assessed by the traditional GMM toolkit. Specifically the spatial fields are dominated by spurs, spines, ridges, and concavities common not only to the T6 group, but also to the other four specimens missed by traditional GMM analysis, and what they have in common is their existence, not their location. It is particularly important to note that these spatial features occur in regions of the septa that Takahashi found to be susceptible to shape disturbances (ridges, spines, bending) as a consequence of evolutionary and developmental forces. This is discussed below in the analysis of individual cases.

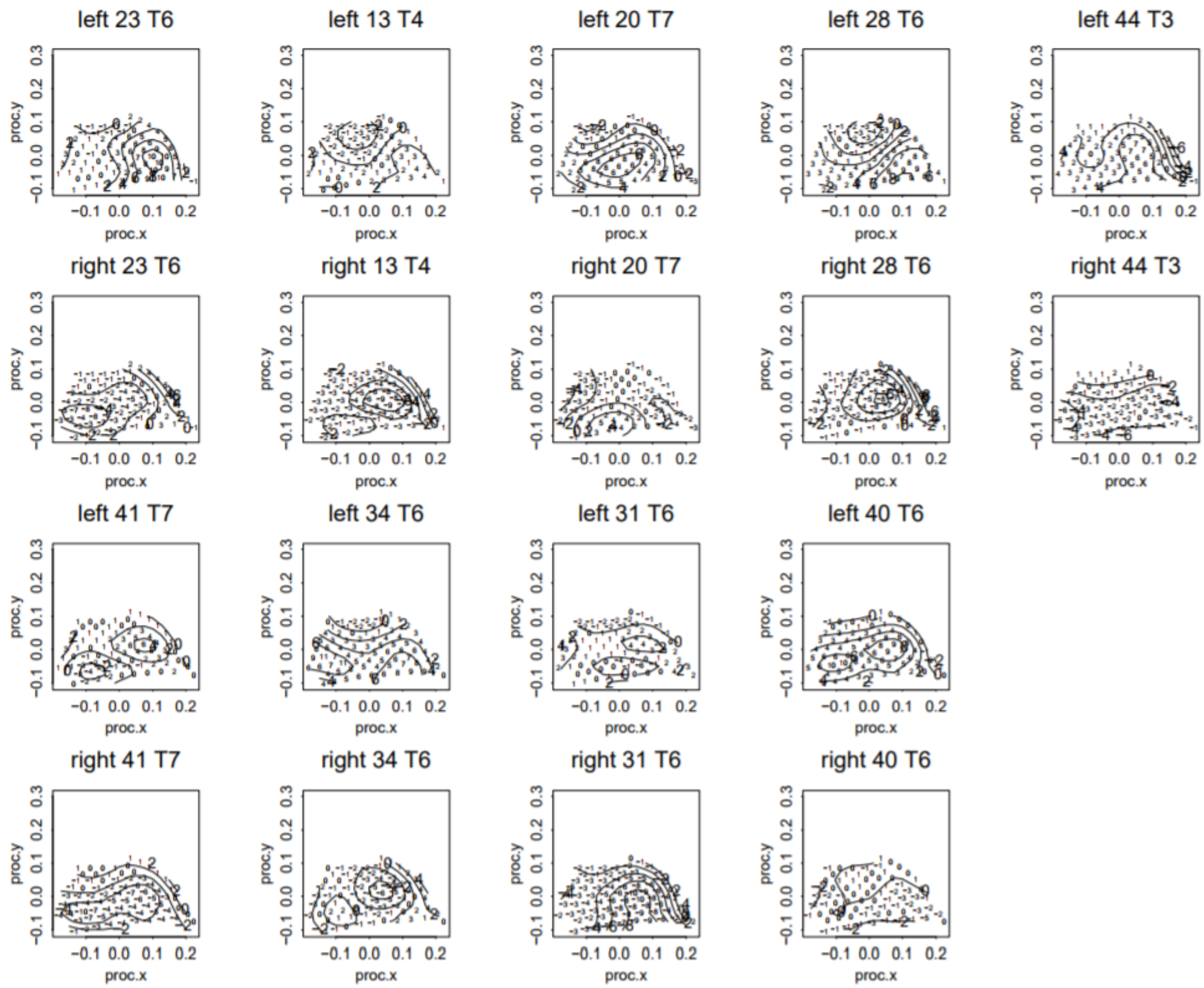

Figure 83: The nine extreme cases from figure 80. Contour maps of left and right surfaces for specimen 23 (071), 13 (036), 20 (015), 28 (064), 44 (009), 41 (043), 34 (007), 31 (061), and 40 (046). Only the even numbered contour lines have been modified.

These forms illustrate the futility of attempting to “classify” deformity into neat categories. While the severe deformities of the T6 were detected, so were four other severely deformed specimens: one T3, one T4, and two T7s. There would appear to be an inherent contradiction between classification and quantification. When classifying according to form there is an implicit unjustified assumption that there is a correlation between form and deformity severity and/or airflow obstruction. This is illustrated by the two non-T6 specimens 41 and 13. Form 41 (T7) combines both a horizontal linear feature running the length of the right side with a strong gradient between a spur and a depression on the left. In contrast form 13 (T4), has a bulge and a depression on the left with a spur on the right approximately between them. This is the surface that you would expect when forces sufficiently strong to cause buckling or bending are applied to what is essentially a flat surface (Takahashi 1949).

Takahashi observed that nasal classification systems have been developed by clinicians based on their clinical observations. His research documented the extent of septal deformity both in the high frequency and the complexity when observed in newborn and as it becomes more frequent during the period of growth and development. In contrast the traditional classifications focus almost entirely on adults, with a single mindedness at creating a surgical connection whilst ignoring the complexities of organismal biology.

Integration – self similarity - disintegration

The Bookstein model of integration – self similarity – disintegration resolves the contradictions of the modularity – integration model, and permits local changes to be considered as change within a module. In that context it is useful to consider the complexity of those modular changes as underscoring Takahashi's concerns regarding simplistic classifications.

Nasal septal "modular changes" would include evolutionary modularity with retraction of the maxilla-facial region and increased flexion of the cranial base with a decreased surface area ratio of the nasal septum but increased surface area ration of the perpendicular plate. Functional modularity with respiration, mastication, and deglutition, accompanied by curving of the upper anterior aspect of the nasal septum, formation of ridges and spines within the nasal septum due to buckling between the septal cartilage and the vomer, and curvature proximal to the ossification line between the perpendicular plate and the septal cartilage.

Developmental modularity associated with growth is documented by the 25% rate of septal deformity at birth, which rises steadily with an increase in septal projection between 0 – 10, increased curvature between age 10 to adolescence, increased curvature during adolescence, and the appearance of a deviated external nose in late adolescence. These changes are often accompanied by a slow increase in the length of the inferior-superior axis.

Thus complex and often uncorrelated local changes account for the failure of nasal septum classifications. Takahashi, rather than attempting to create a clinically descriptive system that would correlate with the severity of airway obstruction and degree of septal deformity, has identified anatomical predictors related to evolutionary and developmental parameters. These predictors are very consistent with our contour maps. Case #23 was reviewed above, the remaining eight severely deformed cases are reviewed below. The contour maps and segmented CT images are in Appendix I.

Case Analysis

Case 13 (036)

On the left surface there is a ridge at the junction of the septal cartilage and the vomer with a concavity superior to the ridge corresponding to the concavity formed by the bending of the cartilaginous septum. With this bending and concavity there is a corresponding bulge on the right surface. The contour maps reflect these deformities.

Case 20 (015)

On the left surface there is a ridge formed along the septal cartilage and vomer junction. Superior to the ridge there is a bulge on the convex septal cartilage surface due bending of the cartilaginous septum/perpendicular plate. The concave surface on the right reflects this bending.

Case 23 (071)

On the left surface there is a sharp bending of the septum along the ossification line of the perpendicular plate which results in a S shaped septum and distortion of the valve region. The concave right surface reflects this bending.

Case 28 (064)

There is a ridge along the cartilaginous septum and vomer junction. On the contralateral surface there is bending and bulging of the cartilaginous septal surface. The combination of the ridge deforming the septum laterally on the left while the bending of the right resulting from growth and development the cartilaginous septum and ossification of the perpendicular plate has produces a complex double “S” (S shaped deformity when viewed both coronally and axially) deformity. This particular case underscores the futility of finding meaning in a simply clinical classification. Without a computerized fluid analysis, it would be impossible to quantify whether airflow had been interrupted at a particular location.

While the contour map and the segmented CT image can give an indication of where the obstruction may occur, it cannot quantify the airflow reduction. The classification type may select a deformed septum (however it has almost an equal chance of missing the selection), it cannot quantify, nor locate where the obstruction occurs.

Case 31 (061)

A septal cartilage/vomeral junction ridge has resulted in a right side bulging over the ridge coupled with bending of the septal cartilage/perpendicular plate to create a pronounced C shape bending of the septum. The above cases are all T6 types, are identified by GMM bending energy/partial warp variance analysis as being among the most deformed, however the classification type provides no useful information pertaining the either the anatomy, location, or quantification of the deformity.

Case 34 (007)

The ridge of the left surface becomes more prominent posteriorly, with several spine like projections at the processus vomerous. Bending of the septal cartilage/Perpendicular plate has produced a complex “S” shaped bend to the right along with a concavity inferiorly.

Case 40 (046)

The ridge on the cartilaginous septum – vomeral junction has several spines projecting in the processus vomerus region. Bending of the perpendicular plate has resulted in a significant C shaped bend with a large concavity on the right surface.

Case 41 (043)

A ridge on the cartilaginous septum – vomeral rises posteriorly to a spine in the processus vomerus region. Bending of the cartilaginous septum/perpendicular plate created a bulging of the right anterior surfaces. The two combine to from a large concavity on the left surface.

Case 44 (009)

A small ridge is present along on the right cartilaginous septum – vomeral junction. Severe bending of the left cartilaginous septum – perpendicular plate has created a large bulging of the left surface and a deep concavity of the right. Disturbance of the septum – vomeral junction has resulted in a severe titling of the septum. The overall morphology is extremely complex, with S shaped curvature when viewed both from the axial and coronal aspect. As with all of the above specimens, these are not amenable to simple classification.

As noted, the limitations and ultimate futility in attempting to gain useful information from a classification system is apparent. The modification of the “GPA of the GMM toolkit” discussed and utilized in this project resolves the issue of biological relevance while providing information pertaining to the nasal septum not previously available. Not only can the Bending energy – partial warp method select the morphologically most severe deformed specimens, the contour maps provide a quantification of the deformity. This mapping and quantification provides added insight when visually assessing the segmented CT images.

Takahashi has created an analytical roadmap for examining the nasal septum:

When deformed cases are viewed in the context of the nasal septal characteristics outlined in figure 83, a systematic method of analysis results where the quantified and localized deformities can considered in the context of their evolutionary, development, and function origins.

With traditional classifications, of particular note is the lack of consideration for the deep creases (concavities) that crater the surface of the nasal septum. While the presence of budges or protrusions that may contact a proximal structure or obstruct an airway are a foundation of classifications, the creases are simply not considered qualitatively or quantitatively. The creases generally have tortuous surfaces, are proximal to the spurs and ridges, and together have a significant effect on airflow. Ignoring their presence or considering only in isolation makes little biological sense.

Finally, all the classifications appear to be disconnected from evolution and development, treating normal variations in nasal septal morphology as pathology rather than natural responses biological restrictions space secondary to an evolutionary paradox. Takahashi's roadmap refocuses analysis on developmental biology.

Chapter 7

Discussion

As reviewed in Chapter I, nasal septal diagnostics combine clinical examination, classification systems founded on clinical examination, and imaging. Both imaging (usually computed tomography) and instrumental methods (rhinomanometry, acoustic rhinometry, and peak nasal inspiratory flow) have limitations. The need for better diagnostics is indisputable, both to prevent unnecessary procedures and to improve cost-effectiveness.

However, advances are unlikely with the current methodologies. Classifications only verbalize, as they are descriptive and cannot quantify. Computed tomography usually does not correlate with subjective symptoms. Automatic segmentation of the images may not provide sufficient resolution to differentiate between soft tissue and cartilage or between cartilage and bone. Semi-automatic and manual segmentation is required to accurately register the morphology of the nasal structures. Furthermore, the unavailability of both landmark points and landmark curves makes this region difficult to measure other than by cross-sectional areas. It is problematic to visually assess the patency of an airway or degree of septal deviation from the CT and then determine a correlation with the patient's subjective symptoms. Visual examination of the CT slices in coronal and axial views (which is the clinical norm) allows a determination of sinonasal anatomy and its variants but does not differentiate between "normal" and pathological findings.

This is illustrated by a recent study which found no significant difference on CTs between patients with minimal radiologic evidence of rhinosinusitis and patients with clinically significant radiologic evidence of rhinosinusitis (Shpilberg 2015). The study was performed by two experienced neuroradiologists examining the CTs independently. Patient had been diagnosed with rhinosinusitis (facial pain, facial pressure, nasal obstruction, hyposomia, or purulent discharge). The patients were divided into two groups: A. minimal radiographic evidence of paranasal sinus disease (mucosal thickening of < 1mm) and no obstruction of drainage. B. Evidence of significant paranasal sinus disease. The authors concluded:

> "We found no significant difference in the prevalence of any of the paranasal sinus or nasal cavity variants between patients with minimal and patients with clinically significant radiologic evidence of rhinosinusitis. Therefore, analysis of every routine CT scan of the paranasal sinuses obtained for sinusitis or rhinitis for the presence of different anatomic variants is of questionable value unless surgery is planned. Failure to recognize these variants is associated with a higher rate of surgical complications." (Shpilberg 2015 p. 1258)

This study raises some interesting questions. Both patient groups were symptomatic with clinical evidence of paranasal sinus disease. Neither group had radiographic evidence of differences in paranasal sinus or nasal cavity variants. The authors conclude that CTs are only useful in reducing surgical risks. Should not the questions be asked?

> Is information being missed in a conventional examination of a CT?
>
> If all presenting patients have clinical indication of paranasal disease, and CT imaging isn't useful differentiating who requires surgery, are current diagnostics sufficient or is this evidence of why surgical outcomes may be problematic.
>
> Would knowledge of whether a patient has a severely deformed nasal septum as objectively determined by the TPS-BE model be useful?
>
> Would a contour map of the nasal septum generated by the TPS-BE model be helpful?

Interesting, Shpilberg found nasal septal deviation in 98.4% of patients in the study (86F, 106M) noting, that this was higher "than was reported in the literature." Takahashi was not cited, however both his sample and our sample report reported similar deviation frequencies as Sphilberg. Shpilberg also reported that one-third of the NSD was associated with a bony nasal septal spur.

Further Studies

The frequent failure of sinonasal surgery was reviewed in Chapter 1. This problem is aggravated by the necessity of revision for many of these surgeries. The UK National Sinonasal Audit (Philpott 2015), found that the surgical revision rate for patients with chronic rhinosinusitis (CRS) is 19.1% at five years, but even worse for certain sinonasal procedures. There is a 52.5% surgical revision rate for those with chronic rhinosinusitis and nasal polyps reporting previous surgery. The NHS of the UK spends £30 million per year on patient with chronic rhinosinusitis with nasal polyps, so with a 50% revision rate there is an increase in costs of £15 million. The study suggested a clinical trial comparing surgical versus medical therapy. This assumes that the surgical procedures themselves are effective and appropriate. The authors conclude "this study emphasises the need for ongoing research to improve the care of patients with CRS in order to minimise the need for repeated specialist care and operative intervention (Philpott 2015).

The modified GMM methodology employed here provides just such an avenue for future research. A one-dimensional calibration of nasal septal deformity via bending energy appears to provide a severity score for deformity while mapping and quantifying morphological variation. What remains to be determined is whether the severity of shape change correlates with interruption of airflow, or whether instead airflow interruption related to roughness is caused not only by the ridges, spines, and bulges, but also the surface textures of the creases and valleys. It might be helpful to view these contour maps with respect to airflow and turbulence around the peaks and valleys. This information would permit the measurement of pressures at predetermined locations. Computed fluid dynamics (CFD), which is the computer modeling of fluid flow has long been used in engineering, more recently in modelling nasal airflow, and appears to offer the functional measures needed to sharpen the distinctions that bending energy is making in a more stringent analysis like figure 85.

Bailie (2006) described many of the limitations of conventional sinonasal diagnostics. These include.

- Our basic understanding of nasal airflow.
- Methods of objective assessment of nasal patency only provide global information: overall resistance, peak flow.
- Local assessment methods are limited: narrowest cross-sectional area.
- Positioning measuring devices within the nose results in interrupting the very airflow that they were intended to measure.
- ENT surgeons tend to rely on clinical judgement regarding whether a patient requires surgery, and where to operate with documented unfavourable results.

It is not enough to “improve diagnostics”, one also needs to improve surgical outcomes.

In the context of these limitations, here is an overview of CFD and the opportunities for the improvement of sino-nasal diagnostics. In an early paper Elad (1993) traced the history of modeling nasal cavity airflow. From models cast from cadavers and smoke flow studies in the 1950s, to velocity studies in the 1960s and 70s, airstream patterns were determined along with localized velocities. They constructed a mathematical simulation of asymmetric airflow through a nose-like model, determining that the airflow is mainly along the nasal cavity floor where the turbinates direct the flow. There is now a sophisticated body of work that models airflow through the nasal cavity.

Bailie summarized CFD methodology:

- A CT or MRI image is obtained that must extend from the tip of the nose as otherwise it will miss the valve, to the posterior wall of the nasopharynx with a maximum slice width of 2mm.
- A fine mesh including the landmarks is created from the image. A balance is required as too large cells will result in averaging over large areas thus missing small details, too small cells increase computing time.
- The mathematical model should treat nasal airflow as a viscous fluid with a laminar flow. Such a flow includes small perturbations.

Early studies assumed steady flow conditions. Ishikawa (2006), demonstrated that a computational model simulating the intranasal vorticities during respiration was possible, permitting a three dimensional display of intranasal velocity and vorticity distributions.

Using a steady flow cross-sectional model, Wen (2008), used a commercial CFD code to predict gas flow through the nasal cavity. The nose was divided into four regions. At the vestibule, air enters through the nostrils into the vestibule. Air flow changes direction 90° towards the horizontal and enters the nasal valve. At the nasal valve region, the airway nasopharynx narrows to its smallest cross-section area. Leaving the valve, the airway expands as it enters the turbinate region where the passages are separated by the septum and must flow around the turbinates. Finally, the passages merge as they enter the nasopharyngeal region. They couldn't quantify airflow continuously over the length of the nasopharynx, and measured flows at 2.6cm and 3.2cm from the anterior nares. At 2.6 cm two vortices were in the right cavity and one in the left, airflow was at 7.5L/min. The airflow increased to 15L/min at 3.2 cm as the size of vortices increased. This region resembles a constriction-expansion region causing the majority of the total airflow resistance. Coinciding with airflow changes, this is the region where ridge formation begins along the septal cartilage – vomeral junction and where bending of the septum occurs as identified by the partial warps/bending energy model.

Wen noted that the main factors contributing to airflow patterns are the nasal cavity geometry and airflow rate, and that nasal resistance can contribute up to half of total airway resistance. Geometric variations produced dramatic increases in resistance, with the highest wall sheer stresses found in regions of greatest resistance (valve and region posterior to the valve). Wen's findings, particularly in the nasal valve region as related to geometry, are of interest. "The maximum shear stresses occurred in the nasal valve region and to a lesser extent in Zone 3 and 4, may lead to dysfunctional effects on nasal sensation of airflow and may play a role in the well-being of nasal breathing. By mapping out the distribution of external stresses on the nasal cavity walls, predictions of the mechanoreceptor response may be estimated.” (Wen 2008, p. 133). The question naturally rises whether there is a correlation between the mapping of bending energy and CFD.

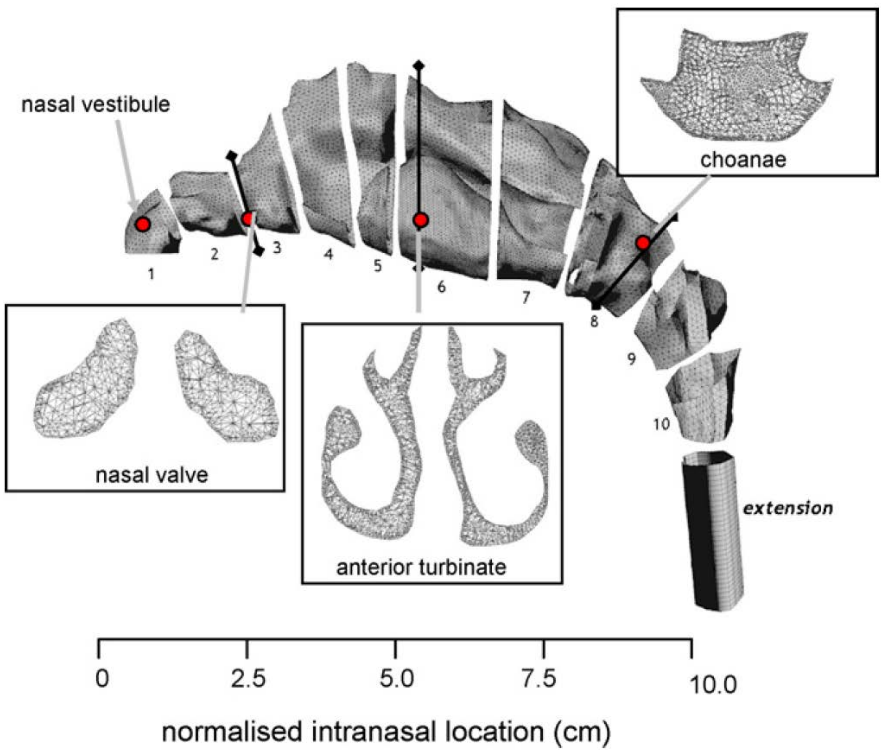

Fig. 1. Nasal cavity model used in the study. Cross-sectional areas taken at the nasal valve, middle turbinate and nasopharynx regions are shown with the computational mesh.

Figure 84: Location of the valve and regions 3 and 4. From Wen 2008.

In a review of the implications of computational fluid dynamics studies on nasal airflow for physiology, Leong (2010) emphasized the problems associated with the nasal valve region, and the difficulty in using traditional methods (endoscopy, acoustic rhinometry, and computerized tomography) to illustrate the relationship between form and function. They measured the cross-sectional area of the valve at its most constricted point, 3cm distance from the nostril. At this point 52.6% to 78.3% of total airway resistance was accounted for. The boundaries of this region include the caudal end of the upper lateral cartilage, the head of the inferior turbinate, the caudal septum, and the remaining tissues surrounding the piriform aperture. For the septum that deviates sufficiently, airflow is channeled away from the deviation toward the floor and roof of the nasal cavity at high velocity. The high airflow velocity results in high wall shear stress. This in turn exaggerates any pressure difference along the nasopharynx.

Note: I have used the term ”valve”, as it appears to be the accepted ENT terminology to describe the angular region described above by Leong (2010). This is an archaic term as there’s no suggested boundary for any named structure “valve”. The term poorly describes both the 3-D structure and is inappropriate for use with fluid mechanics. Tripathi suggests the use of the term “gateway” for medical use as the term “valves” is “…terminology that is otherwise confusing to patients and nonsense to engineers.” (Tripathi, 2017, p. E1). He describes the problematic use of the angular value of the “valve” with medical diagnostics and treatment:

> “The importance of this angle as the fundamental feature of the internal nasal valve is perpetuated in the literature and remains a key concept for physician trainees. In reality, this gateway exists in 3D with a complex geometry, and accurate measurement using physical examination, endoscopy, and imaging is inconsistent at best. Considering this angle in isolation as a means to guide treatment is, therefore, inappropriate. If we treat this angle in rhinoplasty, should this not result in predictable resolution of dynamic obstruction?” (Tripathi. 20178, p. E1)

Figure. Air Velocity Vectors in the Sagittal Plane of the Nasal Airway

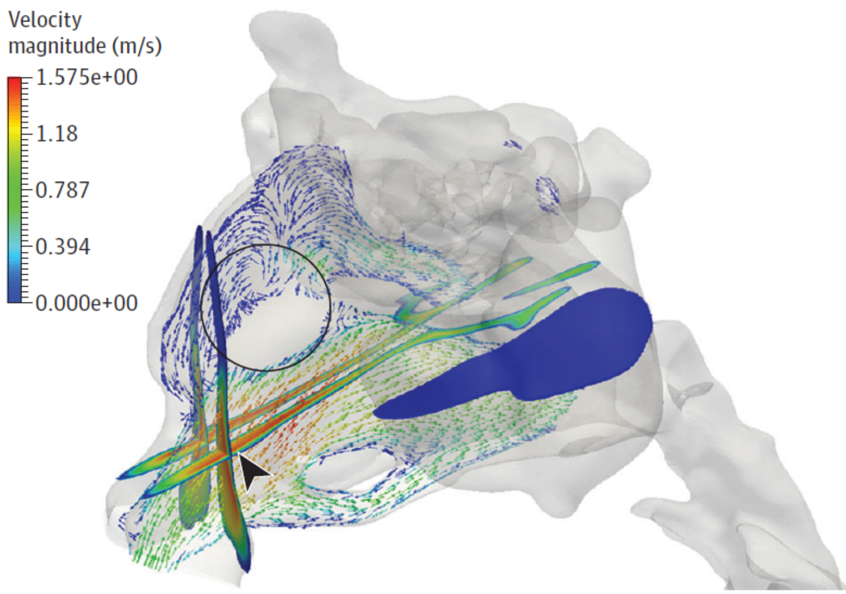

The velocity reaches a maximum within the internal nasal valve (arrowhead). A vortex flow is seen distal to this (black circle) secondary to rapid expansion. Velocity magnitude of each vector is scaled by color. m/s Indicates meters per second.

Figure 85: Sagittal view of air velocity vectors. From Tripathi (2017)

It is significant that the regions of greatest flow velocity are the regions of greatest morphometric variation as determined by bending energy and illustrated by the contour maps of the septum. This is consistent with Takahashi's concept of bending of the anterior septum that affects the valve area where septal deviation redirects airflow at a high velocity, and with the cartilaginous septum/ vomeral junction and ridge formation where there are now abnormal wall stress contours.

Whereas computational fluid dynamics uses the mapping of the nasal septum to determine airflow, and the BE-PWV model maps the contours of the septum, there are obstacles to linking the methodologies, from impaired nasal breathing and the perceived causal relationship with nasal septal deformity. Osman (2016) noted that whereas existing diagnostic tools permit examination of the nasal cavity's geometry (and the methodology employed in this study further expands the toolkit), there is no spatially resolved method for the assessment of airflow. This is further complicated by the self-perception of impaired breathing and a measurement of a reduction of airflow that may not be correlated. The reasons for the sequence of impairment of breathing is unclear, including disturbed airflow, neurological problems, and psychological issues. The use of computational fluid dynamics in a clinical setting is currently problematic as it hasn't been correlated with the most commonly used method of airflow measurement: anterior rhinomamometry (RMM).

While anterior rhinomanometry is widely used to assess nasal function, it is limited to a global assessment of total nasal resistance. CFD can measure local changes and its incorporation into clinical practice would improve diagnosis and treatment but first requires validation against RMM. Osman (2016) assessed RMM and CFD in a comparison study of their ability to determine nasal resistance. RMM measured five breathing cycles for each side of the nose, while numerical simulations were performed on a CT of 0.25mm·0.25mm·0.4mm resolution. The CFD significantly underestimated the nasal resistance as measured using RMM. The authors concluded that while CFD may be underestimating nasal resistance compared to RMM, it may also unclear whether RMM measurements may be altering either breathing behaviour or airflow in a manner that is not understood.

Nevertheless CFD has recently been considered for both preoperative planning of nasal surgery, and as a measure of the efficacy of surgery. Rhee (2012), demonstrated the use of CFD to preplan and evaluate the surgery of a 53 year old woman who underwent septoplasty, turbinate reduction, and nasal valve repair. Noting frequent poor patient satisfaction and the poor correlation between subjective and objective methods of measuring airway obstruction, the authors added inappropriate procedure selection or failure to target the problematics components of the nasal airway. Aiming to seek a balance between under- and over-treatment, Rhee presented a method where a series of computer generated 3D models from CT scans were used to measure airflow on the original and modified (with proposed surgical changes) models. The optimal modified model was chosen as a surgical guide, and following surgery a new 3D model was created and evaluated by CFD.

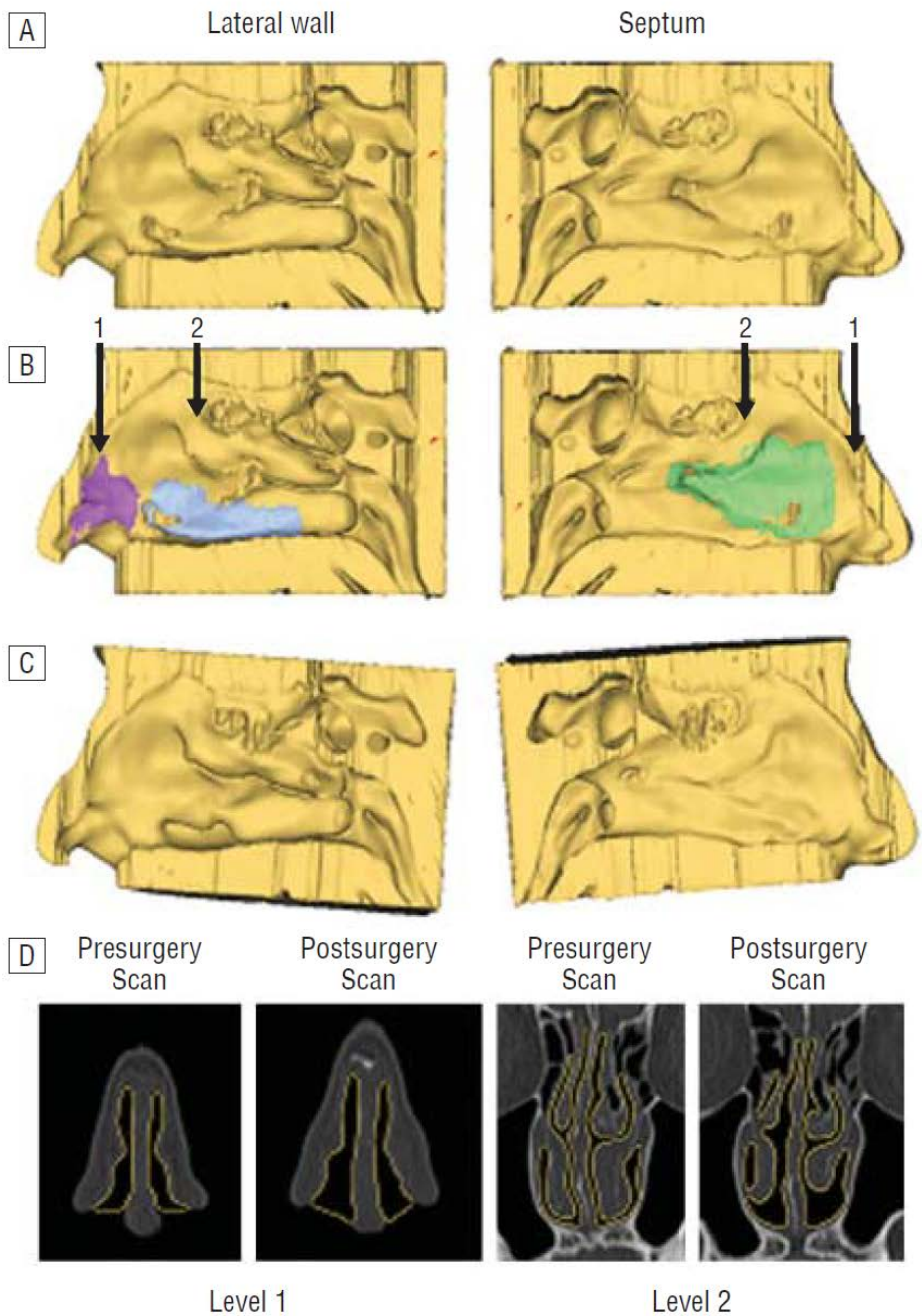

Figure 86: A. Right lateral wall and right side of the septum (pre-surgery. B. Proposed surgical sites, purple = valve repair, blue = inferior turbinate reduction, green = septoplasty. C. Right lateral wall and right septum (post-surgery). D. Coronal views of pre- and post-surgery CTs. Yellow line = border between soft tissue and nasal airspace. From Rhee 2012).

Table 1. Changes in Bilateral Nasal Resistance by Model

Model	Bilateral Nasal Resistance, Pa/(mL/s)	Change, %
Before surgery	0.0979	1 [Reference]
Nasal valve repair alone	0.0922	−5.8
Septoplasty and turbinate reduction alone	0.0788	−19.5
After surgery	0.0742	−24.2

Table 3. Airflow Allocation by Model

Model	Airflow Allocation, %	
	Right	Left
Before surgery	37.1	62.9
Nasal valve repair alone	36.7	63.3
Septoplasty and turbinate reduction alone	61.0	39.0
After surgery	61.6	38.4

Figure 87: Table 1. Bilateral nasal resistance. Table 3. Airflow allocation. From Rhee 2012.

Before surgery, the bilateral nasal resistance was 0.0979 Pa/(mL/s), post-surgery there was a 24.2% reduction. The nasal valve repair model alone predicted a 5.8% reduction, and the septoplasty and inferior turbinate reduction model predicted a 19.5% reduction of resistance. Airflow allocation with the nasal valve surgery model was similar to the pre-surgical result, whereas the septoplasty and inferior turbinate model was similar to the post-surgical result. While demonstrating the feasibility of using CFD for pre-surgical planning, Rhee noted the limitations of such an approach: differences among patients in healing, nasal sensation, and psychological factors, coupled with the great deal of time, technical expertise, and computer capability required.

CFD has also been used to measure the efficacy of specific surgical procedures. Sommer (2016) measured the effects of nasal wall lateralization and pyriform turbinoplasty with CFD, finding that nasal resistance was reduced following surgery.

Jordal (2017) used CFD as a tool for predicting and measuring the outcomes of nasal surgery for alleviation of obstructive sleep apnea syndrome. The past poor outcomes for such surgery (only one third of patients experience improvement) appear to be uncorrelated with clinical findings, with success or failure occurring for unknown reasons or perhaps no reason at all. In an effort to improve surgical predictability, CFD pre- and post-surgical measurements of nasal resistance were compared rhinometric measurements (rhinoresistometry and rhinomanometry (RMM)). While the rhinometric measurements were limited because of nasal passage access, the CFD measurements were lower and similar to CFD measurements noted above by Osman (2016). Jordal suspected that an assumption of a laminar airflow in CFD studies may be producing artificially low measurements, as the airflow may actually be turbulent. Aasgrav (2017) compared four turbulent models of airflow to a laminar flow model and found only minor differences between them. Jordal (2017) further speculates that the low CFD measurements may be a consequence of segmentation of the CTs. They used automatic segmentation along with considerable manual segmentation. They found that the hydraulic diameter (The hydraulic diameter is often used when computing the dimensionless Reynolds number for non-circular ducts) is significantly (60%) lower in the CFD model, speculating that is a consequence of the chosen upper and lower threshold limits in Hounsfield units (HU). Adjusting the HU values to control for hydraulic diameters resulted in similarity between clinical and CFD measurements. The authors concede that this is hardly ideal and conclude that further work is required regarding HU values.

Segmentation smoothing to reduce digitization errors creates a smooth walled model. This is in contrast to the irregular, mucosa and hair covered walls of the nasal cavity, thus producing an idealized and perhaps unrealistic nasal cavity model.

While the absolute measurements of nasal resistance differ between CFD and rhinomanometry, is this measurement relevant? In this section I attempt to make the case for the utility of CFD as a method for interpreting the septal contours as mapped by the bending energy. If those contours could be shown to consistently affect airflow in a predictable manner it would demonstrate a practical utility for the BE method.
CFD and rhinomanometry measures of nasal resistance don't correlate and I have now discussed the reasons for this. But so what. If the morphology of the septum affects airflow in a predictable manner, and if pre- and post-surgery BE derived contour maps and CFD measurements of airflow are consistent is there any need to call on surgeons to simply do before and after conventional measurements? CFD will never become routine but as a validation method in a study of patient subjective satisfaction, clinical symptomology, and BE derived contour maps it would be invaluable.

Gamerra (2017) recently offered an alternative model for preoperative identification of obstructed nasal subsites. "Despite successful surgical correction," he wrote, "many patients are not satisfied with the outcomes after septoplasty or nasal surgery in general." Moreover, some investigators have criticised the high number of unnecessary nasal surgical procedures performed each year. I outlined similar concerns in Chapter I. Gamerra concludes that there are "no diagnostic tools to objectively evaluate the geometry and mechanical properties of the nasal cavities and to measure nasal resistance and degree of nasal obstruction". The method described by Windhager and Bookstein and used in this project resolve the geometric problem (Windhager 2017), and Gamerra's methodologyl present alternative methods of objective measurement of nasal resistance.

Rhinomanometry (RMM) has limited ability to measure sufficient details of dynamic airflow, and is restricted to determining overall nasal airflow and resistance changes, offering little guidance in the formulation of surgical goals. CFD, as discussed previously, has not been validated and requires considerable time and computing resources. To overcome these limitations the Gamerra developed a mathematical model based on Bernoulii's equation, in conjunction with computed tomography and endoscopy.

Notwithstanding the validation still required for CFD, they are other concerns. CFD studies are simulations. The results are derived from the complex Navier-Stokes equation, which may not represent real life conditions (Doorly 2008). As noted previously there are discrepancies between CFD and RMM results. Until these issues are resolved, there is an apparent advantage with the Manometer – Bernoulli method (Gamerra 2017), in that pressure measurement can be localized. Use of the ability to localize and quantify shape change with the method of contour maps (from the BE-PWV method) to determine probe location could make pressure readings relevant. This would provide ENT specialists with information as to where morphological features were located, and whether pressure changes were associated with those features, rather that assuming that because there was septal deformity and concurrent global pressure changes, and that ipso facto surgical correction was desired.

In conclusion, GMM requires homology, but the nasal septum deforms non-homologously, buckling and bending, unpredictably from case to case for reasons that Takahashi has thoroughly explained. While the standard GMM tools are badly suited for rarely making sense of problems in craniofacial biology, less standard, more imaginative uses of the underlying mathematical manipulations (thin plate splines, partial warps) can sometimes match clinical purposes surprisingly well. Using a bending energy centred approach and the approximation of low-pass roughness by a threshold on cumulative scores is a fortuitous application of less familiar GMM tools that may be useful to clinicians who are seeking to reduce unnecessary surgeries and make surgical determination more objective. Long ago, Ryo Takahashi had persuaded me that nasal septal deviation is not pathology, rather a normal evolutionary paradox. Surgeons need to learn this before they decide to operate on everybody.

Summary

In summary, if one examines variation of nasal septal morphology, symptomology associated with that variation, and related diagnostics and treatment, it would be helpful to do so in the context of evolutionary medicine.

> "Evolutionary medicine poses a fundamentally new kind of question about disease. Instead of only asking how bodies work and why some people get sick, evolutionary medicine also asks why natural selection has left all of us with traits that make us vulnerable to disease" (Nesse 2016).

The survey by Takahashi (1988, p. 33) tracing the evolution the nasal septum from Sarcopterygii to Homo, provides ample evidence of where "morphological abnormalities of the nasal cavity, which appear from the sub-human primate stage, are a manifestation of an adaptive failure." Underscoring the evolutionary context, Takahashi notes: "We can consider this as the unavoidable fate of the human nose." The evolution of the nasal septum is described by Takahashi (1988) and diagrammed in figures 88 to 90.

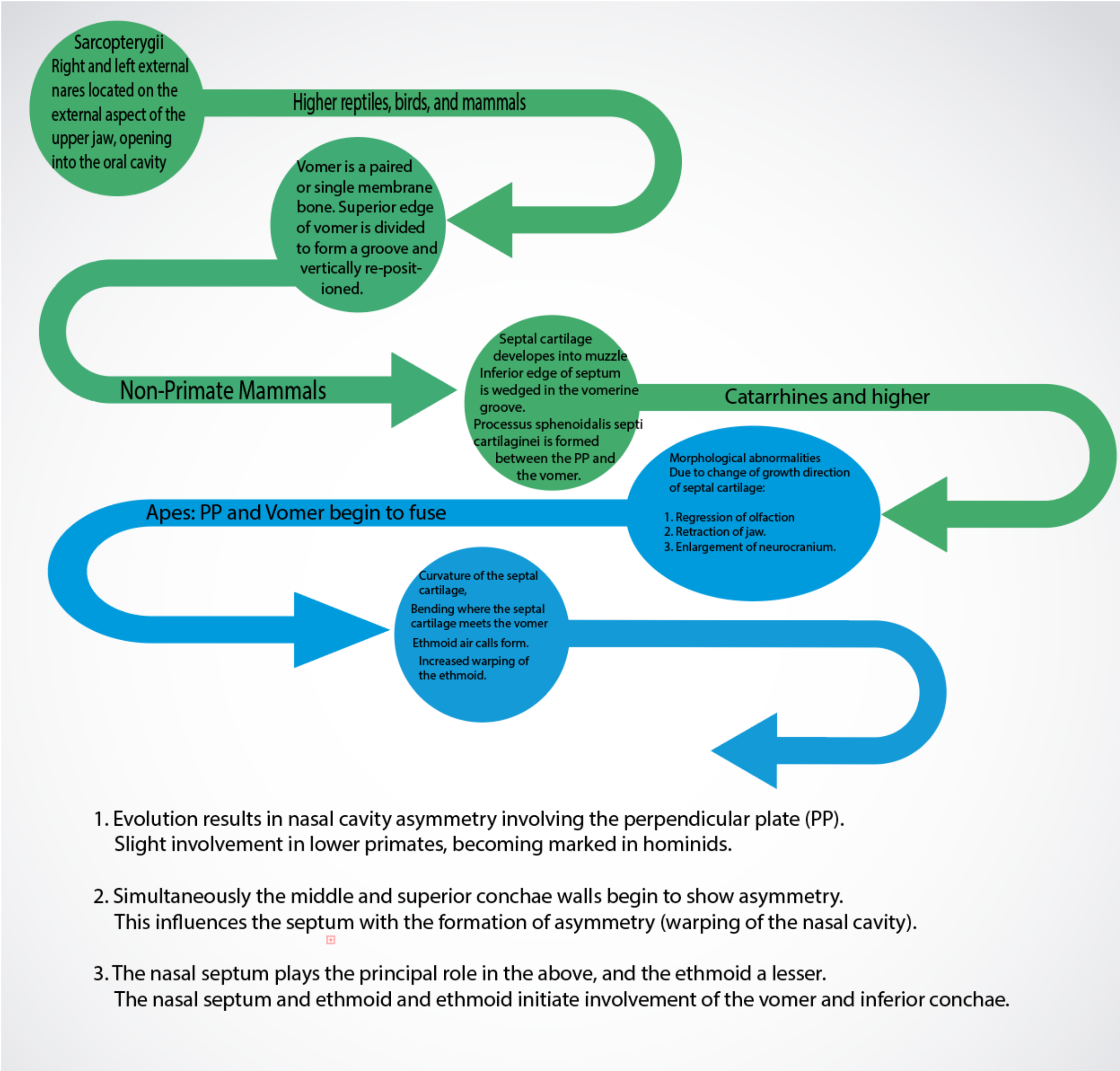

Figure 88: Early evolution of the nasal cavity.

By the evolution of the apes, asymmetry and warping of the conchae walls and nasal septum occurs (figure 88). As man evolves there is a change in both the rotational direction and size of the cranial base angle, resulting in the "adaptive failure".

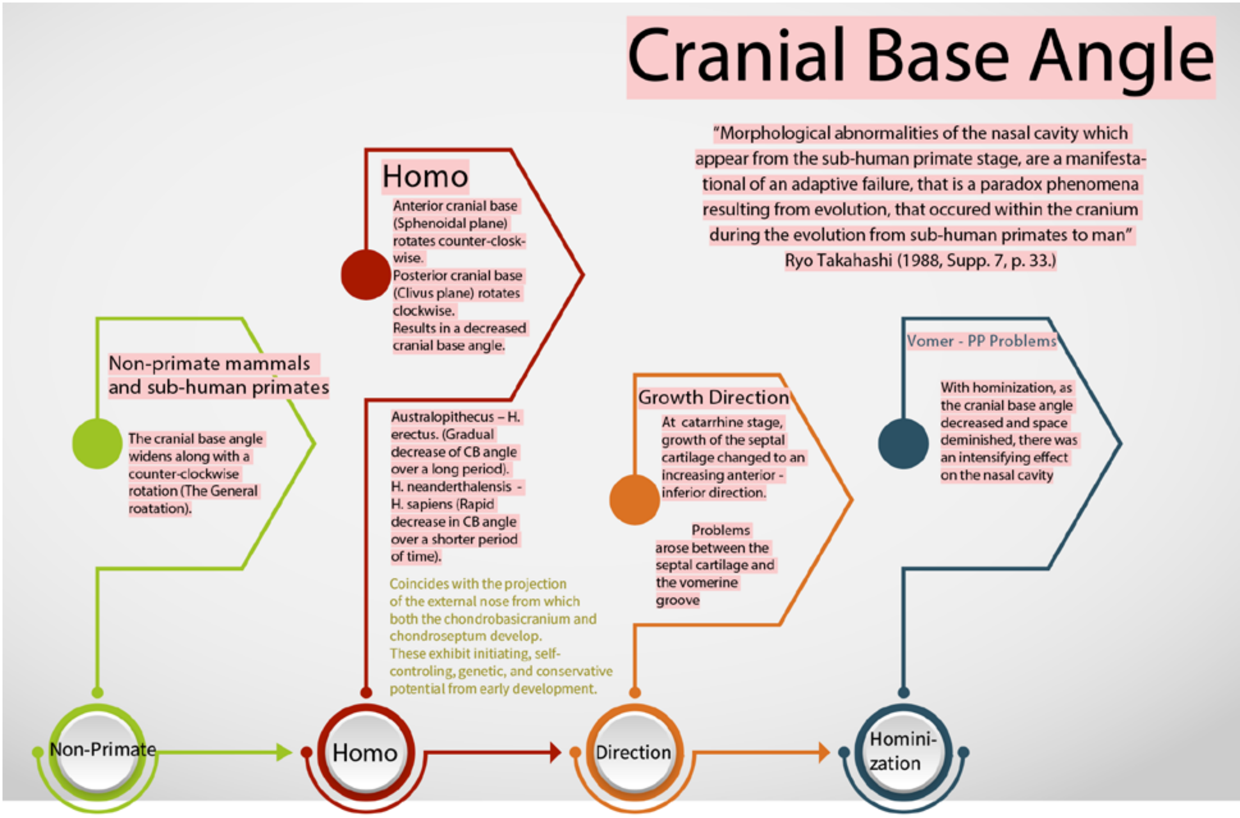

Figure 89: The effect of hominization on the cranial base angle and the nasal cavity.

This “adaptive failure”, the crowding out of the septum, chondrovomeral junction, vomer region resulting in the tortuous morphology that has proved problematic for medical diagnostics and treatment. While sometimes obstructing airflow, but also altering the fluid mechanics of airflow, where the very act of attempting to measure (rhinomanometry) airflow may alter the flow, and where alternative methods of measurement (CFD) have not been validated. If treatment plans are to be evidence based, a bending energy centered model that adapts the thin plate spline and partial warps of the GMM toolkit to map septal morphology may provide a needed quantification.

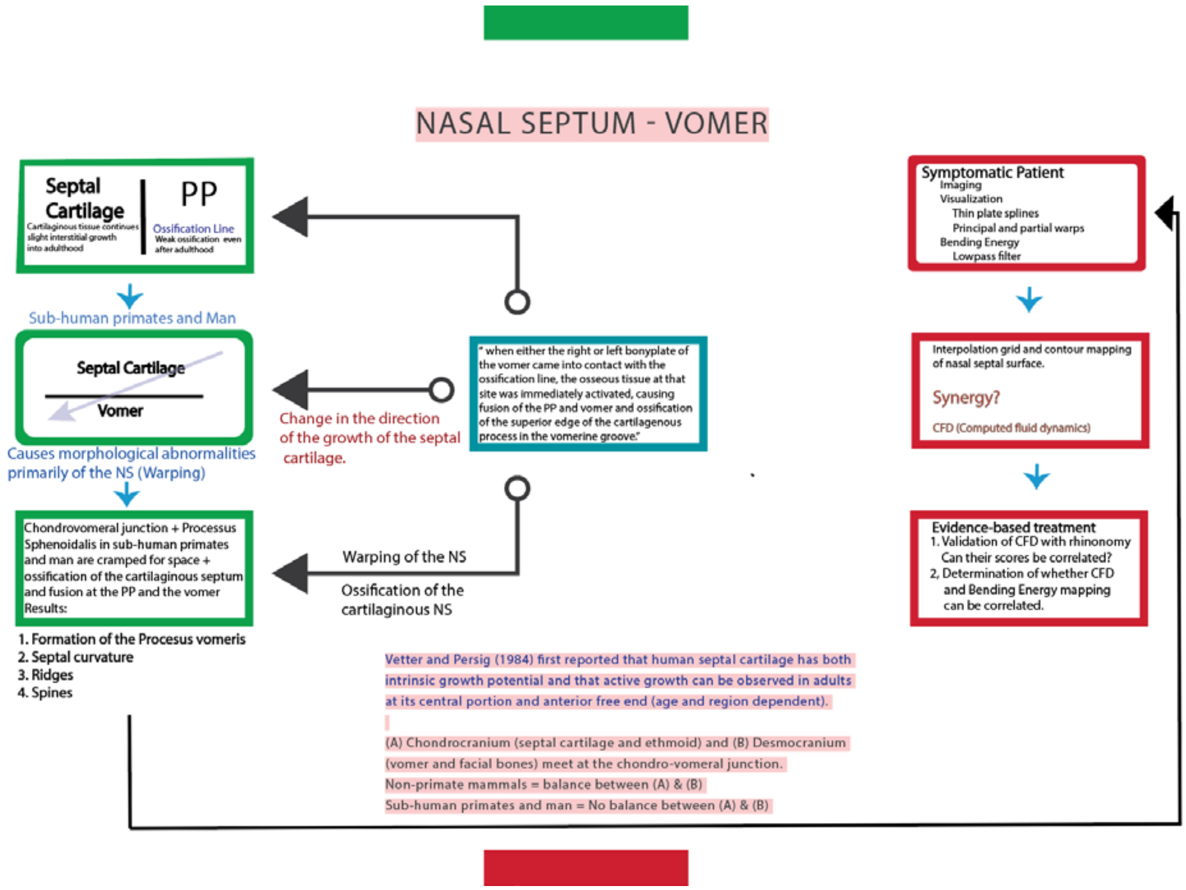

Figure 90: Hominization and the nasal septum/vomer: changes and evidence based treatment.

A prospective trial involving two groups (traditional and modified) would be of great benefit. Questions that remain unanswered include: 1. Do CFD and rhinomanometry correspond, 2. does the mapping of septal morphology by the bending energy model correspond consistently with regions of airflow change identified by CFD, 3. Can the bending energy model provide stand-alone diagnostic information.

The traditional group would use traditional selection methods for surgery: Clinical examination, imaging (CT), rhinomanometry, and endoscopy. The modified group would utilize clinical examination, imaging (CT), BE-PWV analysis, rhinomanometry, endoscopy, and CFD. Such a study would offer some clarity to a field of medicine where outcomes have been less than stellar.

In the context of current medical diagnostics, the various schemes for the classification of nasal septal deformity with the exception of Takahashi's, all seem pretty much worthless because they are neither evidence-based nor theory-based. In the medium term, a prospective trial of pre- and post-surgical CFD would be most persuasive. In the near term, what can be gleaned from my findings that may have some immediate practical value? Following Takahashi's theoretical underpinnings that associate hominization with increased rates and severity of deformity, I believe that the TPS – Bending Energy model for quantifying the severity of deformity offers just such a practical tool.

While my University of Vienna department is the world center for the application of GMM in paleoanthropology, it does not follow that the same tools should work in studies of modern human variability. In particular, studying aspects of variability associated with function may be more productive if the analytical tools present attribution with biophysics. This is not the case for GMM, and is the case for the thin plate spline, the core technology driving the second, successful analysis here.

CFD is the most promising direction of future diagnostics and the TPS-BE model appears to be a bridge in that direction. As previously documented, the success of nasal septal surgery in ameliorating patient's symptoms is problematic. The use of CT imaging in nasal cavity diagnostics while widespread has failed to resolve the problem, as the raw CT image cannot predict the severity of the problem nor correlate with the patient's symptoms.

It appears that clinical examination and CT imaging were unable to assess severity, or to detect the most severely deformed cases. While the Mladina type 6 classified specimens were among the most deformed, they comprised just 5 of the 9 of those cases. I did not have clinical records. It is imperative to run the TPS-BE model where records are available, including the patient's subjective assessments of the severity of their *symptoms* before and after surgery. It would be of great interest to see if the TPS-BE model for determining the severity of septal deformity corresponds with (a) the patient's assessment of symptom severity and (b) surgical outcome.

Should a correspondence exist between the severity of symptoms and deformity, or between the severity of deformity and surgical outcomes, introduction of the TPS-BE model would be a practical diagnostic modality.

Finally, a cautionary note regarding the GMM toolkit. Chapter 4, detailed the analysis of the data using the conventional GMM toolkit. The results were at best ambiguous, finding only 3 of 5 Mladina type 6 specimens, and 3 of 9 severely deformed specimens. Overall it failed to quantify the severity of nasal septal deformity. Conventional GMM is useless for the determination of roughness associated with biological structures except when ridges, etc., are found at reliable locations within an organ; that is not the case for the nasal septum.

It is not surprising that the TPS-BE model succeeds where the use of the GMM toolkit fails so spectacularly. First, with block registration, the Procrustes rotation steps, which are inconsistent with the biophysics of the septum are omitted. Second, one should remember the origin of the thin plate spline. Harder and Desmarais (1972) published “Interpolation using surface splines” in the Journal of Aircraft while employed at MacNeal-Schwendler and NASA - Langley respectively. It is fascinating that a method developed to interpolate wing deflections should prove so useful in measuring surface roughness affecting airflow in the nasal airway.

References

(1892). Notice of Quarterly Meetings for 1892. 60th annual meeting, Nottingham, British Medical Journal.
Adams DC, R. F., Slice DE, (2103). "Afiels comes of age: geometric morphometrics in the 21st century." Hystrix, the Italian Journal of Mammalogy **24**(1): 7-14.
Al Dayeh AA, Rafferty KL, Egbert M, Herring SW (2013). "Real-time monitoring of the growth of the nasal septal cartilage and the nasofrontal suture." American Journal of Orthodontics and Dentofacial Orthopedics 143(6): 773-783.
Andre RF, V. H., Ahmed A, Graamans K, Noist Trenite GJ. (2009). "Correlation between subjective and objective evaluation of the nasal airway. A systematic review of the highest level of evidence." Clinical Otolaryngology **34**: 518-525.
Assgrav E, Johnsen SG, Muller B (2017). "CFD simulations of turbulent flow in the human upper airways." 12th International Conference on CFD in Oil and Gas, Metallurgical and Process Industries, SINTEF, Trondheim, Norway.
Aziz T, B. V., Ansari K, Flores-Mir C (2014). "Measurement tools for the diagnosis of nasal septal deviation: a systematic review." Journal of Otolaryngology Head and Neck Surgery **43**(11): 1-9.
Bailie N, Hanna B, Watterson J, Gallagher G (2006)."An overview of numerical modelling of nasal airflow." Rhinology:44: 53-57.
Barteczko K, Jacob M (2004). "A re-evaluation of the premaxillary bone in humans." Anatomy and Embryology 207(6):417-437.
Baumann I, B. H. (2007). "A new classification of septal deviations." Rhinology **45**(3): 220-223.
Becker, D. (2003). "Septoplasty and turbinate surgery." Aesthetic Surgery Journal **23**(5): 393-403.
Bohlin L, D. A. (1994). "Nasal airway resistance and complications following functional septoplasty: a ten-year follow-up study." Rhinology **32**: 195-197.
Bookstein FL (1978). The measurement of biological shape and shape change. Lecture notes in Biomathematics. New York, Springer.
Bookstein FL (1986). Size and shape spaces for landmark data in two dimensions. Statistical Science I**:** 181-242.
Bookstein FL (1989). "Principal Warps: thin-plate splines and the decomposition of deformations." IEEE Transactions Pattern Analysis and Machine Intelligence **11**: 567-585.
Bookstein FL (1991). Morphometric Tools for Landmark Data: Geometry and Biology. Cambridge, UK., Cambridge University Press.
Bookstein FB (1996). "Biometrics, Biomathematics and the Morphometric Synthesis." Bulletin of Mathematical Biology: 58(2): 313-365.
Bookstein FL, Gunz P, Mitteroecher P, Prossinger H, Schaefer K, Siedler H (2003). "Cranio integration in *Homo*: singular warps analysis of the midsagittal plane in ontogeny and evolution." Journal of Human Evolution 44:167-187.

Mitteroecker P, Bookstein FL (2008). "The evolutionary role of modularity and integration in the Hominoid cranium." Evolution April:943-958.

Bookstein FL, Mitteroecker P (2013). "Compring covariance matrices by relative eigenanalysis, with applications to organismal biology." Evol. Biol: DOI 10.1007/s11692-013-9260-5,

Bookstein FL (2014). "Measuring and Reasoning. Numerical inference in the Sciences." Cambridge, Cambridge University Press.

Bookstein FL (2014). "The relation between geometric morphometrics and functional morphology, as explored by Procrustes interpretation of individual shape measures pertinent to function." Anatomical Record: 1-14.

Bookstein FL, M. P. (2014). "Comparing Covariance Matrices by Relative Eigenanalysis, with Applications to Organismal Biology." Evol. Biol.

Bookstein FL, Domjanic J (2015). "The principal components of adult female insole shape align closely with two of its classic indicators." Plos One: DOI:10.1371/journal.pone.0133303

Bookstein, FL. (2015). "Integration, disintegration, and self-similarity: Characterizing the scales of shape variation in landmark data." Evol Biol.

Bookstein FL (2016). "The inappropriate symmetries of multivariate statistical analysis in geometric morphometrics." Evol Biol 43: 277-313 DOI: 10.1007s11692-016-9382-7

Bookstein FL (2017). "A method of factor analysis for shape coordinates." American Journal of Physical Anthropology DOI: 10.1002/ajpa.23277.

Bookstein FL (2017). "A newly noticed formula enforces fundamental limits on geometric morhometric analysis." Evol Biol DOI: 10.1007/s11692-017-9424-9

Bookstein FL (2018). "A Course in Morphometrics for Biologists: Basics of geometry and statistics for studies of organismal form." Cambridge, Cambridge University Press.

Botti S, Rumeau C, Gallet P, Jankowshi R (2017), "L'articulation vomeropremaxillaire: un temoin de l'evolution des especes." Annales francaises d'oto-rhino-laryngologie et de pathologie cervico-faciale 135: 79-83.

Burns PB, R. R., Chung KC. (2011). "The Levels of Evidence and their role in Evidence-Based Medicine." Plast Reconstr Surg **128**(1): 305-310.

Buyukertan M, K. K., Kokten G. (2003). "A morphometric consideration of nasal septaldeviations by people with paranasal complaints; a computed tomography study." Rhinology **41**: 21-24.

Cannon, D. E. and J. S. Rhee (2012). "Evidence-based practice: functional rhinoplasty." Otolaryngol Clin North Am **45**(5): 1033-1043.

Cerkes N (2011). "The crooked nose: Principles of treatment." Aesthetic Surgery Journal **31**(2): 241-257.

Cleveland WS (1979). "Robust locally weighted regression and smoothing scatterplots." Journal of the American Statistical Association 74(368):829-836.

Cleveland WS, McGill R (1984). "The many faces of a scatterplot." Journal of the American Statistical Association 79(388):807-822.

Coquerelle M, B. F., Braga J, , Halazonetis DJ, Weber GW, Mitteroecker P. (2011). "Sexual dimorphism of the human mandible and its association with dental development." American Journal of Physical Anthropology. **145**: 192-202.

Cottle MH, Loring RM, Fischer GG, Gaynon IE (1958). "The maxilla-premaxilla approach to extensive nasal septum surgery." AMA Archives of Otolaryngology 60:301-312.

Cullen KA, H. M., Golosinskly A. (2009). National Health Statistics Reorts: Ambulatory surgery in the united states_2006. U. S. D. o. H. a. H. Services.

Dias R . "Nonparametric regression: Lowess/Loess. Advanced Geographic Data Analysis Scatter-diagram smoothing. Geod 414/514.
Doorly DJ, Taylor DJ, Schroter RC (2008) "Mechanics of airflow in the human nasal airways." Respiratory Physiology and Neurobiology 163:100-110.
Douglass B (1899). "Treatment of nasal stenosis due to deflective septa, with or without thickening of convex side." Laryngoscope **6**(6): 356-366.
Dryden IL, Mardia KV (2016) "Statistical Shape Analysis with applications in R." Second edition, Wiley, Chichecter, UK.
Duchon J (1976). "Interpolation des fonctions de deux variables suivant le principe de la flexion des plaques minces." Revue Francaise D'Automatique, Informatique, Recherche Operationnelle. Analyse Numerique: 10(12): 5-10.
Earwaker, J. (1993). "Anatomical variants in sinonasal CT." RadioGraphics **13**: 381-415.
Elad D, Liebenthal R, Wenig BL, Einav S (1993). "Analysis of air flow patterns in the human nose." Med. and Biol. Eng. and Compu: 31: 585-592.
Fawcett (1911). "The development of the human maxilla, vomer, and paranasal cartilages." Journal of Anatomy ond Physiology : 378-405.
Gamerra M, Cantone E, Sorrentino G, De Luca R, Russo MB, Be Corso E, Bossa F, De Vivo A, Iengo M (2017). "Mathematical model for preoperative identification of obstructed nasal subsites." Acta Otorhinologica Italica: Doi: 10.14639/0392-100X-1385.
Gibb JS (1907). "Is there an ideal operation for the correction of deviations of the nasal septum?" Annals of Otology, Rhinology, and Laryngology **16**(4): 793-801.
Goergen MJ, Holton NE, Grunheid T (2017). "Morphological interaction between the nasal septum and nasofacial skeleton during human ontology." Journal of Anatomy 230:689-700.
Gower, J. (1975). "Generalized Procrustes Analysis." Psychometrika **40**(1): 33-41.
Gray LP (1965). "Deviated Nasal Septum: Incidence and Etiology." The Journal of Laryngology and Otology **34**(July): 3-20.
Gray LP (1987). "Deviated nasal septum: incidence and etiology." Annals of Otology, Rhinology, and Laryngology Supplement 50 Part 3: 3-20.
Gunz P, Mitteroecker P (2013) "Semilandmarks: a method for quantifying curves and surfaces." Hystrix, the Italian Journal of Mammalogy. 24(1): 103-109.
Guyuron B, U. C., Scull H (1999). "A practical classification of septonasal deviation and an effective guide to septal surgery." Plast Reconstr Surg. **107**(7): 2202-2212.
Hackshaw AK, L. M., Wald NJ. (1997). "The accumulated evidence on lung cancer and environmental tobacco smoke." British Medical Journal **315**: 980-988.
Hafkamp HC, Bruintjes TjD, Huizing EH (1999). "Functional anatomy of the premaxillary area." Rhinology: 37: 21-24.
Harder RL, Desmarais RN (1972). "Interpolation using surface splines." Journal of Aircraft: February: 189-190
Hartman C, Holton N, Miller S, Yokley T, Marshall S, Spinivasan S, Southard T (2016)," Nasal Septal Deviation and Facial Skeletal Asymmetries." The Anatomical Record DOI 10.1002/ar.23303
Harugop A, Mudhol R, Hajare P, Naragund A, Metgudmath V, Chakrabarti S (2012). "Prevalence of nasal septal deviation in new-borns and its precipitating factors: A cross-sectional study. (64) 235-251 DOI: 10.1007/S12070-011-02471.

Hill DLG, Batchelor PG, Holden M, Hawkes D (2001). "Medical image registration." Physics in Medicine and Biology 46: R1-R45.
Horne WJ (1926). "The sorrows of the septum." British Medical Journal - Section of Laryngology and Otology: 1172-1174.
Holton NE, Yokley TR, Figueroa A (2012). "Nasal septal and craniofacial form in European and Africam derived populations." Journal of Anatomy 221:263-274.
Howick J, C. I., Glasziou P, Greenhalgh T, Heneghan C, Liberati A, Moschetti I, Phillips I, Thornton H. (2011) "Explanation of the 2011 Oxford Centre for Evidence-Based Medicine (OCEBM) Levels of Evidence (Background Document)."
Huizing EH (2003). "Incorrect terminology in nasal anatomy and surgery, suggestions for improvement." Rhinology: 41: p 129 - 133.
Hur M-S, Won H-S, Kwak D-S, Chung I-H, Kim I-B (2016). "Morphological patterns and variations of the nasal septal component and their clinical implications." The Journal of Crniofacial Surgery: 27(8):2164-2167.
Ishikawa S, Nakayama T, Watanabe M, Matsuzawa T (2006). "Visualization of flow resistance in physiological nasal respiration." Arch. Otolaryngol Head and Neck Surg: 132: 1203-1209.
Jessen M, M. L. (1984). "The importance of nasal airway resistance and nasal symptoms in the selection of patients for septoplasty." Rhinology **22**: 157-164.
Jessen M, M. L., Ivarsson A. (1989). "Nasal airway resistance and symptoms after functional septoplasty: comparison of findings at 9 months and 9 years." Clun Otolaryngol Allied Sci **14**: 231-234.
Jin HR, L. J., Jung WJ (2007). "New description method and classification system for septal deviation." J Rhinol. **14**(1): 27-31.
Jordal MR, Johnsen SG, Dahl SK, Muller B (2017). " Patient specific simulation of flow in the human upper airways for assessing the effect of nasal surgery." 12th International Conference on CFD in Oil and Gas, Metallurgical and Process Industries, SINTEF, Trondheim, Norway.

Lawson VG (1978). "The management of the twisted nose." The Journal of Otolaryngology **7**(1): 56-66.
Lee JW, B. S. (2013). "Correction of caudal septal deviation and deformity using nasal septal bone graphs." JAMA Facial Plast Surg **15**(2): 96-100.
Leong SC, Chen XB, Lee HP, Wang DY (2010). "A review of the implications of computational fluid dynamic studies on nasal airflow and physiology." Rhinology: 48: 139-145.
Liebermann DE (2011). "The Evolution of the Human Head." Cambridge, Ma. The Belknap Press of the Harvard University Press.
Lin, J. K., F. C. Wheatley, J. Handwerker, N. J. Harris and B. J. Wong (2014). "Analyzing nasal septal deviations to develop a new classification system: a computed tomography study using MATLAB and OsiriX." JAMA Facial Plast Surg 16(3): 183-187.
MacLeod N (2010). "Shape Models II: the thin plate spline." Palaeontological Association Newsletter: 71: 34-47.
Maqbool M, M. S. (2013). Textbook of Ear, Nose, and JThroat Diseases. New Delhi, Jaypee.
Marulanda J, Eimar H, McKee MD, Berkvens M, Nelea V, Roman H, Borras T, Tamini F, Ferron M, Murshed M (2017), **"**Matrix Gla Protein Deficiency Impairs Nasal Septum Growth Causing

Midface Hypoplasia." The American Society for Biochemistry and Molecular Biology, Inc:Journal of Biological Chemistry http://www.jbc.org/cgi/doi/10.1074/jbc.M116.769802
Murthy J, Manisha D (2016). "Pre-maxillary complex morphology in bilateral cleft and hypothesis on laterality of deviated pre-maxilla." Indian Journal of Plastic Surgery 49(3):336-339.
Meyer R (2012). Rhioplasty Including Reconstruction of the Nose. Berlin, Springer.
Miles BA, P. D., Kao H, Finn RA, Throckmorton GS (2007). "Anatomical variation of the nasal septum: analysis of 57 cadaver specimens." Otolaryngol Head Neck Surg **136**(3): 362-368.
Mitteroecker P, Bookstein F (2008). "The evolutionary role of modularity and integration in the hominoid cranium." Evolution DOI: 10.1111/j.1558-5646.2008.0321.x
Mitteroecker P, G. P. (2009). "Advances in Geometric Morphometrics." Evol. Biol. **36**: 235-247.
Mladina, R. (1987). "The role of maxillary morphology in the development of pathological septal defprmities." Rhinology **25**(199-205).
Mladina, R., E. Cujic, M. Subaric and K. Vukovic (2008). "Nasal septal deformities in ear, nose, and throat patients: an international study." Am J Otolaryngol 29(2): 75-82.
Mladina, R., N. Skitarelic, G. Poje and M. Subaric (2015). "Clinical Implications of Nasal Septal Deformities." Balkan Med J **32**(2): 137-146.
Mohebbi A, Ahmadi A, Etemadi M, Safdarian M, Ghourchian S (2012). "An epidmiologic study of factors associated with nasal septal deviation by computed tomography scan: a cross sectional study." BMC Ear, Nose and Throat Disorders DOI: 10.1186/1472-6815-12-15
Moore M, E. R. (2011). "Objective evidence for the efficacy of surgical management of the deviated septum as a treatment for chronic nasal obstruction: a systematic review." Clinical Otolaryngology **36**: 106-113.
Mosher HR (1907). "The premaxillary wings and deviations of the septum." Laryngoscope, November: 840-869.
Moss Ml, Young RW (1960)."A functional approach to craniology." American Journal of Physical Anthropology: 18: 281-292.
Moss ML, Bromberg BE, Song IG, Eisenman G (1968). "The passive role of nasal septal cartilage in mid-facial growth." Plastic andReconstructive Surgery 41(6): 536-542.
Moss ML (1972). "Twenty years of functional cranial analysis." American Journal of Orthodontics and Craniofacial Orthopedics 61(5): 479-485.
Nesse R (2016). "Evolutionary Medicine: The top ten questions." Arizona State University, Center for Evolution and Medicine, Blog.
Osman J, Grossmann F, Brosien K, Kertzscher U, Goubergrits L, Hildebrandt (2016). "Assessment of nasal resistance using computational fluid dynamics." Current Directions in Biomedical Engineering: 2(1): 617-621.
Perrin JB (1926). Discontinuous Structure of Matter. Nobel Lecture in Physics.
Philpott C, Hopkins C, Erskine S, Kumar N, Robertson A, Farboud A, Ahmed S, Anari S, Cathcart R, Khalil H, Jervis P, Carrie S, Kara N, Prinsley P, Almeyda R, Mansell N, Sunkaraneni S, Salam M, Ray J, Panesaar J, Hobson J, Clark A, Morris S (2015). "The burden of revision sinonasal surgery in the UK - data from the chronic rhinosinusitis epidemiology study (CRES): a cross-sectional study." BMJ Open: 5:e006680. doi:10.1136/bmjopen-2014-006680.
Perez-Pinas I, Sabate J, Carmona A, Catalina-Herrera CJ (2000). "Anatomical variations in the human paranasal region studied by CT. Journal of Anatomy 197(2): 221-227

Pirila T, T. J. (2001). "Unilateral and bilateral effects of nasal septum surgery demonstrated with acoustic rhionometry, rhinomanometry, and subjective assessment." Am J Rhinol. **15**(2): 127033.
Rao JJ, K. E., Ram BK, Chowdary SV, Singh J, Rangamani SV. (2005). "Classification of nasal septal deviations—Relation to sinonasal pathology." Indian J Otolaryngol Head Neck Surg. **57**(3): 199-201.
Reyment RA (2010). "Morphometrics: An historical essay". Morphometrics for Nonmorphometricians, Chapter 2: 9-24.
Reitzen SD, R. S., Shah AR. (2011). "Nasal septal deviation in the pediatric and adult populations." Ear, nose & throat journal **90**(3): 112-115.
Rhee J S, M. B., Hannley M, Arganbright JM (2008). "Evidence supporting functional rhinoplasty or nasal valve repair: A 25-year systematic review." Otolaryngology - Head and Neck Surgery **139**(1): 10-20.
Rhee J S, S. C., Frank DO, Kimbell JS, Garcia GJM. (2014). "A systematic review of patient reported nasal obstruction scores: Defining normative and symptomatic ranges in surgical patients." JAMA Facial Plast Surg **16**(3): 219-232.
Rhee, J. S. (2009). "Measuring outcomes in nasal surgery: realities and possibilities." Arch Facial Plast Surg **11**(6): 416-419.
Rhee JS, Cannon DE, Frank DO, Kimbell JS (2012). "Role of vitual surgery in preoperative planning." Arch Facial Plast Surg:14(5) 354-359.
Roe JO (1908). "The correction of nasal deformities." Laryngoscope **18**(10): 782-797.
Rohlf FJ, M. L. (1993). "A revolution in morphometrics." Trends Ecol. Evol. **8**: 129-132.
Rohlf JF, Corti M (2000). "Use of teo-block partial least-squares to study covariation in shape."Systematic Biology 49(4): 740-753.
Rohrich RJ, G. J., Deuber MA, Adams WP (2002). "The deviated nose: Optimizing results using a simplified classification and algorithmic approach." Plast Reconstr Surg **110**(6): 1509-1523.
Salihoglu M, C. E., Altundag A, Cesmeci E (2014). "Examination versus subjective nasal obstruction in the evaluation of the nasal septal deviation." Rhinology **52**(2): 122-126.
Sawhney KL, S. A. (1964). "Diagnosis of deviated septum." Journal of the Oto-laryngolological Society of Australia **38**: 261-263.
Scott JH (1953) "The growth of the human face." Proceedings of the Royal Society of Medicine November 23, p. 91-100.
Scott JH (1958). "The Cranial Base." Americal Journal of Physical Anthropology: 16:319-48.
Senck, S. (2012). New approaches in the virtual reconstruction of fragmented specimens: applications in surgery, forensics, and anthropology. PhD, University of Vienna.
Shpilberg KA, D. S., Doshi AH, Lawson W, Som PM. (2015). "CT of anatomical variants of the paranasal sinuses and nasal cavity: Poor correlation with radiologically significant rhinosinusitis but importance in surgical planning." Neuroradiology/Head and Neck Imaging **204**(June): 1255-1260.
Singh, A., N. Patel, G. Kenyon and G. Donaldson (2006). "Is there objective evidence that septal surgery improves nasal airflow?" J Laryngol Otol **120**(11): 916-920.
Slice DE (2007). "Geometric Morphometrics." Annu. Rev. Anthropol. **36**: 261-281.

Sommer F, Simmen D, Briner HR, Jones N, Hoffmann TK, Lindemann J (2016). "Effects of nasal wall lateralization and pyriform turbinoplasty on nasal air conditioning." Otorhinolaryngology Head Neck Surg:2(1): 1-5.
Stoyanova D, Algee-Hewitt BFB, Slice DE (2015). "An enhanced computational method for age-at-death estimation based on the pubic symphsis uing 3D laser scans and thin plate splines." American Journal of Physical Anthropology:158: 431-440.
Sundh, C. and O. Sunnergren (2015). "Long-term symptom relief after septoplasty." Eur Arch Otorhinolaryngol **272**(10): 2871-2875.
Surgery, A. A. o. O.-H. a. N. (2017). "Patient Health Informtion: Deviated Septum." from http://www.entnet.org/content/deviated-septum.
Takahashi R (1987). "The formation of the nasal septum and the etiology of septal deformity. The concept of evolutionary paradox." Acta Oto-Laryngologica - Supplement 443: 1-155.
Takahashi R (1971). "A collection of ear, nose and throat studies from the Department of Otorhinolaryngology, Jikei University School of Medicine, Tokyo, Japan.
Teixeira, J., V. Certal, E. T. Chang and M. Camacho (2016). "Nasal Septal Deviations: A Systematic Review of Classification Systems." Plast Surg Int **2016**: 7089123.
Thulesius HL, T. H., Jessen M (2009). "What happens to patients with nasal stuffiness and pathological rhinomanometry left without surgery?" Rhinology **47**(1): 24-27.
Toyserkani NM, F. T. (2012). "Are too many septal deviations operated on? A retrospective patient's satisfaction questionaire with 11 years follow-up." Rhinology **50**: 185-190.
Tripathi PB, Eighobashi S, Wong DJF (2017). "The myth of the internal nasal valve." JAMA Facial Plastic Surgery:doi:10.100/jamafcial.2017.0039
UK., E. (2010). Surgery, Nasal Septal. "ENTUK position paper 2010.". ENT UK (the British Academic Conference in Otolaryngology (BACO) and the British Association of Otorhinolaryngology–Head and Neck Surgery (BAO-HNS)). London, England.
Uygur K, Yariktas M, Doner F, Ozgan A (2002). "The incidence of septal deviation in newborns." Journal of Ear, Nose, and Throat 9(2): 117-120
Van Egmond MMHT, R. M., Hendriks CTM, Van Heerbeek N. (2015). "Effectiveness of septoplasties versus non-surgical management for nasal obstruction due to deviated nasal septum in adults: study protocol for a randomized controled study." Trials **16**.
Verwoerd CDA, Verwoerd-Verhoef HL(2005). " Rhinosurgery in children: Basic concepts. Rhinoplasty; a practical guide to functional and aesthetic surgery of the nose". The Hague: Kugler; 2005. *pp. 201-209.*
Verwoerd CDA, Verwoerd-Verhoef HL (2010). "Rhinosurgery in children: developmental and surgical aspects of the growing nose." GMS Current Topics in Otorhinolaryngology - Head and Neck Surgery 9:1-29.
Vetter U, Pirsig W, Heinze, E (1984). "Postnatal growth of the human septal cartilage: Preliminary report." Acta Oto-Laryngologica 97 (1-2): 131-136.
Vidigal TA, H. F., Gregorio LC, Poyares D, Tufik S, Bittencourt LRA (2013). "Subjective, anatomical, and functional nasal evaluation of patients with obstructive sllep apnea syndrome." Sleep and Breathing **17**(1): 427-433.
Wahba G (1990). "Spline models for observational data." Society for Industrial and Applied Mathematics, CBMS-NSF Regional Conference series in applied mathematics.

Weber GW, B. F. (2011). Virtual Anthropology. A guide to a new interdisciplinary field. Wien, New York, Springer.
Weinstock MS, Stupak HD (2018). "Bony/Cartilaginous Mismatch: A Radiologic Investigation into the Cause of Tension Nose Deformity." Plast. Reconstr. Surg. 141: 312-322.
Wen J, Inthavong K, Tu J, Wang S (2008). "Numerical simmulations for detailed airflow dynamics in a human nasal cavity." Respiratory Physiology and Neurobiology: 161: 125-135.
Williams PW (1907). "Operations for deflections and spurs of the nasal septum, with special reference to sub-mucous resection." Bristol Medico-Chirurgical Journal **25**(95): 21-38.

Windhager S, Bookstein FL, Millesi E, Wallner B, Schaefer K (2017). "Patterns of correlation of facial shape with physiological measurements are more integrated than patterns of correlation with ratings." www.nature.com/scientificreports DOI: 10:1038/srep45340.

Appendix I: Images and contour maps of most deformed specimens

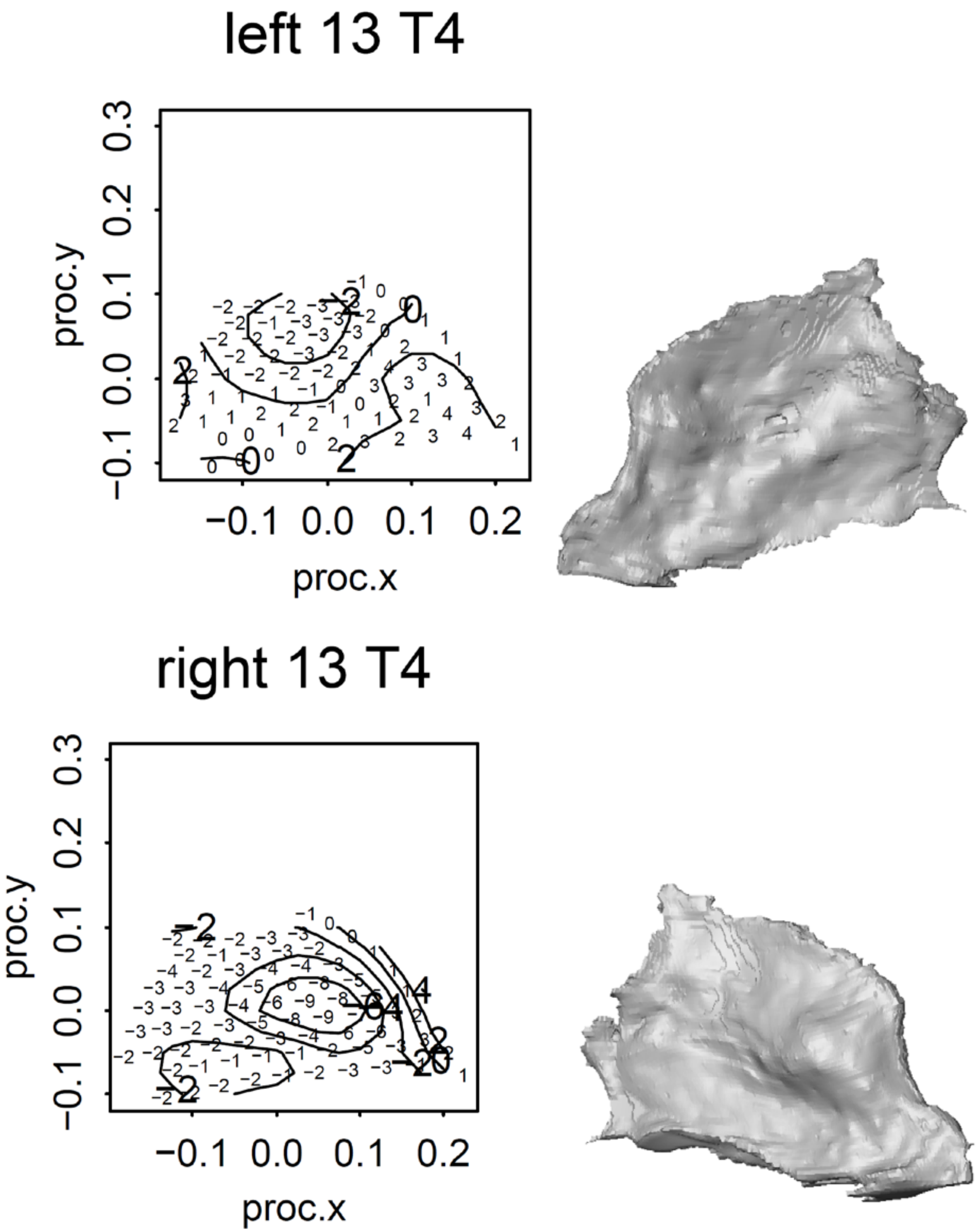

Figure __: Male, age 16, Concha bullosa and adenoids present, (036).

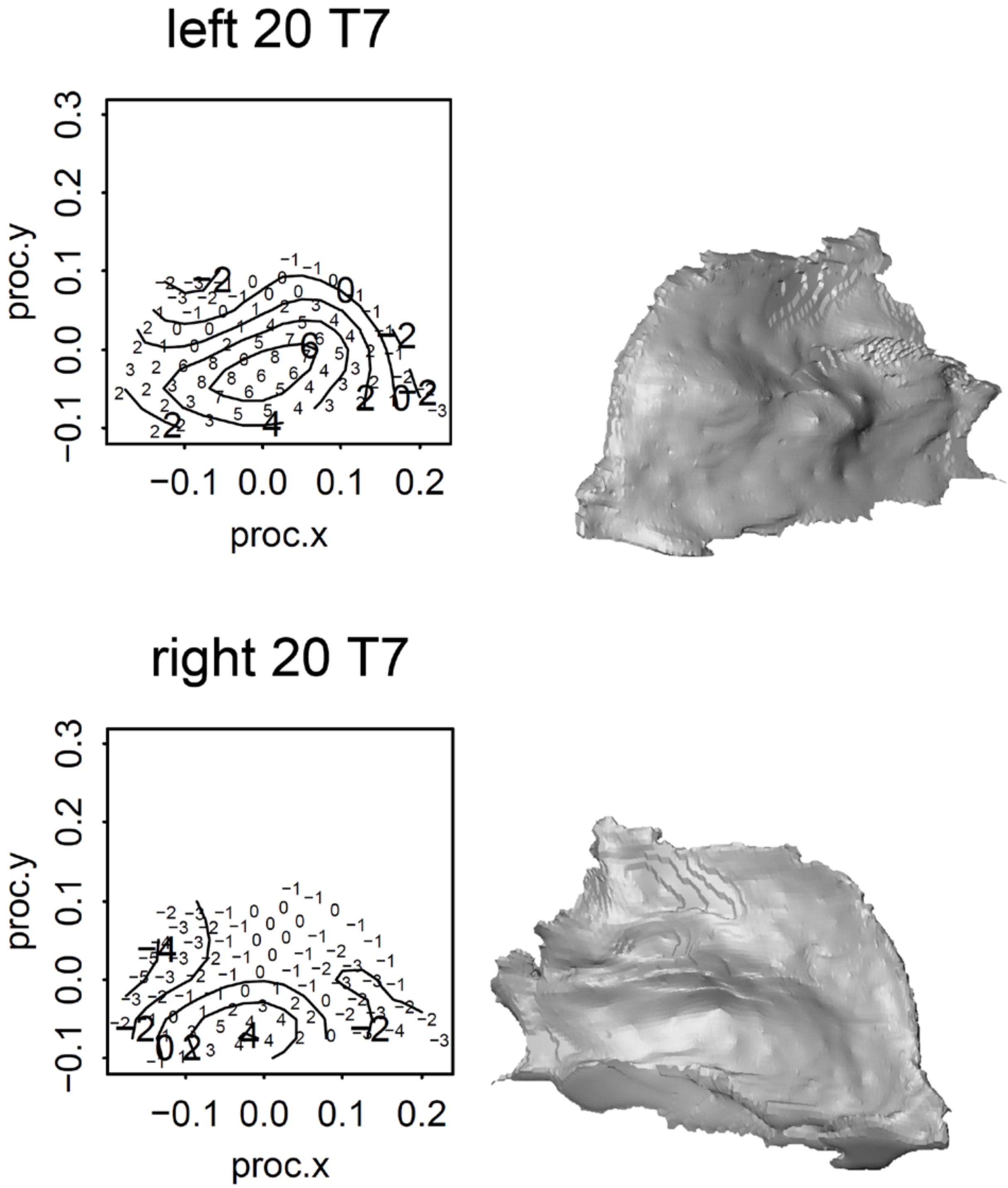

Figure __: Female, age 41, Ridge.

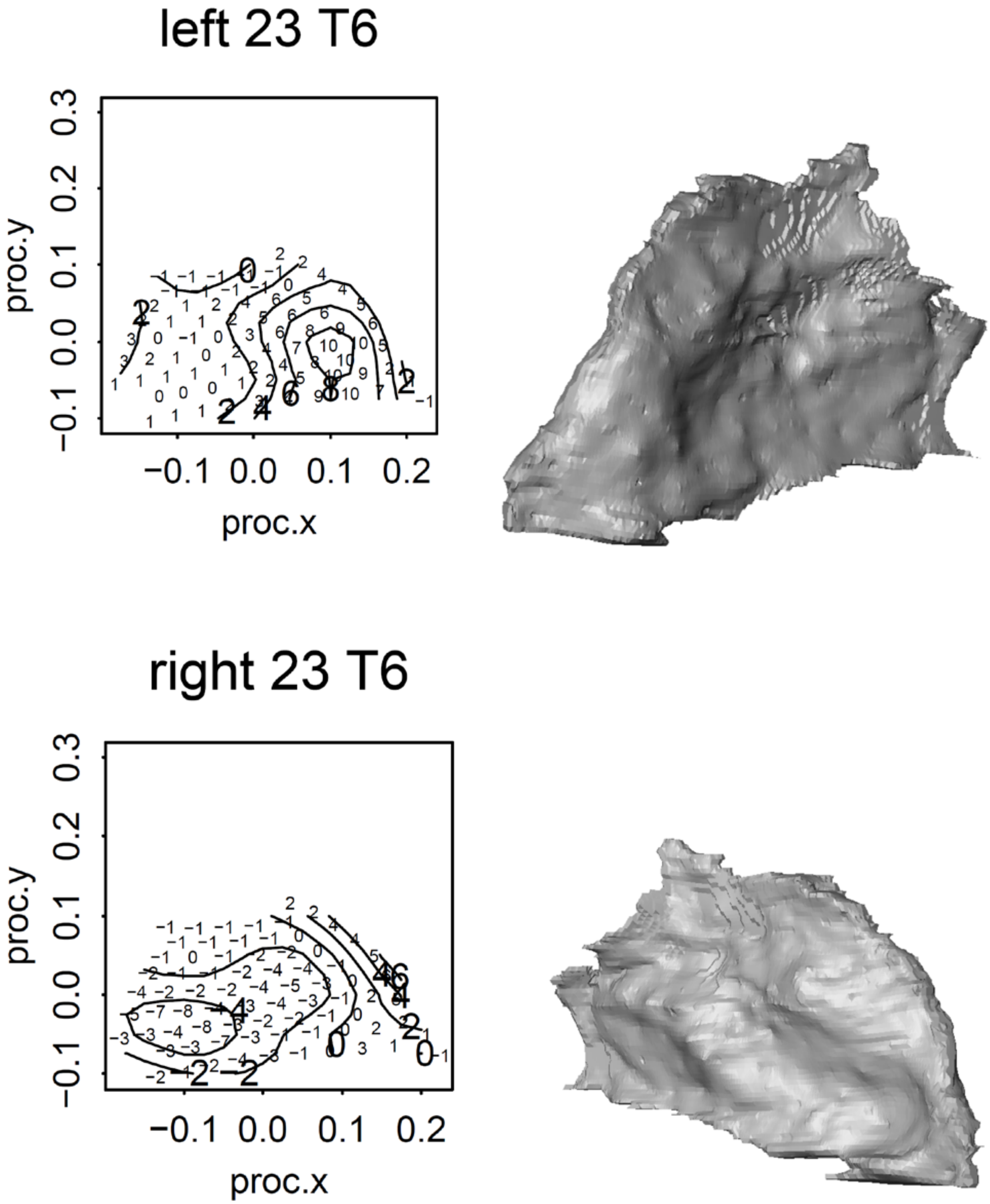

Figure __: Male, Age 33, Ridge

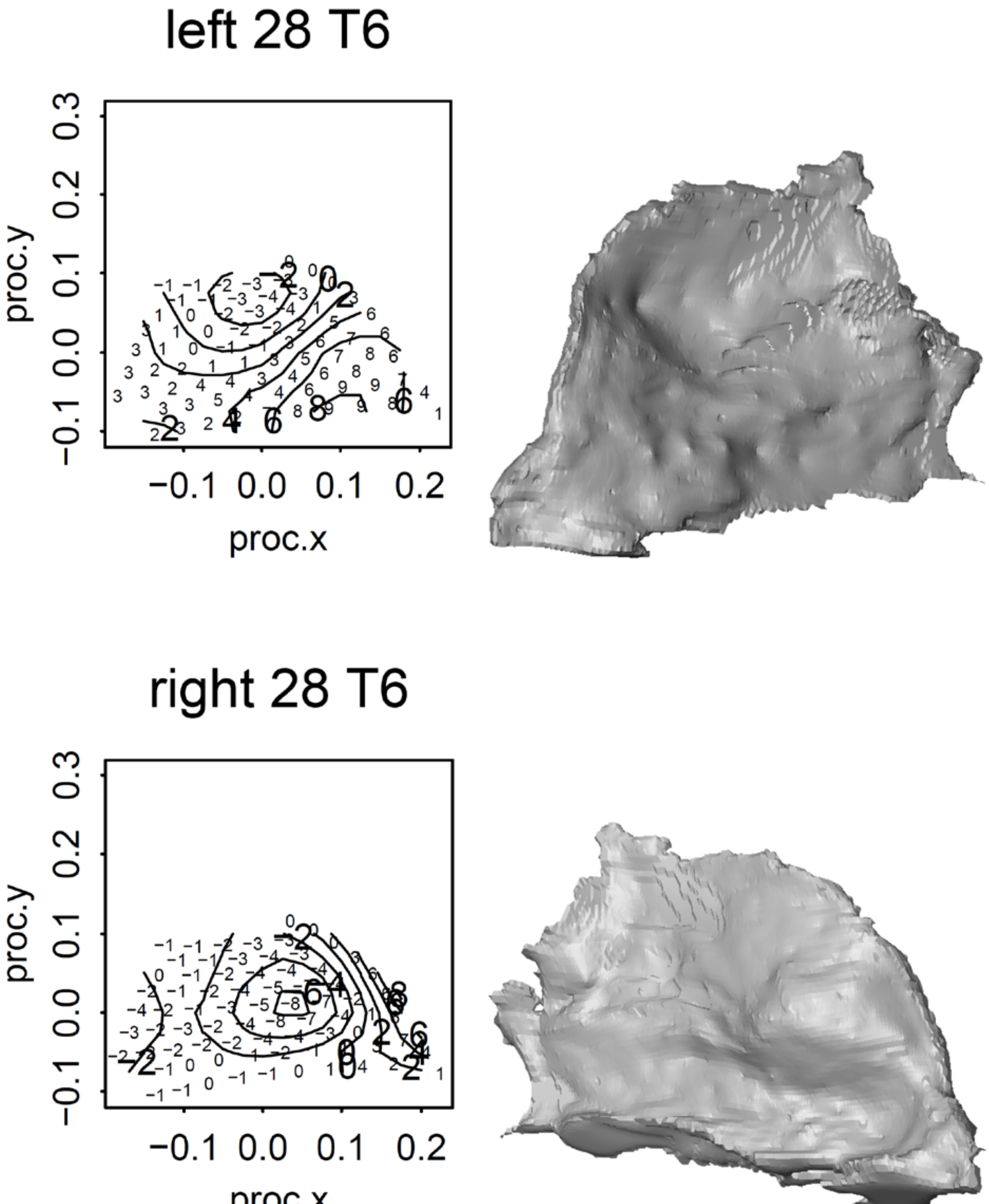

Figure __: Male, Age 53, Ridge.

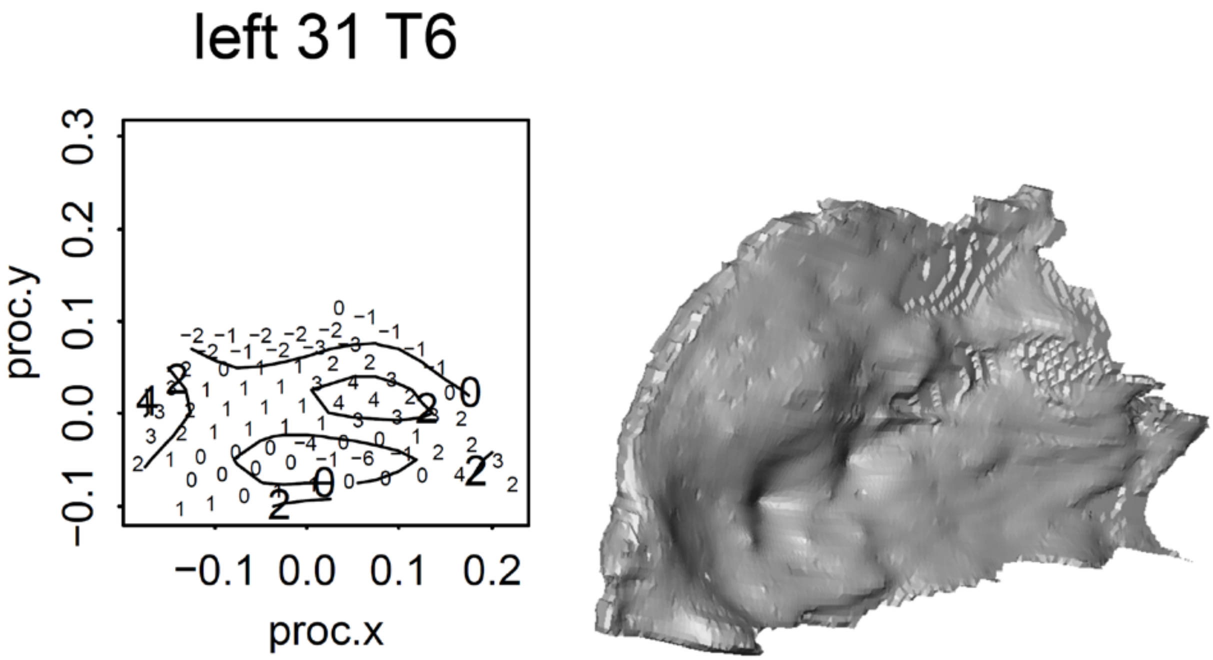

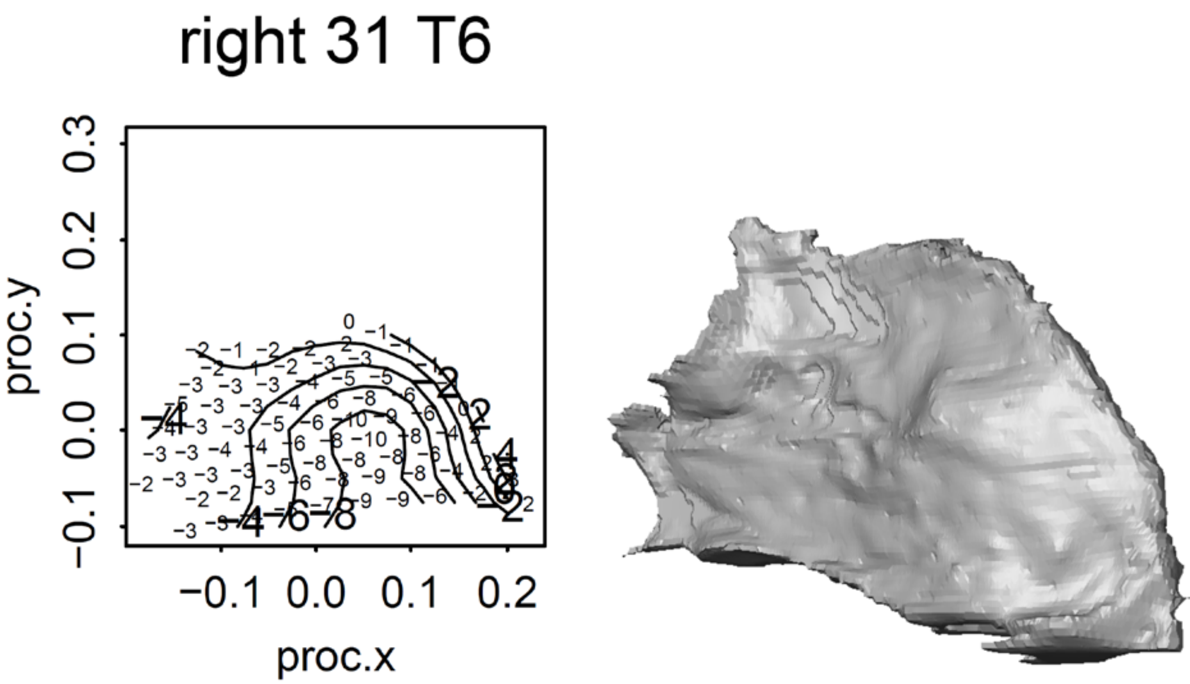

Figure __: Male, Age 54.

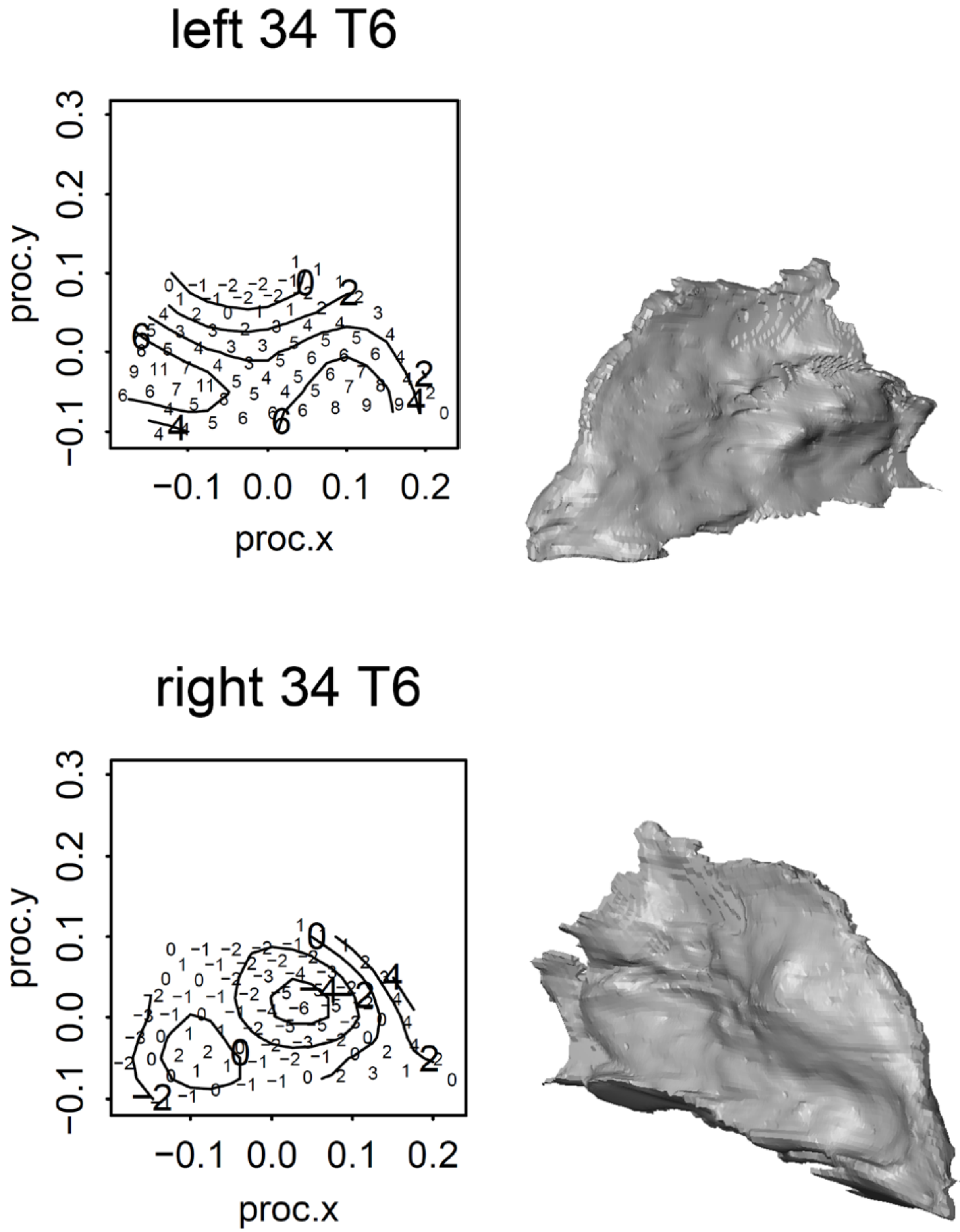

Figure __: Male, Age 44, Ridge.

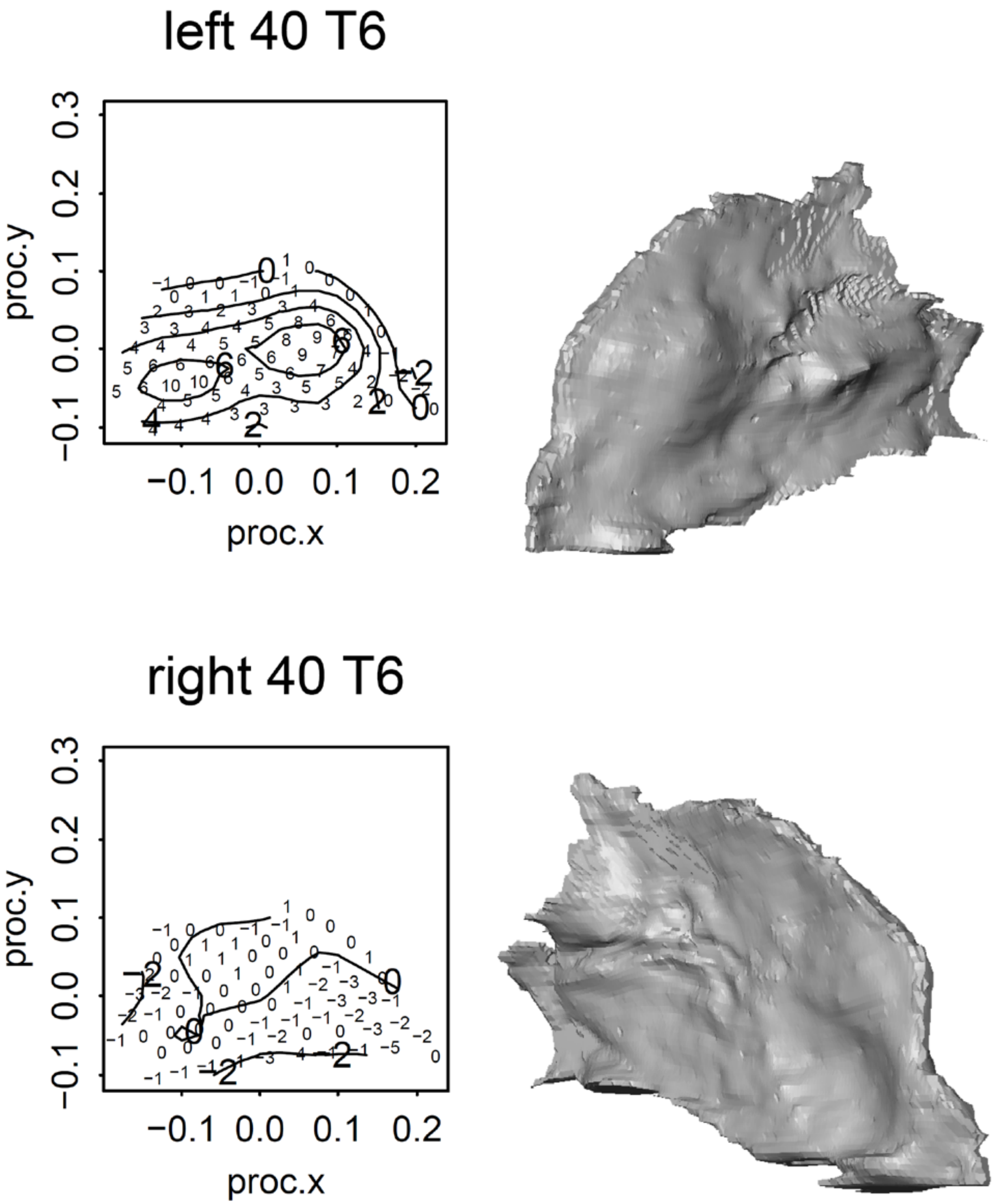

Figure __: Male, Age 56, Concha bullosa

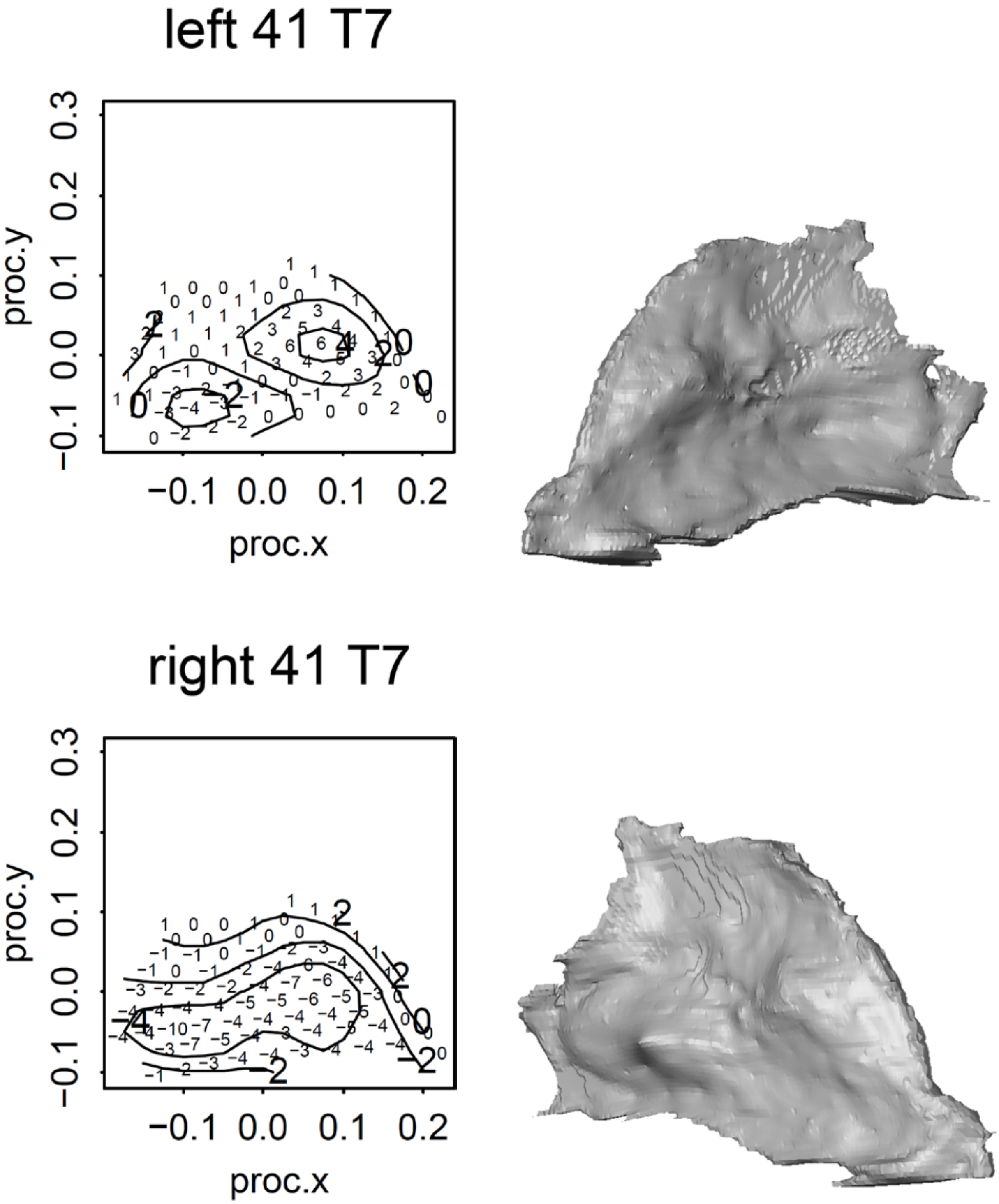

Figure __: Male, Age 21, Ridge

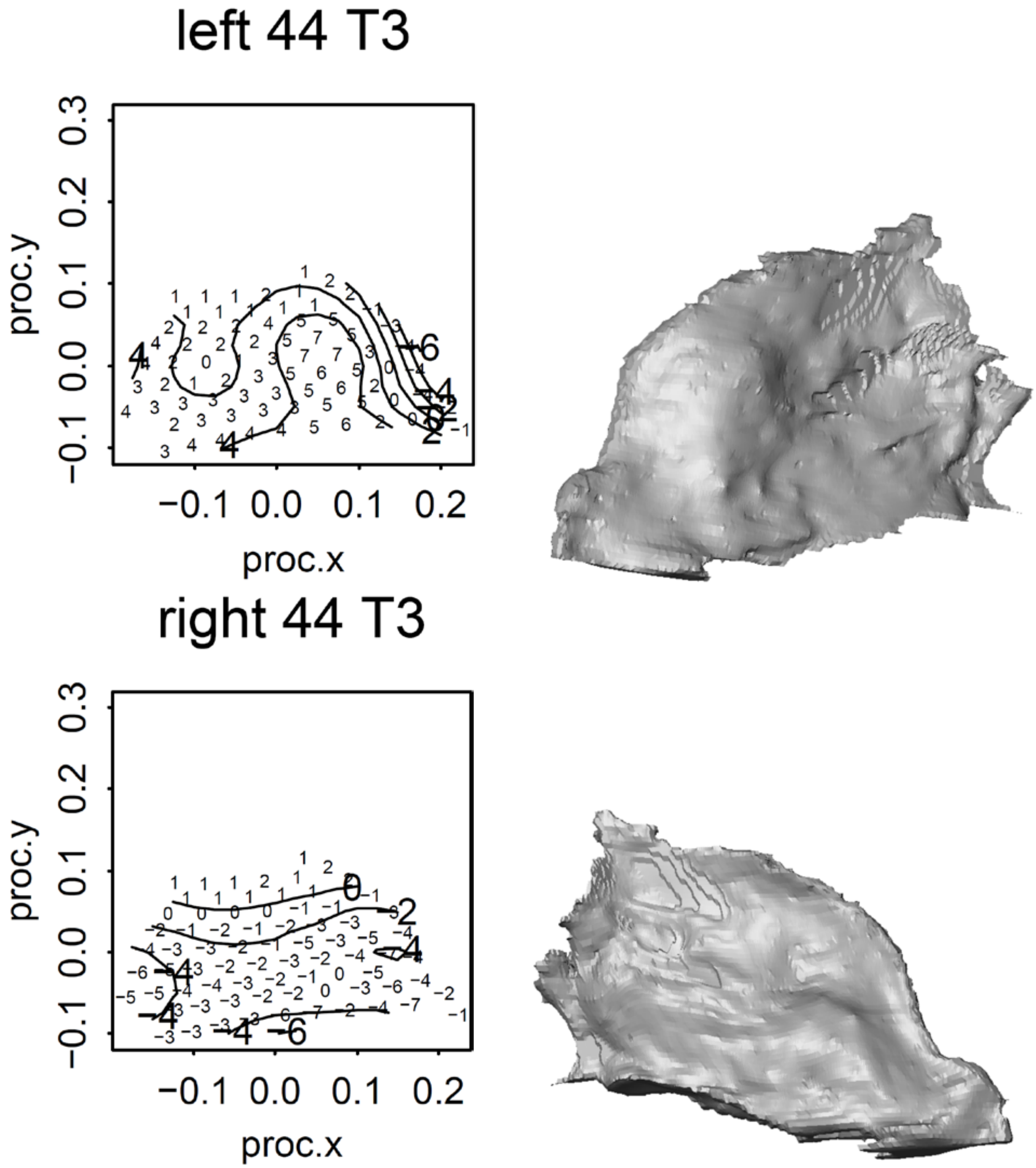

Figure __: Male, Age 48, Concha bullosa.

Appendix II: Dryden – Mardia equations for the thin plate spline.

For a $m = 2$ dimensional case, with deformations given by the bivariate function

$$\mathrm{y} = \Phi(t) = (\Phi_1(t), \Phi_2(t))^T$$

Using a pair of thin-plate splines for the functions $\Phi_1(t)$ and $\Phi_2(t)$

The thin plate spline minimizes the bending energy in transforming between two configurations.

For $(2\ x\ 1)$ landmarks $t_j, i = 1, \dots, k$, on the first figure mapped into $y_i, i = 1, \dots, k$, on the second figure, there are $2k$ interpolation constraints.

$$(y_j)_r = \Phi_r(t_j), \quad r = 1{,}2, \;\; j = 1, \dots., k, \qquad \text{(a)}$$

And we write $\Phi(t_j) = (\Phi_1(t_j), \Phi_2(t_j))^T, j = 1, \dots, \dots, k$, for the 2D deformation. Let

$$T = [t_1 \quad t_2 \quad \dots \quad t_k\,]^T, \quad Y = [y_1 \quad y_2 \quad \dots \quad y_k]^T$$

So that T and Y are both $(k\ x\ 2)$ matrices

A pair of thin plate splines (PTPS) is given by the bivariate function

$$\Phi(t) = (\Phi_1(t), \Phi_2(t))^T$$
$$= c + At + W^T s(t),$$

$where\ t\ is\ (2\ x\ 1), s(t) = (\sigma(t - t_k))^T, (k\ x\ 1)\ and$

$$\sigma(h) = \begin{cases} \|h\|^2 \log(\|h\|), & \|h\| > 0, \\ 0, & \|h\| = 0 \end{cases}$$

The $2k + 6$ parameters of the mapping are $c(2\ x\ 1), A(2\ x\ 2)$ and $W(K\ x\ 2)$. There are $2k$ interpolation constraints in equation (a), and six more are introduced in order for the bending energy in equation (c) to be defined:

$$1_k^T W = 0, \;\; T^T W = 0. \qquad \text{(b)}$$

The pair of thin plate splines which satisfy the constraints of equation (b) are called natural thin-plate splines. Equations (a) and (b) can be re-written in matrix form

$$\begin{bmatrix} S & 1_k & T \\ 1_k^T & 0 & 0 \\ T^T & 0 & 0 \end{bmatrix} \begin{bmatrix} W \\ c^T \\ A^T \end{bmatrix} = \begin{bmatrix} Y \\ 0 \\ 0 \end{bmatrix},$$

where $(S)_{ij} = \sigma(t_i - t_j)$ and 1_k is the k-vector of ones. The matrix

$$\Gamma = \begin{bmatrix} S & 1_k & T \\ 1^T & 0 & 0 \\ T^T & 0 & 0 \end{bmatrix}$$

is non-singular provided S is non-singular. Hence

$$\begin{bmatrix} W \\ c^T \\ A^T \end{bmatrix} = \begin{bmatrix} S & 1_k & T \\ 1_k^T & 0 & 0 \\ T^T & 0 & 0 \end{bmatrix}^{-1} \begin{bmatrix} Y \\ 0 \\ 0 \end{bmatrix} = \Gamma^{-1} \begin{bmatrix} Y \\ 0 \\ 0 \end{bmatrix},$$

writing this partition of Γ^{-1} as

$$\Gamma^{-1} = \begin{bmatrix} \Gamma^{11} & \Gamma^{12} \\ \Gamma^{21} & \Gamma^{22} \end{bmatrix},$$

where Γ^{11} is $k\ x\ k$, it follows that

$$W = \Gamma^{11} Y$$

$$\begin{bmatrix} c^T \\ A^T \end{bmatrix} = [\hat{\beta}_1, \hat{\beta}_2] = \Gamma^{21} Y,$$

giving the parameter values for the mapping. If S^{-1} exists, then we have:

$$\Gamma^{-11} = S^{-1} - S^{-1} Q (Q^T S^{-1} Q)^{-1} Q^T S^{-1},$$

$$\Gamma^{21} = (Q^T S^{-1} Q)^{-1} Q^T S^{-1} = (\Gamma^{12})^T ,$$

$$\Gamma^{22} = -(Q^T S^{-1} Q)^{-1} ,$$

where $Q = [1_k, T]$,

The $k\ x\ k$ matrix B_e is called the bending energy matrix

$$B_e = \Gamma^{11}. \qquad \text{(c)}$$

There are three constraints on the bending energy matrix

$$1_k^T B_e = 0, \qquad T^T B_e = 0$$

And the rank of the bending energy matrix is $k - 3$. (Dryden 2016)

Appendix III: Abstract (German)

Dieses Projekt befasst sich mit einem Paradox in der derzeit angewandten **Anthropologie der menschlichen Nasenscheidewand (die Trennwand, die die** Nasenhöhle teilt). Weltweit werden jährlich etwa eine Million Septoplastien durchgeführt (im Jahr 2006 wurden 600.000 in den USA durchgeführt, wobei die Rate von 2000 auf 2014 jährlich um 3,7% gestiegen ist). Die Operation wurde durchgeführt, um "Abweichungen" der Nasenscheidewand zu korrigieren – gemeint sind Abweichungen von der Ebenheit der gemischten knorpeligen Knochenplatte. Das Problem ist, dass die Erfolgsmessungen des Chirurgen häufig von der Wahrnehmung der Symptome durch die Patienten abweichen, wobei nur wenige qualitativ hochwertige Beweise die Behauptung stützen, dass diese Operationen förderlich sind.

Die "Arten von abweichendem Septum" sind vielen Klassifizierungsschemata unterworfen worden, die oft untereinander widersprüchlich sind, nicht mit spezifischen Verfahren verbunden sind, und nicht evidenzbasiert im Hinblick auf die Übereinstimmung mit akzeptierten Standards der Beurteilung der präoperativen Funktion und der postoperativen Verbesserung. Ziel dieser Dissertation war es, zu untersuchen, ob das Standard-Toolkit der geometrischen Morphometrie (GMM) - die Statistik der biologischen Form bei der Segmentierung der (zweiseitigen) septalen Oberfläche - diesen Problemzusammenhang klären könnte, entweder durch Bestätigung der Gültigkeit einer bestehenden Klassifikation, oder durch die Entwicklung von funktionellen Messungen, die eine Operation rechtfertigen könnten.

Die gewählte Klassifikation wurde 1987 vom kroatischen Hals-Nasen-Ohrenarzt Ranko Mladina entwickelt (mit späteren Revisionen). Mladina hat die Welt der Abweichungen in sieben Typen unterteilt, von denen die schwerwiegendste, "T6" (Typ 6), ein Schwerpunkt meiner Ergebnisse sein wird. Diese Klassen wurden subjektiv basierend auf veröffentlichten verbalen Beschreibungen des Septums zugeordnet, wie sie aus CT und klinischer Untersuchung visualisiert wurden. An der Zuordnung dieser Klassen waren keine Quantifizierungen beteiligt.

Zunächst erfolgte die Quantifizierung dieser Klassen durch Anwendung des GMM-Toolkits auf meine Segmentierung der Septumoberflächen. GMM, eine Spezialität der Abteilung für Bioanthropologie der Universität Wien, drückt einen Datensatz biologischer Formen als eine Sammlung von kartesischen Koordinaten (x, y und z) von markierten Punkten (Orientierungspunkten) zusammen mit Punktketten (Semi- Orientierungspunkten) entlang von Kurven und Maschen von Punkten auf Oberflächen (Oberflächen-Semi-Orientierungspunkten). Die Punkte, die ich digitalisierte, beinhalteten fünf Orientierungspunkte (am meisten anteriorer / inferiorer Punkt an der NS, Foramen caecum, Ethmoid-Sphenoid, Sphenoid-Vomer, Vomer-Palatin), zwei Kurven (anteriores Nasenseptum, hinteres Nasenseptum) und jeweils ein Netz der zwei Oberflächen mit 132 getrennten Punkten. Zusätzlich wurden 5 weitere Landmarken (Basion, Pharynxbefestigung am Sphenoid, Sella turcica (Boden), Sella turcica (posterior) und Opisthion) auf der hinteren Schädelbasis ausgewählt, um eine "anatomische Mittelebene" mit Bezug zu definieren, zu welchem die Septumabweichungen bewertet würden.

Eine GMM-Analyse durchläuft drei Schritte: Reduktion der Daten in ein gemeinsames Koordinatensystem, multivariate statistische Analyse der standardisierten Formen und graphische Darstellung der durch die Analyse aufgedeckten Muster, beschränkt auf die Septumdaten selbst oder in Kombination mit der klinischen Typologie. Die untersuchte Probe umfasste 49 Septen mit einer nicht-trivialen Mladina-Klassifikation, ausgewählt aus einem Angebot von 92 von einer Klinik der Universität Graz, die sie wiederum aus ihrer Anhäufung von 2000 erwachsenen CTs auswählten.

Die septalen Formen wurden nach der sogenannten Procrustes-Technik (Anpassung für durchschnittliche Position, Größe und Orientierung) auf einen gemeinsamen Mittelwert registriert, die statistische Analyse erfolgte nach der herkömmlichen Technik der "relativen Ketten" (Hauptkomponenten aller drei kartesischen Koordinaten zur gleichen Zeit), und die Anzeige erfolgte durch eine Kombination von TPS-Graphen (Thin-Plate Spline) für die Septumdeformation in der Ebene zusammen mit Streuungen von Hauptkomponenten-Scores, die durch die entsprechende Mladina-Typennummer gekennzeichnet sind. GMM geht davon aus, dass korrespondierende Punkte des Septumnetzes biologisch gleichwertigen Formmerkmalen entsprechen. Diese Analyse ist offensichtlich fehlgeschlagen, da sogar die Mladina-Art der größten Deformität (T6) ihre Mitglieder über die resultierenden Hauptkomponenten-Streudiagramme verteilt fand: Es gab keine besondere Beziehung zwischen den Septalenformkoordinaten und der Mladina-Klassifikation.

Die Erkenntnis, dass ein anderer Ansatz zur Datenanalyse erforderlich war, kam zur gleichen Zeit wie die Entdeckung einer großen nicht erkannten Ressource: das Lebenswerk eines selten übersetzten japanischen HNO-Arztes Ryo Takahashi, der die Veränderung der Nasenscheidewand beim Homo Sapiens als Folge der Entwicklungstendenzen unserer Arten betrachtete. Diese Septumabweichung, die bei 98% aller erwachsenen Männer und bei über 90% der Frauen beobachtet wurde, war ein Ausdruck der inkompatiblen Kräfte auf die verschiedenen Rahmenstrukturen der Nasenhöhle. Insbesondere entsprachen die schwersten Fälle einer Abweichung dem Knicken der entsprechenden knorpeligen Knochenoberflächen während des Wachstums und der Entwicklung. Statt einer vereinfachten Klassifikation bot Takahashi diagnostische Systematik an, um ein verformtes Septum zu analysieren, das letztendlich die Kräfte und ihre Auswirkung auf die Morphologie der verschiedenen Unterbereiche des Septums in verschiedenen Richtungen und unter Berücksichtigung des Wechselspiels zwischen den angrenzenden Strukturen erklären würde - Strukturen wie die Nasenmuscheln. Von dieser Theorie folgte sofort eine Kritik des klassischen GMM-Ansatzes: Da die Position des Knickens mehr oder weniger unabhängig von dessen Größe war, war die Annahme von GMM in Bezug auf Homologie nicht gültig.

Die alternative Methode, die im Lichte von Takahashis Theorie konstruiert wurde, wählte zwei spezifische Werkzeuge von GMM aus und verwirft den Rest. Erstens registrierten wir alle Fälle von Septumoberflächen auf der hinteren anatomischen Mittelebene und nicht auf ihrem eigenen Durchschnitt. Zweitens haben wir anstelle des standardmäßigen relativen Verzerrungsschemas (Hauptkomponenten in 3D) diese Variationen ohne Zentrierung betrachtet, nur in einer Dimension (der mediolateralen), ausgedrückt in einem apriorischem System von orthogonalen Mustern, den partiellen Ketten. Diese beschreiben die Art und Weise, wie ein Spline mit dünnen Platten bei der Minimierung der Biegungsenergie durch ein Spektrum von Mustern auf verschiedenen räumlichen Skalen ankommt. Meine Musteranalyse erfolgte in Form eines Bandpassfilters, einer Untersuchung der Bandbreite von Teilspektren, um zu sehen, welche die Mladina T6-Kategorie am besten erklären könnte.

Diese stark modifizierte Methode hat hervorragend funktioniert. Ein spezieller Bandpassfilter (Tiefpass summiert über die ersten 19 Teilketten in der Reihenfolge der Biegeenergie) trennte die fünf Mladina's T6 unter den neun Proben mit der höchsten Biegeenergie von der Probe von 49 perfekt. Von den zusätzlichen vier stark verformten Proben, waren zwei Mladina Klasse T7, ein T4 und ein T3. Die Gütezahl für dieses Bandpassfilter kann als ein sorgfältig abgestimmtes Maß für die Oberflächenrauigkeit mehrerer Skalen erklärt werden. Es bleibt abzuwarten, ob Rauheitsmessungen mit den subjektiven Symptomen der respiratorischen Schwierigkeit übereinstimmen, die die Hauptgründe dafür sind, dass Patienten sich überhaupt behandeln lassen. Eine solche Verbindung ist plausibel, da diese schweren Deformitäten häufig die Nasenklappenregion betreffen, wo die Obstruktion die größte Auswirkung auf die Luftströmung hat.

Ein abschließender Überblick über den aktuellen Stand der rechnerischen fluid-dynamischen Analysen der Nasenhöhle, ein biotechnischer Schub, der ebenfalls auf der Annahme beruht, dass der Luftfluss die Ursache der Symptomatologie ist, skizziert eine Reihe quantitativer Untersuchungen, die die Diagnostik in diesem Bereich optimieren könnten, um die Anzahl der Operationen zu reduzieren, bei denen keine Symptome gemildert werden. Wir glauben, dass dieses Projekt ein nützliches Licht auf die Frage geworfen hat, was erforderlich ist, um Visualisierungstechniken von einem Bereich der Biologie (Paläoanthropologie) auf einen anderen zu übertragen, der viel enger mit der Biophysik einer essentiellen menschlichen Funktion (hier Atmung) ausgerichtet ist. Wir haben vielleicht einen ganz neuen Zweig für angewandte Anthropologie eröffnet.

Appendix IV: Abstract (English)

This project is concerned with a paradox in the current applied anthropology of the human nasal septum (the partition that halves the nasal cavity). Worldwide, perhaps a million septoplasties are performed annually (In 2006, 600,000 were performed in the USA, with the rate increasing from 2000 to 2014 at 3.7% annually). The surgery was performed to “correct deviations” of the nasal septum, meaning deviations from flatness of the mixed cartilaginous-bony panel. The problem is that the surgeon’s measures of success are frequently at variance with patients’ perception of symptom alleviation, with little high-quality evidence supporting claims that these surgeries are beneficial.

The “types of deviated septum” have been subjected to many classification schemes, often contradictory among themselves, not associated with specific procedures, and not evidence-based in terms of matching any accepted standards of assessment of presurgical function and postsurgical improvement. The purpose of this dissertation was to assess if the standard toolkit of geometric morphometrics (GMM) – the statistics of biological form when applied to segmentations of the (two-sided) septal surface would clarify this nexus of problems, either by confirming the validity of an existing classification or through the development of functional measurements that might justify surgery.

The classification chosen was developed by the Croatian otorhinolaryngologist Ranko Mladina in 1987 (with later revisions). Mladina divided the world of deviations into seven types of which the most serious, “T6” (Type 6), will be a focus of my findings. These classes were assigned subjectively based on published verbal descriptions of the septum as visualized from CT and clinical examination. There were no quantifications involved in the assignment of these classes. Initially the quantification of these classes was by applying the GMM toolkit to my segmentation of the septal surfaces. GMM, a specialty of the department of bioanthropology of the University of Vienna, expresses a data set of biological forms as a collection of Cartesian coordinates (x, y, and z) of labelled points (landmarks) along with chains of points (semilandmarks) along curves and meshes of points upon surfaces (surface semilandmarks). The points I digitized included five landmarks (most anterior/inferior point on the NS, foramen caecum, ethmoid-sphenoid, sphenoid-vomer, vomer-palatine), two curves (anterior nasal septum, posterior nasal septum), and a mesh for each of the two surfaces with 132 separate points. In addition there were 5 other landmarks (Basion, pharyngeal attachment to the sphenoid, sella turcica (floor), sella turcica (posterior), and opisthion) chosen on the posterior cranial base in order to define an “anatomical mid-plane” with respect to which the septum’s deviations would be assessed.

A GMM analysis proceeds through three steps: reduction of the data to a common coordinate system, multivariate statistical analysis of the standardized forms, and graphical display of the patterns revealed by the analysis, restricted to the septal data itself or in combination with the clinical typology. The sample studied comprised 49 septa having a nontrivial Mladina classification, selected from an offering of 92 from a clinic at the University of Graz that selected them, in turn, from their accumulation of some 2000 adult CTs.

The septal forms were registered to a common average by the so-called Procrustes technique (adjustment for average position, size, and orientation), statistical analysis was by the conventional technique of “relative warps” (principal components of all three Cartesian coordinates at the same time), and display was by a combination of thin-plate spline (TPS) graphs for in-plane septal deformation together with scatters of principal component scores tagged by the corresponding Mladina type number. GMM assumes that corresponding points of the septal mesh corresponded to biologically homologous shape features. This analysis obviously failed, as even the Mladina type of greatest deformity (T6) found its members distributed all over the resulting principal component scatterplots: there was no particular relation between the septal shape coordinates and the Mladina classification.

The realization that another approach to data analysis was required came at the same time as the discovery of a major unrecognized resource: the life work of a rarely translated Japanese otorhinolaryngologist, Ryo Takahashi, who couched the variation of the nasal septum in Homo sapiens as a consequence of trends in the evolution of our species. That septal deviation observed in 98% of all adult males and over 90% of females was an expression of the incompatible forces on the various framing structures of the nasal cavity. In particular, the most severe cases of deviation corresponded to buckling of the corresponding cartilaginous-osseous surfaces during growth and development. Rather than a simplistic classification, Takahashi offered diagnostic systematics to analyse a deformed septum that would ultimately account for the forces and their effect on the morphology of the various sub-regions of the septum, in different directions, and with consideration of the interplay between adjoining structures such as the nasal turbinates. From this theory a critique of the classic GMM approach immediately followed: since the position of the buckling was more or less independent of its magnitude, the assumption of GMM in respect to homology was not valid.

The alternative method constructed in light of Takahashi’s theory selected two specific tools from GMM and discarded the rest. First, we registered all instances of either septal surface on the posterior anatomical mid-plane rather than on their own average. Second, in place of the standard relative warp scheme (principal components in 3D), we considered these variations without centering, in only one dimension (the mediolateral), as expressed in terms of an a-priori system of orthogonal patterns, the partial warps that describe the way a thin-plate spline arrives at its minimization of bending energy by a spectrum of patterns at different spatial scales. My pattern analysis took the form of a bandpass filter, an exploration of the range of partial spectra to see which best might account for the Mladina T6 category.

This highly modified method worked superbly. One particular bandpass filter (low-pass summed over the first 19 partial warps in order of bending energy) perfectly segregated the five Mladina's T6s among the nine specimens having the highest bending energy from the sample of 49. Of the additional four severely deformed specimens, two were Mladina class T7, one T4, and one T3. The figure of merit for this bandpass filter can be explained as a carefully tuned measure of multiscale surface roughness. It remains to be determined if measures of roughness are aligned with the subjective symptoms of respiratory difficulty that are the main reasons that patients seek treatment in the first place. Such a connection is plausible as these severe deformities frequently involve the nasal valve region, where obstruction has the greatest effect on airflow.

A closing review of the current state of computational fluid dynamic analyses of the nasal cavity, a bioengineering thrust likewise based on the assumption that airflow is at the root of symptomatology, sketches a series of quantitative investigations that might optimize diagnostics in this area so as to reduce the number of surgeries that fail to ameliorate whatever symptoms are reported. We believe that this project has shed a useful light on what is required to translate visualization techniques from one domain of biology (paleoanthropology) to another that is much more tightly aligned with the biophysics of an essential human function (here, breathing). We may have opened a whole new branch for applied anthropology.